

UC Davis

UC Davis Electronic Theses and Dissertations

Title

New approaches exploring cytochrome P450 pathway-derived metabolites of polyunsaturated fatty acids as effectors and markers of health and disease

Permalink

<https://escholarship.org/uc/item/1nr7j01p>

Author

Singh, Nalin

Publication Date

2022

Peer reviewed|Thesis/dissertation

New approaches exploring cytochrome P450 pathway-derived metabolites of polyunsaturated fatty acids as effectors and markers of health and disease

By

NALIN SINGH
DISSERTATION

Submitted in partial satisfaction of the requirements for the degree of

DOCTOR OF PHILOSOPHY

in

Agricultural and Environmental Chemistry

in the

OFFICE OF GRADUATE STUDIES

of the

UNIVERSITY OF CALIFORNIA

DAVIS

Approved:

Bruce D. Hammock

Heike Wulff

John W. Newman

Committee in Charge

2022

Table of Contents

Acknowledgments	iii
Abstract	iv
Introduction	1
Chapter 1: Adrenic Acid-Derived Epoxy Fatty Acids Are Naturally Occurring Lipids and Their Methyl Ester Prodrug Reduces Endoplasmic Reticulum Stress and Inflammatory Pain	5
Chapter 2: <i>N</i> -Benzyl-linoleamide, a Constituent of <i>Lepidium meyenii</i> (Maca), Is an Orally Bioavailable Soluble Epoxide Hydrolase Inhibitor That Alleviates Inflammatory Pain.....	51
Chapter 3: New Alkoxy- Analogues of Epoxyeicosatrienoic Acids Attenuate Cisplatin Nephrotoxicity In Vitro via Reduction of Mitochondrial Dysfunction, Oxidative Stress, Mitogen-Activated Protein Kinase Signaling, and Caspase Activation	103
Chapter 4: Improved ELISA for linoleate-derived diols in human plasma utilizing a polyHRP-based secondary tracer	162
Conclusion	205
Appendix	210

Acknowledgments

Firstly, I want to thank my PI, Dr. Bruce D. Hammock for allowing me the opportunity to work in his laboratory over the past five years and for his encouragement and ideas along the way. I would also like to thank my dissertation committee members, Drs. Heike Wulff and John W. Newman for their assistance and input. I would like to express my gratitude to several members of the Hammock Lab for their guidance and insights, most notably Drs. Christophe Morisseau, Bogdan Barnych, Karen M. Wagner, Cindy B. McReynolds, Debin Wan, Dongyang Li, and Daniel B. Lybrand. Finally, I wish to thank my family for their continued encouragement and support of my endeavors.

Abstract

Ubiquitous exposure to various exogenous factors imparts both acute and chronic adverse effects on human health. Common molecular modes of action include induction of inflammation and activation of the mitochondrial dysfunction-reactive oxygen species-endoplasmic reticulum (ER) stress axis. The kidney is especially susceptible to noxious impacts due to several structural and functional characteristics. Preservation of inflammation-mediated and organelle-linked health impacts is further hampered by a lack of safe and efficacious reno-protective agents and unreliable biomarkers.

The cytochrome P450 (CYP) branch of polyunsaturated fatty acid (PUFA) metabolism oxygenates PUFAs to a class of signaling molecules known as epoxy fatty acids (EpFAs). These are primarily inflammation resolving and mitochondria-ER stabilizing lipid mediators. Since numerous points within the P450 pathway can be capitalized upon and/or manipulated, CYP-mediated EpFA biosynthesis and metabolism offer novel therapeutic targets to ameliorate and monitor disease.

Thus, this dissertation describes new and complementing research methodologies that were explored to elucidate the pharmacological and diagnostic potential of this PUFA metabolizing route. More precisely, Chapter 1 reveals the prevalence and therapeutic relevance of an overlooked group of EpFAs. Chapter 2 furthers the quest for naturally occurring, dietarily-attained enzyme inhibitors that block the primary route of EpFA metabolism and exert desired medicinal effects. Chapter 3 illuminates a biochemically active functional group that can be employed as a lead for the design of new and improved EpFA-like therapies. Chapter 4 delivers a modern and clinically pertinent analytical method for quantitation of the downstream

metabolites of EpFAs derived from a pervasive dietary fat to exploit their exceptional biomarker functions.

Arachidonic acid-derived epoxyeicosatrienoic acids (EETs) are the most widely pharmacologically utilized group of EpFAs. However, the presence and therapeutic activity of their 22 carbon- homologues, adrenic acid-derived epoxydocosatrienoic acids (EDTs), is unstudied, despite the abundance of its parent PUFA in the kidney and vasculature. EDTs were found to occur naturally *in vivo* and exert anti-ER stress effects in kidney cells and relief from inflammatory pain in an animal model, thus illuminating another medicinally relevant group of EpFAs. Inhibition of the soluble epoxide hydrolase (sEH) enzyme curbs the major route of EpFA degradation, facilitating their bioactivities. sEH inhibitors (sEHI) derived from natural sources, such as botanicals, offer unique applicatory benefits over synthetic drugs. Accordingly, macamides derived from maca (*Lepidium meyenii*) were found to be the most promising natural sEHI group to date for a combination of inhibitory potency towards sEH and abundance in plant root. The single most relevant macamide was orally available and alleviated inflammatory pain pre-clinically. Design of structural analogues of EpFAs provides biochemically robust therapeutics that mimic EpFA activity. Accordingly, replacement of the labile epoxide group with more stable alkyl ether groups yielded a new class of EpFA analogues. These alkoxy-based analogues of EETs attenuated nephrotoxicity of a widely used chemotherapeutic (i.e., cisplatin) *in vitro* through downregulation of mitochondrial oxidative stress and termination of downstream apoptotic signaling. Downstream sEH-generated dihydroxy fatty acids, most notably the predominant linoleic acid-derived dihydroxyoctadecenoic acids (DiHOMEs), have been closely implicated in numerous pro-inflammatory pathologies and hence provide a promising biomarker for assessment of health outcomes. Reliable analytical methods are necessary for their detection

and enzyme-linked immunoassays (ELISA) possess distinct benefits as complements to classically used liquid chromatography-tandem mass spectrometry (LC-MS/MS). Therefore, utilizing polyHRP technology, a highly sensitive ELISA for DiHOMEs was developed, validated for use in human plasma, the most clinically relevant matrix, and authenticated with LC-MS/MS.

In conclusion, the multitude of strategies discussed here highlight the medicinal potential and malleability of the CYP route of PUFA metabolism and advance the pursuit of potential biochemical means to mitigate and track the deleterious health effects of environmental stressors.

Introduction

In the modern world, humans are constantly exposed to a battery of environmental factors with the potential to adversely affect health. These include xenobiotics such as pesticides, pharmaceuticals, heavy metals, industrial and consumer chemicals, harmful dietary components, and viral and bacterial pathogens. Detrimental effects can range from acute toxicities to the onset of diseases resulting from low-level, chronic exposures. Certain molecular mechanisms appear to underlie and tie together the pathophysiology of stress exerted, namely induction of a robust pro-inflammatory response in conjunction with disruptions to mitochondrial function, stimulation of reactive oxygen species (ROS), and perturbations to endoplasmic reticulum (ER) homeostasis.¹⁻³ Persistent inflammatory signaling, frequently mediated by the mitochondrial ROS-ER stress axis, and other downstream effects of the mitochondrial dysfunction-oxidative stress-ER stress network dysregulate cellular processes, activating pro-apoptotic pathways and lead to eventual cell death.

Adverse impacts include both systemic effects, such as a generalized inflammatory reaction, as well as organ-specific damage. For instance, factors such as a high perfusion rate, high metabolic activity, and cellular uptake mechanisms make the kidneys especially vulnerable to environmental stressors.⁴ The dearth of protective agents with an acceptable therapeutic index and unfeasible treatment alternatives (e.g., organ transplants, dialysis), as well as ambiguous and inconsistent biomarkers of health compound the challenges faced when shielding health from exogenous agents. Hence, there is a high and urgent demand for innovative approaches that can potentially unlock new biochemical tools for effective management of disease.

Polyunsaturated fatty acids (PUFAs), such as the ω -6 arachidonic acid (ARA, 20:4), are derived from the phospholipids of cell membranes and are metabolized to bioactive oxylipids by

three main enzymatic pathways: cyclooxygenase (COX), lipoxygenase (LOX), and cytochrome P450 (CYP).¹ The COX and LOX routes generate many pro-inflammatory lipid mediators and hence several of drugs currently available on the market act on inhibiting or antagonizing these two pathways. In contrast, aside from producing certain pro-inflammatory ω -hydroxy molecules (e.g., 20-HETE), the relatively unexplored CYP oxidase route primarily forms mono-epoxides known as epoxy fatty acids (EpFAs). These are largely anti-inflammatory lipid mediators and ARA-derived epoxyeicosatrienoic acids (EETs) are the most well studied group of beneficial EpFAs. EpFAs are principally substrates of the soluble epoxide hydrolase (sEH), and, to a lesser extent, the microsomal epoxide hydrolase (mEH), distantly related enzymes in the α/β -hydrolase fold protein family. They are converted downstream to vicinal diols (i.e., alcohols on neighboring carbons) known as dihydroxy fatty acids (DHFAs). EpFAs are autocrine and paracrine-acting molecules that resolve inflammation and mitigate mitochondrial dysfunction and ER stress.¹⁻³ These molecular actions have been shown to underpin the amelioration of pathologies in a whole host of pre-clinical disease models. Conversely, DHFAs, especially the abundant linoleic acid-derived dihydroxyoctadecenoic acids (DiHOMEs),⁵ are proinflammatory and tend to closely correlate with many poor disease outcomes.

Hence, CYP-dependent EpFA metabolism provides a novel and promising biochemical mode for pharmacological preservation of health and analytical diagnosis of disease. Taking advantage of the multiple and diverse targets within this metabolizing route, numerous approaches can be employed: 1) direct administration of EpFAs themselves, 2) inhibition of the sEH enzyme to stabilize endogenous EpFA levels, 3) design and application of more stable EpFA analogues 4) deployment of DHFAs as surrogate biomarkers for phenotypic outcomes. Accordingly, this dissertation covers the unique methodologies that were investigated within each of these realms.

More specifically, Chapter 1 reports occurrence and therapeutic potential of Adrenic acid (22:4)-derived epoxides, 22-carbon homologues of EETs that are a relatively unexplored group of EpFAs. Chapter 2 describes a new group of orally active, natural product sEH inhibitors. Chapter 3 elucidates a new class of EET analogues which employ more stable bioisosteric alternatives for the epoxide. Finally, Chapter 4 details development of a sensitive immunoassay-based analytical method for detection of DiHOMEs in biological matrices.

References

1. Singh N, Hammock BD. Soluble Epoxide Hydrolase. In: Offermanns S, Rosenthal W, editors. *Encyclopedia of Molecular Pharmacology*. Cham: Springer International Publishing; 2020. p. 1-7.
2. McReynolds C, Morisseau C, Wagner K, Hammock B. Epoxy Fatty Acids Are Promising Targets for Treatment of Pain, Cardiovascular Disease and Other Indications Characterized by Mitochondrial Dysfunction, Endoplasmic Stress and Inflammation. In: Kihara Y, editor. *Druggable Lipid Signaling Pathways*. Cham: Springer International Publishing; 2020. p. 71-99.
3. Inceoglu B, Bettaieb A, Haj FG, Gomes AV, Hammock BD. Modulation of mitochondrial dysfunction and endoplasmic reticulum stress are key mechanisms for the wide-ranging actions of epoxy fatty acids and soluble epoxide hydrolase inhibitors. *Prostaglandins Other Lipid Mediat*. 2017;133:68-78.
4. Perazella MA. Renal Vulnerability to Drug Toxicity. 2009;4(7):1275-1283

5. McReynolds CB, Cortes-Puch I, Ravindran R, Khan IH, Hammock BG, Shih P-aB, et al. Plasma Linoleate Diols Are Potential Biomarkers for Severe COVID-19 Infections. *Frontiers in Physiology*. 2021;12:403.

**Chapter 1: Adrenic Acid-Derived Epoxy Fatty Acids are Naturally Occurring
Lipids and Their Methyl Ester Prodrug Reduces Endoplasmic Reticulum Stress and
Inflammatory Pain**

Nalin Singh, Bogdan Barnych, Karen M. Wagner, Debin Wan, Christophe Morisseau, and Bruce
D. Hammock*

Department of Entomology and Nematology and UC Davis Comprehensive Cancer Center,
University of California Davis, Davis, California 95616, United States

ABSTRACT: Adrenic acid (AdA, 22:4) is an ω -6 polyunsaturated fatty acid (PUFA), derived from arachidonic acid. Like other PUFAs, it is metabolized by cytochrome P450s to a group of epoxy fatty acids (EpFAs), epoxydocosatrienoic acids (EDTs). EpFAs are lipid mediators with various beneficial bioactivities, including exertion of analgesia and reduction of endoplasmic reticulum (ER) stress, that are degraded to dihydroxy fatty acids by the soluble epoxide hydrolase (sEH). However, the biological characteristics and activities of EDTs are relatively unexplored, and, alongside dihydroxydocosatrienoic acids (DHDTs), they had not been detected *in vivo*. Herein, EDT and DHDT regioisomers were synthesized, purified, and used as standards for analysis with a selective and quantitative HPLC-MS/MS method. Biological verification in AdA-rich tissues suggests basal metabolite levels are highest in the liver, with 16,17-EDT concentrations consistently being the greatest across the analyzed tissues. Enzyme hydrolysis assessment revealed that EDTs are sEH substrates, with greatest relative rate preference for the 13,14-EDT regioisomer. Pretreatment with an EDT methyl ester regioisomer mixture significantly reduced the onset of tunicamycin-stimulated ER stress in human embryonic kidney cells. Finally, administration of the regioisomeric mixture effectively alleviated carrageenan-induced inflammatory pain in rats. This study indicates EDTs and DHDTs are naturally occurring lipids, and EDTs could be another therapeutically relevant group of EpFAs.

INTRODUCTION

A sub-set of Cytochrome P450s (CYPs) mediate oxidation of polyunsaturated fatty acids (PUFAs), generating mono-epoxide metabolites known as epoxy fatty acids (EpFAs). EpFAs are signaling molecules that play a role in various pathologies and exert primarily anti-inflammatory, anti-hypertensive, analgesic, anti-apoptotic, and anti-endoplasmic reticulum (ER) stress effects.¹⁻⁵ Epoxyeicosatrienoic acids (EETs), derived from the ω -6 PUFA arachidonic acid (ARA, 20:4), are the most widely studied group of EpFAs. Other relevant EpFAs include ω -3 PUFAs docosahexaenoic acid (DHA, 22:6) and eicosapentaenoic acid (EPA, 20:5) derived epoxydocosapentaenoic acids (EDPs) and epoxyeicosatetraenoic acids (EEQs), respectively. EpFAs are rapidly degraded *in vivo* to less active dihydroxy fatty acids (DHFAs) chiefly by the soluble epoxide hydrolase (sEH). sEH inhibition is a common therapeutic approach that stabilizes EpFA levels *in vivo*, enhancing their bioavailability and biological functions.

All-*cis*-7,10,13,16-docosatetraenoic acid (DTA, 22:4), more commonly known as adrenic acid (AdA), is another ω -6 PUFA. It is formed via 2-carbon elongation of ARA at the carboxylic end or elongation and desaturation of linoleic acid (LA, 18:2).⁶⁻⁸ It is present in the adrenal gland, liver, kidney, brain, and vasculature.⁸⁻¹¹ Exogenous administration of AdA in *ex vivo* arterial models induced CYP-mediated formation of a group of EpFAs, epoxydocosatrienoic acids (EDTs, also known as DH-EETs).^{12,13} Diol metabolites, dihydroxydocosatrienoic acids (DHDTs, also known as DH-DHETs) were also detected,¹³ presumably formed by downstream sEH hydrolysis.

EDTs were found to be endothelium-derived hyperpolarizing factors with strong vasorelaxant effects.^{12,13} Another study demonstrated the ability of EDTs to dilate coronary microvessels.¹⁴ The mode of action was consistent with the established vasodilatory mechanism of EETs.¹⁵⁻¹⁷

Despite this biological activity and structural relevance, the role of EDTs is not well studied and the occurrence of EDTs and DHDTs has not been previously reported *in vivo*. The lack of a sufficiently sensitive and reliable analytical method is a key limiting factor, as is the absence of commercially available EDT and DHDT standards.

Hence, to illuminate the physiological characteristics and bioactivities of a relatively unexplored metabolite pairing, the epoxy and dihydroxy metabolites of AdA were synthesized and purified. A sensitive, selective, and reliable HPLC-MS/MS method was developed and used to quantify basal metabolite concentrations and distributions in AdA-rich tissues. The method was then applied to an enzyme kinetics study to assess the rate of sEH mediated hydrolysis of EDT regioisomers. Finally, the therapeutic action of an EDT methyl ester regioisomer mixture was investigated 1) *in vitro* against tunicamycin-triggered ER Stress in human embryonic kidney (HEK293) cells 2) *in vivo* against carrageenan-induced inflammatory pain in rats.

RESULTS AND DISCUSSION

MRM Transitions, Retention Times, and Method Validation. Since the m/z of each parent epoxide or diol ion was the same, the developed HPLC-MS/MS analytical method emphasized both unique, quantitative ion transitions and chromatographic separation in order to effectively distinguish regioisomers. Most molecular fragmentation occurred near the epoxide or diol functional groups. Since the position of those groups varies depending on the location of the double bond, a specific fragmentation pattern followed, yielding distinctive daughter ions for every regioisomer (**Table 1**). With regards to chromatography, the DHDTs expectedly eluted much earlier than the EDTs from the reverse phase LC column (**Table 1**) since they are considerably more polar.¹³ Furthermore, within each metabolite group, regioisomers with groups at the terminal double bond (i.e., 16,17) eluted first (**Table 1**) as the distance between the

epoxide or diol moiety and the carboxylic end of the acid directly correlates with polarity.¹³ The large linear, dynamic range and low limits of detection and quantitation (**Table 1**) indicate that the method can be applied in making quantitative assessments over a varying range of analyte concentrations, including at very low levels. Both intraday and interday precision and accuracy were consistently >84% (Table S1, Supporting Information), signifying reliable and reproducible quantitation of samples. Analytical recovery of the method at low, moderate, and high compound concentrations was >85% (Figure S1, Supporting Information), demonstrating efficient and consistent biological sample preparation and analyte extraction.

Table 1. Optimized MRM Transitions, Retention Times, Method Limits of Detection and Quantitation, and Linear Ranges for EDTs and DHDTs

Analyte	Q1 (Da)	Q3 (Da)	t _R (min)	LOD (pM)	LOQ (pM)	Linear Range (nM)
16,17- DHDT	365.5	235.0	6.44	50	100	0.125-200
13,14- DHDT	365.5	195.1	6.58	50	100	0.125-200
10,11- DHDT	365.5	154.9	6.67	10	50	0.125-200
7,8- DHDT	365.5	96.9	6.78	100	500	0.625-200
16,17- EDT	347.2	246.9	8.25	5	10	0.0125-200

13,14- EDT	347.2	194.9	8.44	5	10	0.0125-200
10,11- EDT	347.2	182.9	8.50	10	50	0.125-200
7,8-EDT	347.2	134.9	8.71	500	1000	1.25-200

Occurrence and Distribution of Basal EDT and DHDT Levels in Rat Tissues. Previously, CYP-mediated generation of EDTs was demonstrated through exogenous administration of adrenergic acid in *ex vivo* arterial systems.^{12,13} However, their occurrence *in vivo* was unclear. Hence, basal EDT and DHDT concentrations were quantified in tissues reported to have abundant levels of AdA. Most of the metabolites were detected in rat liver, kidney and brain samples, and levels were found to be highest in the liver (**Table 2**). This finding can potentially be attributed to greater hepatic CYP and sEH expression,^{18,19} relative to other organs, resulting in more localized biosynthesis. DHDTs were below the limit of quantitation in the brain (**Table 2**) which may be due to the greater polarity of DHFAs, which is considered to facilitate rapid transport to and accumulation in the cerebrospinal fluid, as has been observed for dihydroxyeicosatrienoic acids (DHETs).²⁰ The 16,17-EDT regioisomer was consistently present at the highest concentrations across all three tissues, particularly in the liver (**Table 2**). This indicates that CYP facilitated epoxidation of AdA likely occurs preferably at the terminal olefin. The phenomenon would be consistent with the catalytic preference CYP monooxygenases have for the terminal double bond in several PUFAs and endocannabinoids.^{21,22} 13,14-EDT and 16,17-EDT were also detected in rat plasma, at concentrations of 0.112 and 0.369 nM, respectively. In general, relative levels of EDTs (0.6 – 9 %) and DHDTs (0.3 – 1 %) in tissues were considerably

lower than those of structurally analogous EETs and DHETs (defined as the metabolite with corresponding functional group located at identical olefin position e.g., terminal epoxides 16,17-EDT and 14,15-EET, **Table 2**). The finding would be in line with the lower systemic abundance of the parent AdA, relative to ARA. The notable exception was hepatic 16,17-EDT, which was present at nearly one-third of the concentrations of 14,15-EET.

Table 2. Concentrations of EDTs and DHDTs in AdA-Rich Rat Tissues^a

Absolute Concentrations (pg/g of tissue)				Relative Concentrations (% of Analogous ARA Metabolite)			
	Liver	Brain	Kidney		Liver	Brain	Kidney
7,8-EDT	N/D	N/D	N/D	7,8-EDT/5,6-EET	N/D	N/D	N/D
10,11-EDT	40.6	N/D	N/D	10,11-EDT/8,9-EET	7.03	N/D	N/D
13,14-EDT	47.0	18.8	8.31	13,14-EDT/11,12-EET	4.73	2.67	0.55
16,17-EDT	186	41.6	45.5	16,17-EDT/14,15-EET	31.7	8.50	3.25
7,8-DHDT	N/D	N/D	N/D	7,8-DHDT/5,6-DHET	N/D	N/D	N/D

10,11- DHDT	N/D	N/D	20.9	10,11- DHDT/8,9- DHET	N/D	N/D	0.63
13,14- DHDT	107	N/D	16.8	13,14- DHDT/11,12- DHET	0.97	N/D	0.94
16,17- DHDT	115	N/D	24.3	16,17- DHDT/14,15- DHET	0.66	N/D	0.32

^aN/D indicates < LOQ.

Kinetic Parameters of EDTs for Human sEH. Previously, formation of DHDTs has been observed following administration of AdA in adrenal cortical arteries.¹³ sEH hydrolysis of EDTs was the suspected route of metabolism since it is the primary pathway of degradation for other EpFAs. However, this hypothesis was not tested until this study, which reveals EDTs to be sEH substrates. The ability of sEH to hydrolyze each EDT regioisomer was studied under steady-state conditions using purified, recombinant human sEH. The enzyme catalysis for all the substrates fit the Michaelis-Menten model well ($R^2 = 0.95 - 0.99$, **Figure 1**) and variability in kinetic constants was observed (**Table 3**). K_M and V_{max} were acquired through non-linear regression and k_{cat} (i.e., turnover number) was obtained by dividing maximal velocity by enzyme concentration. The mechanism of sEH hydrolysis is a two-step base-catalyzed process that involves formation of a covalent hydroxyl-alkyl-enzyme ester intermediate, followed by ester hydrolysis by water and release of the vicinal diol.²³ Hence, the K_M value is a measurement for the substrate concentration at which velocity is half-maximal, rather than a measure of enzymatic affinity for

the substrate. The k_{cat} value represents primarily the rate constant for hydrolysis of the covalent intermediate since that is the slower, rate limiting step.²⁴ The $k_{\text{cat}}/K_{\text{M}}$ ratio is a measure of enzyme efficiency and is the most comprehensive indicator of the rate of reaction for a substrate. The ratio was greatest for 13,14-EDT (**Table 3**), indicating it was the best sEH substrate within the group. Accordingly, 16,17-EDT and 10,11-EDT were the next most preferred substrates, respectively, while 7,8-EDT was the worst (**Table 3**). The variable regioisomeric selectivity was consistent with sEH hydrolysis trends observed for other EpFAs such as EETs, EDPs, and EEQs.²⁵ Generally, within each EpFA group, the regioisomer with the epoxide around carbon-14 (e.g., 13,14-EDP or 14,15-EET) is degraded most rapidly²⁵ and the greatest relative substrate selectivity for 13,14-EDT was in line with this phenomenon. Rate of metabolism worsens or ceases as the epoxide in the molecule approaches the terminal or carboxylic ends (e.g., 19,20-EDP or 5,6-EET).²⁵ Expectedly, 7,8-EDT was the most slowly hydrolyzed regioisomer due to the proximity of its epoxide group to the acid function. The sEH active site is probably the key consideration in determining selectivity.²⁶ It includes large hydrophobic pockets on either side of the catalytic triad residues and, hence, accommodates EpFAs that possess the epoxide closer to the middle of the chain most effectively. A comparison with the kinetics of hydrolysis for EETs²⁵ indicates that EDTs are, in general, poorer substrates for the sEH (**Table 3**). While the rates of hydrolysis for 10,11-EDT and 13,14-EDT were quite similar to those of homologous EETs (i.e., 8,9-EET and 11,12-EET, respectively, **Table 3**), the $k_{\text{cat}}/K_{\text{M}}$ of 16,17-EDT was smaller than that of 14,15-EET by more than one order of magnitude (**Table 3**). This indicates 16,17-EDT is hydrolyzed significantly more slowly than its EET homologue and hence would possess greater resistance to degradation, which could be a factor that accounts for its relatively higher concentrations *in vivo* compared to other EDT/EET pairings (**Table 2**).

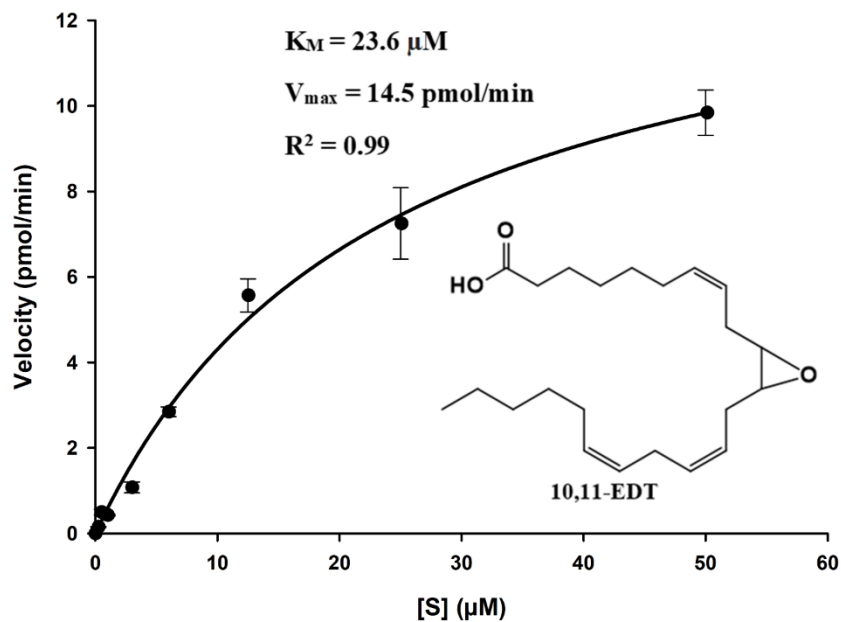


Figure 1. Velocity vs. [S] plot for hydrolysis of 10,11-EDT by recombinant, human sEH ([E] = 3 nM). The kinetic constants (K_M and V_{max}) were determined by nonlinear regression using the enzyme kinetic module of SigmaPlot 14.0 (Systat Software, Inc). An R^2 of 0.99 indicates the reaction fit the Michaelis-Menten model well.

Table 3. Kinetic Parameters for Hydrolysis of EDT Regioisomers by Recombinant Human sEH

	R^2	$K_M (\mu\text{M})$	$k_{\text{cat}} (\text{s}^{-1})$	$k_{\text{cat}}/K_M (\text{s}^{-1}/\mu\text{M}^{-1})$
7,8-EDT	0.95	30.2	0.26	0.009
10,11-EDT	0.99	23.6	0.40	0.017
13,14-EDT	0.97	6.37	0.58	0.091
16,17-EDT	0.98	23.1	0.67	0.029
8,9-EET ^b	0.97	26.0	0.56	0.022
11,12-EET ^b	0.97	2.0	0.26	0.13

14,15-EET ^b	0.95	7.0	3.0	0.43
------------------------	------	-----	-----	------

^bLiterature Values.²⁵

Downregulation of Tunicamycin-Triggered Endoplasmic Reticulum Stress in Human Embryonic Kidney Cells. Disruptions to endoplasmic reticulum (ER) homeostasis result in accumulation of misfolded proteins in the ER lumen, a phenomenon known as ER Stress.²⁷ The downstream unfolded protein response (UPR) is activated, which is adaptive during early-stage ER Stress but shifts towards apoptotic signaling if the system is overwhelmed under late-stage conditions. EETs and soluble epoxide hydrolase inhibitors have demonstrated the ability to stabilize the ER Stress response and, consequently, ameliorate a variety of pathologies.²⁸ Hence, the ability of EDTs to mediate ER Stress was explored in HEK293 cells, utilizing a tunicamycin model to simulate ER Stress conditions.²⁹ Pre-treatment with EDT methyl esters improved cell viability following prolonged exposure to tunicamycin (**Figure 2**), in a dose-dependent manner (**Figure 2B**). EDTs also reduced UPR markers in cells exposed to tunicamycin, during conditions of both early- (5 h, **Figure 3**) and late- (16 h, **Figure 4**) stage ER Stress. Finally, EDTs decreased the activity of a tunicamycin-activated inflammatory caspase (i.e., Caspase-1, **Figure 4C**). The magnitude of effects exerted was comparable to that of EET methyl esters pre-treated cells (**Figures 2A, 3, and 4**). During early-stage ER Stress, restoration of the master ER chaperone binding immunoglobulin protein (BiP) to basal levels (**Figure 3B**), diminished phosphorylated/total ratio of the UPR transducing inositol-requiring enzyme 1 α (IRE1 α) (**Figure 3C**), and abolished activation of the chaperone-transcribing spliced X-box binding protein 1 (XBP-1s) (**Figure 3A**) imply EDTs help ameliorate the misfolded protein burden on the ER and re-establish homeostatic folding capacity. Diminished levels of transcription factor

activating transcription factor 4 (ATF4) (**Figure 4B**) and termination of C/EBP homologous protein (CHOP) upregulation (**Figure 4A**) during late-stage ER Stress indicate EDTs play a role in blocking augmentation of downstream pro-apoptotic pathways. ER Stress has shown to induce caspase-1, an inflammasome-linked caspase implicated in apoptotic and pyroptotic cell death signaling.³⁰ Its activity was elevated by tunicamycin but substantially curbed by EDT pre-treatment (**Figure 4C**), suggesting EDTs might mitigate pro-inflammatory responses initiated by perturbations to the ER.

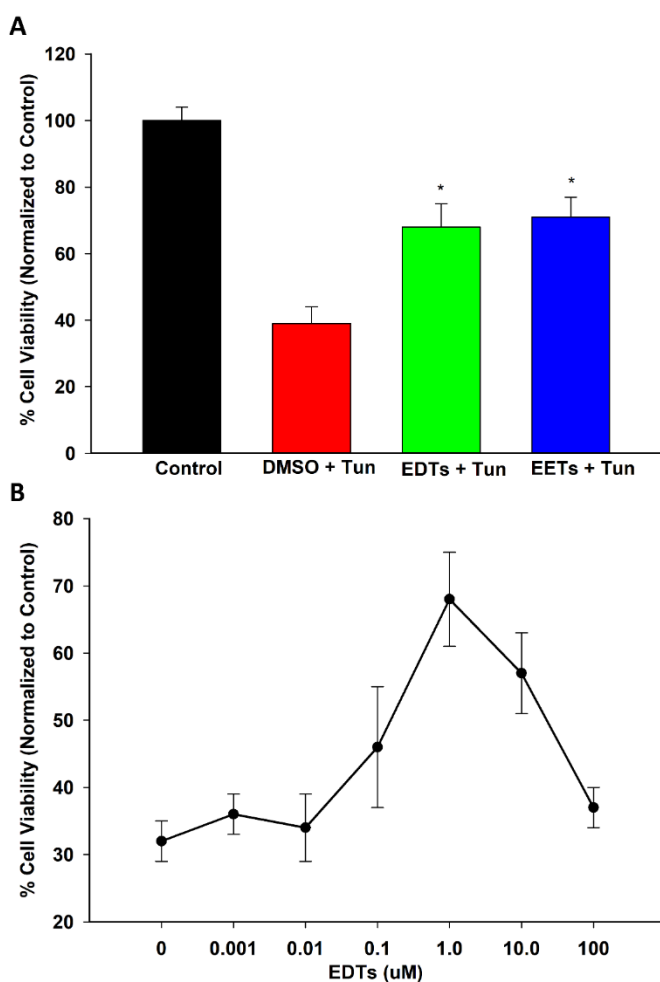


Figure 2. EDTs restore viability of HEK293 cells exposed to Tunicamycin (Tun). (**A**) Pre-treatment with EDTs (methyl esters, regioisomeric mixture, 1 µM) or EETs significantly improved cell viability following prolonged (24 h) exposure to 4 µg/mL Tun (One Way Analysis

of Variance, Holm-Sidak method, * $p < 0.001$ vs. DMSO + Tun group, $\alpha = 0.05$) **(B)** Dose-response of the protective action of EDTs, with maximal therapeutic activity occurring at a 1 μ M dose of EDT methyl esters (regioisomer mixture).

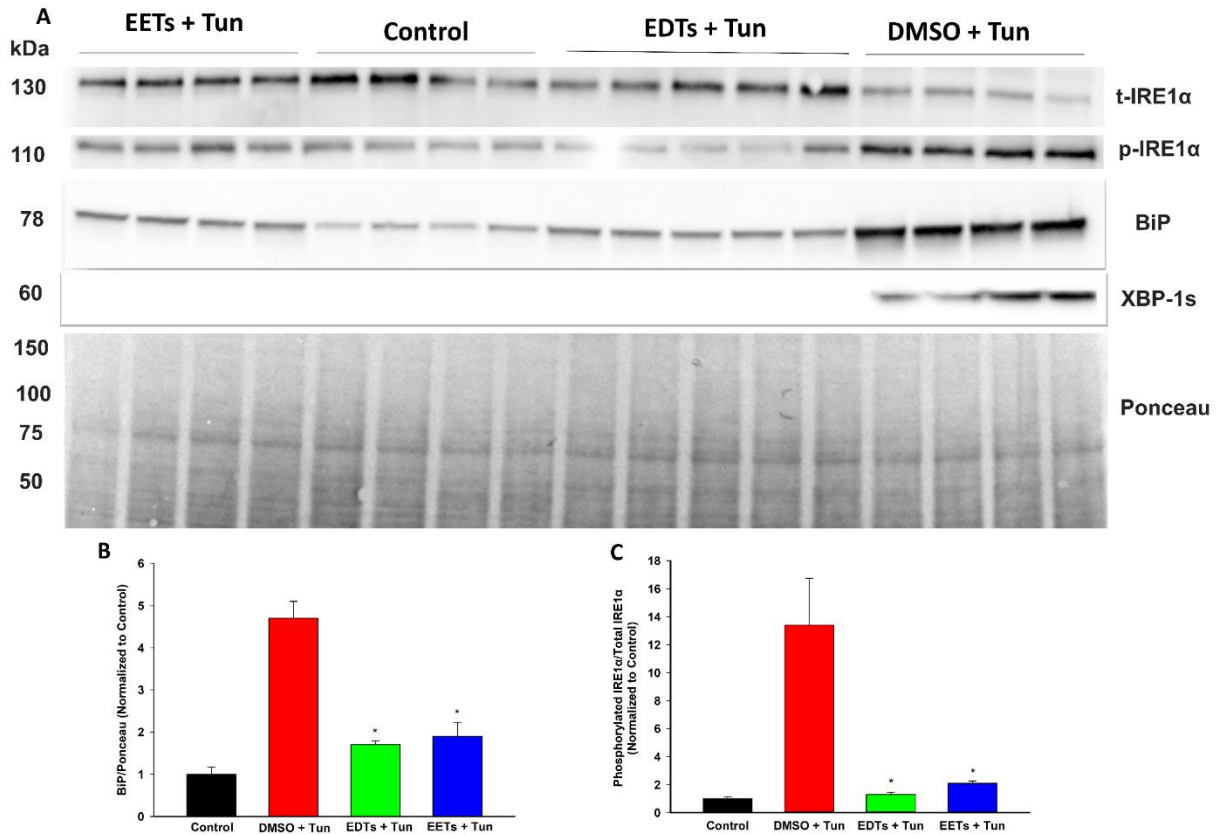


Figure 3. EDTs attenuate early-stage UPR markers in Tunicamycin (Tun)-triggered ER Stress in HEK293 cells. **(A)** Immunoblots of t-IRE1 α , p-IRE1 α , BiP, and XBP-1s for cells pre-treated with EDTs (methyl esters, regioisomeric mixture, 1 μ M), EETs, or DMSO for 1 h and exposed to 4 μ g/mL Tun for 5 h. **(B)** EDTs (and EETs) significantly reduced BiP levels, relative to Ponceau loading control (One Way Analysis of Variance, Holm-Sidak method, * $p < 0.001$ vs. DMSO + Tun group, $\alpha = 0.05$). **(C)** EDTs (and EETs) significantly reduced the ratio of phosphorylated IRE1 α to total IRE1 α (One Way Analysis of Variance, Holm-Sidak method, * $p < 0.001$ vs. DMSO + Tun group, $\alpha = 0.05$).

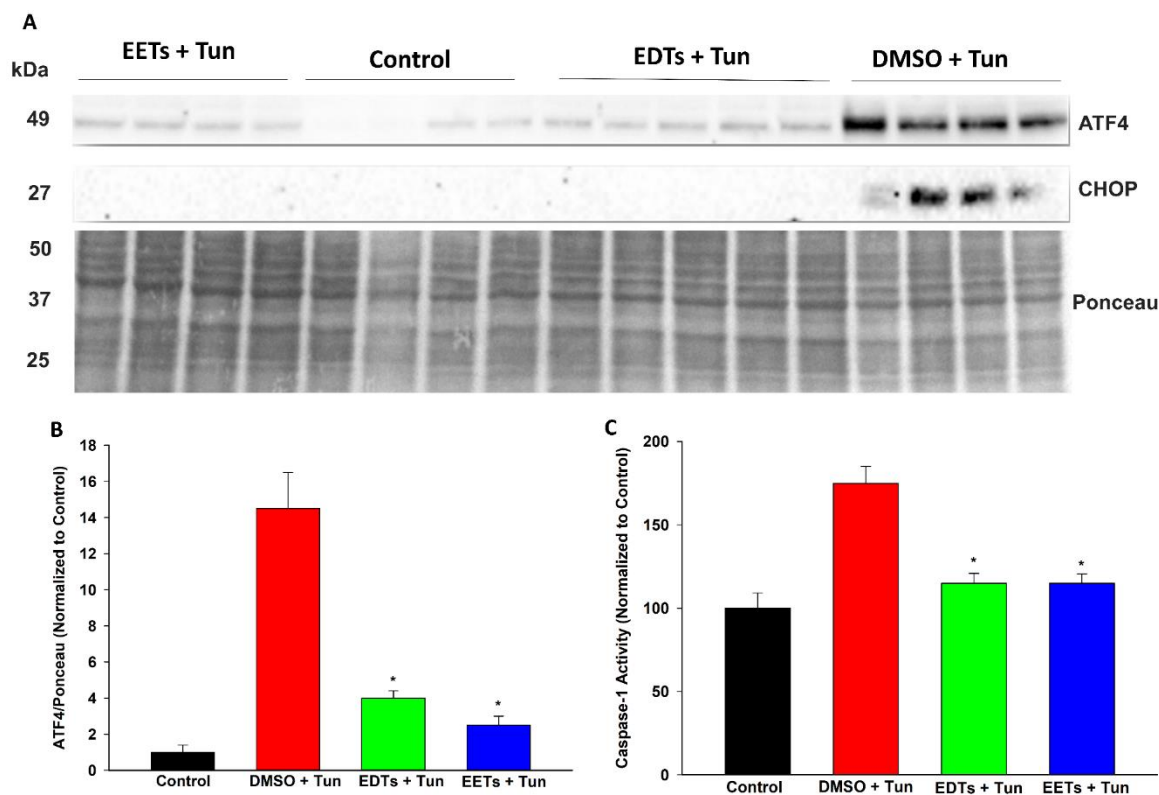
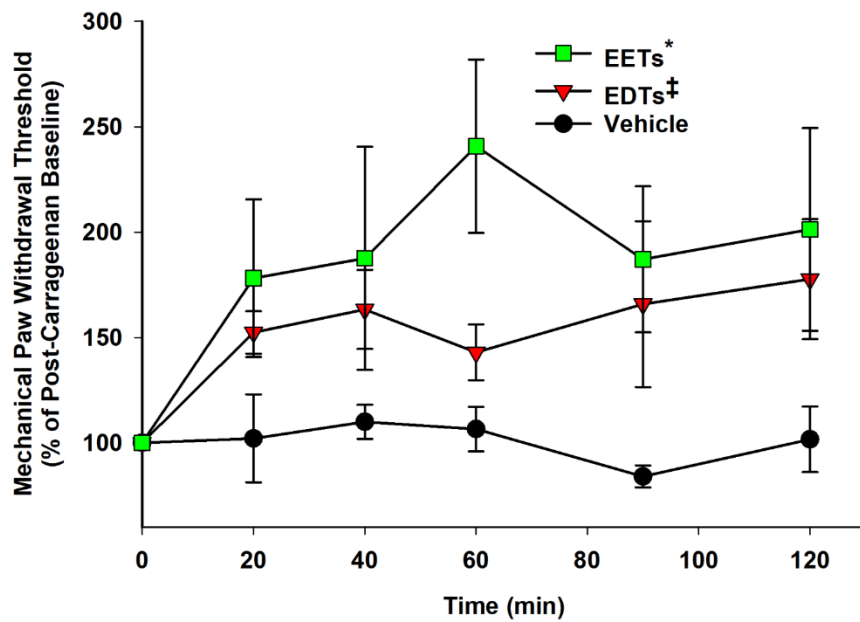


Figure 4. EDTs attenuate late-stage UPR markers and activity of an inflammatory caspase in Tunicamycin (Tun)-triggered ER Stress in HEK293 cells. **(A)** Immunoblots of ATF4 and CHOP for cells pre-treated with EDTs (methyl esters, regioisomeric mixture, 1 μ M), EETs, or DMSO for 1 h and exposed to 4 μ g/mL Tun for 16 h. **(B)** EDTs (and EETs) significantly reduced ATF4 levels, relative to Ponceau loading control (One Way Analysis of Variance, Holm-Sidak method, * $p < 0.001$ vs. DMSO + Tun group, $\alpha = 0.05$). **(C)** EDTs (and EETs) significantly decreased Caspase-1 activity (One Way Analysis of Variance, Holm-Sidak method, * $p < 0.001$ vs. DMSO + Tun group, $\alpha = 0.05$).

Analgesia Against Carrageenan-Induced Inflammatory Pain. Regioisomeric mixtures of EETs, EDPs, and EEQs and soluble epoxide hydrolase inhibitors have shown to effectively alleviate inflammation-mediated pain.^{25,31} Hence, the potential anti-nociceptive activity of EDTs was also investigated, utilizing a previously described carrageenan-induced inflammatory pain

model in rats.²⁵ Administration of carrageenan considerably reduced paw withdrawal thresholds (compared to naïve baseline), indicating development of a severely painful state. Treatment with EDT methyl esters significantly increased paw withdrawal thresholds (**Figure 5A and 5B**), over a 2 h time course, indicating pain relief. The intensity of effect was also comparable to that of EET methyl esters-treated rats (**Figure 5**).

A



B

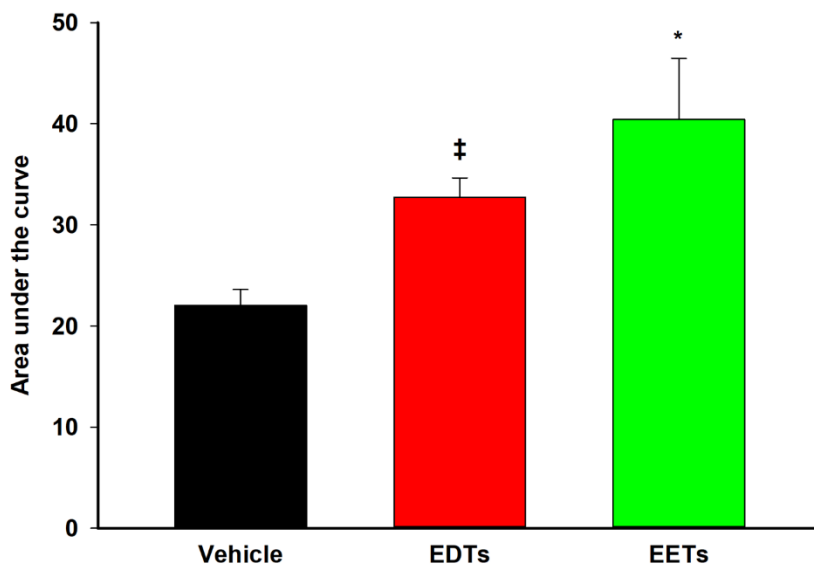


Figure 5. EDTs attenuate Carrageenan-induced inflammatory pain in rats. **(A)** Following carrageenan (CARR, 0.5 mg/paw) administration, the painful post-CARR baseline was normalized to 100% and subsequent scores were calculated as the score \times 100/CARR baseline. Thus, the increase in MWT scores (i.e., above the painful CARR baseline) observed with EDTs (methyl esters, regioisomeric mixture, 300 ng/paw) treatment is indicative of antinociceptive effects. Scores are reported as the means \pm SEM of a group of rats per time point. Analgesic efficacy of EDTs (and EETs) was significant compared to the vehicle control (10% EtOH in saline) over a 2 h time course (Two Way Analysis of Variance, Holm-Sidak method [Factor: Treatment], * p < 0.001 vs. Vehicle, ‡ p = 0.021 vs. Vehicle, α = 0.05). **(B)** Area under the curve (integrated from 0-120 min) represents the cumulative efficacy of a treatment and was significantly different for EDTs (and EETs) compared to the vehicle control (One Way Analysis of Variance, Holm-Sidak method, * p = 0.043 vs. Vehicle, ‡ p = 0.004 vs. Vehicle, α = 0.05).

CONCLUSION

The inhibition of soluble epoxide hydrolase is a novel and promising therapeutic approach that could potentially tackle several unmet clinical needs, ranging from acute and chronic pain to various fibrotic, metabolic, renal, and neurodegenerative disorders.^{28,31-33} The underlying bioactivity of EpFAs dictates the efficacy of sEH inhibitors (sEHI) and has primarily been attributed to the ARA-derived EETs, though more recently there is growing interest in the biological roles of epoxy metabolites of ω -3 PUFAs, namely EDPs and EEQs. Based on the results of this study, AdA-derived EDTs (**Figure 6**) appear to be another relevant class of EpFAs. With synthesis of regioisomer standards and through validated HPLC-MS/MS analysis of AdA-rich tissues, this study establishes that EDTs are indeed naturally occurring lipids *in*

in vivo. Furthermore, the demonstrated capability of EDTs to attenuate ER Stress, the signaling response that underlies several aforementioned pathologies, as well as reduce inflammatory pain strengthens the case that EDTs are pertinent lipid mediators. Finally, the finding that EDTs are metabolized by sEH (**Figure 6**) implies that inhibition of sEH would stabilize their levels *in vivo*. This suggests EDTs may in part contribute to the efficacy of sEHI and hence future studies should consider the bioactivity of EDTs when the therapeutic effects of sEHI are examined in disease models.

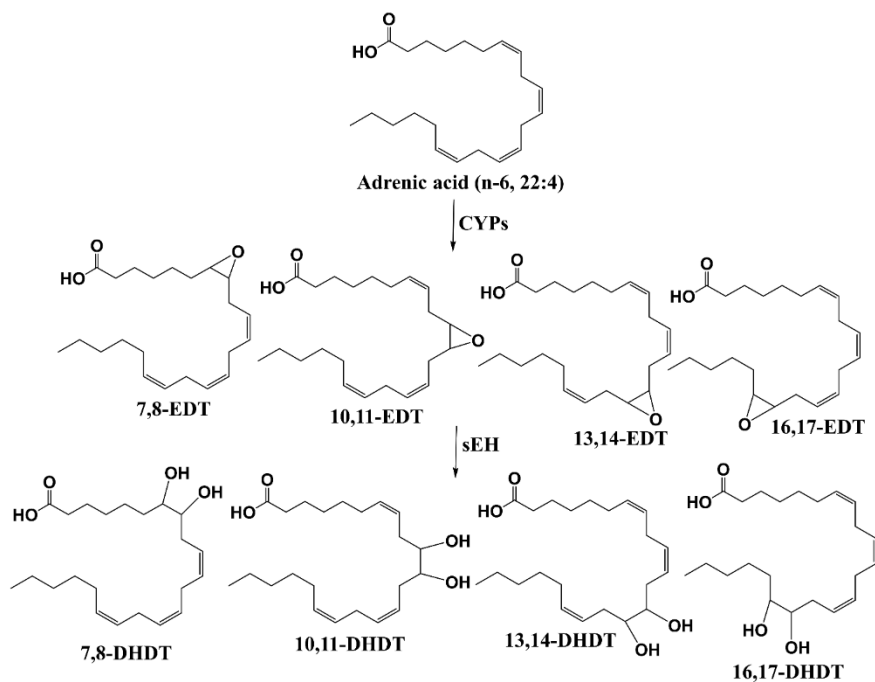


Figure 6. Cytochrome P450 (CYP) Pathway of Adrenic acid Metabolism. Epoxydocosatrienoic acids (EDTs) are formed by CYP-mediated epoxidation of adrenic acid and are degraded downstream to Dihydroxydocosatrienoic acids (DHDTs) by the soluble epoxide hydrolase (sEH).

METHODS

Reagents and General Experimental Procedures. Adrenic methyl ester was purchased from Nu-Chek Prep, Inc. (Elysian, MN). All chemicals purchased from commercial sources were used as received without further purification. Acetonitrile, methanol, ethyl acetate, and glacial acetic acid of HPLC grade or better were purchased from Fisher Scientific (Pittsburgh, PA). The internal standard, 12-(3-cyclohexyl-ureido)-dodecanoic acid (CUDA), was synthesized in-house and dissolved in methanol. Deionized water (18.1 M Ω /cm) was prepared in-house and used for mobile phase preparation and solid phase extraction (SPE). Tunicamycin (10 mg/mL in DMSO) was purchased from Alfa Aesar (Haverhill, MA). Ac-VAD-AFC, a fluorogenic Caspase-1 substrate, was purchased from Santa Cruz Biotechnology, Inc. (Dallas, TX). Primary antibodies against BiP (C50B12), IRE1 α (14C10), p-IRE1 α (Ser724), XBP-1s (D2C1F), ATF4 (D4B8), and CHOP (L63F7) were purchased from Cell Signaling Technology (Danvers, MA) or Thermo Fisher Scientific (Waltham, MA). Analytical TLC was performed on Merck TLC silica gel 60 F254 plates and spots were visualized via potassium permanganate staining. Flash chromatography was performed on silica gel (230–400 mesh) from Macherey Nagel. ¹H and ¹³C NMR spectra were recorded on 400 MHz Bruker Avance III HD Nanobay or 800 MHz Avance III NMR spectrometers and referenced to the residual solvent peak at δ 7.28 or δ 1.94 (CDCl₃ or CD₃CN) and δ 77.14 (CDCl₃), respectively. Multiplicity is described by the abbreviations, s = singlet, t = triplet, m = multiplet. HRESIMS was recorded on a Thermo Q-Exactive High-field Orbitrap mass spectrometer, equipped with an electrospray ionization source operating in the positive- or negative-ion mode.

Synthesis, Characterization, and Application of EDT Methyl Esters (Regioisomeric Mixture). Adrenic methyl ester (1.00 g, 2.89 mmol, 1.0 eq.) was quickly added to a vigorously stirring solution of 70% *meta*-chloroperoxybenzoic acid (143 mg, 0.578 mmol, 0.20 eq.) in

dichloromethane and stirred for 90 min at room temperature. The reaction was quenched with saturated sodium carbonate (aq.) and the mixture was extracted with diethyl ether (4X), dried (MgSO₄), and concentrated under reduced pressure. EDT methyl esters were purified by flash chromatography (ethyl acetate-hexanes 10:90). Colorless oil; ¹H NMR (400 MHz, CDCl₃) δ 5.52-5.26 (6H, m, vinylic), 3.62 (3H, s, methyl ester), 2.96-2.84 (2H, m), 2.83-2.75 (2H, m), 2.44-2.15 (5H, m), 2.06-1.98 (3H, m), 1.65-1.56 (2H, m), 1.54-1.47 (2H, m), 1.40-1.21 (10H, m), 0.86 (3H, t, *J* = 6.4 Hz, terminal aliphatic); ¹³C NMR (100 MHz, CDCl₃) δ 173.98, 132.75, 132.34, 130.84, 130.71, 130.60, 130.46, 130.43, 130.36, 130.20, 130.03, 128.72, 128.59, 127.71, 127.56, 127.45, 127.39, 127.13, 124.47, 124.35, 124.17, 124.04, 124.01, 123.67, 57.05, 56.87, 56.39, 56.35, 56.26, 56.23, 51.33, 33.95, 33.85, 31.69, 31.47, 29.66, 29.27, 29.20, 29.13, 28.97, 28.73, 27.72, 27.59, 27.37, 27.19, 26.99, 26.32, 26.26, 26.19, 26.16, 25.77, 25.61, 24.79, 22.56, 22.53, 14.00; HRESIMS *m/z* 385.2749 [M + Na]⁺ (calcd for C₂₃H₃₈NaO₃⁺, 385.2713). The ratio of 16,17-, 13,14-, 10,11-, and 7,8-EDT methyl ester regioisomers in the mixture was determined to be 2.0:1.7:1.7:1.0, respectively. The methyl ester form is frequently employed as a pro-drug for EpFA application in both *in vitro* and *in vivo* disease models,^{25,34-37} and hence was utilized for pharmacological applications. The major advantages of the methyl esters are greater long-term stability and improved cell membrane permeability. They are rapidly cleaved to the biologically active carboxylic acid form by cellular esterases.^{38,39} A time course for formation of EDT free acids in HEK293 cells has been described in the Supporting Information (Figure S2).

Isolation of EDT methyl ester regioisomers. The four EDT regioisomers were separated and isolated using a preparative chromatography system: Phenomenex Luna Silica 100 Å, LC 250 × 21.2 mm, 5 μm column in conjunction with a Waters 2489 UV/Vis detector (monitoring at 200

nm) and a Waters Fraction Collector III. Preparative chromatography gradient conditions are given in the Supporting Information (Table S2).

Synthesis of DHDT methyl esters. Shown with the representative 16,17-DHDT methyl ester. 5.8 mg (0.016 mmol) of 16,17-EDT methyl ester was dissolved in a solution of 0.5 ml acetonitrile, 0.25 ml H₂O, and 0.25 ml 8% perchloric acid and stirred overnight at room temperature. The mixture was directly purified by flash chromatography (ethyl acetate-hexanes 30:70).

Synthesis of EDT and DHDT free acids. Shown with the representative 16,17-EDT free acid. To 30 μ L of 30 mM 16,17-EDT methyl ester (in THF, 0.9 μ mol, 1.00 eq.), 9 μ L of 10 M NaOH (aq., 90 μ mol, 100 eq.) was added. The reaction was stirred for 30 h at room temperature and quenched with 15 μ L of acetic acid. The mixture was directly purified by flash chromatography (ethyl acetate-hexanes-acetic acid 40:60:0.3). The ¹H NMR spectra and HRESIMS for the eight free acid analytes are described in the Supporting Information.

HPLC-MS/MS Method Optimization. The liquid chromatography system used for analysis was an Agilent 1200 SL liquid chromatography series (Agilent Technologies, Inc., Santa Clara, CA). The samples were placed in an autosampler and a volume of 5 μ L was injected on a Kinetex C18 100 Å, LC 100 X 2.1 mm, 1.7 μ m column, which was kept at 50 °C. Mobile Phase A was water with 0.1% glacial acetic acid while Mobile Phase B was acetonitrile with 0.1% glacial acetic acid. A gradient elution (Table S3, Supporting Information) with a flow rate of 250 μ L/min was employed and the chromatographic run was optimized to be 11 min for separation of analytes. The column was coupled to a 4000 Q-Trap tandem mass spectrometer (Applied Biosystems, Waltham, MA) equipped with an electrospray source (Turbo V), operating under a negative Multiple Reaction Monitoring (MRM) mode. Mass spectrometer conditions are

described in the Supporting Information (Table S4). Individual analyte standards were infused into the mass spectrometer to optimize source parameters (Table S5, Supporting Information) and identify unique MRM transitions. Source parameters and optimized MRM transitions of the internal standard CUDA, EETs, and DHETs are described in the Supporting Information (Table S6)

Calibration Curves and Linearity. All eight free acid analytes were dissolved in acetonitrile and stock solutions were stored at -80 °C prior to use. Standard mixtures of eight different concentrations were prepared in 200 nM CUDA solution to determine calibration curves, linear ranges, and R^2 values via least-squares linear regression.

Solid Phase Extraction. To obtain analytes from biological matrices for method validation and biological applications, solid phase extraction was conducted, as previously described.⁴⁰ Oasis HLB 3cc Vac SPE Cartridges (60 mg Sorbent/Cartridge and 30 μ m particle size), purchased from Waters Corp. (Milford, MA), were pre-conditioned, loaded with sample, washed, and dried. Analytes were then eluted, concentrated, and reconstituted in 200 nM CUDA.

Method Validation. The sensitivity, accuracy, precision, and recovery of the method were determined by analyzing quality control (QC) samples: human pooled plasma samples spiked with corresponding analytes. The limit of detection (LOD) and quantitation (LOQ) were estimated to be the minimum analyte concentration giving a signal to noise (S/N) ratio of >3 and >10, in a QC sample, respectively. Four replicates for each of four QC groups (unspiked, spiked at 1 nM, 10 nM, and 100 nM pre-extraction) were quantified within 24 h to estimate the intra-day accuracy and precision. Inter-day accuracy and precision were assessed by analyzing samples over 3 different days. Similarly, analytical recovery was estimated by comparing

recovered concentrations from QC samples spiked pre-extraction to QC samples spiked post-extraction.

Biological Verification. All animal experiments were performed according to protocols approved by the Institutional Animal Care and Use Committee (IACUC) of University of California, Davis. For quantitation of basal EDT and DHDT levels, liver, kidney, brain, and plasma samples were collected from male Sprague-Dawley (SD) rats ($n = 6$), purchased from Charles River Laboratories. The animals were placed under deep isoflurane anesthesia and blood was collected via cardiac puncture. The plasma fraction was separated through cold centrifugation at 4000 rpm for 10 min. Animals were euthanized with isoflurane and perfused with saline prior to tissue sampling. Tissue and plasma samples were flash frozen and stored at $-80\text{ }^{\circ}\text{C}$ until metabolite extraction.

sEH Kinetics. To assess sEH mediated hydrolysis of EDTs, a previously described enzyme kinetics assay was modified and applied.²⁵ A range of concentrations (0.04 - 5 mM) for each EDT methyl ester regioisomer were prepared in DMSO. One μL of substrate solution was added to 90 μL of human carboxylesterase 2 ($[\text{E}]_{\text{final}} = 27\text{ }\mu\text{g}/\text{mL}$) in sodium phosphate buffer (0.1 M, pH 7.4 w/ freshly added 0.1 mg/mL BSA) and incubated overnight at $37\text{ }^{\circ}\text{C}$ to facilitate complete conversion to the free acids. 10 μL of purified, recombinant human sEH, in sodium phosphate buffer, was added ($[\text{E}]_{\text{final}} = 0.2\text{ }\mu\text{g}/\text{mL}$), followed by incubation for 5 - 15 min at $37\text{ }^{\circ}\text{C}$. The reaction was quenched with 100 μL of 400 nM CUDA and amount of the corresponding DHDT formed was quantified via HPLC-MS/MS analysis. The rate of formation was plotted as a function of initial substrate concentration and kinetic constants (K_M and V_{max}) were calculated via nonlinear regression using the enzyme kinetic module of SigmaPlot 14.0 (Systat Software, Inc., Chicago, IL). All measurements were performed in triplicates and the mean is reported.

Cell Culture. Human embryonic kidney (HEK293) cells were purchased from American Type Culture Collection and cultured in Dulbecco's modified Eagle's medium supplemented with 10% fetal bovine serum and 1% penicillin-streptomycin. Cultures were maintained in a humidified incubator at 37 °C under an atmosphere of 5% CO₂/95% air.

MTT Assay. HEK293 cells were seeded in poly-L-lysine coated, clear-bottom black 96-well microplates at a density of approximately 1×10^4 cells/well and incubated overnight. Following pre-treatment with EDT or EET methyl ester regioisomer mixtures (0.001 – 100 μ M) for 1 h, cells were exposed to tunicamycin (4 μ g/mL) for 24 h. The media was replaced with fresh media containing 0.5 mg/ml of the MTT reagent and cells were incubated for 3 h at 37 °C. After the media was removed, the crystals were dissolved in 100% DMSO, and absorbance was read at 562 nm using a Tecan Infinite Pro microplate reader.

Caspase-1 Activity Assay. HEK293 cells were seeded in 6-well plates at a density of approximately 3×10^5 cells/well and incubated overnight. Following pre-treatment with EDT or EET methyl ester regioisomer mixtures (1 μ M) for 1 h, cells were exposed to tunicamycin (4 μ g/mL) for 16 h. An assay measuring caspase-1 activity was conducted as previously described.⁴¹ Briefly, cells were rinsed with phosphate-buffered saline (PBS) and lysed with ice-cold RIPA buffer. Following centrifugation, the supernatants were collected and stored on ice. 60 μ L of supernatants were incubated with 60 μ L of caspase activity buffer (containing 50 μ M Ac-VAD-AFC, a fluorogenic caspase-1 substrate) for 2 h at 37 °C, after which fluorescence was read at $\lambda_{Ex}/\lambda_{Em} = 400 \text{ nm}/505 \text{ nm}$ using a Molecular Devices microplate reader.

Western Blotting. Confluent HEK293 cells in T75 flasks were pre-treated with EDT or EET methyl ester regioisomer mixtures (1 μ M) for 1 h, followed by tunicamycin (4 μ g/mL) exposure for 5 or 16 h. Cells were rinsed with PBS, lysed with ice-cold RIPA buffer (containing freshly

added protease and phosphatase inhibitors), homogenized, and centrifuged to collect supernatants. Protein concentrations in the lysates were estimated using a BCA Assay (Pierce). Proteins were denatured, separated by SDS-PAGE, and transferred to nitrocellulose membranes. Membranes were stained with Ponceau stain and imaged using a CCD-based digital imager for the protein loading control. Membranes were then blocked with 5% BSA or non-fat milk in tris-buffered saline with 0.05% Tween-20 for 1 h at room temperature, followed by incubation with the primary antibody (1:1000) overnight at 4 °C. Unbound antibody was washed off and membranes were incubated with an HRP-conjugated secondary antibody (1:10000) for 1 h at room temperature. Following washes, blots were exposed to an ECL substrate (BioRad) under dark conditions for 2 min and bands were imaged.

Inflammatory Pain Model. A von Frey assay measuring mechanical withdrawal thresholds (MWT) was performed in male SD rats ($n = 4-6/\text{group}$), as previously described.⁴² The study was conducted in a randomized and blinded manner. Prior to compound administration, rats were placed in clear, acrylic chambers and a baseline was assessed using an electronic von Frey aesthesiometer apparatus (IITC, Woodland Hills, CA). Carrageenan (CARR, 50 μL of a 1% solution, 0.5 mg) was then injected into the plantar area of the right hind paw. After three-and-a-half hours, post-CARR MWT were measured and normalized to 100%. Immediately after ($t = 0$), 10 μL of the vehicle control (10% EtOH in saline), EDT, or EET methyl ester regioisomer mixture (300 ng/paw) was administered via intraplantar injection in the same paw. Ipsilateral MWT were assessed three to five times per rat per time point, over a 2 h time course (at 20-, 40-, 60-, 90-, and 120-min intervals), and scores were normalized relative to the post-CARR baseline.

ASSOCIATED CONTENT

Supporting Information. Intra and inter-day accuracy and precision and recovery of the developed analytical HPLC-MS/MS method, Preparative HPLC Gradient, Analytical HPLC Gradient, 4000 Q-Trap Mass Spectrometer Conditions, MRM Transitions for Internal Standard, EETs, and DHETs, Source Parameters for all analytes, ¹H NMR and HRESIMS for EDT and DHDT regioisomers, *In Vitro* time course of EDT free acid formation

AUTHOR INFORMATION

Corresponding Author

*Email: bdhammock@ucdavis.edu. Tel: 530-752-7519. Fax: 530-752-1537

Authors

Nalin Singh – Email: nalsingh@ucdavis.edu

Bogdan Barnych – Email: bbarnych@ucdavis.edu

Karen M. Wagner – Email: kmwagner@ucdavis.edu

Debin Wan – Email: dbwan@ucdavis.edu

Christophe Morisseau – Email: chmorisseau@ucdavis.edu

ACKNOWLEDGEMENTS

This work was partially funded by National Institutes of Health grants, National Institute of Environmental Health Sciences (NIEHS) RIVER Award (R35 ES030443-01), NIEHS/Superfund Research Program (P42 ES004699), and National Institute of Diabetes and Digestive and Kidney Diseases (R01DK103616 and R01DK107767). N.S. thanks the NIEHS/UC Davis Superfund Research Program for financial support in the form of GSR fellowships.

REFERENCES

- (1) Fisslthaler, B.; Popp, R.; Kiss, L.; Potente, M.; Harder, D. R.; Fleming, I.; Busse, R.
Cytochrome P450 2C is an EDHF synthase in coronary arteries. *Nature* **1999**, *401*, 493-497.
- (2) Imig, J. D.; Zhao, X.; Capdevila, J. H.; Morisseau, C.; Hammock, B. D. Soluble epoxide hydrolase inhibition lowers arterial blood pressure in angiotensin II hypertension. *Hypertension* **2002**, *39*, 690-694.
- (3) Inceoglu, B.; Jinks, S. L.; Ulu, A.; Hegedus, C. M.; Georgi, K.; Schmelzer, K. R.; Wagner, K.; Jones, P. D.; Morisseau, C.; Hammock, B. D. Soluble epoxide hydrolase and epoxyeicosatrienoic acids modulate two distinct analgesic pathways. *Proc. Natl. Acad. Sci. U. S. A.* **2008**, *105*, 18901-18906.
- (4) Liu, L.; Chen, C.; Gong, W.; Li, Y.; Edin, M. L.; Zeldin, D. C.; Wang, D. W.
Epoxyeicosatrienoic acids attenuate reactive oxygen species level, mitochondrial dysfunction, caspase activation, and apoptosis in carcinoma cells treated with arsenic trioxide. *J. Pharmacol. Exp. Ther.* **2011**, *339*, 451-463.
- (5) Xu, X.; Tu, L.; Feng, W.; Ma, B.; Li, R.; Zheng, C.; Li, G.; Wang, D. W. CYP2J3 gene delivery up-regulated adiponectin expression via reduced endoplasmic reticulum stress in adipocytes. *Endocrinology* **2013**, *154*, 1743-1753.
- (6) Rosenthal, M. D.; Hill, J. R. Elongation of arachidonic and eicosapentaenoic acids limits their availability for thrombin-stimulated release from the glycerolipids of vascular endothelial cells. *Biochim. Biophys. Acta, Lipids Lipid Metab.* **1986**, *875*, 382-391.

- (7) Mann, C. J.; Kaduce, T. L.; Figard, P. H.; Spector, A. A. Docosatetraenoic acid in endothelial cells: formation, retroconversion to arachidonic acid, and effect on prostacyclin production. *Arch. Biochem. Biophys.* **1986**, *244*, 813-823.
- (8) Rosenthal, M. D.; Hill, J. R. Human vascular endothelial cells synthesize and release 24- and 26-carbon polyunsaturated fatty acids. *Biochim. Biophys. Acta, Lipids Lipid Metab.* **1984**, *795*, 171-178.
- (9) Mimouni, V.; Narce, M.; Huang, Y. S.; Horrobin, D. F.; Poisson, J. P. Adrenic acid $\Delta 4$ desaturation and fatty acid composition in liver microsomes of spontaneously diabetic Wistar BB rats. *Prostaglandins, Leukotrienes Essent. Fatty Acids* **1994**, *50*, 43-47.
- (10) Wijendran, V.; Lawrence, P.; Diau, G. Y.; Boehm, G.; Nathanielsz, P. W.; Brenna, J. T. Significant utilization of dietary arachidonic acid is for brain adrenic acid in baboon neonates. *J. Lipid Res.* **2002**, *43*, 762-767.
- (11) Sprecher, H.; VanRollins, M.; Sun, F.; Wyche, A.; Needleman, P. Dihomo-prostaglandins and -thromboxane. A prostaglandin family from adrenic acid that may be preferentially synthesized in the kidney. *J. Biol. Chem.* **1982**, *257*, 3912-3918.
- (12) Yi, X. Y.; Gauthier, K. M.; Cui, L.; Nithipatikom, K.; Falck, J. R.; Campbell, W. B. Metabolism of adrenic acid to vasodilatory 1 α ,1 β -dihomo-epoxyeicosatrienoic acids by bovine coronary arteries. *Am. J. Physiol.: Heart Circ. Physiol.* **2007**, *292*, H2265-2274.
- (13) Kopf, P. G.; Zhang, D. X.; Gauthier, K. M.; Nithipatikom, K.; Yi, X. Y.; Falck, J. R.; Campbell, W. B. Adrenic acid metabolites as endogenous endothelium-derived and zona glomerulosa-derived hyperpolarizing factors. *Hypertension* **2010**, *55*, 547-554.

- (14) Zhang, Y.; Oltman, C. L.; Lu, T.; Lee, H. C.; Dellsperger, K. C.; VanRollins, M. EET homologs potently dilate coronary microvessels and activate BK(Ca) channels. *Am. J. Physiol.: Heart Circ. Physiol.* **2001**, *280*, H2430-2440.
- (15) Gebremedhin, D.; Ma, Y. H.; Falck, J. R.; Roman, R. J.; VanRollins, M.; Harder, D. R. Mechanism of action of cerebral epoxyeicosatrienoic acids on cerebral arterial smooth muscle. *Am. J. Physiol.: Heart Circ. Physiol.* **1992**, *263*, H519-525.
- (16) Campbell, W. B.; Gebremedhin, D.; Pratt, P. F.; Harder, D. R. Identification of epoxyeicosatrienoic acids as endothelium-derived hyperpolarizing factors. *Circ. Res.* **1996**, *78*, 415-423.
- (17) Archer, S. L.; Gragasin, F. S.; Wu, X.; Wang, S.; McMurtry, S.; Kim, D. H.; Platonov, M.; Koshal, A.; Hashimoto, K.; Campbell, W. B.; Falck, J. R.; Michelakis, E. D. Endothelium-derived hyperpolarizing factor in human internal mammary artery is 11,12-epoxyeicosatrienoic acid and causes relaxation by activating smooth muscle BK(Ca) channels. *Circulation* **2003**, *107*, 769-776.
- (18) Sadler, N. C.; Nandhikonda, P.; Webb-Robertson, B. J.; Ansong, C.; Anderson, L. N.; Smith, J. N.; Corley, R. A.; Wright, A. T. Hepatic Cytochrome P450 Activity, Abundance, and Expression Throughout Human Development. *Drug Metab. Dispos.* **2016**, *44*, 984-991.
- (19) Gill, S. S.; Hammock, B. D. Distribution and properties of a mammalian soluble epoxide hydrolase. *Biochem. Pharmacol.* **1980**, *29*, 389-395.
- (20) Hakansson, I.; Gouveia-Figueira, S.; Ernerudh, J.; Vrethem, M.; Ghafouri, N.; Ghafouri, B.; Nording, M. Oxylipins in cerebrospinal fluid in clinically isolated syndrome and relapsing remitting multiple sclerosis. *Prostaglandins Other Lipid Mediators* **2018**, *138*, 41-47.

- (21) Lucas, D.; Goulitquer, S.; Marienhagen, J.; Fer, M.; Dreano, Y.; Schwaneberg, U.; Amet, Y.; Corcos, L. Stereoselective epoxidation of the last double bond of polyunsaturated fatty acids by human cytochromes P450. *J. Lipid Res.* **2010**, *51*, 1125-1133.
- (22) McDougale, D. R.; Watson, J. E.; Abdeen, A. A.; Adili, R.; Caputo, M. P.; Krapf, J. E.; Johnson, R. W.; Kilian, K. A.; Holinstat, M.; Das, A. Anti-inflammatory ω -3 endocannabinoid epoxides. *Proc. Natl. Acad. Sci. U. S. A.* **2017**, *114*, E6034-E6043.
- (23) Singh, N.; Hammock, B. D. Soluble Epoxide Hydrolase. In *Encyclopedia of Molecular Pharmacology*, 3rd ed.; Offermanns, S.; Rosenthal, W., Eds.; Springer International Publishing: Cham, 2020; pp 1-7.
- (24) Morisseau, C.; Weckslar, A. T.; Deng, C.; Dong, H.; Yang, J.; Lee, K. S.; Kodani, S. D.; Hammock, B. D. Effect of soluble epoxide hydrolase polymorphism on substrate and inhibitor selectivity and dimer formation. *J. Lipid Res.* **2014**, *55*, 1131-1138.
- (25) Morisseau, C.; Inceoglu, B.; Schmelzer, K.; Tsai, H. J.; Jinks, S. L.; Hegedus, C. M.; Hammock, B. D. Naturally occurring monoepoxides of eicosapentaenoic acid and docosahexaenoic acid are bioactive antihyperalgesic lipids. *J. Lipid Res.* **2010**, *51*, 3481-3490.
- (26) Argiriadi, M. A.; Morisseau, C.; Goodrow, M. H.; Dowdy, D. L.; Hammock, B. D.; Christianson, D. W. Binding of alkylurea inhibitors to epoxide hydrolase implicates active site tyrosines in substrate activation. *J. Biol. Chem.* **2000**, *275*, 15265-15270.
- (27) Sano, R.; Reed, J. C. ER stress-induced cell death mechanisms. *Biochim. Biophys. Acta, Mol. Cell Res.* **2013**, *1833*, 3460-3470.
- (28) Inceoglu, B.; Bettaieb, A.; Haj, F. G.; Gomes, A. V.; Hammock, B. D. Modulation of mitochondrial dysfunction and endoplasmic reticulum stress are key mechanisms for the

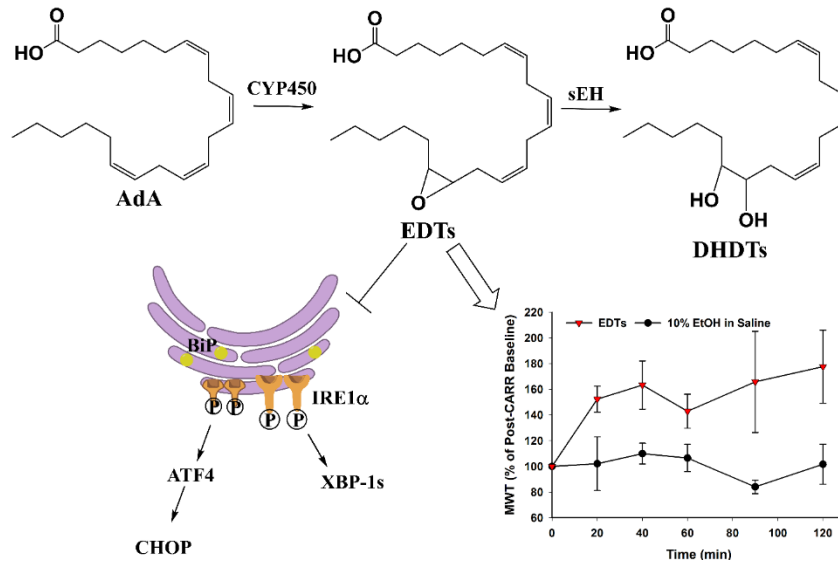
wide-ranging actions of epoxy fatty acids and soluble epoxide hydrolase inhibitors.

Prostaglandins Other Lipid Mediators **2017**, *133*, 68-78.

- (29) Abdullahi, A.; Stanojic, M.; Parousis, A.; Patsouris, D.; Jeschke, M. G. Modeling Acute ER Stress in Vivo and in Vitro. *Shock* **2017**, *47*, 506-513.
- (30) Lebeaupin, C.; Proics, E.; de Bievilleville, C. H.; Rousseau, D.; Bonnafous, S.; Patouraux, S.; Adam, G.; Lavallard, V. J.; Rovere, C.; Le Thuc, O.; Saint-Paul, M. C.; Anty, R.; Schneck, A. S.; Iannelli, A.; Gugenheim, J.; Tran, A.; Gual, P.; Bailly-Maitre, B. ER stress induces NLRP3 inflammasome activation and hepatocyte death. *Cell Death Dis.* **2015**, *6*, e1879.
- (31) Inceoglu, B.; Schmelzer, K. R.; Morisseau, C.; Jinks, S. L.; Hammock, B. D. Soluble epoxide hydrolase inhibition reveals novel biological functions of epoxyeicosatrienoic acids (EETs). *Prostaglandins Other Lipid Mediators* **2007**, *82*, 42-49.
- (32) Liu, J. Y. Inhibition of Soluble Epoxide Hydrolase for Renal Health. *Front. Pharmacol.* **2018**, *9*, 1551.
- (33) Hashimoto, K. Role of Soluble Epoxide Hydrolase in Metabolism of PUFAs in Psychiatric and Neurological Disorders. *Front. Pharmacol.* **2019**, *10*.
- (34) Abdu, E.; Bruun, D. A.; Yang, D.; Yang, J.; Inceoglu, B.; Hammock, B. D.; Alkayed, N. J.; Lein, P. J. Epoxyeicosatrienoic acids enhance axonal growth in primary sensory and cortical neuronal cell cultures. *J. Neurochem.* **2011**, *117*, 632-642.
- (35) Inceoglu, B.; Zolkowska, D.; Yoo, H. J.; Wagner, K. M.; Yang, J.; Hackett, E.; Hwang, S. H.; Lee, K. S. S.; Rogawski, M. A.; Morisseau, C.; Hammock, B. D. Epoxy Fatty Acids and Inhibition of the Soluble Epoxide Hydrolase Selectively Modulate GABA Mediated Neurotransmission to Delay Onset of Seizures. *PLoS One* **2013**, *8*, e80922.

- (36) Supp, D. M.; Hahn, J. M.; McFarland, K. L.; Combs, K. A.; Lee, K. S. S.; Inceoglu, B.; Wan, D.; Boyce, S. T.; Hammock, B. D. Soluble Epoxide Hydrolase Inhibition and Epoxyeicosatrienoic Acid Treatment Improve Vascularization of Engineered Skin Substitutes. *Plast. Reconstr. Surg.* **2016**, *4*, e1151.
- (37) Wagner, K.; Lee, K. S.; Yang, J.; Hammock, B. D. Epoxy fatty acids mediate analgesia in murine diabetic neuropathy. *Eur. J. Pain* **2017**, *21*, 456-465.
- (38) Greene, J. F.; Williamson, K. C.; Newman, J. W.; Morisseau, C.; Hammock, B. D. Metabolism of monoepoxides of methyl linoleate: bioactivation and detoxification. *Arch. Biochem. Biophys.* **2000**, *376*, 420-432.
- (39) Greene, J. F.; Newman, J. W.; Williamson, K. C.; Hammock, B. D. Toxicity of epoxy fatty acids and related compounds to cells expressing human soluble epoxide hydrolase. *Chem. Res. Toxicol.* **2000**, *13*, 217-226.
- (40) Yang, J.; Schmelzer, K.; Georgi, K.; Hammock, B. D. Quantitative Profiling Method for Oxylipin Metabolome by Liquid Chromatography Electrospray Ionization Tandem Mass Spectrometry. *Anal. Chem.* **2009**, *81*, 8085-8093.
- (41) Furuoka, M.; Ozaki, K.; Sadatomi, D.; Mamiya, S.; Yonezawa, T.; Tanimura, S.; Takeda, K. TNF- α Induces Caspase-1 Activation Independently of Simultaneously Induced NLRP3 in 3T3-L1 Cells. *J. Cell. Physiol.* **2016**, *231*, 2761-2767.
- (42) Wagner, K.; Inceoglu, B.; Dong, H.; Yang, J.; Hwang, S. H.; Jones, P.; Morisseau, C.; Hammock, B. D. Comparative efficacy of 3 soluble epoxide hydrolase inhibitors in rat neuropathic and inflammatory pain models. *Eur. J. Pharmacol.* **2013**, *700*, 93-101.

Table of Contents Graphic



Supporting Information for

Chapter 1: Adrenic Acid-Derived Epoxy Fatty Acids are Naturally Occurring Lipids and Their Methyl Ester Prodrug Reduces Endoplasmic Reticulum Stress and Inflammatory Pain

Nalin Singh, Bogdan Barnych, Karen M. Wagner, Debin Wan, Christophe Morisseau, and Bruce

D. Hammock*

Department of Entomology and Nematology and UC Davis Comprehensive Cancer Center,

University of California Davis, Davis, California 95616, United States

Table S1. Intra-day and Inter-day Accuracy and Precision of HPLC-MS/MS method for EDTs and DHDTs

Metabolite	Spiked Concentration (nM)	Detected Concentration (Mean [SD], nM)	Intra-day Accuracy (%)	Intra-day Precision (%)	Inter-day Accuracy (%)	Inter-day Precision (%)
10,11-EDT	1	0.845 [0.112]	13.6	16.4	15.5	13.3
	10	8.86 [1.05]	9.88	15.4	11.3	11.9
	100	87.3 [4.48]	12.9	3.64	12.7	5.13
13,14-EDT	1	0.892 [0.127]	14.5	14.1	10.7	14.2
	10	9.18 [0.687]	5.74	10.3	8.20	7.48
	100	89.3 [6.71]	10.3	5.94	10.7	7.51
16,17-EDT	1	0.913 [0.151]	14.9	9.27	8.67	16.5
	10	9.21 [0.831]	4.29	8.73	7.93	9.02
	100	90.2 [3.62]	8.81	3.63	9.83	4.01

7,8-	1	0.936 [0.002]	6.20	16.6	6.41	2.50
DHDT						
	10	9.37 [0.045]	6.00	6.61	6.32	4.85
	100	90.2 [3.85]	12.5	8.37	9.79	4.27
10,11-	1	0.913 [0.166]	7.22	12.2	8.62	18.2
DHDT						
	10	9.14 [0.833]	10.9	16.0	7.75	9.11
	100	90.2 [10.5]	13.3	6.77	8.78	11.6
13,14-	1	0.938 [0.053]	12.2	4.10	6.21	5.66
DHDT						
	10	9.98 [0.759]	5.21	9.64	10.2	7.61
	100	97.8 [4.69]	3.49	3.33	2.22	4.80
16,17-	1	0.911 [0.087]	11.1	11.0	8.93	9.52
DHDT						
	10	9.31 [0.849]	1.83	7.53	6.68	9.12
	100	93.0 [4.87]	2.49	5.98	6.99	5.24

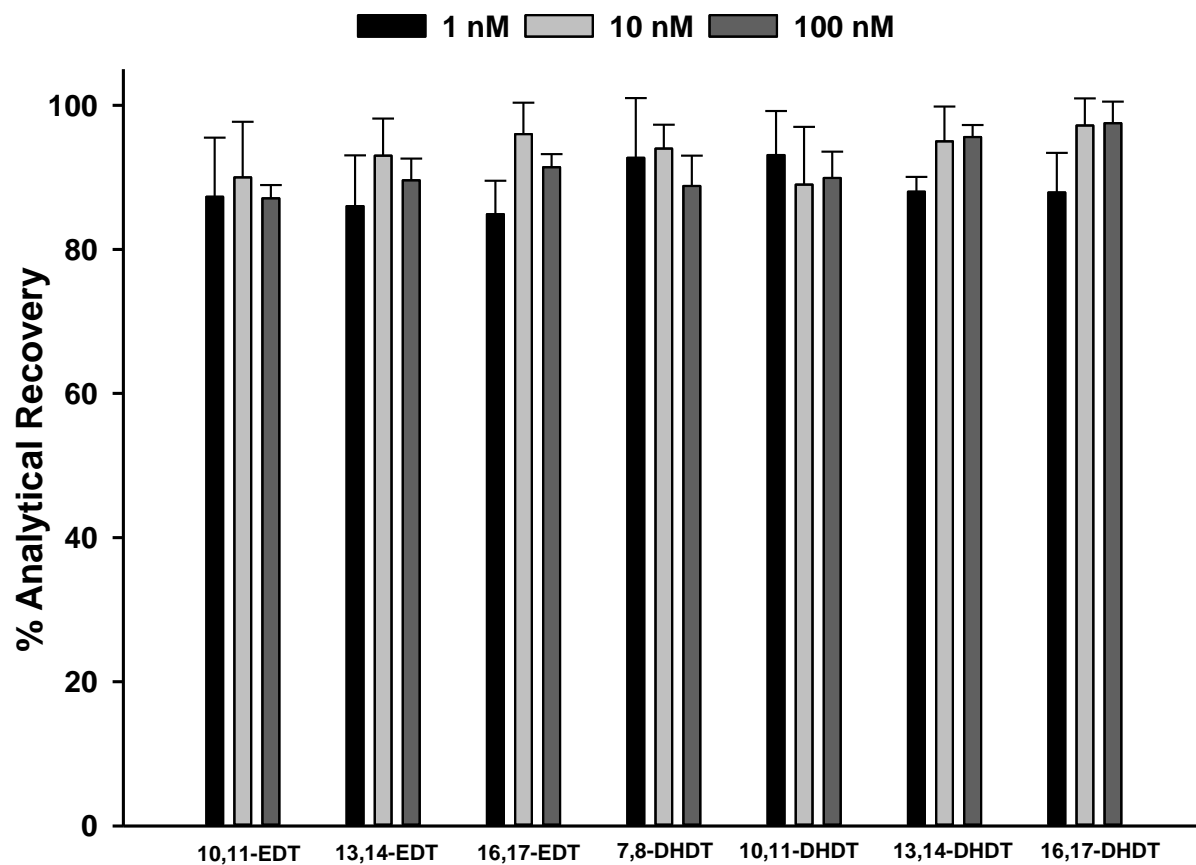


Figure S1. Analytical Recovery of EDTs and DHDTs at Low (1 nM), Moderate (10 nM), and High (100 nM) Analyte Concentrations.

Table S2. Preparative HPLC Conditions for Purification of EDT-me Regioisomers

Time (min)	Flow Rate (mL/min)	A ^a (%)	B ^b (%)
0	30	75	25
100	30	75	25
100.1	30	25	75

122	30	25	75
122.1	30	75	25
145	30	75	25

^aHexanes with 0.1% glacial acetic acid.

^bHexanes with 0.4% Isopropanol and 0.1% glacial acetic acid.

Table S3. Analytical HPLC Gradient for Chromatographic Separation of EDTs and DHDTs

Time (min)	Flow Rate ($\mu\text{L}/\text{min}$)	B (%)
0	250	30
4	250	75
8	250	90
9	250	95
9.5	250	95
9.6	250	30
11	250	30

Table S4. Q-Trap Mass Spectrometer Conditions

Parameter	Value
Curtain Gas (CUR)	30 psi
Collision Gas (CAD)	Medium
IonSpray Voltage (IS)	-4500
Temperature (TEM)	600 °C

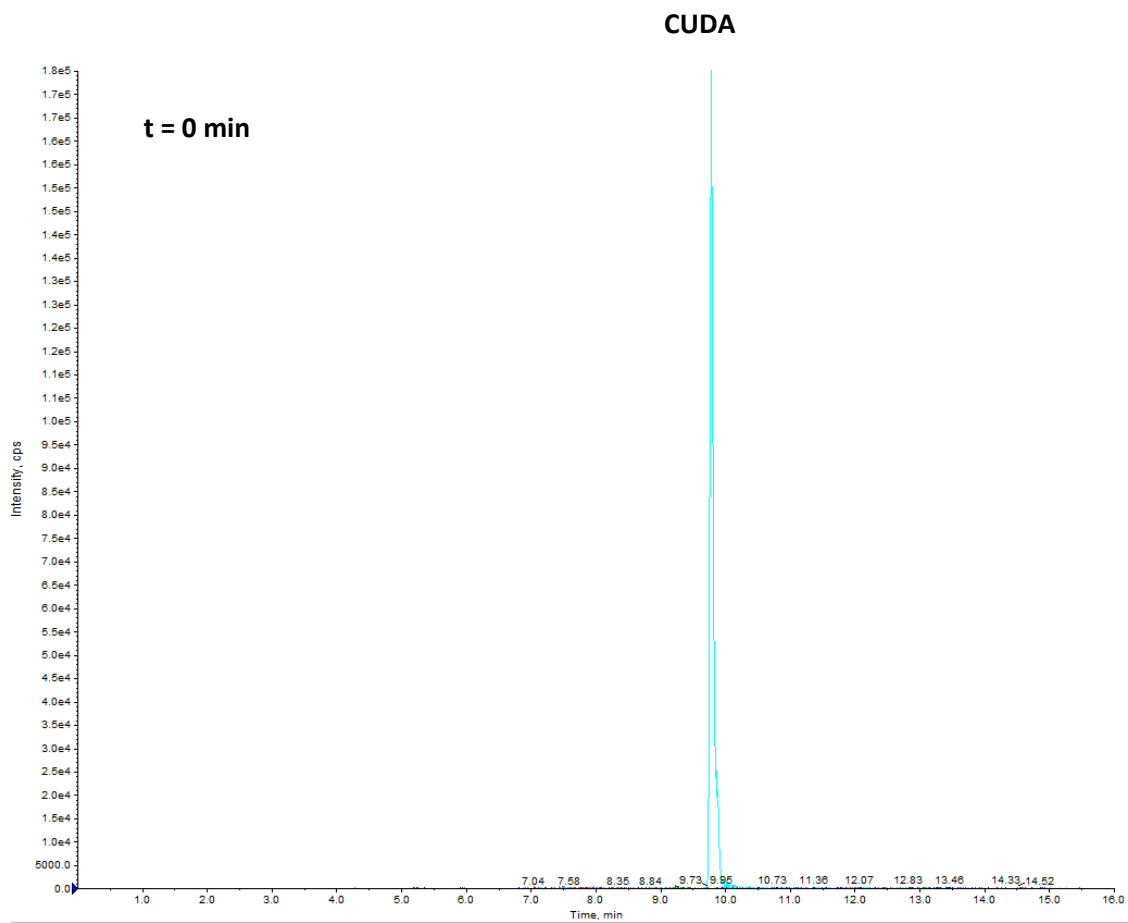
Ion Source Gas 1 (GS1)	60 psi
Ion Source Gas 2 (GS2)	50 psi
Interface Heater (ihe)	ON
Entrance Potential (EP)	-10

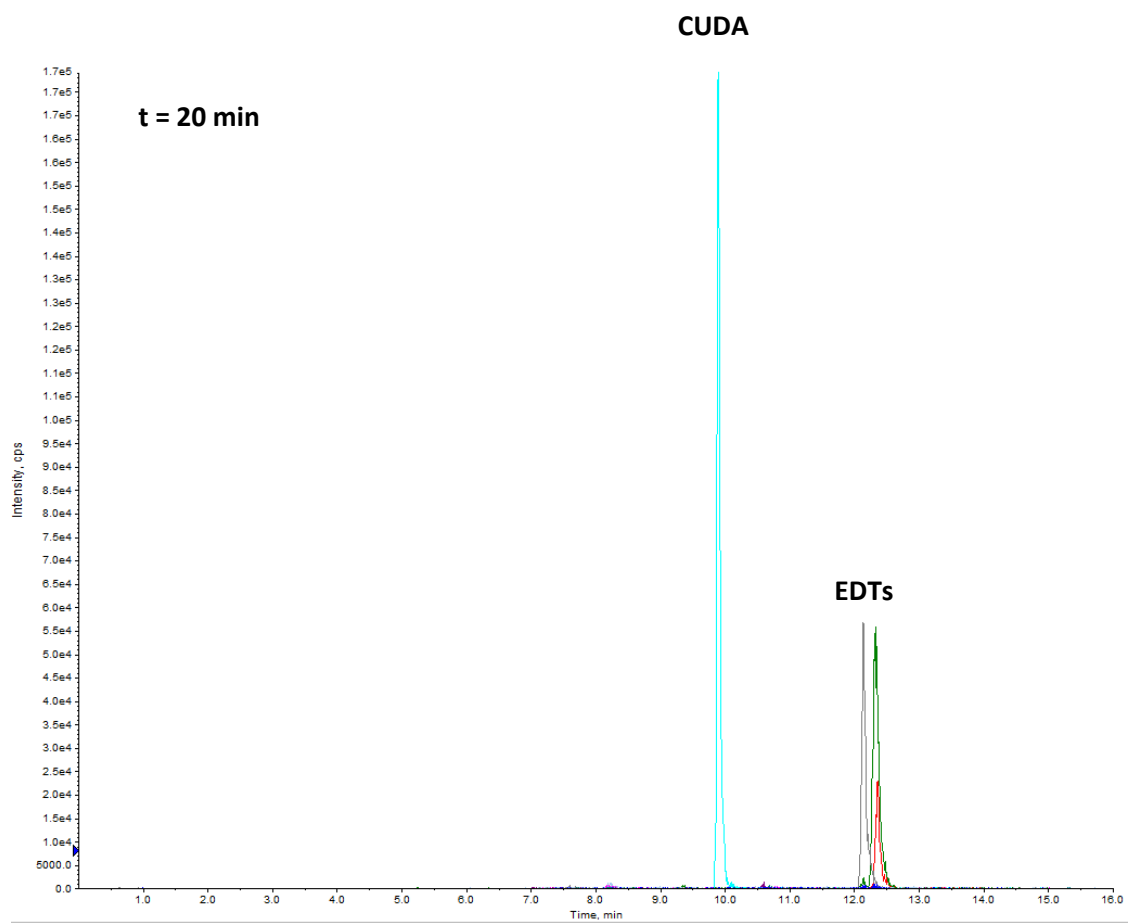
Table S5. Source Parameters for EDTs and DHDTs

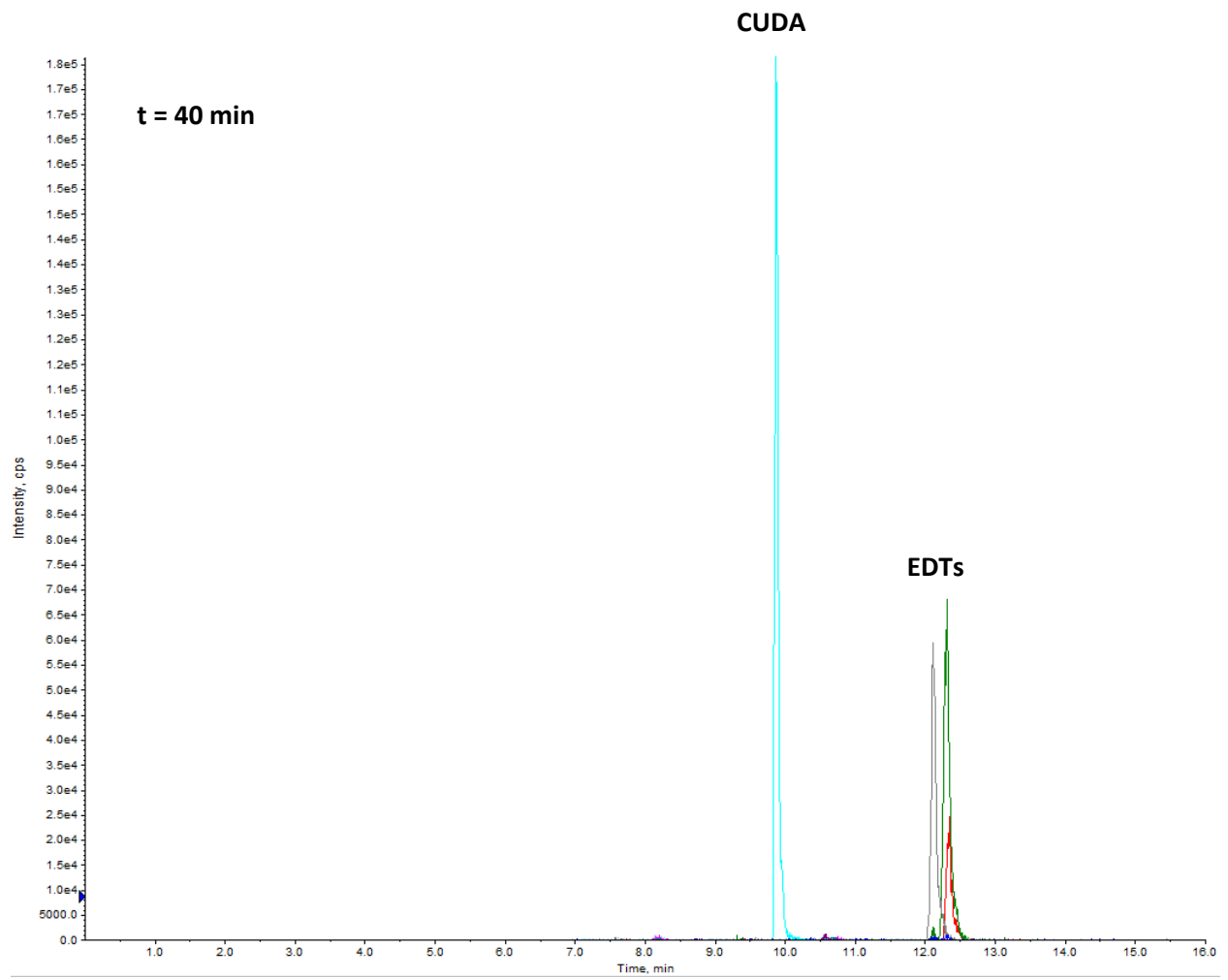
Analyte	DP(V)	CE(V)	CXP(V)
7,8-EDT	-45	-18	-7
10,11-EDT	-45	-18	-13
13,14-EDT	-45	-22	-9
16,17-EDT	-50	-20	-11
7,8-DHDT	-65	-42	-5
10,11-DHDT	-50	-32	-9
13,14-DHDT	-95	-30	-9
16,17-DHDT	-75	-30	-11

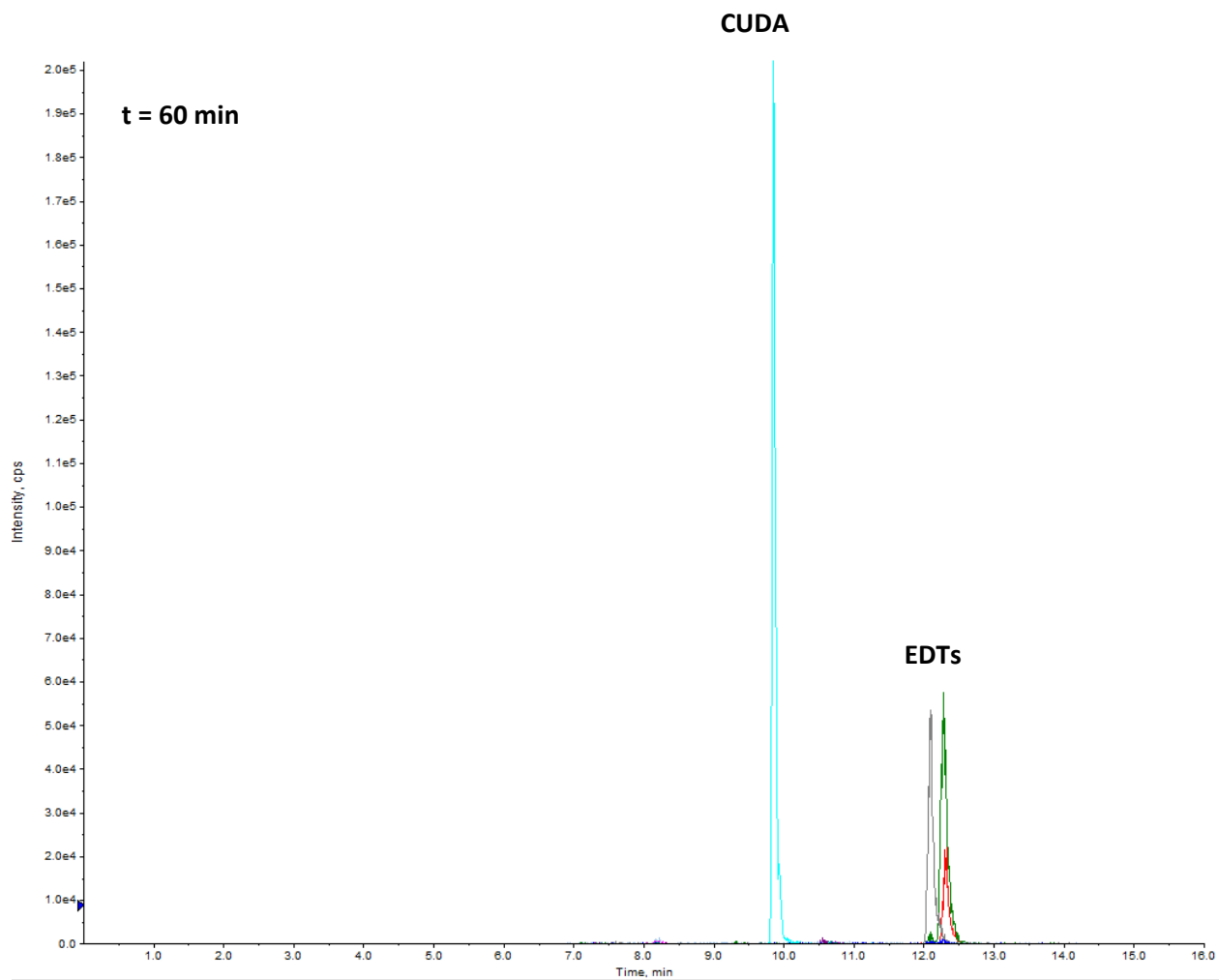
Table S6. Optimized MRM Transitions and Source Parameters for CUDA, EETs and DHETs

Analyte	Q1 (Da)	Q3(Da)	DP(V)	CE(V)	CXP(V)
CUDA	339.2	214.1	-65	-22	-8
5,6-EET	319.3	191.1	-60	-20	-7
8,9-EET	319.3	155.2	-65	-20	-6
11,12-EET	319.3	167.2	-60	-20	-7
14,15-EET	319.3	219.3	-65	-20	-4
5,6-DHET	337.2	145.1	-70	-26	-10
8,9-DHET	337.2	127.1	-70	-30	-8
11,12-DHET	337.2	167.1	-65	-26	-8
14,15-DHET	337.2	207.1	-65	-25	-10









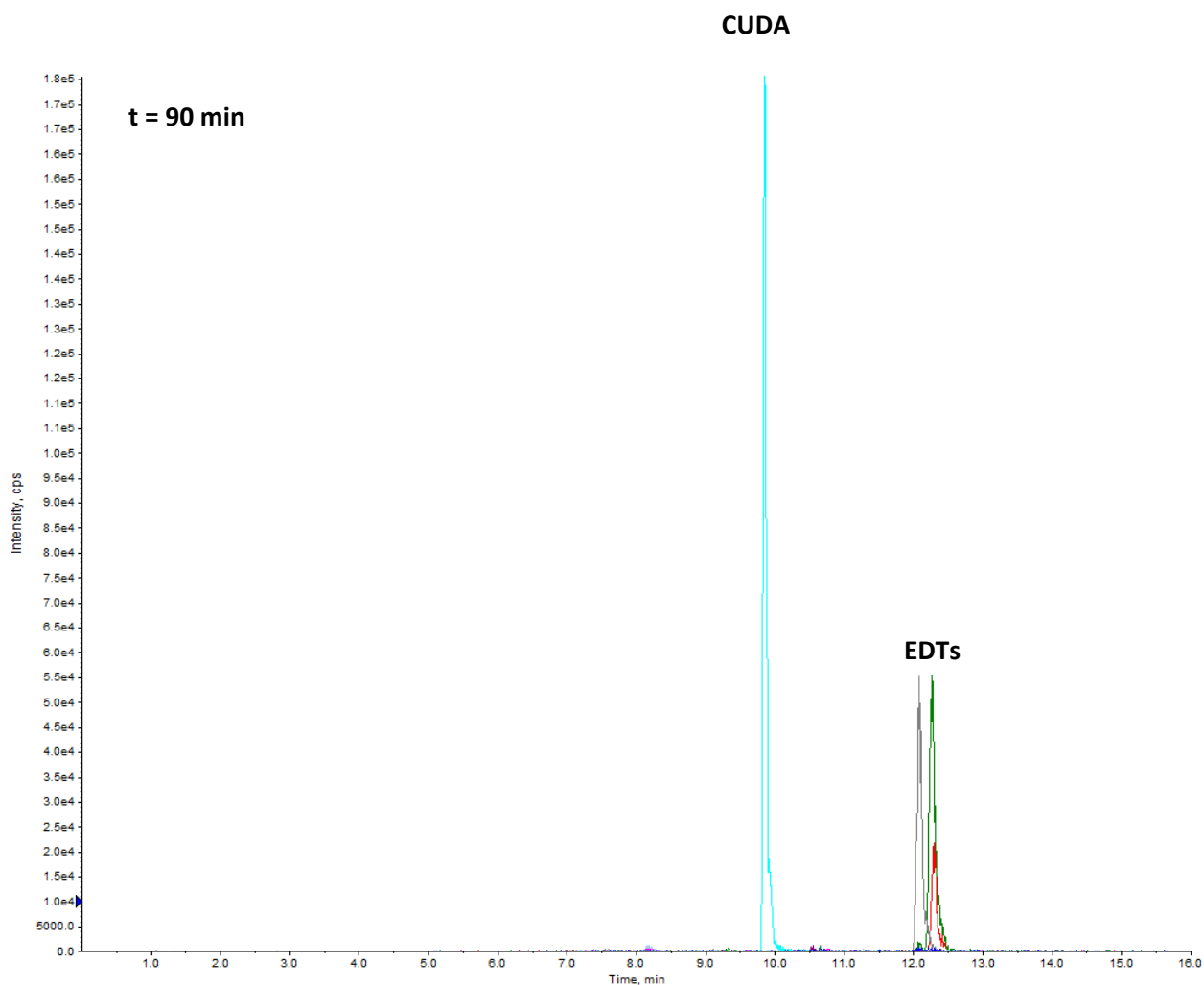


Figure S2. *In Vitro* Time Course demonstrating EDT free acid formation in HEK293 Cells. EDT methyl esters (regioisomer mixture) were incubated in a suspension of HEK293 cells for 20-, 40-, 60-, or 90-min at 37 °C under an atmosphere of 5% CO₂. The reaction was quenched with the internal standard CUDA (in methanol) and EDTs were detected by HPLC-MS/MS analysis. EDT free acids were observed at the 20 min time point and their levels appear to plateau after 20 min, suggesting rapid (i.e., within 20 min) cleavage of methyl esters to the carboxylic acids by cellular esterases.

¹H NMR and HRESIMS for EDT and DHDT Regioisomers

7,8-Epoxydocosatrienoic acid. ¹H NMR (800 MHz, CD₃CN) δ 5.52-5.32 (6H, m), 2.89-2.81 (4H, m), 2.36-2.06 (8H, m), 1.61-1.57 (2H, m), 1.39-1.23 (12H, m), 0.89 (3H, t); HRESIMS *m/z* 347.2585 [M - H]⁻ (calcd for C₂₂H₃₅O₃⁻, 347.2592).

10,11-Epoxydocosatrienoic acid. ¹H NMR (800 MHz, CD₃CN) δ 5.54-5.32 (6H, m), 2.91-2.80 (4H, m), 2.42-1.99 (10H, m), 1.59-1.52 (2H, m), 1.39-1.24 (10H, m), 0.90 (3H, t); HRESIMS *m/z* 347.2583 [M - H]⁻ (calcd for C₂₂H₃₅O₃⁻, 347.2592).

13,14-Epoxydocosatrienoic acid. ¹H NMR (800 MHz, CD₃CN) δ 5.56-5.31 (6H, m), 2.92-2.80 (4H, m), 2.40-1.95 (10H, m), 1.59-1.49 (2H, m), 1.38-1.20 (10H, m), 0.87 (3H, t); HRESIMS *m/z* 347.2583 [M - H]⁻ (calcd for C₂₂H₃₅O₃⁻, 347.2592).

16,17-Epoxydocosatrienoic acid. ¹H NMR (800 MHz, CD₃CN) δ 5.57-5.32 (6H, m), 2.92-2.77 (4H, m), 2.41-1.97 (8H, m), 1.59-1.47 (2H, m), 1.38-1.20 (12H, m), 0.88 (3H, t); HRESIMS *m/z* 347.2582 [M - H]⁻ (calcd for C₂₂H₃₅O₃⁻, 347.2592).

7,8-Dihydroxydocosatrienoic acid. ¹H NMR (800 MHz, CD₃CN) δ 5.50-5.32 (8H, m), 3.36-3.24 (2H, m), 2.86-2.81 (4H, m), 2.30-2.01 (6H, m), 1.59-1.53 (2H, m), 1.37-1.20 (12H, m), 0.91 (3H, t); HRESIMS *m/z* 365.2693 [M - H]⁻ (calcd for C₂₂H₃₇O₄⁻, 365.2697).

10,11-Dihydroxydocosatrienoic acid. ¹H NMR (800 MHz, CD₃CN) δ 5.48-5.32 (8H, m), 3.41-3.35 (2H, m), 2.83-2.77 (4H, m), 2.32-2.00 (8H, m), 1.58-1.52 (2H, m), 1.38-1.21 (10H, m), 0.91 (3H, t); HRESIMS *m/z* 365.2686 [M - H]⁻ (calcd for C₂₂H₃₇O₄⁻, 365.2697).

13,14-Dihydroxydocosatrienoic acid. ^1H NMR (800 MHz, CD_3CN) δ 5.49-5.31 (8H, m), 3.41-3.37 (2H, m), 2.82-2.79 (4H, m), 2.32-2.01 (8H, m), 1.59-1.54 (2H, m), 1.38-1.24 (10H, m), 0.90 (3H, t); HRESIMS m/z 365.2697 $[\text{M} - \text{H}]^-$ (calcd for $\text{C}_{22}\text{H}_{37}\text{O}_4^-$, 365.2697).

16,17-Dihydroxydocosatrienoic acid. ^1H NMR (800 MHz, CD_3CN) δ 5.49-5.31 (8H, m), 3.38-3.32 (2H, m), 2.85-2.80 (4H, m), 2.30-2.02 (6H, m), 1.59-1.54 (2H, m), 1.39-1.25 (12H, m), 0.90 (3H, t); HRESIMS m/z 365.2686 $[\text{M} - \text{H}]^-$ (calcd for $\text{C}_{22}\text{H}_{37}\text{O}_4^-$, 365.2697).

Chapter 2: *N*-Benzyl-linoleamide, a Constituent of *Lepidium meyenii* (Maca), is an Orally Bioavailable Soluble Epoxide Hydrolase Inhibitor that Alleviates Inflammatory Pain

Nalin Singh,^{†,‡} Bogdan Barnych,^{†,‡} Christophe Morisseau,[†] Karen M. Wagner,[†] Debin Wan,[†] Ashley Takeshita,[†] Hoang Pham,[†] Ting Xu,[§] Abhaya Dandekar,[⊥] Jun-Yan Liu,^{||} and Bruce D. Hammock^{*,†}

[†]Department of Entomology and Nematology and UC Davis Comprehensive Cancer Center, University of California Davis, Davis, CA, 95616, United States

[§]Beijing Advanced Innovation Center for Food Nutrition and Human Health, College of Resources and Environmental Sciences, China Agricultural University, Beijing, 100193, People's Republic of China

[⊥]Department of Plant Sciences, University of California Davis, Davis, CA, 95616, United States

^{||}Institute of Life Sciences, Chongqing Medical University, Chongqing, 400016, People's Republic of China

ABSTRACT

Lepidium meyenii (maca), a plant indigenous to the Peruvian Andes, recently has been utilized globally for claimed health or recreational benefits. The search for natural products that inhibit soluble epoxide hydrolase (sEH), with therapeutically relevant potencies and concentrations, led to the present study on bioactive amide secondary metabolites found in *L. meyenii*, the macamides. Based on known and suspected macamides, 19 possible macamides were synthesized and characterized. The majority of these amides displayed excellent inhibitory potency ($IC_{50} \approx 20\text{-}300$ nM) towards the recombinant mouse, rat and human sEH. Quantitative analysis of commercial maca products revealed that certain products contain known macamides (**1-5**, **8-12**) at therapeutically relevant total concentrations (≥ 3.29 mg/g of root), while the inhibitory potency of *L. meyenii* extracts directly correlates with the sum of concentration/ IC_{50} ratios of macamides present. Considering both its in vitro efficacy and high abundance in commercial products, *N*-benzyl-linoleamide (**4**) was identified as a particularly relevant macamide that can be utilized for in vivo studies. Following oral administration in the rat, compound **4** not only displayed acceptable pharmacokinetic characteristics, but it effectively reduced lipopolysaccharide-induced inflammatory pain. Inhibition of sEH by macamides provides a plausible biological mechanism of action to account for several beneficial effects previously observed with *L. meyenii* treatments.

Epoxy fatty acids (EpFAs), derived from cytochrome P450 oxidation of polyunsaturated fatty acids, are lipid mediators with primarily anti-inflammatory, analgesic, antihypertensive and antiapoptotic activities.¹⁻⁴ However, they are rapidly degraded to less bioactive dihydroxy fatty acids by soluble epoxide hydrolase (sEH). sEH inhibitors (sEHI) stabilize endogenous levels of EpFAs, enhancing their bioavailability and biological functions. Hence, inhibition of sEH is a novel and powerful therapeutic approach that could be utilized to tackle a number of unmet clinical needs. Thousands of highly potent urea, amide and carbamate-based sEHI have been synthesized and characterized. Despite this, only a handful have entered clinical trials and, currently, no drug on the market is used intentionally as an sEH inhibitor. One huge barrier is the extremely costly and time-consuming approval process for synthetic drugs due to very stringent regulatory requirements.

Alternatively, sEHI from natural sources, such as botanicals, can act as possible nutraceuticals and, through dietary supplementation, might provide a significantly faster and inexpensive means to treat patients. This could be particularly important in developing countries. Previously, a number of chemicals from a variety of natural sources have been identified as sEHI,⁵⁻¹² including urea and amide-based inhibitors from plants in the order Brassicales.^{13,14} However, a large number of these compounds have either a low potency or their concentrations in the plant are insufficient for clinical application.

Lepidium meyenii Walp. (*L. meyenii*), commonly known as maca or “Peruvian ginseng”, belongs to the family Brassicaceae and is indigenous to the high altitude of central Peruvian Andes. Its root is a native food crop and there is rising global interest in *L. meyenii* products as herbal remedies.¹⁵⁻¹⁷ Characterization of *L. meyenii* has revealed several secondary metabolites including glucosinolates, flavonolignans, and macamides.^{18,19} Macamides are *N*-benzylamides of

long-chain fatty acids (LCFAs) and are the key bioactive components of *L. meyenii*. They have demonstrated therapeutic potential against neurological disorders, including antidepressant effects²⁰ and protective action in models of Parkinson's disease.^{21,22} Improvements in neural cell viability are attributed to the prevention of mitochondrial membrane depolarization and reduced induction of reactive oxygen species (ROS). Attenuation of oxidative stress has also been shown to mediate non-neurological effects including protection against erythrocyte hemolysis,²³ antifatigue effects in muscles,²⁴ and decreased lipid peroxidation in a diabetic rat model.²⁵ Moreover, combining a Chinese clive seed extract with a maca extract significantly synergized beneficial effects on male sexual health.²⁶

Macamides have been characterized as inhibitors of fatty acid amide hydrolase (FAAH),^{27,28} an enzyme that degrades neuroprotective endocannabinoids such as anandamide.²⁹ Hence, FAAH inhibition has been proposed as a mechanism of action for macamides in the central nervous system. However, the potency is poor ($IC_{50} > 10 \mu M$), insufficient for the degree of FAAH inhibition typically required to exert biological effects such as analgesia.³⁰ Thus, FAAH inhibition is unlikely to fully account for the neuroprotective activity of macamides. sEH inhibition stabilizes the mitochondrial dysfunction-ROS-Endoplasmic Reticulum stress axis and, consequently, underlies the amelioration of several pathologies.³ Therefore, potentially it provides an alternative mode of action that captures macamide bioactivity. sEHI have also been shown to dramatically synergize with and expand the biological activity of FAAH inhibitors.³¹

Considering their structural similarities to previously identified amide pharmacophore containing sEHI,³²⁻³⁴ 19 possible macamides were synthesized, characterized, and tested as novel inhibitors of sEH in vitro. Additionally, macamide content in a number of commercial maca products was quantified to investigate compound distribution and abundance among products.

Finally, the most pertinent macamides were studied *in vivo* to assess pharmacokinetic parameters and analgesic effects in an inflammatory pain model.

RESULTS AND DISCUSSION

Macamide Design and Synthesis. A proposed route of biosynthesis of macamides involves LCFAs and benzylamine derivatives as substrates, which accumulate during traditional post-harvest treatments as catabolic processes accelerate.³⁵⁻³⁸ LCFAs are released from membrane lipids while glucosinolates are broken down to benzyl isothiocyanates, converted to benzylamines and enzymatically linked to the fatty acids, forming macamides (Figure 1). Thus, the macamides designed include a benzylamine moiety, which was either unsubstituted or possessed methoxy groups at *meta/para* positions, similar to certain parent glucosinolates. They also contain a fatty acid portion and a range of common saturated, mono- or polyunsaturated LCFAs were selected to account for effects of varying tail lengths and unsaturation sites.

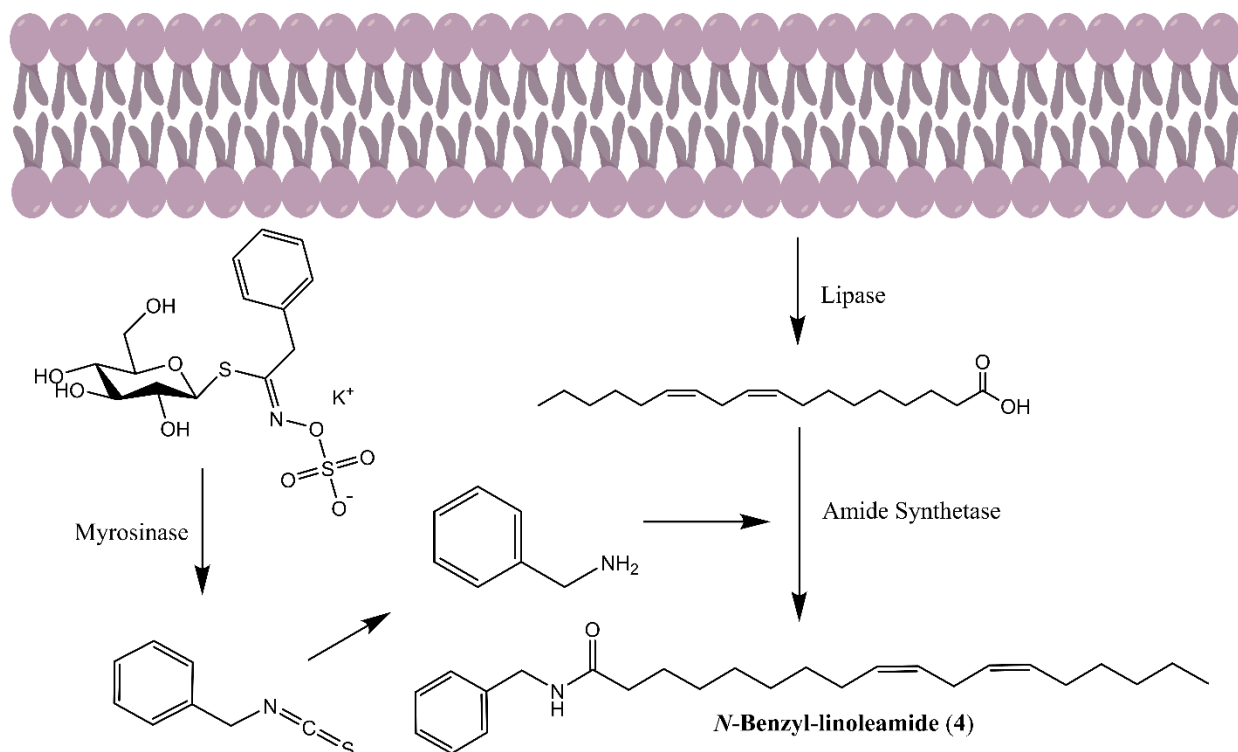
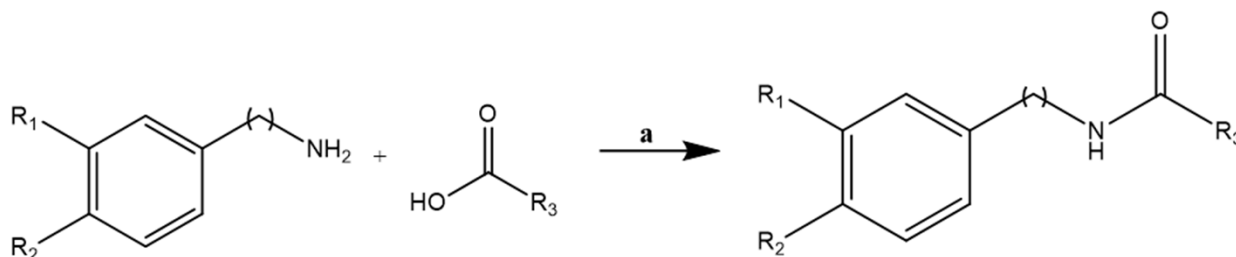


Figure 1. Schematic of hypothesized route for biosynthesis of macamides.³⁵⁻³⁸ Shown with the representative *N*-Benzylamide of linoleic acid (**4**).

Scheme 1. General Synthesis of Compounds 2-19. a: EDC, DMAP (cat.), CH₂Cl₂



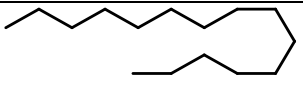
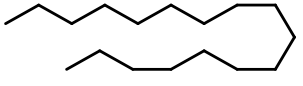
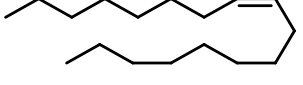
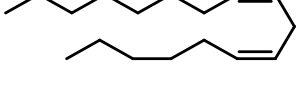
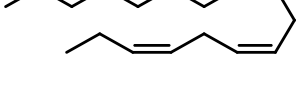
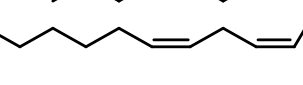
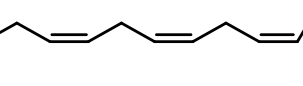
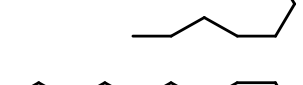
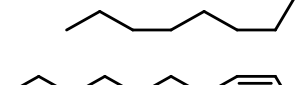
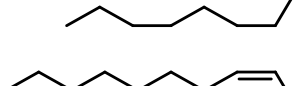
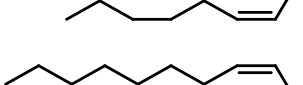
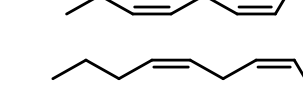
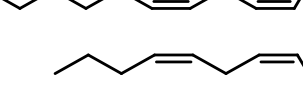
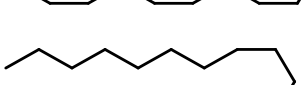

Accordingly, the central synthetic method employed was amide synthesis (Scheme 1). In general, the appropriate LCFA was activated with 1-ethyl-3-(3-dimethylaminopropyl)carbodiimide, and a catalytic amount of 4-dimethylaminopyridine, under dry and inert conditions. This was followed by addition of benzylamine to generate compounds **2-7**, 3-methoxybenzylamine to generate compounds **8-14**, 3,4-dimethoxybenzylamine to generate compounds **15-17**, and phenylethylamine to generate compounds **18** and **19**.

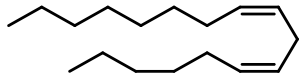
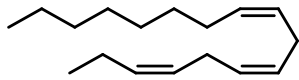
Inhibition of Recombinant Human, Rat, and Mouse sEH. Inhibitory potency of the synthesized amides was tested against recombinant human, rat, and mouse sEH (Table 1). Compounds with polyunsaturated fatty acid tails were more potent than the corresponding benzylamide analogue with saturated tails (**4-7** vs. **1-2** and **11-14** vs. **8-9**). The difference was especially prominent relative to the saturated 18-carbon chains (**2** and **9**), which were between two and three orders of magnitude less potent and were the weakest of the characterized inhibitors. The addition of a single double bond at the C-9-C-10 position (**3** and **10**) increased potency by almost two orders of magnitude. These observations suggest olefinic bonds are important for the inhibitory potential of macamides with longer fatty acid tails. However, within

inhibitor groups with two or more double bonds in their tails (**4-7** and **11-14**), there was little discernible difference in potencies. The addition of a *meta*-methoxy to the phenyl ring (**8-14**) generally decreased IC₅₀ values compared to unsubstituted analogs (**1-7**). This indicated that methoxy groups at *meta* positions can enhance sEH inhibition, as has been demonstrated with benzyl-containing urea-based natural sEH inhibitors.¹⁴ A second, *para*-methoxy (**15-17**), however, did not improve inhibitory potency. In fact, it significantly reduced potency of compounds with a saturated 16-carbon tail (**15** vs. **1** and **8**) and also lessened the efficacy of compounds with unsaturated tails (**16** and **17** vs. **4** and **5**, and **11** and **12**). Insertion of a methylene between the phenyl ring and amide function (**18** and **19**) increased inhibitory potency towards the human enzyme by almost one order of magnitude, compared to analogues **4-5**. The influence might be due to reduced steric hindrance in the active site.

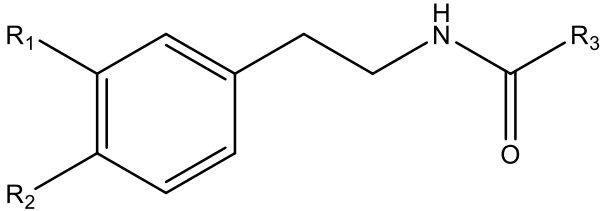
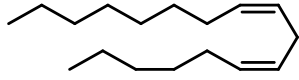
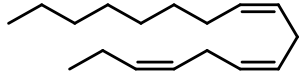
Table 1. Effects of Phenyl Substituents and Fatty Acid Chains on the sEH Inhibitory Potency of 19 Macamide-like Compounds

R ₁	R ₂	R ₃	Natural	Human	Rat	Mouse	Human
			Product	sEH	sEH	sEH	FAAH
			(+/-)	IC ₅₀	IC ₅₀	IC ₅₀	IC ₅₀ ^a
				(nM)	(nM)	(nM)	(nM)

1	H	H		+	524	370	422	>100,000
2	H	H		+	>100,000	35,800	59,600	>100,000
3	H	H		+	893	198	265	16,700
4	H	H		+	155	41	44	10,800
5	H	H		+	134	23	28	41,800
6	H	H		-	123	40	50	N/A
7	H	H		-	111	29	43	N/A
8	OCH ₃	H		+	235	113	159	N/A
9	OCH ₃	H		+	16,077	28,676	89,850	N/A
10	OCH ₃	H		+	241	84	126	11,000
11	OCH ₃	H		+	92	43	38	10,300
12	OCH ₃	H		+	76	9.3	27	13,700
13	OCH ₃	H		-	55	22	73	N/A
14	OCH ₃	H		-	63	18.6	49	N/A
15	OCH ₃	OCH ₃		+	7,059	15,910	>100,000	N/A

16	OCH ₃	OCH ₃		-	104	111	148	N/A
17	OCH ₃	OCH ₃		-	84	90	122	N/A

^aLiterature values²⁷

				Natural	Human	Rat	Mouse	Human
R ₁	R ₂	R ₃		Product	sEH	sEH	sEH	FAAH
				(+/-)	IC ₅₀	IC ₅₀	IC ₅₀	IC ₅₀ ^a
					(nM)	(nM)	(nM)	(nM)
18	H	H		-	28	33	91	N/A
19	H	H		-	15	15	39	N/A

^aLiterature values.²⁷

Macamide Levels in *L. meyenii* Products and Inhibitory Potency of Extracts. Thirteen commercially available *L. meyenii* root products were extracted and analyzed to quantify the amount of macamides present. Product types and sources are described in the Supporting Information (Table S1). Total macamide concentration estimates were based only on compounds with synthetic standards. Levels of macamides present varied significantly (> two orders of magnitude) from product to product (Table 2), with an average of around 1.24 mg/g of root. The key determinant for differences is likely variability in post-harvest treatment factors such as drying temperature, storage time and air exposure, since these conditions dictate substrate release

and subsequent biosynthesis efficiency.³⁵⁻³⁸ Certain extracts (e.g., E2 and E9) contained concentrations (≥ 3.29 mg/g of root) that were nearly two orders of magnitude greater than those of urea sEHI (< 0.058 mg/g of root) found in plants such as *Pentadiplandra brazzeana* Baill.¹³ This suggests that, under the right post-harvest conditions, dried *L. meyenii* root extracts might have sufficiently high macamide concentrations to be of nutraceutical value as a source of naturally derived sEHI. To support this claim, the inhibitory potency of the *L. meyenii* extracts was measured for the human and mouse sEH (Table 2). Biological activity of extracts also varied dramatically, but the IC₅₀ values obtained inversely correlated with the amount of macamides in the extracts (Spearman's rank correlation coefficient $\rho_{\text{human sEH}} = -0.928$ and $\rho_{\text{mouse sEH}} = -0.956$), suggesting that the sEH inhibition was mostly due to the presence of macamides in the extracts.

Table 2: Macamide Content and Inhibitory Potency of Thirteen *L. meyenii* Product Extracts

	Total	Human	Mouse
<i>L. meyenii</i>	Macamide	sEH	sEH
Extracts	Concentrations	IC ₅₀	IC ₅₀
	($\mu\text{g/g}$ of root)	(ng/mL)	(ng/mL)
E1	22.4	11,700	12,600
E2	3,602	329	138
E3	1,804	377	169
E4	1,780	450	139
E5	210	6,380	6,530
E6	217	4,550	3,400
E7	66.5	5,085	6,290

E8	2,480	422	207
E9	3,290	287	157
E10	301	2,620	1,701
E11	1,490	980	456
E12	870	1,606	869
E13	16.0	4,380	> 14,000

Ten out of the 19 synthesized compounds were detected in all extracts, and these are known natural products,^{26,27} specifically *N*-benzylamides of palmitic acid (**1**), stearic acid (**2**), oleic acid (**3**), linoleic acid (**4**) and α -linolenic acid (**5**) and their 3-methoxy substituted analogues (**8-12**). Compound **15**, the 3,4-dimethoxy substituted analogue of *N*-benzylpalmitamide (**1**) has also been detected previously in *L. meyenii*.²⁵ However, it was below the limit of quantitation (Table S2, Supporting Information) in the analyzed samples, possibly due to the difference in origin of maca. Amides with fatty acid tails containing 20 carbons, i.e. arachidonic acid (**6**, **13**) and eicosapentaenoic acid (**7**, **14**), were below the limit of quantitation (Table S2, Supporting Information), likely due to the relatively low concentrations of 20- and 22-carbon fatty acids in plant membrane lipids.^{39,40} In the most abundant extract (E2), levels of compound **4** were the highest, with concentrations nearly three and four times greater than those of the next two most abundant macamides, **1** and **5**, respectively (Table 3). In order to gauge inhibitory contributions of individual macamides within the extract, the ratio of concentrations to the corresponding IC₅₀ values was determined (Table 3), to obtain a metric that accounted for both abundance in *L. meyenii* and potency towards sEH. The ratio was easily the greatest for macamide **4**, suggesting it is likely the most biologically relevant macamide found in *L. meyenii* roots to date. Macamide

5 was the next most relevant product, while the potential activity of the 3-methoxy substituted analogues of **4** and **5** (i.e. **11** and **12**) as well as macamide **1** was also noteworthy. Higher abundance would largely account for the contribution of **1** while, conversely, the excellent potency of **11** and **12** (Table 1) would compensate for their relatively lower levels in extracts.

Table 3. Concentrations and Abundance/IC₅₀ Ratios of Individual Macamides in Extract 2

Compound	Concentration ($\mu\text{g/g}$ of Root)	Abundance/hsEH IC ₅₀ ($\mu\text{g/nM}$)	Abundance/msEH IC ₅₀ ($\mu\text{g/nM}$)
1	680	1.30	1.61
2	269	<0.003	0.005
3	275	0.308	1.04
4	1,640	10.6	37.3
5	464	3.46	16.6
8	39.6	0.168	0.249
9	24.0	0.001	<0.001
10	21.6	0.090	0.171
11	146	1.59	3.84
12	42.8	0.563	1.58

Furthermore, the potency of extracts E1-13 directly correlated with the sum (Table S3, Supporting Information) of detected macamide abundance/IC₅₀ ratios (Spearman's rank correlation coefficient $\rho_{\text{human sEH}} = 0.929$ and $\rho_{\text{mouse sEH}} = 0.887$), signifying that the inhibitory

potency towards sEH is likely a function of the concentrations and bioactivity of individual macamides present in the *L. meyenii* product.

Pharmacokinetics. Based on a combination of strong inhibitory potency and abundance in *L. meyenii* samples (Table 3), compounds **4** and **5** were selected for in vivo studies. To assess oral bioavailability of **4** and **5**, a pharmacokinetic study in rats was conducted to study their fate following oral administration of 100 mg/kg of each compound. A 96-h time-course of plasma concentrations of **4** and **5** was generated to assess key pharmacokinetic characteristics and is displayed in the Supporting Information (Figure S1).

Table 4. Pharmacokinetic Parameters for a 100 mg/kg Oral Dose of Compounds **4** and **5**^a

Compound	C _{max} (nM)	T _{max} (hours)	AUC (nM × hours)	t _{1/2} (hours)
4	519 ± 149	3	3690 ± 664	9
5	54 ± 11	6	723 ± 230	14.6

^aResults are the mean ± SEM (n=4/group).

Pharmacokinetic parameters (Table 4) indicated that the concentration of compound **4** peaked in the blood within 3 h and was around one order of magnitude greater than its rat sEH IC₅₀ (Table 1). However, the pharmacokinetic profile of compound **5** was poorer than that of **4**. It took double the time to reach its maximum blood concentration, which was nearly one order of

magnitude smaller, relative to **4**. The total body exposure to the macamides (i.e., AUC) was also approximately five times lower for **5**, compared to **4**. It is possible the additional olefin bond in **5** increases susceptibility to secondary metabolism, autoxidation, and allylic and bisallylic hydroxylation,^{41,42} decreasing in vivo stability.

Analgesia in Inflammatory Pain Model. Compound **4** demonstrated antinociceptive effects in a lipopolysaccharide (LPS)-induced inflammatory pain model in rat. Baseline paw withdrawal thresholds were scored before administration of compounds and normalized to 100%. LPS results in lower than baseline scores, indicating a painful state. Oral administration of **4** (100 mg/kg) significantly increased paw withdrawal thresholds (interpreted as pain relief), relative to the vehicle control (Figure 2). Therapeutic effects persisted over a 6-h time-course, similar to activity of classic, synthetic sEHI against LPS induced allodynia.⁴³ Effects of **5** were not significant (Figure S2, Supporting Information), probably due to its poor bioavailability.

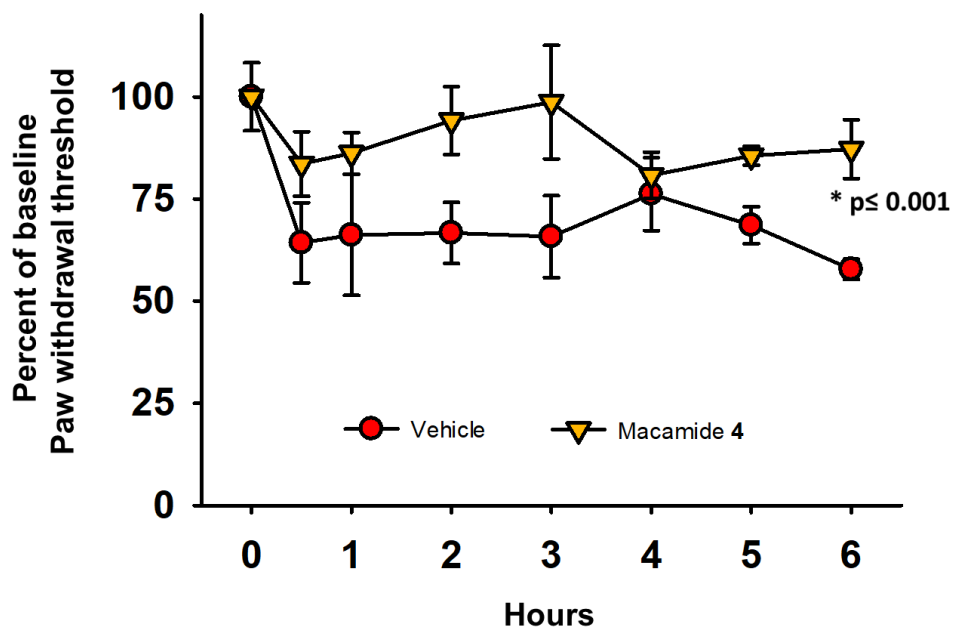


Figure 2. Macamide **4** (100 mg/kg) was efficacious against LPS-induced inflammatory pain in rat. Scores are the means \pm SEM reported as percent of baseline (normalized to 100%), calculated as the score \times 100/baseline score. The median value of efficacy was statistically significant compared to the vehicle control (NEOBEE 1053) over a 6-h time-course (Kruskal-Wallis One Way Analysis of Variance on Ranks, $\alpha=0.05$, $*p \leq 0.001$, $n=4/\text{group}$).

The discovery of macamides as sEHI can at least partially explain the vast majority of biological effects observed with *L. meyenii* extract or macamide treatments. Through restoration of mitochondrial health and attenuation of oxidative stress, sEHI have proven therapeutically promising using in vitro and in vivo models of Parkinson's disease.⁴⁴⁻⁴⁶ sEHI have also demonstrated antidepressant effects in mice, through improved brain-derived neurotrophic factor signaling in a stress model.⁴⁷ Mechanistically and/or functionally, the effects parallel macamide-mediated neuroprotection under these disease conditions.²⁰⁻²² Similarly, protection against ROS underlies the efficacy of sEHI against seemingly distinct pathologies³ and mirrors macamide activity in dissimilar disease conditions tied together by oxidative stress.²³⁻²⁵ The significantly greater potency towards sEH, compared to FAAH (Table 1), also strengthens the case for sEH inhibition as the more prevalent biological mechanism of action for macamides. However, macamides could in fact act as dual inhibitors of sEH and FAAH, potentially leading to synergism of biological effects, such as analgesia,³¹ by facilitating both EpFA bioactivity and endocannabinoid-mediated agonism of cannabinoid (CB) receptors. The mixture of bioactive natural products in an *L. meyenii* extract could have further additive or synergistic effects and could provide another advantage over classic small-molecule therapeutics. Finally, macamides (such as compound **4**) themselves selectively bind to the CB1 receptor,⁴⁸ and hence might directly exert some of the observed analgesic effects. The cannabimimetic activity could help

explain the recreational use of maca, though it suggests perhaps some caution should be exercised when considering *L. meyenii* for medicinal applications.

CONCLUSION

Nineteen potential macamides were synthesized, their inhibitory potency towards sEH was tested and their levels in commercial *L. meyenii* products were quantified. These compounds, several of which are known natural products, were found to be a novel and promising class of potent sEHI. *N*-Benzyl-linoleamide (**4**) is the most therapeutically significant macamide studied so far, based on a combination of its dominant abundance in maca products, in vitro potency, and in vivo efficacy. Two unsaturation sites in the fatty acid tail appear to provide an optimal balance between inhibitory potency and oral bioavailability, leading to significant analgesia in an inflammatory pain model. The therapeutic relevance of total macamides in maca products depends on the post-harvest treatment of *L. meyenii*, due to its significant influence on macamide biosynthesis. Certain samples contained levels that were nearly two orders of magnitude greater than those of sEHI found in previously identified dietary sources. Hence, careful selection and preparation of maca products is the key consideration in their potential application as nutraceuticals. In this study, analysis of macamides in *L. meyenii* products was conducted only using compounds with synthetic standards. However, it is probable other macamides exist and should be investigated in future studies. Current and new synthetic standards may facilitate efforts in breeding, post-harvest handling and other agronomic practices to increase the efficacy and concentration of macamides in commercial extracts.

EXPERIMENTAL SECTION

General Experimental Procedures. Compound **1** and most reagents required for synthesis are commercially available and were purchased from one of the following commercial vendors: Nu-Chek Prep, Inc. (Elysian, MN), Sigma Aldrich Chemical Co. (Milwaukee, WI), Fisher Scientific (Houston, TX), Eanmine LLC (Monmouth Jct, NJ), Oakwood Chemical (Estill, SC), Chem-Impex Inc (Wood Dale, IL) or Combi-Blocks (San Diego, CA). All reactions were carried out in anhydrous solvents, under an atmosphere of nitrogen or argon and at room temperature. All chemicals purchased from commercial sources were used as received without further purification. NMR spectra were recorded on a 400 MHz Bruker Avance III HD Nanobay NMR spectrometer. Multiplicity is described by the abbreviations, b = broad, s = singlet, d = doublet, t = triplet, m = multiplet. Chemical shifts (δ) are expressed as ppm. ^1H NMR spectra were referenced to the residual solvent peak at δ 7.26 (CDCl_3) or 2.51 ($\text{DMSO-}d_6$). ^{13}C NMR spectra were referenced to the solvent peak at δ 77.16 (CDCl_3) or 40.01 ($\text{DMSO-}d_6$). HRESIMS were recorded on a Thermo Electron LTQ-Orbitrap XL Hybrid mass spectrometer, equipped with an electrospray ionization (ESI) source operating in the positive-ion mode. Analytical TLC was performed on Merck TLC silica gel 60 F254 plates and spots were revealed under 254 nm UV light or developed with a potassium permanganate stain. Flash chromatography was performed on silica gel (230–400 mesh) from Macherey Nagel. Commercial *L. meyenii* product extracts were analyzed via HPLC-MS/MS. An Agilent 1200 SL liquid chromatography series (Agilent Corporation, Palo Alto, CA, USA), utilizing a Kinetex C_{18} 100 Å, LC 100 x 2.1 mm, 1.7 μm column was employed. It was coupled to a 4000 Q-Trap tandem mass spectrometer (Applied Biosystems Instrument Corp.), equipped with an ESI source (Turbo V) operating in the positive-ion mode. Multiple Reaction Monitoring (MRM) transitions were optimized via direct infusion of standards.

Chemistry. General Synthetic Method for Compounds 2-19, as shown with the Representative *N*-**Benzyl**octadeca-9Z,12Z-dienamide (**4**). Linoleic acid (2.00 g, 7.13 mmol), 1-ethyl-3-(3-dimethylaminopropyl)carbodiimide hydrochloride (1.71 g, 8.91 mmol) and 4-dimethylaminopyridine (catalytic amount) were stirred in dichloromethane (10 mL) for 15 min. Benzylamine (1.09 mL, 10.0 mmol) was added and the mixture was stirred overnight. After completion (confirmed by TLC), the crude mixture was concentrated under reduced pressure, redissolved in hexanes and purified by flash chromatography (ethyl acetate-hexanes 15:85 → 20:80). Yield 2.21g (84%).

N-Benzyloctadecanamide (**2**): Yield 29%; white powder, mp 89-91 °C; ¹H NMR (400 MHz, CDCl₃) δ 7.38-7.29 (5H, m, aromatic), 5.70 (1H, bs, NH), 4.47 (2H, d, *J* = 5.6 Hz, benzylic), 2.23 (2H, t, *J* = 7.6 Hz, α-H), 1.72-1.64 (2H, m, β-H), 1.34-1.27 (28H, m, CH₂), 0.90 (3H, t, *J* = 6.8 Hz, CH₃); ¹³C NMR (100 MHz, CDCl₃) δ 173.00 (CC(=O)N), 138.46 (C), 128.71 (CH), 127.90 (CH), 127.84 (CH), 43.59 (CH₂), 36.84 (CH₂), 31.94 (CH₂), 29.72 (CH₂), 29.70 (CH₂), 29.67 (CH₂), 29.63 (CH₂), 29.52 (CH₂), 29.38 (CH₂), 29.37 (CH₂), 29.34 (CH₂), 25.80 (CH₂), 22.71 (CH₂), 14.14 (CH₃); MS/MS MRM transition (Q1 → Q3) *m/z* 374.30 [M + H]⁺ → 91.00 [benzylum].

N-Benzyloctadec-9Z-enamide (**3**): Yield 90%; white powder, mp 48-50 °C; ¹H NMR (400 MHz, DMSO-*d*₆) δ 8.28 (1H, t, *J* = 6.0 Hz, NH), 7.33-7.21 (5H, m, aromatic), 5.37-5.29 (2H, m, vinylic), 4.25 (2H, d, *J* = 6.4 Hz, benzylic), 2.12 (2H, t, *J* = 7.6 Hz, α-H), 2.01-1.97 (4H, m, allylic), 1.53-1.50 (2H, m, β-H), 1.32-1.25 (20H, m, CH₂), 0.86 (3H, t, *J* = 7.2 Hz, CH₃); ¹³C NMR (100 MHz, DMSO-*d*₆) δ 172.54 (CC(=O)N), 140.26 (C), 130.11 (CH), 128.68 (CH), 127.61 (CH), 127.12 (CH), 42.41 (CH₂), 35.80 (CH₂), 31.75 (CH₂), 29.57 (CH₂), 29.30 (CH₂), 29.16 (CH₂), 29.13 (CH₂), 29.11 (CH₂), 29.06 (CH₂), 29.03 (CH₂), 27.08 (CH₂), 27.05 (CH₂),

25.78 (CH₂), 22.56 (CH₂), 14.42 (CH₃); MS/MS MRM transition (Q1 → Q3) *m/z* 372.30 [M + H]⁺ → 91.10 [benzylum].

N-Benzyl-octadeca-9*Z*,12*Z*-dienamide (**4**): Yield 84%; white powder, mp 30-32 °C; ¹H NMR (400 MHz, CDCl₃) δ 7.38-7.30 (5H, m, aromatic), 5.74 (1H, bs, NH), 5.44-5.32 (4H, m, vinylic), 4.47 (2H, d, *J* = 6.0 Hz, benzylic), 2.80 (2H, t, *J* = 6.4 Hz, bisallylic), 2.23 (2H, t, *J* = 7.2 Hz, α-H), 2.10-2.04 (4H, m, allylic), 1.72-1.64 (2H, m, β-H), 1.40-1.33 (14H, m, CH₂), 0.92 (3H, t, *J* = 6.4 Hz, CH₃); ¹³C NMR (100 MHz, CDCl₃) δ 172.92 (CC(=O)N), 138.40 (C), 130.21 (CH), 130.03 (CH), 128.69 (CH), 128.02 (CH), 127.88 (CH), 127.81 (CH), 127.48 (CH), 43.96 (CH₂), 36.78 (CH₂), 31.90 (CH₂), 29.98 (CH₂), 29.33 (CH₂), 29.27 (CH₂), 29.24 (CH₂), 29.12 (CH₂), 27.18 (CH₂), 25.74 (CH₂), 25.60 (CH₂), 22.95 (CH₂), 14.07 (CH₃); HREIMS *m/z* 370.3117 [M + H]⁺ (calcd for C₂₅H₄₀NO⁺, 370.3104); MS/MS MRM transition (Q1 → Q3) *m/z* 370.30 [M + H]⁺ → 91.00 [benzylum].

N-Benzyl-octadeca-9*Z*,12*Z*,15*Z*-trienamide (**5**): Yield 83%; colorless oil; ¹H NMR (400 MHz, CDCl₃) δ 7.36-7.29 (5H, m, aromatic), 5.73 (1H, bs, NH), 5.45-5.31 (6H, m, vinylic), 4.46 (2H, d, *J* = 5.2 Hz, benzylic), 2.83 (4H, t, *J* = 6.4 Hz, bisallylic), 2.22 (2H, t, *J* = 7.6 Hz, α-H), 2.12-2.05 (4H, m, allylic), 1.72-1.68 (2H, m, β-H), 1.39-1.33 (8H, m, CH₂), 1.00 (3H, t, *J* = 7.2 Hz, CH₃); ¹³C NMR (100 MHz, CDCl₃) δ 173.20 (CC(=O)N), 138.61 (C), 131.96 (CH), 130.26 (CH), 128.80 (CH), 128.30 (CH), 128.26 (CH), 127.75 (CH), 127.70 (CH), 127.33 (CH), 127.14 (CH), 43.43 (CH₂), 36.65 (CH₂), 29.62 (CH₂), 29.33 (CH₂), 29.31 (CH₂), 29.19 (CH₂), 27.24 (CH₂), 25.82 (CH₂), 25.65 (CH₂), 25.56 (CH₂), 20.58 (CH₂), 14.32 (CH₃); HREIMS *m/z* 368.2958 [M + H]⁺ (calcd for C₂₅H₃₈NO⁺, 368.2948); MS/MS MRM transition (Q1 → Q3) *m/z* 368.30 [M + H]⁺ → 108.10 [benzylaminium].

N-Benzylicosa-5*Z*,8*Z*,11*Z*,14*Z*-tetraenamide (**6**): Yield 91%; colorless oil; ¹H NMR (400 MHz, CDCl₃) δ 7.34-7.25 (5H, m, aromatic), 6.38 (1H, bs, NH), 5.45-5.33 (8H, m, vinylic), 4.39 (2H, d, *J* = 6.0 Hz, benzylic), 2.87-2.79 (6H, m, bisallylic), 2.23 (2H, t, *J* = 7.6 Hz, α-H), 2.14-2.05 (4H, m, allylic), 1.77-1.69 (2H, m, β-H), 1.42-1.29 (6H, m, CH₂), 0.92 (3H, t, *J* = 7.2 Hz, CH₃); ¹³C NMR (100 MHz, CDCl₃) δ 172.72 (CC(=O)N), 138.46 (C), 130.53 (CH), 129.13 (CH), 128.71 (CH), 128.22 (CH), 127.84 (CH), 127.52 (CH), 43.60 (CH₂), 36.06 (CH₂), 34.68 (CH₂), 31.61 (CH₂), 29.36 (CH₂), 29.09 (CH₂), 27.26 (CH₂), 26.73 (CH₂), 25.66 (CH₂), 22.66 (CH₂), 20.69 (CH₂), 14.12 (CH₃); MS/MS MRM transition (Q1 → Q3) *m/z* 394.30 [M + H]⁺ → 91.00 [benzylum].

N-Benzylicosa-5*Z*,8*Z*,11*Z*,14*Z*,17*Z*-pentaenamide (**7**): Yield 90%; colorless oil; ¹H NMR (400 MHz, CDCl₃) δ 7.33-7.24 (5H, m, aromatic), 6.41 (1H, bs, NH), 5.43-5.30 (10H, m, vinylic), 4.39 (2H, d, *J* = 5.6 Hz, benzylic), 2.89-2.79 (8H, m, bisallylic), 2.21 (2H, t, *J* = 7.6 Hz, α-H), 2.13-2.06 (4H, m, allylic), 1.76-1.69 (2H, m, β-H), 0.99 (3H, t, *J* = 7.6 Hz, CH₃); ¹³C NMR (100 MHz, CDCl₃) δ 172.91 (CC(=O)N), 138.55 (C), 132.04 (CH), 129.19 (CH), 128.69 (CH), 128.61 (CH), 128.60 (CH), 128.28 (CH), 128.26 (CH), 128.15 (CH), 128.11 (CH), 127.88 (CH), 127.70 (CH), 127.36 (CH), 127.04 (CH), 43.46 (CH₂), 35.94 (CH₂), 26.74 (CH₂), 25.67 (CH₂), 25.60 (CH₂), 25.58 (CH₂), 20.60 (CH₂), 14.32 (CH₃); MS/MS MRM transition (Q1 → Q3) *m/z* 392.30 [M + H]⁺ → 91.00 [benzylum].

N-(3-Methoxybenzyl)hexadecanamide (**8**): Yield 36%; white powder, mp 60-62 °C; ¹H NMR (400 MHz, CDCl₃) δ 7.27-7.25 (1H, m, aromatic), 6.89 (1H, d, *J* = 7.6 Hz, aromatic), 6.84-6.83 (2H, m, aromatic), 5.75 (1H, bs, NH), 4.45 (2H, d, *J* = 5.6 Hz, benzylic), 3.82 (3H, s, H-C-O), 2.25 (2H, t, *J* = 7.2 Hz, α-H), 1.71-1.66 (2H, m, β-H), 1.34-1.28 (24H, m, CH₂), 0.92 (3H, t, *J* = 6.8 Hz, CH₃); ¹³C NMR (100 MHz, CDCl₃) δ 172.97 (CC(=O)N), 159.92 (CC(=C)O), 140.01

(C), 129.76 (CH), 120.04 (CH), 113.39 (CH), 112.99 (CH), 55.25 (O-CH₃), 43.57 (CH₂), 36.87 (CH₂), 31.94 (CH₂), 29.71 (CH₂), 29.67 (CH₂), 29.62 (CH₂), 29.51 (CH₂), 29.37 (CH₂), 29.34 (CH₂), 25.79 (CH₂), 22.70 (CH₂), 14.13 (CH₃); MS/MS MRM transition (Q1 → Q3) m/z 376.30 [M + H]⁺ → 121.00 [3-methoxybenzylum].

N-(3-Methoxybenzyl)octadecanamide (**9**): Yield 83%; white powder, mp 77-79 °C; ¹H NMR (400 MHz, CDCl₃) δ 7.22-7.18 (1H, m, aromatic), 6.83 (1H, d, J = 7.6 Hz, aromatic), 6.79-6.76 (2H, m, aromatic), 6.41 (1H, bs, NH), 4.34 (2H, d, J = 5.6 Hz, benzylic), 3.76 (3H, s, H-C-O), 2.18 (2H, t, J = 7.6 Hz, α-H), 1.66-1.58 (2H, m, β-H), 1.31-1.26 (28H, m, CH₂), 0.89 (3H, t, J = 7.2 Hz, CH₃); ¹³C NMR (100 MHz, CDCl₃) δ 173.25 (CC(=O)N), 159.82 (CC(=C)O), 140.22 (C), 129.98 (CH), 119.88 (CH), 113.25 (CH), 112.72 (CH), 55.10 (O-CH₃), 43.35 (CH₂), 36.66 (CH₂), 31.95 (CH₂), 29.74 (CH₂), 29.72 (CH₂), 29.71 (CH₂), 29.69 (CH₂), 29.67 (CH₂), 29.57 (CH₂), 29.43 (CH₂), 29.39 (CH₂), 25.86 (CH₂), 22.71 (CH₂), 14.13 (CH₃); MS/MS MRM transition (Q1 → Q3) m/z 404.30 [M + H]⁺ → 121.00 [3-methoxybenzylum].

N-(3-Methoxybenzyl)octadec-9*Z*-enamide (**10**): Yield 98%; colorless oil; ¹H NMR (400 MHz, CDCl₃) δ 7.27-7.24 (1H, m, aromatic), 6.88 (1H, d, J = 7.2 Hz, aromatic), 6.84-6.82 (2H, m, aromatic), 5.76 (1H, bs, NH), 5.41-5.32 (2H, m, vinylic), 4.44 (2H, d, J = 5.6 Hz, benzylic), 3.82 (3H, s, H-C-O), 2.23 (2H, t, J = 7.2 Hz, α-H), 2.05-2.00 (4H, m, allylic), 1.69-1.64 (2H, m, β-H), 1.36-1.29 (20H, m, CH₂), 0.90 (3H, t, J = 6.8 Hz, CH₃); ¹³C NMR (100 MHz, CDCl₃) δ 172.95 (CC(=O)N), 159.91 (CC(=C)O), 140.03 (C), 130.01 (CH), 129.75 (CH), 120.02 (CH), 113.39 (CH), 112.95 (CH), 55.23 (O-CH₃), 43.55 (CH₂), 36.82 (CH₂), 31.92 (CH₂), 29.78 (CH₂), 29.72 (CH₂), 29.54 (CH₂), 29.33 (CH₂), 29.32 (CH₂), 29.28 (CH₂), 29.16 (CH₂), 27.24 (CH₂), 27.19 (CH₂), 25.78 (CH₂), 22.70 (CH₂), 14.13 (CH₃); MS/MS MRM transition (Q1 → Q3) m/z 402.30 [M + H]⁺ → 121.00 [3-methoxybenzylum].

N-(3-Methoxybenzyl)octadeca-9*Z*,12*Z*-dienamide (**11**): Yield 39%; colorless oil; ¹H NMR (400 MHz, CDCl₃) δ 7.28-7.24 (1H, m, aromatic), 6.89 (1H, d, *J* = 7.6 Hz, aromatic), 6.84-6.82 (2H, m, aromatic), 5.75 (1H, bs, NH), 5.44-5.31 (4H, m, vinylic), 4.43 (2H, d, *J* = 5.6 Hz, benzylic), 3.82 (3H, s, H-C-O), 2.80 (2H, t, *J* = 6.8 Hz, bisallylic), 2.23 (2H, t, *J* = 7.6 Hz, α-H), 2.09-2.04 (4H, m, allylic), 1.69-1.66 (2H, m, β-H), 1.42-1.28 (14H, m, CH₂), 0.91 (3H, t, *J* = 6.8 Hz, CH₃); ¹³C NMR (100 MHz, CDCl₃) δ 172.91(CC(=O)N), 159.91 (CC(=C)O), 140.01 (C), 130.24 (CH), 130.06 (CH), 129.76 (CH), 128.06 (CH), 127.91 (CH), 120.03 (CH), 113.41 (CH), 112.96 (CH), 55.24 (O-CH₃), 43.56 (CH₂), 36.82 (CH₂), 31.54 (CH₂), 29.72 (CH₂), 29.62 (CH₂), 29.36 (CH₂), 29.31 (CH₂), 29.27 (CH₂), 29.16 (CH₂), 27.21 (CH₂), 25.77 (CH₂), 25.64 (CH₂), 22.53 (CH₂), 14.09 (CH₃); MS/MS MRM transition (Q1 → Q3) *m/z* 400.30 [M + H]⁺ → 121.00 [3-methoxybenzylum].

N-(3-Methoxybenzyl)octadeca-9*Z*,12*Z*,15*Z*-trienamide (**12**): Yield 71%; colorless oil; ¹H NMR (400 MHz, CDCl₃) δ 7.28-7.24 (1H, m, aromatic), 6.89 (1H, d, *J* = 7.2 Hz, aromatic), 6.84-6.82 (2H, m, aromatic), 5.77 (1H, bs, NH), 5.45-5.30 (6H, m, vinylic), 4.44 (2H, d, *J* = 5.6 Hz, benzylic), 3.82 (3H, s, H-C-O), 2.82 (4H, t, *J* = 6.0 Hz, bisallylic), 2.22 (2H, t, *J* = 7.6 Hz, α-H), 2.11-2.04 (4H, m, allylic), 1.69-1.66 (2H, m, β-H), 1.38-1.28 (8H, m, CH₂), 1.00 (3H, t, *J* = 7.6 Hz, CH₃); ¹³C NMR (100 MHz, CDCl₃) δ 172.95 (CC(=O)N), 159.91 (CC(=C)O), 140.02 (C), 131.98 (CH), 130.28 (CH), 129.75 (CH), 128.30 (CH), 128.27 (CH), 127.74 (CH), 127.13 (CH), 120.02 (CH), 113.40 (CH), 112.94 (CH), 55.24 (O-CH₃), 43.55 (CH₂), 36.81 (CH₂), 29.71 (CH₂), 29.59 (CH₂), 29.31(CH₂), 29.27 (CH₂), 29.15 (CH₂), 27.22 (CH₂), 25.77 (CH₂), 25.63 (CH₂), 25.54 (CH₂), 20.57 (CH₂), 14.29 (CH₃); MS/MS MRM transition (Q1 → Q3) *m/z* 398.30 [M + H]⁺ → 121.00 [3-methoxybenzylum].

N-(3-Methoxybenzyl)icosa-5*Z*,8*Z*,11*Z*,14*Z*-tetraenamide (**13**): Yield 90%; colorless oil; ¹H NMR (400 MHz, CDCl₃) δ 7.28-7.24 (1H, m, aromatic), 6.88 (1H, d, *J* = 7.2 Hz, aromatic), 6.84-6.83 (2H, m, aromatic), 5.73 (1H, bs, NH), 5.45-5.34 (8H, m, vinylic), 4.43 (2H, d, *J* = 6.0 Hz, benzylic), 3.82 (3H, s, H-C-O), 2.86-2.80 (6H, m, bisallylic), 2.24 (2H, t, *J* = 7.6 Hz, α-H), 2.17-2.04 (4H, m, allylic), 1.81-1.73 (2H, m, β-H), 1.45-1.28 (6H, m, CH₂), 0.90 (3H, t, *J* = 6.8 Hz, CH₃); ¹³C NMR (100 MHz, CDCl₃) δ 172.68 (CC(=O)N), 159.91 (CC(=C)O), 139.90 (C), 130.54 (CH), 129.78 (CH), 129.08 (CH), 128.83 (CH), 128.25 (CH), 128.16 (CH), 127.87 (CH), 127.53 (CH), 120.08 (CH), 120.04 (CH), 113.47 (CH), 112.96 (CH), 55.24 (O-CH₃), 43.60 (CH₂), 36.10 (CH₂), 31.52 (CH₂), 29.33 (CH₂), 27.23 (CH₂), 26.70 (CH₂), 25.65 (CH₂), 25.54 (CH₂), 22.58 (CH₂), 14.08 (CH₃); MS/MS MRM transition (Q1 → Q3) *m/z* 424.30 [M + H]⁺ → 121.00 [3-methoxybenzylum].

N-(3-Methoxybenzyl)icosa-5*Z*,8*Z*,11*Z*,14*Z*,17*Z*-pentaenamide (**14**): Yield 97%; colorless oil; ¹H NMR (400 MHz, CDCl₃) δ 7.28-7.24 (1H, m, aromatic), 6.86 (1H, d, *J* = 7.2 Hz, aromatic), 6.83-6.81 (2H, m, aromatic), 5.78 (1H, bs, NH), 5.45-5.31 (10H, m, vinylic), 4.42 (2H, d, *J* = 5.6 Hz, benzylic), 3.81 (3H, s, H-C-O), 2.87-2.80 (8H, m, bisallylic), 2.24 (2H, t, *J* = 7.6 Hz, α-H), 2.17-2.05 (4H, m, allylic), 1.80-1.72 (2H, m, β-H), 0.99 (3H, t, *J* = 7.2 Hz, CH₃); ¹³C NMR (100 MHz, CDCl₃) δ 172.72 (CC(=O)N), 159.90 (CC(=C)O), 139.90 (C), 132.07 (CH), 129.77 (CH), 129.10 (CH), 129.04 (CH), 128.80 (CH), 128.60 (CH), 128.29 (CH), 128.22 (CH), 128.10 (CH), 127.87 (CH), 127.01 (CH), 120.04 (CH), 113.47 (CH), 112.93 (CH), 55.24 (O-CH₃), 43.59 (CH₂), 36.09 (CH₂), 29.71 (CH₂), 26.70 (CH₂), 25.64 (CH₂), 25.55 (CH₂), 25.54 (CH₂), 20.57 (CH₂), 14.28 (CH₃); MS/MS MRM transition (Q1 → Q3) *m/z* 422.30 [M + H]⁺ → 121.00 [3-methoxybenzylum].

N-(3,4-Dimethoxybenzyl)hexadecanamide (**15**): Yield 33%; white, amorphous solid; ¹H NMR (400 MHz, CDCl₃) δ 6.84 (3H, bs, aromatic), 5.66 (1H, bs, NH), 4.41 (2H, d, *J* = 6.0 Hz, benzylic), 3.89 (6H, s, H-C-O), 2.22 (2H, t, *J* = 7.6 Hz, α-H), 1.56-1.51 (2H, m, β-H), 1.34-1.31 (24H, m, CH₂), 0.86 (3H, t, *J* = 6.8 Hz, CH₃); ¹³C NMR (100 MHz, CDCl₃) δ 172.90 (CC(=O)N), 149.20 (CC(=C)O), 148.51 (CC(=C)O), 131.07 (C), 120.11 (CH), 111.23 (CH), 111.18 (CH), 55.96 (O-CH₃), 55.89 (O-CH₃), 43.45 (CH₂), 36.09 (CH₂), 31.65 (CH₂), 29.71 (CH₂), 29.69 (CH₂), 29.67 (CH₂), 29.63 (CH₂), 29.51 (CH₂), 29.37 (CH₂), 29.35 (CH₂), 29.07 (CH₂), 25.35 (CH₂), 22.66 (CH₂), 14.21 (CH₃); MS/MS MRM transition (Q1 → Q3) *m/z* 406.30 [M + H]⁺ → 151.10 [3,4-dimethoxybenzylum].

N-(3,4-Dimethoxybenzyl)octadeca-9*Z*,12*Z*-dienamide (**16**): Yield 85%; white, amorphous solid; ¹H NMR (400 MHz, CDCl₃) δ 6.84 (3H, bs, aromatic), 5.68 (1H, bs, NH), 5.39-5.36 (4H, m, vinylic), 4.41 (2H, d, *J* = 6.0 Hz, benzylic), 3.89 (6H, s, H-C-O), 2.79 (2H, t, *J* = 6.4 Hz, bisallylic), 2.22 (2H, t, *J* = 7.8 Hz, α-H), 2.09-2.04 (4H, m, allylic), 1.79-1.72 (2H, m, β-H), 1.39-1.27 (14H, m, CH₂), 0.92 (3H, t, *J* = 6.4 Hz, CH₃); ¹³C NMR (100 MHz, CDCl₃) δ 172.84 (CC(=O)N), 149.20 (CC(=C)O), 148.51 (CC(=C)O), 131.08 (C), 130.23 (CH), 130.01 (CH), 128.07 (CH), 127.90 (CH), 120.10 (CH), 111.24 (CH), 111.18 (CH), 55.93 (O-CH₃), 55.87 (O-CH₃), 43.45 (CH₂), 36.86 (CH₂), 31.43 (CH₂), 29.62 (CH₂), 29.15 (CH₂), 29.07 (CH₂), 27.28 (CH₂), 27.21 (CH₂), 25.76 (CH₂), 25.28 (CH₂), 22.66 (CH₂), 14.10 (CH₃); HREIMS *m/z* 430.3324 [M + H]⁺ (calcd for C₂₇H₄₄NO₃⁺, 430.3316); MS/MS MRM transition (Q1 → Q3) *m/z* 430.30 [M + H]⁺ → 151.10 [3,4-dimethoxybenzylum].

N-(3,4-Dimethoxybenzyl)octadeca-9*Z*,12*Z*,15*Z*-trienamide (**17**): Yield 87%; white, amorphous solid; ¹H NMR (400 MHz, CDCl₃) δ 6.84 (3H, bs, aromatic), 5.66 (1H, bs, NH), 5.42-5.33 (6H, m, vinylic), 4.41 (2H, d, *J* = 5.6 Hz, benzylic), 3.89 (6H, s, H-C-O), 2.83 (4H, t, *J* = 6.8 Hz,

bisallylic), 2.22 (2H, t, $J = 7.6$ Hz, α -H), 2.12-2.05 (4H, m, allylic), 1.69-1.62 (2H, m, β -H), 1.40-1.32 (8H, m, CH₂), 1.00 (3H, t, $J = 7.2$ Hz, CH₃); ¹³C NMR (100 MHz, CDCl₃) δ 172.83 (CC(=O)N), 149.20 (CC(=C)O), 148.52 (CC(=C)O), 131.98 (C), 131.06 (CH), 130.24 (CH), 128.31 (CH), 128.25 (CH), 127.76 (CH), 127.12 (CH), 120.11 (CH), 111.25 (CH), 111.18 (CH), 55.95 (O-CH₃), 55.89 (O-CH₃), 43.36 (CH₂), 36.87 (CH₂), 31.60 (CH₂), 29.59 (CH₂), 29.27 (CH₂), 29.14 (CH₂), 29.07 (CH₂), 27.68 (CH₂), 25.78 (CH₂), 25.35 (CH₂), 22.66 (CH₂), 14.31 (CH₃); HREIMS m/z 428.3165 [M + H]⁺ (calcd for C₂₇H₄₂NO₃⁺, 428.3159); MS/MS MRM transition (Q1 \rightarrow Q3) m/z 428.30 [M + H]⁺ \rightarrow 151.10 [3,4-dimethoxybenzylum].

N-Phenethyloctadeca-9*Z*,12*Z*-dienamide (**18**): Yield 82%; white powder, mp 31-33 °C; ¹H NMR (400 MHz, CDCl₃) δ 7.36-7.21 (5H, m, aromatic), 5.71 (1H, bs, NH), 5.44-5.32 (4H, m, vinylic), 3.57-3.52 (2H, m, H-C-N), 2.86-2.78 (4H, m, bisallylic, benzylic), 2.15-2.04 (6H, m, allylic, α -H), 1.63-1.59 (2H, m, β -H), 1.41-1.28 (14H, m, CH₂), 0.91 (3H, t, $J = 7.2$ Hz, CH₃); ¹³C NMR (100 MHz, CDCl₃) δ 173.07 (CC(=O)N), 138.96 (C), 130.25 (CH), 130.07 (CH), 128.79 (CH), 128.65 (CH), 128.06 (CH), 127.92 (CH), 126.52 (CH), 40.48 (CH₂), 36.86 (CH₂), 35.74 (CH₂), 31.54 (CH₂), 29.63 (CH₂), 29.36 (CH₂), 29.27 (CH₂), 29.25 (CH₂), 29.15 (CH₂), 27.22 (CH₂), 25.74 (CH₂), 25.65 (CH₂), 22.59 (CH₂), 14.09 (CH₃); MS/MS MRM transition (Q1 \rightarrow Q3) m/z 384.30 [M + H]⁺ \rightarrow 105.10 [1-phenylethan-1-ylum].

N-Phenethyloctadeca-9*Z*,12*Z*,15*Z*-trienamide (**19**): Yield 88%; colorless oil; ¹H NMR (400 MHz, CDCl₃) δ 7.35-7.20 (5H, m, aromatic), 5.73 (1H, bs, NH), 5.48-5.30 (6H, m, vinylic), 3.57-3.52 (2H, m, H-C-N), 2.85-2.81 (6H, m, bisallylic, benzylic), 2.15-2.05 (6H, m, allylic, α -H), 1.64-1.57 (2H, m, β -H), 1.39-1.28 (8H, m, CH₂), 1.00 (3H, t, $J = 7.8$ Hz, CH₃); ¹³C NMR (100 MHz, CDCl₃) δ 173.09 (CC(=O)N), 138.97 (C), 131.98 (CH), 130.28 (CH), 128.78 (CH), 128.64 (CH), 128.30 (CH), 128.26 (CH), 127.74 (CH), 127.13 (CH), 126.51 (CH), 40.50 (CH₂),

36.84 (CH₂), 35.74 (CH₂), 29.72 (CH₂), 29.61 (CH₂), 29.25 (CH₂), 29.14 (CH₂), 27.22 (CH₂), 25.74 (CH₂), 25.63 (CH₂), 25.55 (CH₂), 20.57 (CH₂), 14.29 (CH₃); HREIMS *m/z* 382.3115 [M + H]⁺ (calcd for C₂₆H₄₀NO⁺, 382.3104); MS/MS MRM transition (Q1 → Q3) *m/z* 382.30 [M + H]⁺ → 105.10 [1-phenylethan-1-ylum].

sEH Inhibition Assay. The assay was performed as previously described.⁴⁹ All IC₅₀ values for recombinant human, mouse, and rat sEHs were determined by a fluorescence-based assay system in a 96-well, serial dilution format. Non-fluorescent cyano(6-methoxy-naphthalen-2-yl)methyl *trans*-[(3-phenyloxiran-2-yl)methyl] carbonate (MNPC) was used as the assay substrate at a final concentration of 5 μM. MNPC is hydrolyzed by sEH to the fluorescent 6-methoxynaphthaldehyde. Formation of the product was measured by a Molecular Devices M-2 plate reader ($\lambda_{\text{ex}} = 330 \text{ nm}$, $\lambda_{\text{em}} = 465 \text{ nm}$). All measurements were performed in triplicate and the means are reported. *t*-TUCB, a classic sEHI, was run in parallel and the obtained IC₅₀ values were corroborated with reported literature values,⁴³ to validate the experimental results (Table S4, Supporting Information).

Extraction and Analysis of Macamides from *L. meyenii* Products. Products 1-7 (Table S1, Supporting Information) were first homogenized via mortar and pestle grinding. For products 1-12 (Table S1, Supporting Information), 1 g of *L. meyenii* root powder was extracted with a 40 mL mixture of hexanes-ethanol (7:1) at 50 °C, under ultra-sonication for 15 min. Each suspension was filtered, evaporated under reduced pressure, and reconstituted in 5 mL of ethyl acetate. Aliquots were diluted in HPLC-grade methanol and filtered through a 0.22 μm filter prior to analysis. Product 13 (Table S1, Supporting Information) was directly diluted, filtered, and analyzed. Other solvent and extraction systems were also tested, and normalized extraction efficiencies are described in the Supporting Information (Table S5). Maca extract samples were

placed in an autosampler, and 10 μ L aliquots were injected on the HPLC column and macamide concentrations were quantified by HPLC-MS/MS analysis using standard curves and dilution factors. The HPLC trace for the mixture of macamides detected in the extract of Product 2 is displayed in the Supporting Information (Figure S3).

Pharmacology. All animal experiments were performed according to protocols approved by the Institutional Animal Care and Use Committee (IACUC) of University of California, Davis (approval nos. 21204 for Pharmacokinetics and 21509 for Inflammatory Pain Model to Prof. Bruce D. Hammock).

Pharmacokinetics. Male Sprague–Dawley (SD) rats ($n=4$ /group, 8 weeks old, 250–300 g), purchased from Charles River Laboratories, were used in the pharmacokinetic study of compounds **4** and **5**. Each compound (100 mg/kg) was dissolved in 100% NEOBEE 1053 and administered via oral gavage. Whole blood (10 μ L) was collected with a pipet from the tail vein, punctured by a lancet at 0, 0.25, 0.5, 1, 2, 4, 8, 12, 24, 48, 72 and 96 h after dosing. Each blood sample was immediately transferred to a tube containing 100 μ L of water with 0.1% EDTA, vortexed and stored at -80 °C until analysis. According to a previously reported method,⁵⁰ the blood samples were processed, and compound concentrations were determined.

Inflammatory Pain Model. A von Frey assay measuring mechanical allodynia was performed, as previously described,⁵¹ in male SD rats ($n=4$ /group). The study was conducted in a randomized and blinded manner. Mechanical withdrawal thresholds (MWT) were determined before dosing to establish a baseline score. Then, 1 mL of 100% NEOBEE 1053 vehicle, 100 mg/kg compound **4** or 100 mg/kg compound **5** was oral gavaged. Immediately following oral gavage, 50 μ L of a 0.2 μ g/mL solution of LPS in saline were injected intraplantarly in a hind (ipsilateral) paw. The rats were then assessed for MWT over a 6-h time-course. The ipsilateral

MWT were measured three-five times per rat per time point, and scores are reported as the means of a group of rats.

ASSOCIATED CONTENT

Supporting Information. Descriptions of thirteen commercial *L. meyenii* products, normalized extraction efficiencies, analytical method limits of quantitation, sums of abundance/IC₅₀ ratios, IC₅₀s of in vitro positive control, blood concentration profiles of compounds **4** and **5**, analgesic efficacy of **5**, HPLC trace of commercial *L. meyenii* product extract (E2) and ¹H and ¹³C NMR spectra for new compounds (**16**, **17**, and **19**).

AUTHOR INFORMATION

Corresponding Author

*Tel: 530-752-7519. Fax: 530-752-1537. Email: bdhammock@ucdavis.edu.

Notes

‡N.S. and B.B. contributed equally.

ACKNOWLEDGMENTS

This study was partially supported by National Institutes of Health grants, National Institute of Environmental Health Sciences (NIEHS) RIVER Award (R35 ES030443-01), NIEHS/Superfund Research Program (P42 ES004699), and National Institute of Neurological Disorders and Stroke (R01 DK107767).

REFERENCES

- (1) Imig, J. D.; Hammock, B. D. *Nat. Rev. Drug Discov.* **2009**, *8*, 794-805.
- (2) Morisseau, C.; Hammock, B. D. *Annu. Rev. Pharmacol. Toxicol.* **2013**, *53*, 37-58.
- (3) Inceoglu, B.; Bettaieb, A.; Haj, F. G.; Gomes, A. V.; Hammock, B. D. *Prostaglandins Other Lipid Mediat.* **2017**, *133*, 68-78.
- (4) Wagner, K. M.; McReynolds, C. B.; Schmidt, W. K.; Hammock, B. D. *Pharmacol. Ther.* **2017**, *180*, 62-76.
- (5) Jo, A. R.; Kim, J. H.; Yan, X.-T.; Yang, S. Y.; Kim, Y. H. *J. Enzyme Inhib. Med. Chem.* **2016**, *31*, 70-78.
- (6) Thao, N. P.; Luyen, B. T. T.; Lee, J. S.; Kim, J. H.; Kim, Y. H. *Bioorg. Med. Chem. Lett.* **2017**, *27*, 1874-1879.
- (7) Thao, N. P.; Kim, J. H.; Thuy Luyen, B. T.; Dat, N. T.; Kim, Y. H. *Int. J. Biol. Macromol.* **2017**, *98*, 526-534.
- (8) Kim, J. H.; Jo, Y. D.; Kim, H. Y.; Kim, B. R.; Nam, B. *Comput. Struct. Biotechnol. J.* **2018**, *16*, 404-411.
- (9) Kim, J. H.; Jo, Y. D.; Jin, C. H. *Int. J. Biol. Macromol.* **2019**, *135*, 1202-1207.
- (10) He, X.; Zhao, W. Y.; Shao, B.; Zhang, B. J.; Liu, T. T.; Sun, C. P.; Huang, H. L.; Wu, J. R.; Liang, J. H.; Ma, X. C. *Int. J. Biol. Macromol.* **2020**, *158*, 1362-1368.
- (11) Sun, C.-P.; Zhang, J.; Zhao, W.-Y.; Yi, J.; Yan, J.-K.; Wang, Y.-L.; Morisseau, C.; Liu, Z.-B.; Hammock, B. D.; Ma, X.-C. *Bioorg. Chem.* **2020**, *96*, 103637.
- (12) Xuan Duy, L.; Le Ba, V.; Gao, D.; Hoang, V. D.; Quoc Toan, T.; Yang, S. Y.; Duy Quang, D.; Kim, Y. H.; Cuong, N. M. *Nat. Prod. Res.* **2020**, 1-6. (DOI: 10.1080/14786419.2020.1774759)

- (13) Kitamura, S.; Morisseau, C.; Inceoglu, B.; Kamita, S. G.; De Nicola, G. R.; Nyegue, M.; Hammock, B. D. *PloS One* **2015**, *10*, e0117438.
- (14) Kitamura, S.; Morisseau, C.; Harris, T. R.; Inceoglu, B.; Hammock, B. D. *PloS One* **2017**, *12*, e0176571.
- (15) Shin, B. C.; Lee, M. S.; Yang, E. J.; Lim, H. S.; Ernst, E. *BMC Complement Altern. Med.* **2010**, *10*, 44.
- (16) Gonzales, G. F. *Evid. -Based Complement. Altern. Med.* **2011**, *2012*, 193496.
- (17) Dording, C. M.; Schettler, P. J.; Dalton, E. D.; Parkin, S. R.; Walker, R. S.; Fehling, K. B.; Fava, M.; Mischoulon, D. *Evid. -Based Complement. Altern. Med.* **2015**, *2015*, 949036.
- (18) Piacente, S.; Carbone, V.; Plaza, A.; Zampelli, A.; Pizza, C. *J. Agric. Food Chem.* **2002**, *50*, 5621-5625.
- (19) Yi, F.; Tan, X.-l.; Yan, X.; Liu, H.-B. *Chinese Med.* **2016**, *11*, 42.
- (20) Ai, Z.; Cheng, A. F.; Yu, Y. T.; Yu, L. J.; Jin, W. *J. Med. Food* **2014**, *17*, 535-542.
- (21) Zhou, Y.; Li, P.; Brantner, A.; Wang, H.; Shu, X.; Yang, J.; Si, N.; Han, L.; Zhao, H.; Bian, B. *Sci. Rep.* **2017**, *7*, 44660.
- (22) Gugnani, K. S.; Vu, N.; Rondón-Ortiz, A. N.; Böhlke, M.; Maher, T. J.; Pino-Figueroa, A. *J. Toxicol. Appl. Pharmacol.* **2018**, *340*, 67-76.
- (23) Lin, L.; Huang, J.; Sun-Waterhouse, D.; Zhao, M.; Zhao, K.; Que, J. *Int. J. Food Sci. Technol.* **2018**, *53*, 304-312.
- (24) Yang, Q.; Jin, W.; Lv, X.; Dai, P.; Ao, Y.; Wu, M.; Deng, W.; Yu, L. *Pharm. Biol.* **2016**, *54*, 827-834.
- (25) Qiu, C.; Zhu, T.; Lan, L.; Zeng, Q.; Du, Z. *Braz. Arch. Biol. Technol.* **2016**, *59*, e16150462.

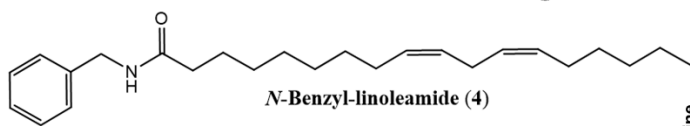
- (26) Zhang, Y.; Zhou, F.; Ge, F. *BMC Complement. Altern. Med.* **2019**, *19*, 135.
- (27) Wu, H.; Kelley, C. J.; Pino-Figueroa, A.; Vu, H. D.; Maher, T. J. *Bioorg. Med. Chem.* **2013**, *21*, 5188-5197.
- (28) Alasmari, M.; Böhlke, M.; Kelley, C.; Maher, T.; Pino-Figueroa, A. *Mol. Neurobiol.* **2019**, *56*, 1770-1781.
- (29) Deutsch, D. G.; Ueda, N.; Yamamoto, S. *Prostaglandins Leuk. Essent. Fatty Acids* **2002**, *66*, 201-210.
- (30) Nantermet, P. G.; Henze, D. A. In *Annual Reports in Medicinal Chemistry*; Macor, J. E.; Ed.; Academic Press: Cambridge, MA, 2011; Vol. 46, pp 19-32.
- (31) Sasso, O.; Wagner, K.; Morisseau, C.; Inceoglu, B.; Hammock, B. D.; Piomelli, D. *Pharmacol. Res.* **2015**, *97*, 7-15.
- (32) Morisseau, C.; Goodrow, M. H.; Newman, J. W.; Wheelock, C. E.; Dowdy, D. L.; Hammock, B. D. *Biochem. Pharmacol.* **2002**, *63*, 1599-1608.
- (33) Kim, I.-H.; Heirtzler, F. R.; Morisseau, C.; Nishi, K.; Tsai, H.-J.; Hammock, B. D. *J. Med. Chem.* **2005**, *48*, 3621-3629.
- (34) Pecic, S.; Deng, S.-X.; Morisseau, C.; Hammock, B. D.; Landry, D. W. *Bioorg. Med. Chem. Lett.* **2012**, *22*, 601-605.
- (35) Esparza, E.; Hadzich, A.; Kofer, W.; Mithofer, A.; Cosio, E. G. *Phytochemistry* **2015**, *116*, 138-148.
- (36) Chen, J.-J.; Zhao, Q.-S.; Liu, Y.-l.; Gong, P.-f.; Cao, L.-l.; Wang, X.-D.; Zhao, B. *Int. J. Food Prop.* **2017**, *20*, 3112-3123.
- (37) Huang, Y.-J.; Peng, X.-R.; Qiu, M.-H. *Nat. Prod. Bioprospect.* **2018**, *8*, 405-412.

- (38) Zhang, S.-Z.; Yang, F.; Shao, J.-L.; Pu, H.-M.; Ruan, Z.-Y.; Yang, W.-L.; Li, H. *Int. J. Food Sci. Technol.* **2020**, *55*, 2428-2440
- (39) Ohlrogge, J.; Browse, J. *Plant Cell* **1995**, *7*, 957-970.
- (40) Somerville, C. In *Biochemistry and Molecular Biology of Plants*; Buchanan, B. B., Gruissem, W., Jones, R. L., Eds.; American Society of Plant Physiologists: Rockville, MD, 2000, pp 456-527.
- (41) Falck, J. R.; Kodela, R.; Manne, R.; Atcha, K. R.; Puli, N.; Dubasi, N.; Manthathi, V. L.; Capdevila, J. H.; Yi, X. Y.; Goldman, D. H.; Morisseau, C.; Hammock, B. D.; Campbell, W. *B. J. Med. Chem.* **2009**, *52*, 5069-5075.
- (42) Oliw, E. H.; Brodowsky, I. D.; Hörnsten, L.; Hamberg, M. *Arch. Biochem. Biophys.* **1993**, *300*, 434-439.
- (43) Wagner, K.; Inceoglu, B.; Dong, H.; Yang, J.; Hwang, S. H.; Jones, P.; Morisseau, C.; Hammock, B. D. *Eur. J. Pharmacol.* **2013**, *700*, 93-101.
- (44) Ren, Q.; Ma, M.; Yang, J.; Nonaka, R.; Yamaguchi, A.; Ishikawa, K. I.; Kobayashi, K.; Murayama, S.; Hwang, S. H.; Saiki, S.; Akamatsu, W.; Hattori, N.; Hammock, B. D.; Hashimoto, K. *Proc. Natl. Acad. Sci. U.S.A.* **2018**, *115*, E5815-e5823.
- (45) Huang, H. J.; Wang, Y. T.; Lin, H. C.; Lee, Y. H.; Lin, A. M. *Mol. Neurobiol.* **2018**, *55*, 138-144.
- (46) Lakkappa, N.; Krishnamurthy, P. T.; Pandareesh, M. D.; Hammock, B. D.; Hwang, S. H. *Neurotoxicology* **2019**, *70*, 135-145.
- (47) Ren, Q.; Ma, M.; Ishima, T.; Morisseau, C.; Yang, J.; Wagner, K. M.; Zhang, J. C.; Yang, C.; Yao, W.; Dong, C.; Han, M.; Hammock, B. D.; Hashimoto, K. *Proc. Natl. Acad. Sci. U.S.A.* **2016**, *113*, E1944-52.

- (48) Hajdu, Z.; Nicolussi, S.; Rau, M.; Lorántfy, L.; Forgo, P.; Hohmann, J.; Csupor, D.; Gertsch, J. *J. Nat. Prod.* **2014**, *77*, 1663-1669.
- (49) Jones, P. D.; Wolf, N. M.; Morisseau, C.; Whetstone, P.; Hock, B.; Hammock, B. D. *Anal. Biochem.* **2005**, *343*, 66-75.
- (50) Liu, J. Y.; Lin, Y. P.; Qiu, H.; Morisseau, C.; Rose, T. E.; Hwang, S. H.; Chiamvimonvat, N.; Hammock, B. D. *Eur. J. Pharm. Sci.* **2013**, *48*, 619-627.
- (51) Inceoglu, B.; Jinks, S. L.; Schmelzer, K. R.; Waite, T.; Kim, I. H.; Hammock, B. D. *Life Sci.* **2006**, *79*, 2311-2319.

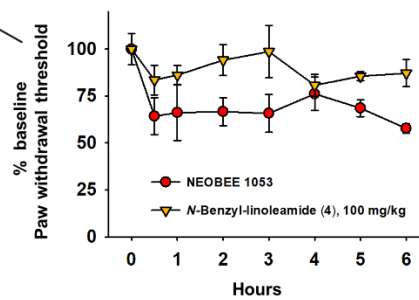
Table of Contents Graphic

Analgesic Natural Product



In vitro
hsEH IC₅₀ – 155 nM
rsEH IC₅₀ – 41 nM
msEH IC₅₀ – 44 nM

In vivo at 100 mg/kg p.o. in rat
C_{max} – 519 nM
T_{max} – 3 h
AUC – 3685 nM×h



Supporting Information for

Chapter 2: *N*-Benzyl-linoleamide, a Constituent of *Lepidium meyenii* (Maca), is an Orally Bioavailable Soluble Epoxide Hydrolase Inhibitor that Alleviates Inflammatory Pain

Nalin Singh,^{†,‡} Bogdan Barnych,^{†,‡} Christophe Morisseau,[†] Karen M. Wagner,[†] Debin Wan,[†] Ashley Takeshita,[†] Hoang Pham,[†] Ting Xu,[§] Abhaya Dandekar,[⊥] Jun-Yan Liu,^{||} and Bruce D. Hammock^{*,†}

[†]Department of Entomology and Nematology and UC Davis Comprehensive Cancer Center, University of California Davis, Davis, CA, 95616, United States

[§]Beijing Advanced Innovation Center for Food Nutrition and Human Health, College of Resources and Environmental Sciences, China Agricultural University, Beijing, 100193, People's Republic of China

[⊥]Department of Plant Sciences, University of California Davis, Davis, CA, 95616, United States

^{||}Institute of Life Sciences, Chongqing Medical University, Chongqing, 400016, People's Republic of China

Table S1. Descriptions of thirteen commercial *L. meyenii* (maca) products

<i>L. meyenii</i> product	Description
Product 1	Purple maca root slices from Lijiang, China
Product 2	Yellow maca root from Lijiang, China
Product 3	Black maca root from Shaotong City, China
Product 4	Black maca root from Lijiang, China
Product 5	Black maca root from Peru
Product 6	Yellow maca root from Peru
Product 7	Black maca root from Qujing, China
Product 8	Yellow maca root powder from Zhaotong, China
Product 9	Yellow maca root powder from Qujing, China
Product 10	Black maca root powder from The Maca Team LLC
Product 11	Yellow maca root powder from The Maca Team LLC
Product 12	Red maca root powder from The Maca Team LLC

Table S2. HPLC-MS/MS method Limits of Quantitation

ID	LOQ (ng/ml)
2	0.4
3	0.002
4	0.002
5	0.002
6	0.01
7	0.1
8	0.002
9	1
10	0.002
11	0.01
12	0.01
13	0.1
14	0.1
15	0.1
16	1
17	0.1
18	0.1

Table S3. Sum of abundance/IC₅₀ ratios of individual macamides in *L. meyenii* extracts

<i>L. meyenii</i> extract	Σ Abundance/hsEH IC ₅₀ ($\mu\text{g/nM}$)	Σ Abundance/msEH IC ₅₀ ($\mu\text{g/nM}$)
E1	0.100	0.339
E2	18.0	62.3
E3	6.72	22.2
E4	7.75	24.8
E5	0.866	2.41
E6	0.597	1.58
E7	0.282	0.978
E8	9.72	31.5
E9	14.1	46.8
E10	1.28	4.04
E11	6.43	20.3
E12	3.37	11.2
E13	0.050	0.179

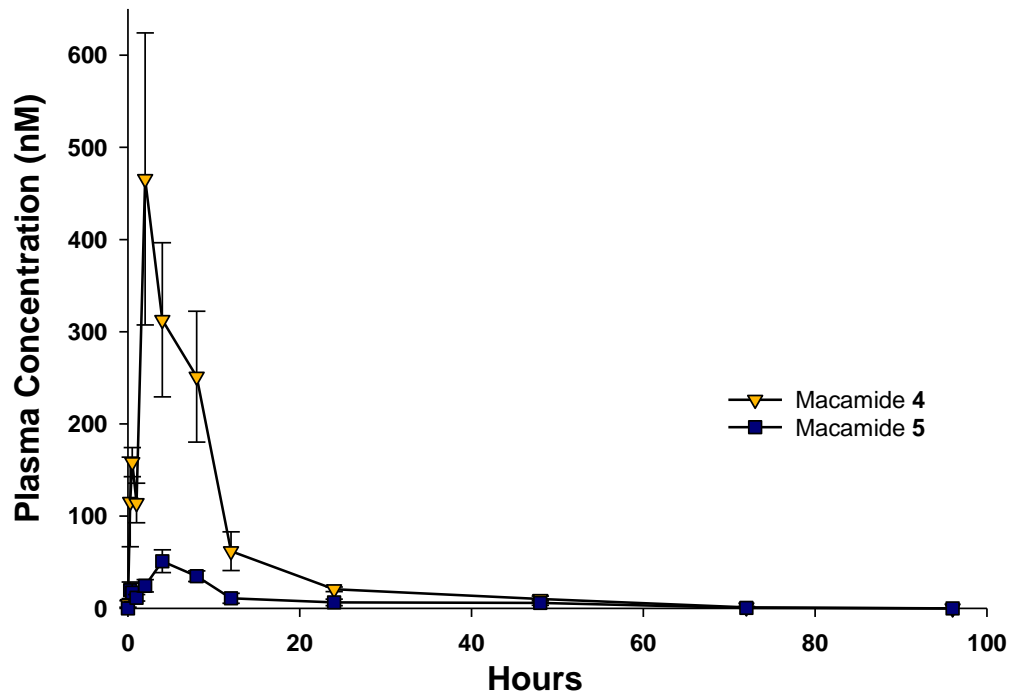


Figure S1. Pharmacokinetic study in rat: 96-hr time course for plasma concentrations of macamides **4** and **5**

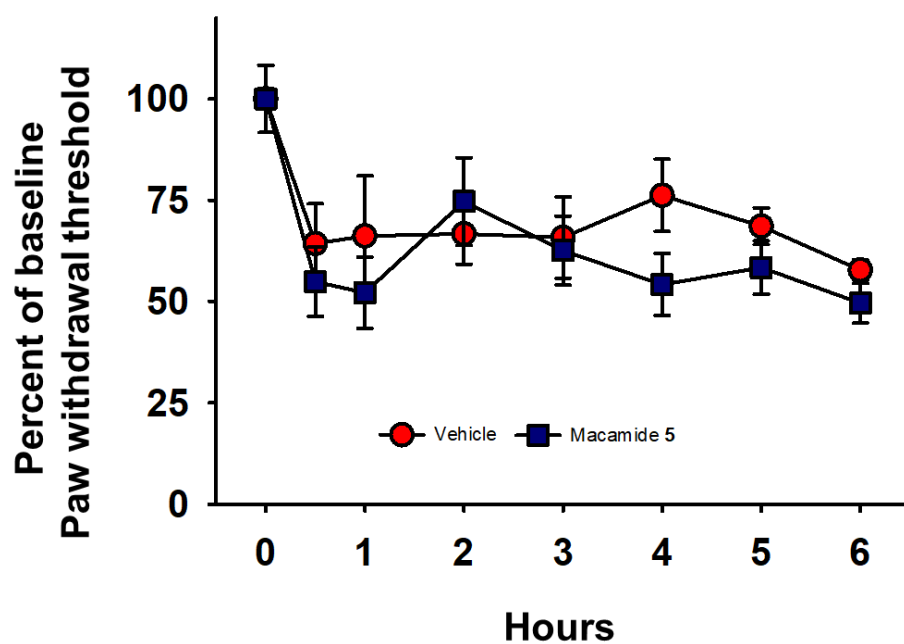


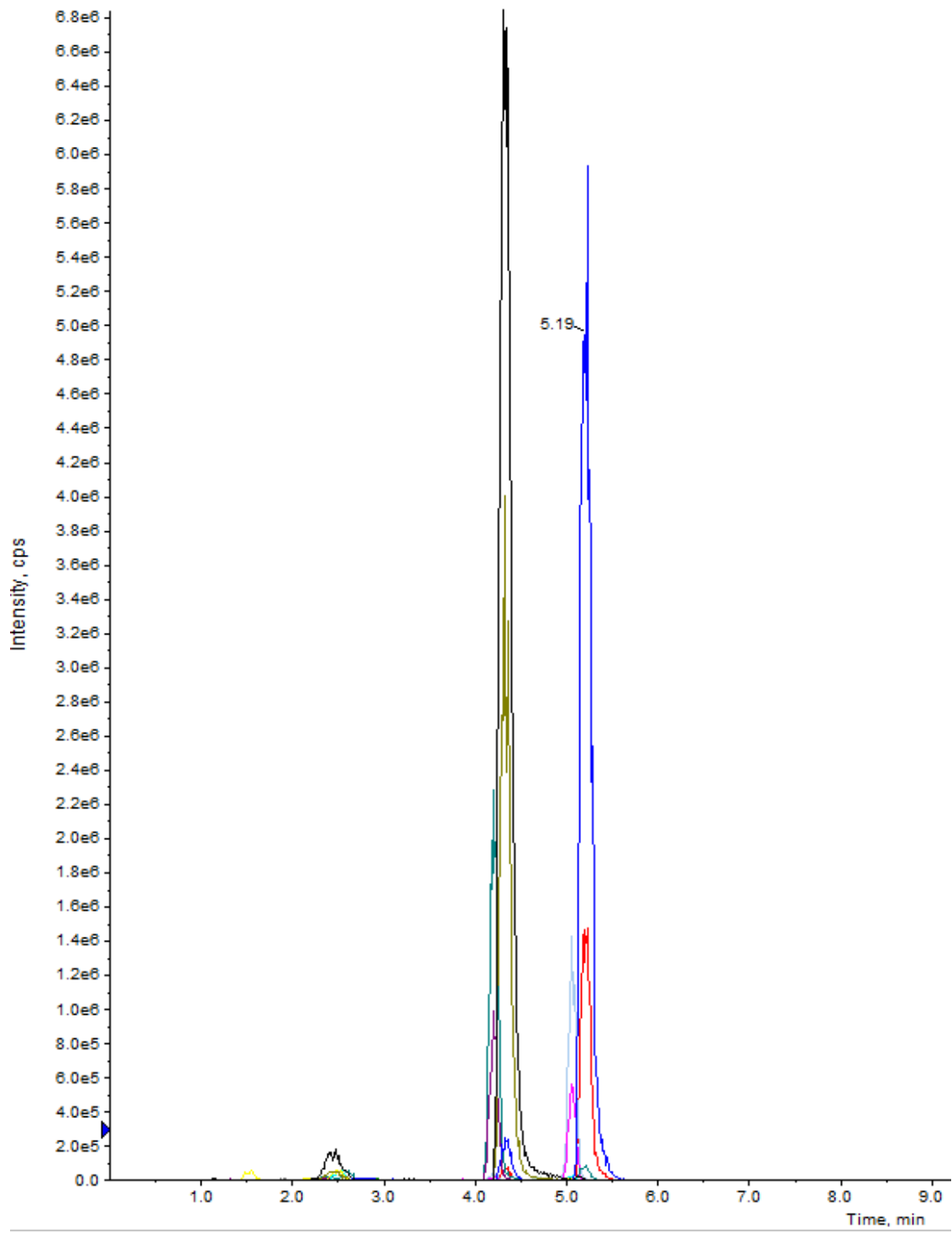
Figure S2. Analgesic efficacy of macamide **5** (100 mg/kg) against LPS induced inflammatory pain in rat was not statistically significant compared to the vehicle control. Scores are the mean \pm SEM reported as percent of baseline (normalized to 100%) calculated as the score \times 100/baseline score (Kruskal-Wallis One Way Analysis of Variance on Ranks, $\alpha=0.05$, $p=0.407$, $n=4$ /group)

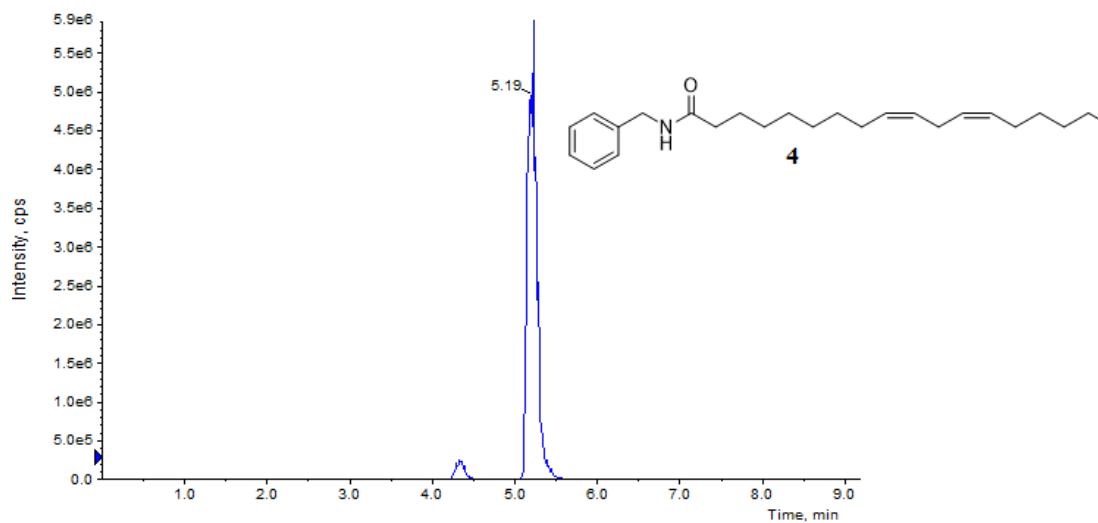
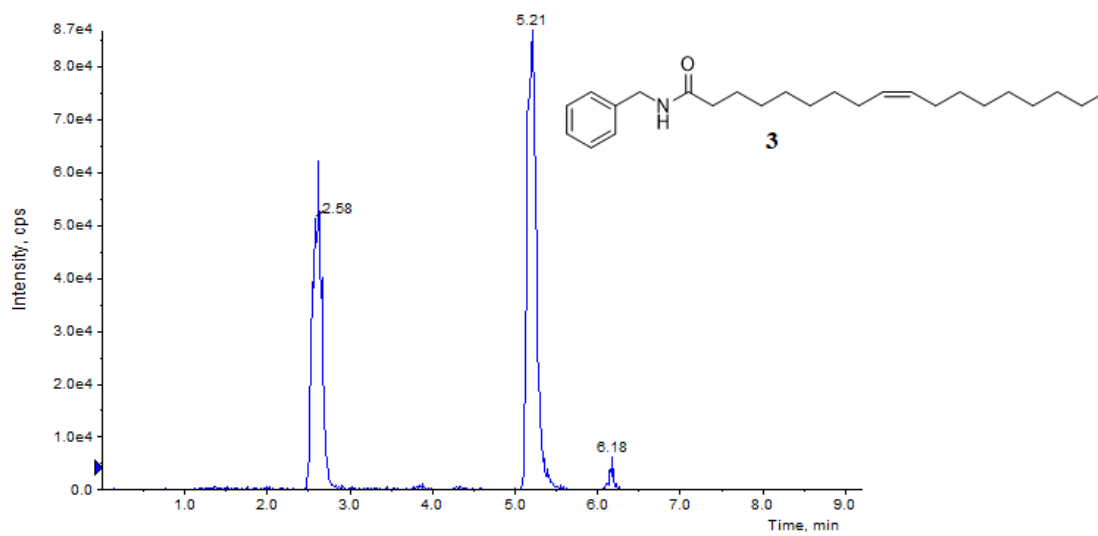
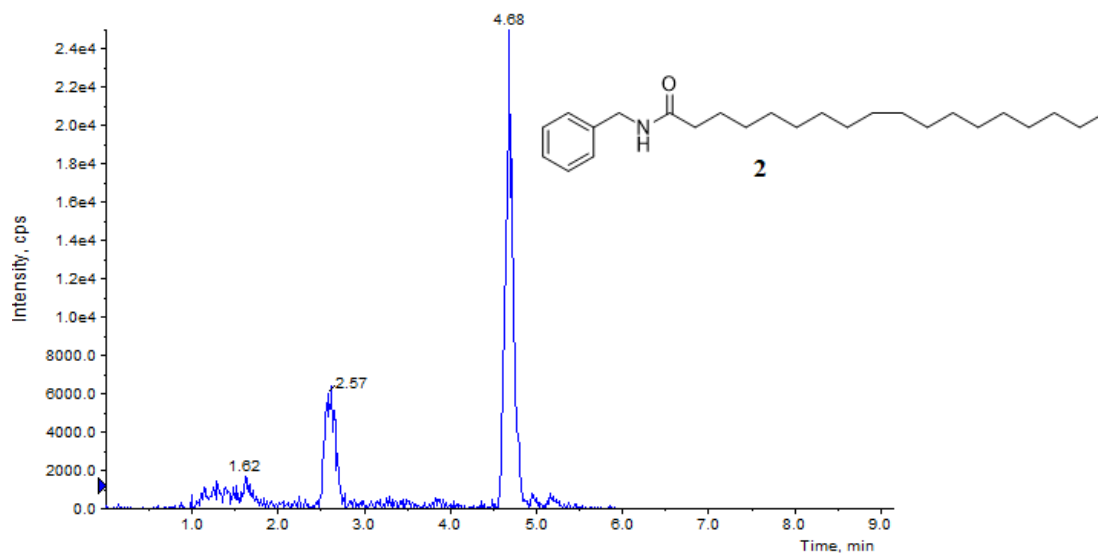
Table S4. Experimental and Literature IC₅₀ values of positive control, *t*-TUCB

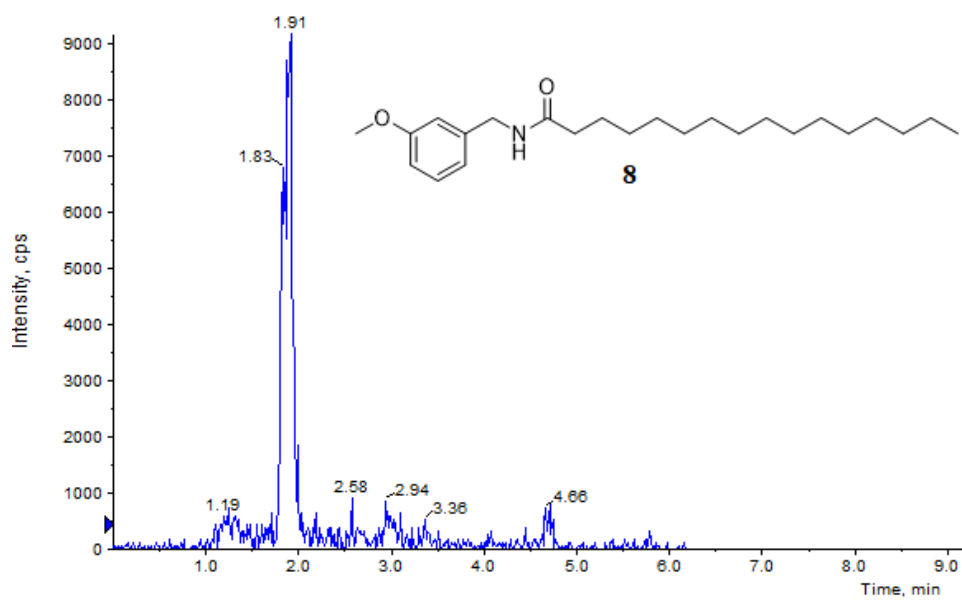
	hsEH IC ₅₀ (nM)	rsEH IC ₅₀ (nM)	msEH IC ₅₀ (nM)
Experimental	0.4	11	2.5
Literature	0.9	16	1.3

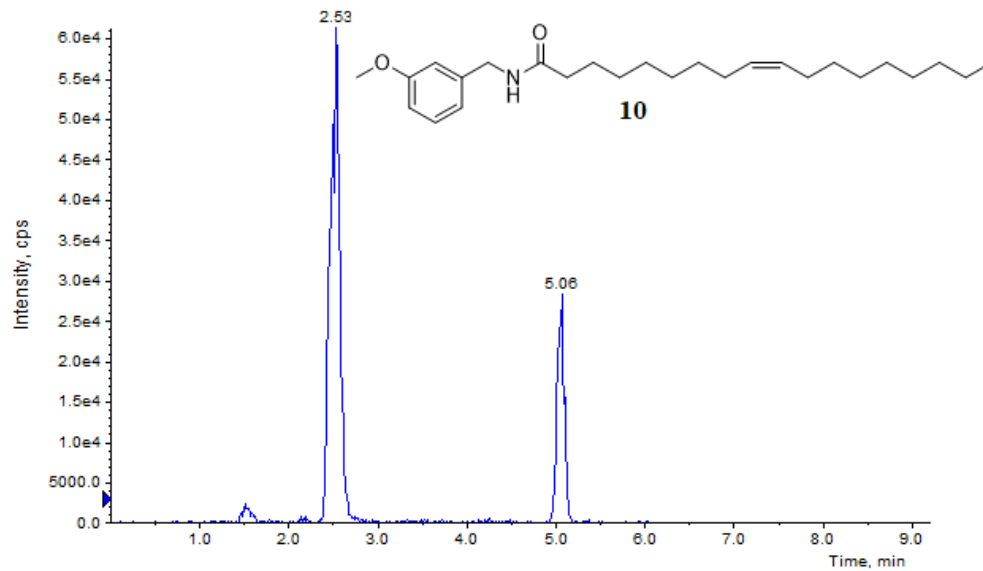
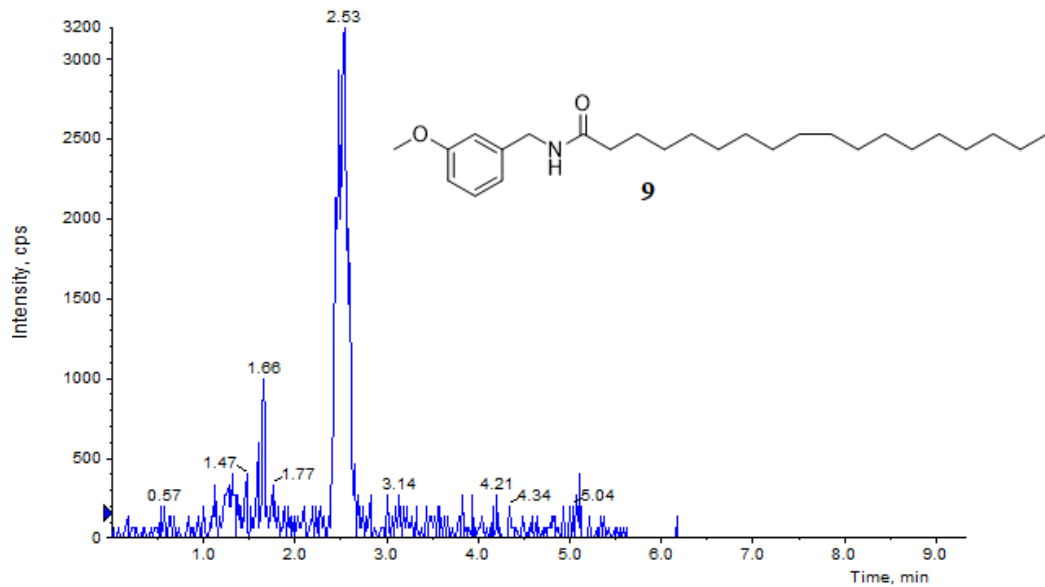
Table S5. Normalized efficiencies of macamide extraction procedures

ID	Hexanes: EtOH (7:1)/Ultrasonication (%)	Hexanes/Ultrasonication (%)	Hexanes/Soxhlet (%)
2	100	90.0	93.1
3	100	98.7	86.4
4	100	95.0	62.8
5	100	78.1	75.2
8	100	96.9	96.4
9	100	146	87.7
10	100	113	97.1
11	100	89.8	81.5
12	100	98.9	83.9









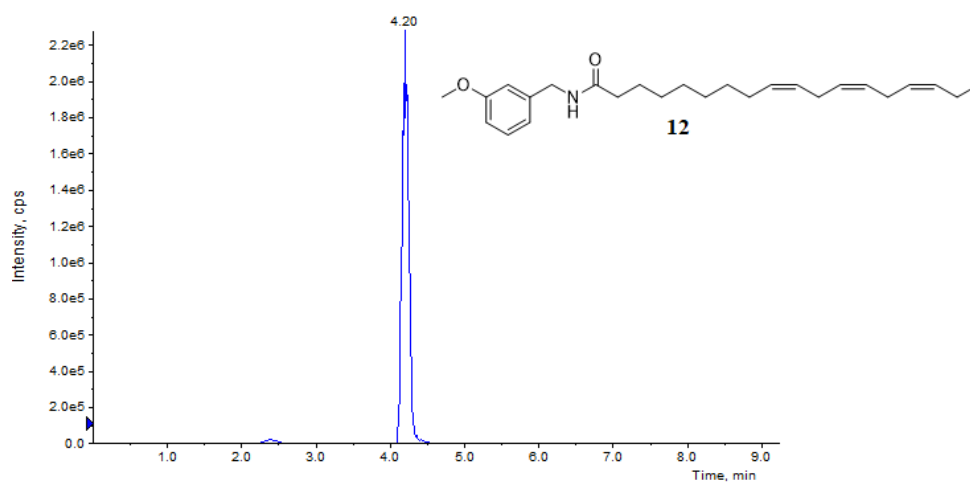
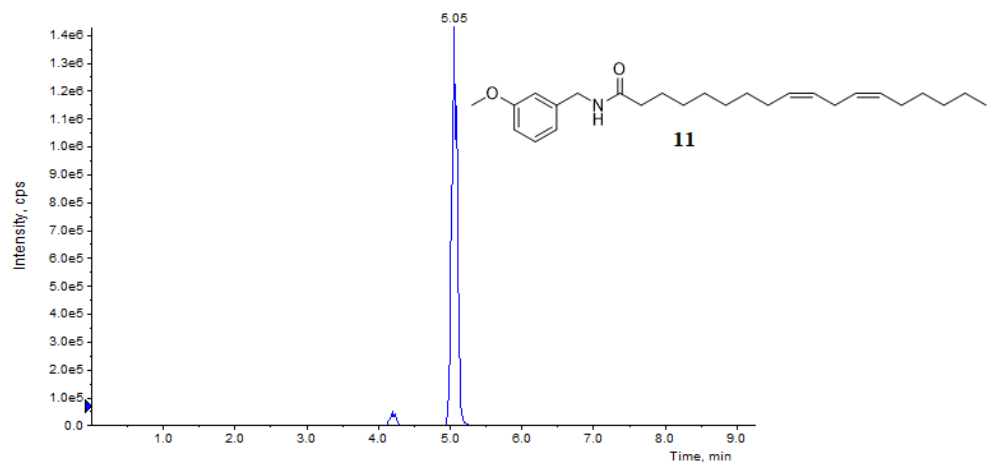
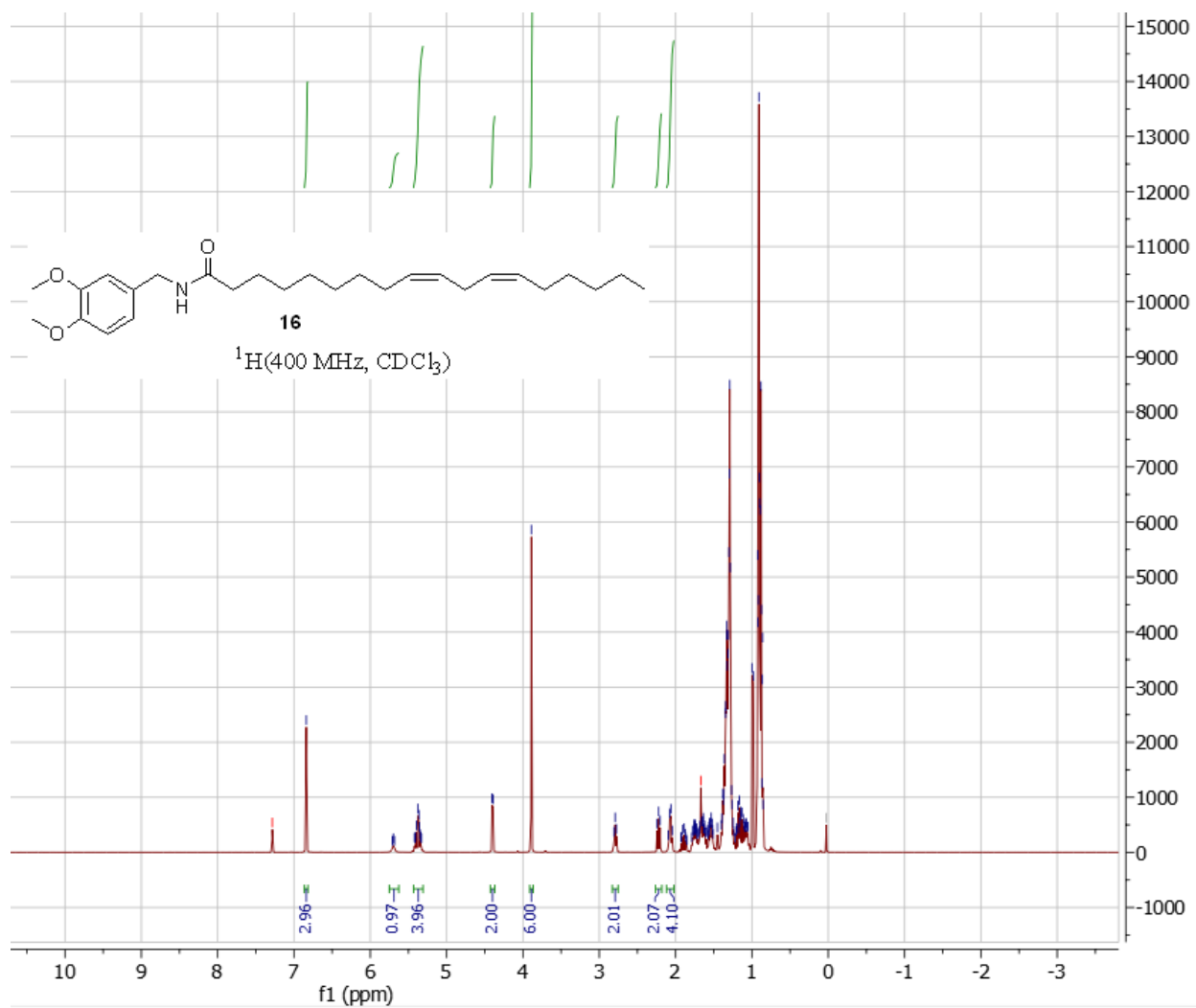
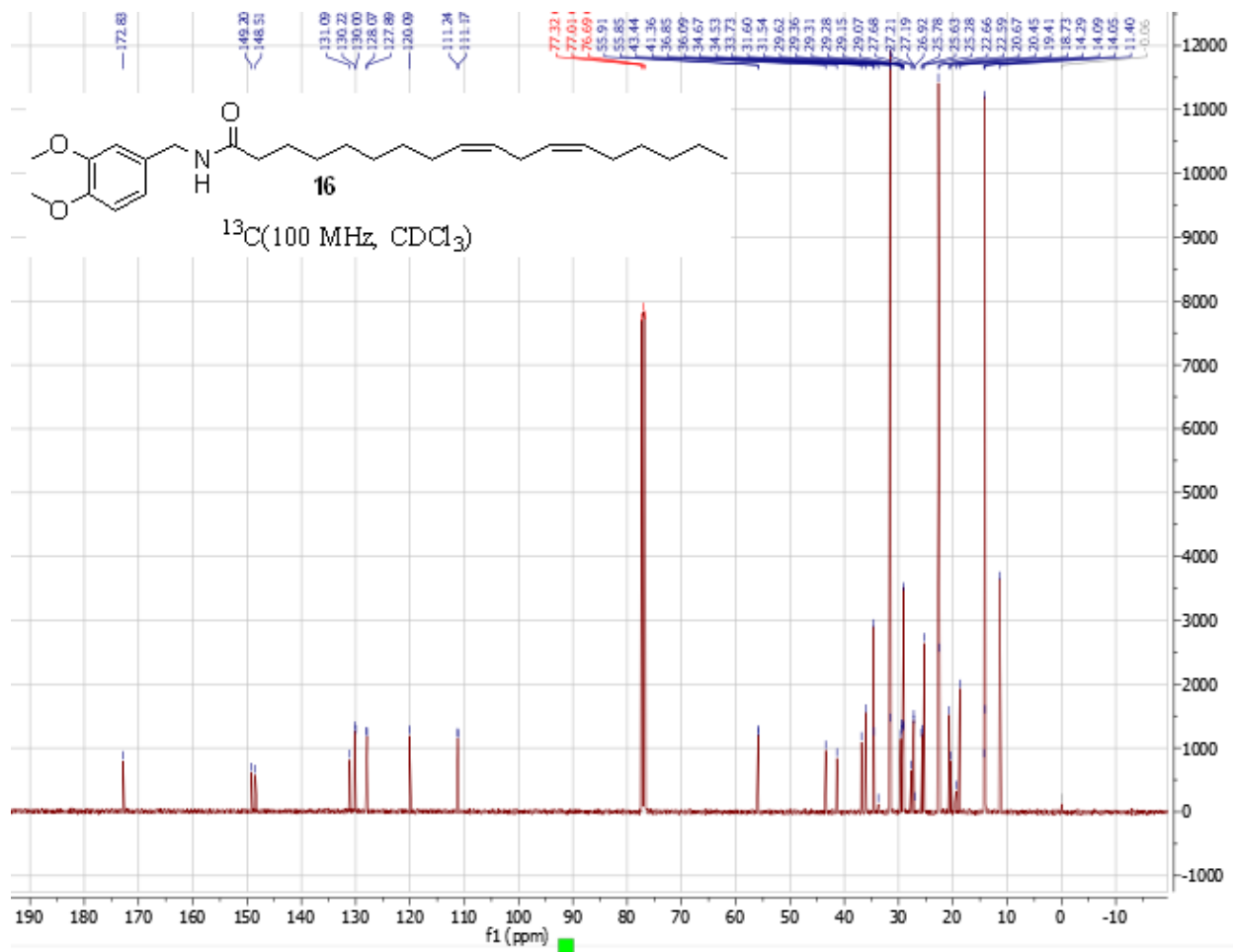
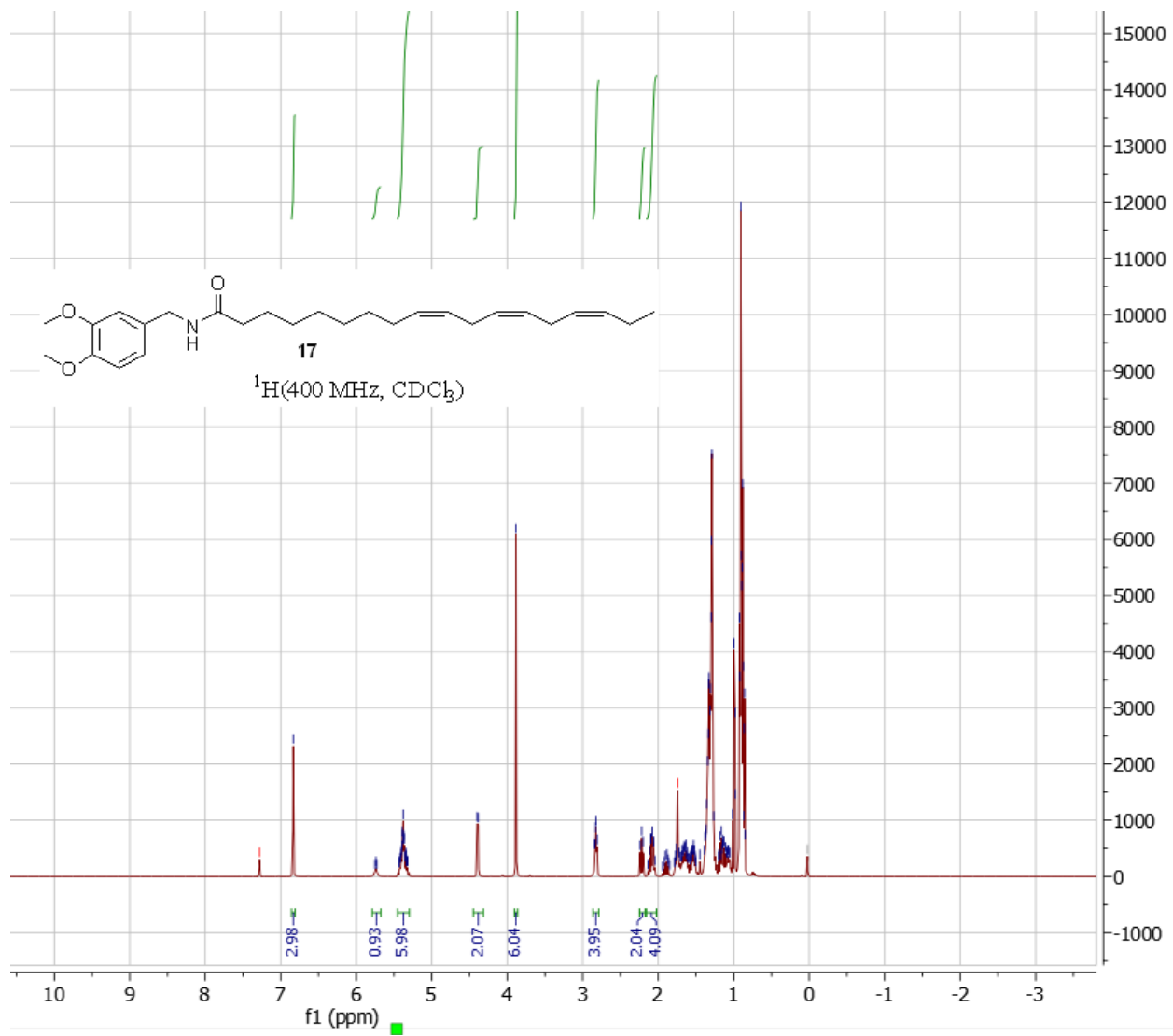


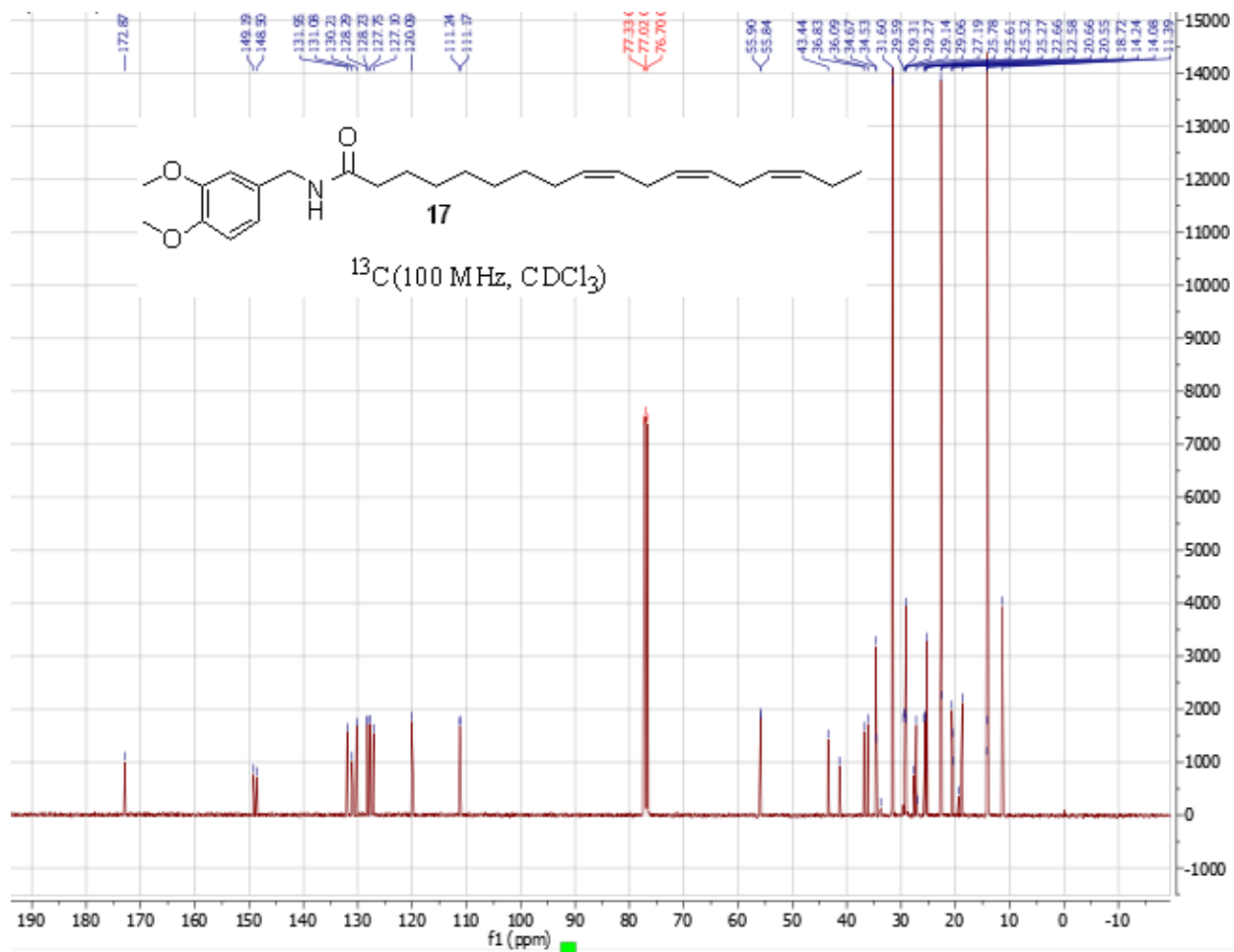
Figure S3. HPLC Trace of the extract of commercial *L. meyenii* product 2 and the known natural product macamides detected (**2-5**, **8-12**).

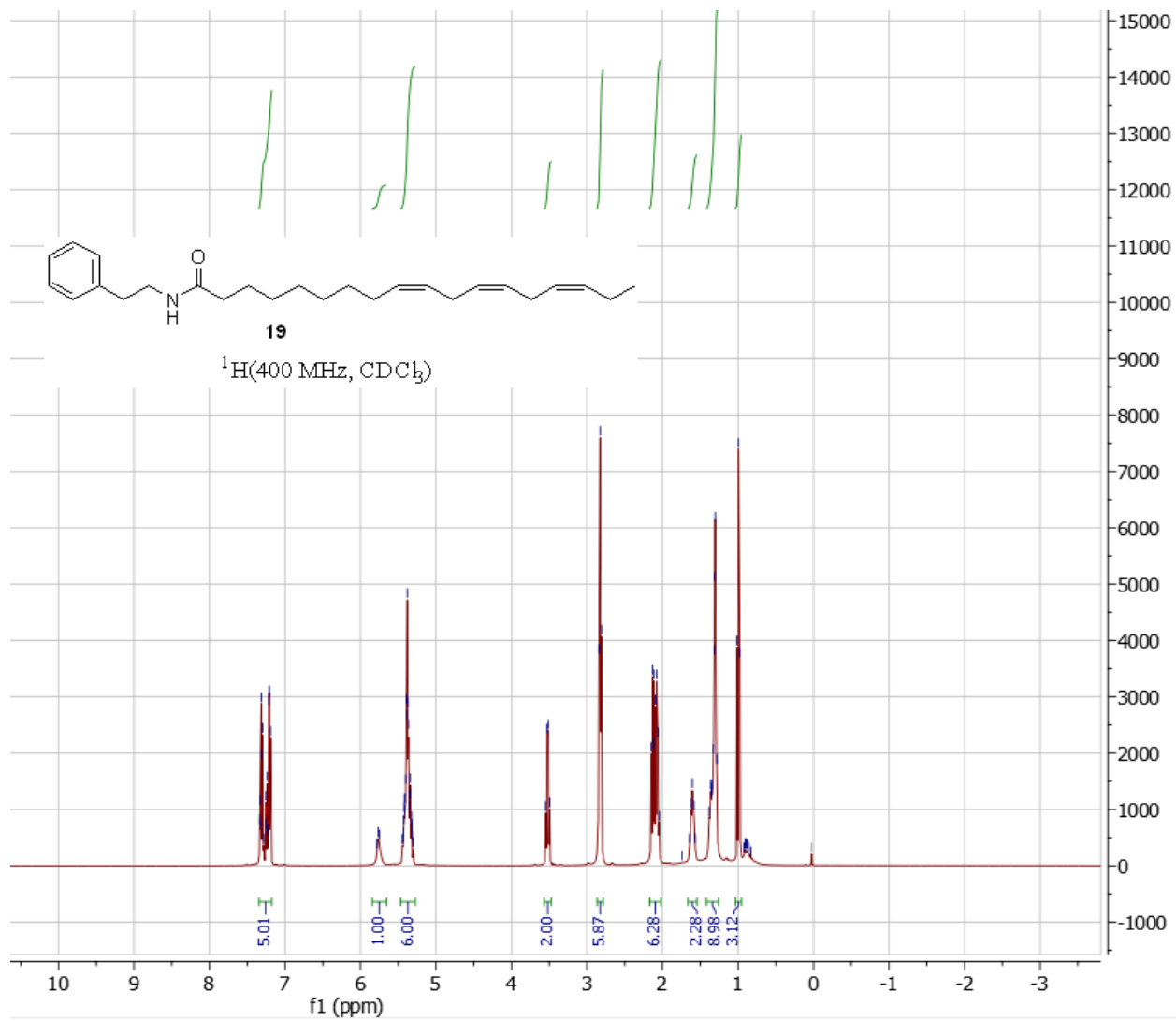
^1H and ^{13}C NMR Spectra of new compounds (**16**, **17** and **19**)

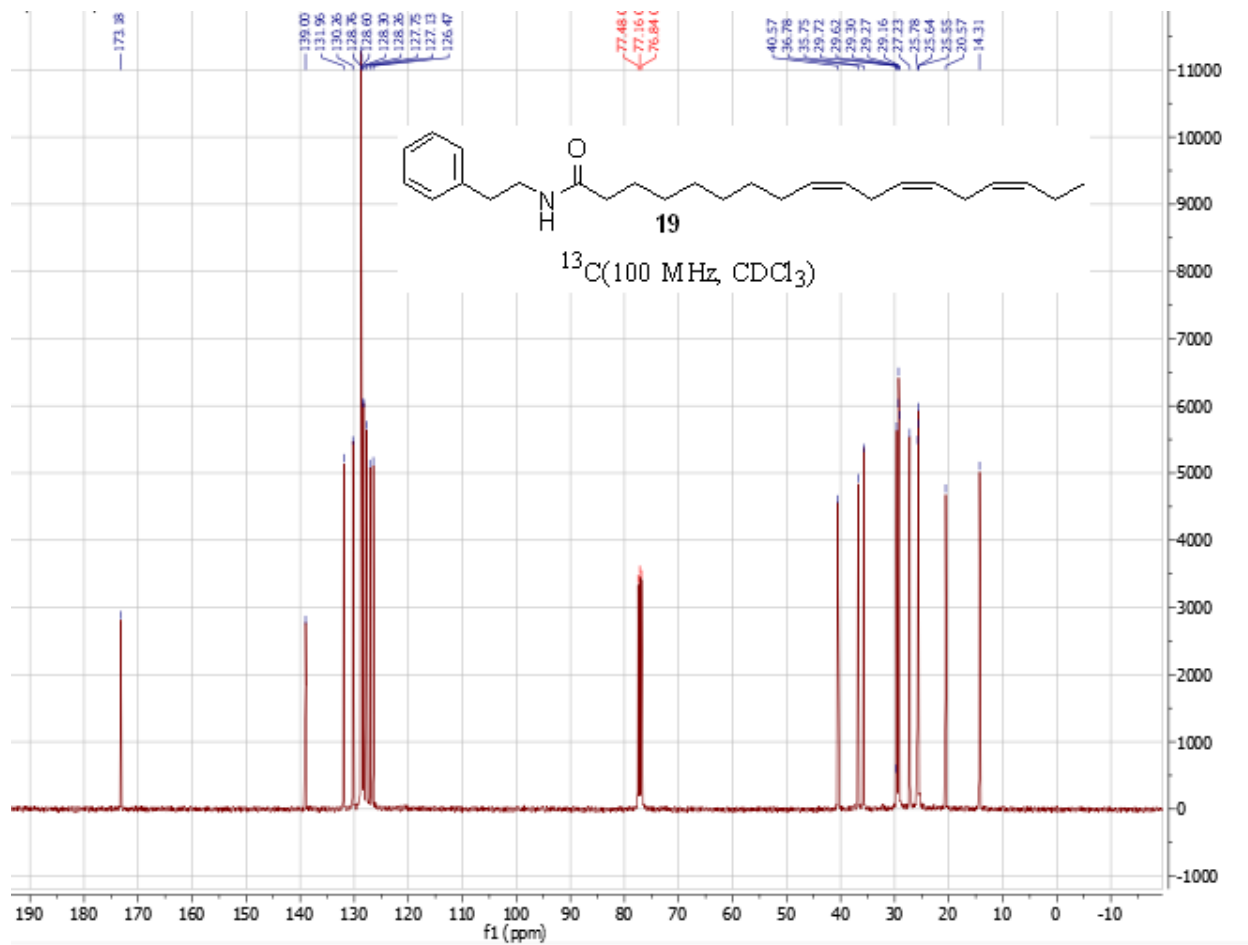












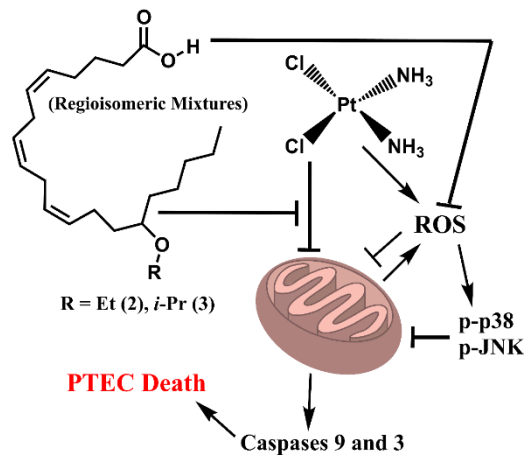
**Chapter 3: New Alkoxy- Analogues of Epoxyeicosatrienoic Acids Attenuate
Cisplatin Nephrotoxicity in vitro via Reduction of Mitochondrial Dysfunction,
Oxidative Stress, Mitogen-Activated Protein Kinase Signaling, and Caspase
Activation**

Nalin Singh,[†] Anders Vik,[§] Daniel B. Lybrand,[†] Christophe Morisseau,[†] and Bruce D.
Hammock^{†,*}

[†]Department of Entomology and Nematology and UC Davis Comprehensive Cancer Center,
University of California Davis, Davis, CA, 95616, United States

[§] Department of Pharmacy, Section for Pharmaceutical Chemistry, University of Oslo, PO Box
1068 Blindern, N-0316 Oslo, Norway

Table of Contents Graphic



ABSTRACT

Usage of cisplatin, a highly potent chemotherapeutic, is limited by its severe nephrotoxicity. Arachidonic acid (ARA)-derived epoxyeicosatrienoic acids (EETs) and soluble epoxide hydrolase (sEH) inhibitors were shown to ameliorate this dose-limiting side effect, but both approaches have some pharmacological limitations. Analogues of EETs are an alternative avenue with unique benefits, but the current series of analogues face concerns regarding their structure and mimetic functionality. Hence, in this study, regioisomeric mixtures of four new ARA alkyl-ethers were synthesized, characterized, and assessed as EET analogues against the concentration- and time-dependent toxicities of cisplatin in porcine proximal tubular epithelial cells. All four ether groups displayed bioisostere activity, ranging from marginal for methoxy- (**1**), good for *n*-propoxy- (**4**), and excellent for ethoxy- (**2**) and *i*-propoxy- (**3**). Compounds **2** and **3** displayed cytoprotective effects comparable to that of an EET regioisomeric mixture (**5**) against high, acute cisplatin exposures but were more potent against low to moderate, chronic exposures. Compounds **2** and **3** (and **5**) acted through stabilization of the mitochondrial transmembrane potential and attenuation of reactive oxygen species, leading to reduced phosphorylation of mitogen-activated protein kinases p38 and JNK and decreased activation of caspase-9 and -3. This study demonstrates that alkoxy- groups are potent and more metabolically stable bioisostere alternatives to the epoxide within EETs that enable sEH-independent activity. It also illustrates the potential of ether-based mimics of EETs and other epoxy fatty acids as promising nephroprotective agents to tackle the clinically relevant side effect of cisplatin, without compromising its antineoplastic function.

INTRODUCTION

cis-Diamminedichloroplatinum (II), commonly known as cisplatin (CDDP), is a potent inorganic antineoplastic agent that is widely used for treatment of several types of cancers.¹ However, it has many side effects, the most severe being dose-limiting nephrotoxicity.¹ Due to selective basolateral uptake, cisplatin is particularly damaging to the proximal tubules.² Mitochondrial disruptions,³ generation of reactive oxygen species (ROS),⁴ activation of mitogen-activated protein kinases (MAPKs),^{5,6} and recruitment of caspases⁷ are major implicated molecular modes of toxicity that lead to apoptosis of epithelial tubular cells. Currently, the lack of safe and efficacious therapeutic agents and impractical treatment alternatives make preserving kidney health during CDDP-based chemotherapy especially challenging. Since there is justified pressure on oncologists to administer higher levels of cisplatin to overcome drug resistance in tumors, therapeutics are urgently needed to mitigate its renal toxicity.

Cytochromes P450 (CYPs)-catalyzed epoxidation of polyunsaturated fatty acids (PUFAs) generates mono-epoxide lipid mediators known as epoxy fatty acids (EpFAs). ω -6 Arachidonic acid (ARA, 20:4)-derived epoxyeicosatrienoic acids (EETs) are the most widely studied group of EpFAs.⁸⁻¹⁰ EETs exhibit primarily tissue-healing and organ-protective activities but are hydrolyzed to less active vicinal diols by the soluble epoxide hydrolase (sEH). sEH inhibitors (sEHIs) stabilize endogenous levels of EETs, enhancing their bioavailability and facilitating their functions. EETs *in vitro* and the inhibition or knockout of sEH *in vivo* have been shown to attenuate cisplatin nephrotoxicity.¹¹⁻¹³ Thus, this pathway provides a novel and promising therapeutic target to manage the major side effects of cisplatin.

While administration of EETs and sEHIs are the two most common therapeutic approaches, both have certain disadvantages. sEH-mediated degradation of EETs occurs rapidly and hence

EETs are poorly bioavailable *in vivo* following most routes of administration. The activity of sEHIs is dependent on endogenous levels of EETs and other EpFAs. Therefore, under certain conditions of renal or cardiovascular dysfunction where release of membrane fatty acids or CYP metabolism is impaired, EET biosynthesis could be compromised, limiting efficacy of sEHIs. EET analogues (or mimics) are an alternative approach.^{14,15} They are designed to be more biologically stable than EETs and act independently of endogenous EET generation. Several potential EET analogues are being investigated and the most promising compounds have demonstrated therapeutic effects in multiple disease models. Some EET analogues have also been shown to ameliorate cisplatin nephrotoxicity *in vivo*.^{16,17}

However, many current EET analogues utilize classic sEHI pharmacophores (i.e., ureas and amides) as epoxide bioisosteres. For molecules where demonstrable mimetic function, verified in systems such as sEH-deficient mesenteric vessels,¹⁸ is absent, there is ensuing debate and uncertainty about their functionality as analogues (or dual-acting agents) as opposed to sEHIs. Furthermore, modified chain lengths and altered unsaturation sites in the fatty acid moieties of some of these analogues have raised questions about off-target effects and a diminished therapeutic index. Since an epoxide is a cyclic ether, linear or branched ethers are plausible alternative bioisosteres. Alkoxy groups would allow direct replacement of the epoxide with more metabolically stable functional groups and permit retention of the core molecular backbone. Incidentally, alkoxy groups were employed as epoxide bioisosteres in compounds mimicking the juvenile hormones (JHs) of insects, and these analogues have been utilized successfully for decades as potent growth regulators for pest control.^{19,20}

Thus, in this study, alkoxy-containing EET analogues were synthesized and characterized. Concentration- and time-dependent activities of bioisosteres were screened, relative to the

epoxide within EETs, against cisplatin toxicity in the porcine LLC-PK1 proximal tubular epithelial cell (PTEC) line, the standard in vitro model for PTECs. Furthermore, based on the molecular pathways of cisplatin kidney toxicity, the mechanism of therapeutic action for the most promising analogue series was investigated, namely stabilization of mitochondrial dysfunction, anti-oxidative stress action, reduced relative MAPK phosphorylation, and anti-caspase activation.

EXPERIMENTAL PROCEDURE

Reagents and Apparatus. *cis*-diamminedichloroplatinum (II) of 99.99% purity (trace metal basis) was purchased from Fisher Scientific Company LLC (Pittsburg, PA, USA). MTT (3-(4,5-dimethylthiazol-2-yl)-2,5-diphenyltetrazolium bromide) and CM-H₂DCFDA indicator were purchased from Life Technologies (Carlsbad, CA, USA). JC-10 dye, FCCP (Carbonyl cyanide-*p*-trifluoromethoxyphenylhydrazone), and MitoSOX Red indicator were purchased from Fisher Scientific. Primary antibodies against p38, phospho-p38, SAPK/JNK, and phospho-SAPK/JNK were purchased from Cell Signaling Technology (Danvers, MA, USA). Cyano(6-methoxynaphthalen-2-yl)methyl *trans*-[(3-phenyloxiran-2-yl)methyl] carbonate (CMNPC), WST-8 (CCK-8) cell proliferation assay kit, 14,15-EE-5(Z)-E (14,15-Epoxyeicosa-5(Z)-enoic Acid), and Ac-DEVD-AMC were purchased from Cayman Chemical Company (Ann Arbor, MI, USA). Ac-LEHD-pNa and Erythromycin (EM) were purchased from Millipore Sigma (St. Louis, MO, USA). *trans*-4-[4-(3-adamantan-1-yl-ureido)-cyclohexyloxy]-benzoic acid (*t*-AUCB) was generated in-house.²¹ Arachidonic acid methyl ester was purchased from Nu-Chek Prep, Inc. (Elysian, MN, USA). The reagents required for synthesis are commercially available and were purchased from one of the following vendors: Fisher Scientific, Millipore Sigma, or VWR

International (Radnor, PA, USA). All chemicals purchased from commercial sources were used as received without further purification. Analytical thin layer chromatography (TLC) was performed on Merck TLC silica gel 60 F₂₅₄ plates (Darmstadt, Germany) and spots were revealed via development with a potassium permanganate stain. Flash chromatography was performed on silica gel (230–400 Mesh, Grade 60) from Fisher Scientific. ¹H and ¹³C nuclear magnetic resonance (NMR) spectra were recorded on a 400 MHz Bruker Avance III HD Nanobay NMR spectrometer. Multiplicity is described by the abbreviations, s = singlet, t = triplet, m = multiplet. High resolution electrospray ionization mass spectrometry (HRESIMS) data were recorded on a Thermo Q-Exactive High-field Orbitrap mass spectrometer equipped with an electrospray ionization (ESI) source operating in positive ion mode. High-performance liquid chromatography-mass spectrometry (HPLC-MS) traces and product ion spectra (Figures S1-S5, Supporting Information) were recorded on an Agilent 1200 SL HPLC, coupled to a SCIEX 4000 Q-TRAP tandem mass spectrometer, equipped with an ESI source, and operating in positive ion mode. For HPLC-MS analyses, compounds **1-5** were injected onto a reverse-phase 2.1 x 150 mm 1.8- μ m Zorbax Eclipse C18 RRHT column, held at 50 °C. Mobile phase A was water with 0.1% glacial acetic acid (AA) and mobile phase B was acetonitrile with 0.1% glacial AA. A gradient elution was employed, and the chromatographic run was optimized to be 90 min for separation of peaks. Gradient conditions and MS source parameters are described in the Supporting Information (Tables S1, S2).

Synthesis and characterization of mono-ethers (1-4, regioisomeric mixtures) of arachidonic acid methyl ester. The general synthesis is illustrated with the representative ethoxyeicosatrienoic methyl esters (**2**). Arachidonic acid methyl ester (1.10 g, 3.45 mmol, 1.0 equiv.) was dissolved in ethanol (5 mL) and quickly added to a stirring solution of Hg(OAc)₂

(1.65 g, 5.18 mmol, 1.5 equiv.) in ethanol (12 mL). The mixture was stirred under nitrogen or argon overnight at room temperature. The mixture was then cooled to 0 °C (via ice bath), and a solution of NaBH₄ (0.26 g, 6.90 mmol, 2.0 equiv.) in water (10 mL) was slowly added. After stirring for 10 min, 10 drops of acetic acid were added, the stirring was stopped, and the solution was allowed to settle. The supernatant was collected, and the mercury precipitate was washed with ethanol (2 x 10 mL). The combined supernatant fractions were concentrated in vacuo, reconstituted in hexanes (20 mL) and saturated aq. NaHCO₃ (15 mL), after which the organic layer was isolated. The aqueous layer was extracted with hexanes (3 x 10 mL). The combined organic layers were washed once with aq. NaHCO₃, dried (MgSO₄), and concentrated in vacuo. The crude mixture was reconstituted in hexanes and, by monitoring fractions with TLC, purified using flash chromatography (ethyl acetate-hexanes 4:96 → 8:92) to yield the mono-ethyl-ethers of arachidonic acid methyl ester. Compound structures of **1-4** were consistent with the acquired ¹H NMR spectra, including ratios of olefinic protons, ether protons, and other indicator peaks (e.g., methyl ester, terminal methyl) on integration. Observed high resolution *m/z* of adduct ions concurred with calculated values. Relative retention times were also consistent with the polarity of the corresponding alkoxy- substituent.

Compounds **1-4** are complex mixtures expected to contain eight possible regioisomers as the alkoxy- group can be inserted at one of two positions across each of the four ARA olefins. Furthermore, every regioisomer would possess a chiral center, suggesting sixteen potential stereoisomers. Hence, HPLC-MS traces predictably revealed multiple peaks of the parent *m/z* that eluted as a group within a narrow time window. Similarly, the number of peaks detected by ¹³C NMR for **1-4** exceeded the number of carbons present within an individual isomer of a group. Slight differences in chemical shifts for an equivalent carbon in different regioisomers

would account for these “duplicate” or “triplicate” peaks since the position of the carbon in question varies depending on specific molecule.

Methoxyeicosatrienoic methyl esters (1, regioisomer mixture). Yield 9% (112 mg); Colorless oil; ^1H NMR (400 MHz, CDCl_3) δ 5.46-5.36 (6H, m, **vinyllic**), 3.69 (3H, s, **CO₂Me**), 3.37 (3H, s, **OMe**) 3.24-3.14 (1H, m), 2.85-2.78 (3H, m), 2.37-2.21 (3H, m), 2.17-2.02 (4H, m), 1.75-1.67 (2H, m), 1.58-1.45 (3H, m), 1.42-1.26 (7H, m), 0.91 (3H, t, $J = 7.2$ Hz, **Me**); ^{13}C NMR (100 MHz, CDCl_3) δ 174.1, 132.1, 130.5, 130.5, 130.4, 130.4, 130.1, 130.0, 129.9, 129.8, 129.7, 129.5, 129.5, 129.2, 129.2, 129.1, 128.9, 128.9, 128.9, 128.6, 128.5, 128.4, 128.2, 128.2, 128.2, 128.1, 127.9, 127.8, 127.8, 127.6, 127.5, 126.4, 126.0, 125.8, 125.7, 125.4, 125.1, 80.9, 80.6, 80.4, 80.3, 80.2, 80.2, 79.9, 56.6, 56.6, 56.5, 56.4, 51.5, 33.6, 33.6, 33.6, 33.5, 33.5, 33.5, 33.4, 33.3, 32.1, 31.9, 31.6, 31.5, 31.1, 31.1, 31.0, 31.0, 29.5, 29.4, 29.4, 29.3, 29.3, 27.4, 27.2, 27.2, 27.2, 26.6, 26.6, 25.8, 25.8, 25.6, 25.6, 25.6, 24.9, 24.8, 24.8, 23.2, 23.2, 23.1, 23.1, 22.7, 22.6, 22.6, 14.1, 14.1; HRESIMS observed m/z 373.2738 $[\text{M} + \text{Na}]^+$ (calculated m/z for $\text{C}_{22}\text{H}_{38}\text{NaO}_3^+$, 373.2719); HPLC-MS observed multiple peaks of m/z 351 $[\text{M} + \text{H}]^+$ ($\text{C}_{22}\text{H}_{39}\text{O}_3^+$), retention times (t_R) 39.2 - 41.5 min

Ethoxyeicosatrienoic methyl esters (2, regioisomer mixture). Yield 22% (280 mg); Colorless oil; ^1H NMR (400 MHz, CDCl_3) δ 5.43-5.33 (6H, m, **vinyllic**), 3.66 (3H, s, **CO₂Me**), 3.60-3.39 (2H, m, **O-CH₂**) 3.30-3.20 (1H, m), 2.81-2.77 (3H, m), 2.34-2.21 (3H, m), 2.14-2.00 (4H, m), 1.74-1.66 (2H, m), 1.57-1.43 (3H, m), 1.40-1.26 (7H, m), 1.21-1.18 (3H, m, **CH₃-CH₂-O**), 0.89 (3H, t, $J = 7.0$ Hz, **Me**); ^{13}C NMR (100 MHz, CDCl_3) δ 174.0, 131.9, 130.3, 130.2, 130.1, 129.9, 129.6, 129.5, 129.3, 129.2, 129.1, 128.9, 128.9, 128.8, 128.7, 128.6, 128.4, 128.1, 128.0, 127.9, 127.8, 127.8, 127.6, 125.9, 125.3, 78.7, 78.6, 78.5, 78.4, 64.4, 64.3, 64.2, 64.1, 51.4, 34.1, 34.1, 34.0, 34.0, 33.5, 33.4, 33.4, 32.0, 31.9, 31.8, 31.8, 31.7, 31.5, 31.5, 29.4, 29.3, 29.3, 29.2, 27.4,

27.2, 27.2, 27.1, 26.7, 26.6, 26.5, 25.8, 25.7, 25.6, 25.6, 25.6, 25.5, 25.0, 24.8, 24.7, 23.3, 23.3, 23.2, 22.7, 22.6, 22.5, 15.7, 15.6, 14.1, 14.0; HRESIMS observed m/z 387.2900 [M + Na]⁺ (calculated m/z for C₂₃H₄₀NaO₃⁺, 387.2875); HPLC-MS observed multiple peaks of m/z 365 [M + H]⁺ (C₂₃H₄₁O₃⁺), t_R 51.2 - 54.1 min

i-Propoxyeicosatrienoic methyl esters (**3**, regioisomer mixture). Yield 16% (210 mg); Colorless oil; ¹H NMR (400 MHz, CDCl₃) δ 5.44-5.33 (6H, m, **vinyllic**), 3.67 (3H, s, **CO₂Me**), 3.64-3.59 (1H, m, **O-CH**), 3.36-3.27 (1H, m), 2.84-2.77 (3H, m), 2.34-2.21 (3H, m), 2.14-2.03 (4H, m), 1.73-1.67 (2H, m), 1.52-1.42 (3H, m), 1.38-1.26 (7H, m), 1.16-1.12 (6H, m, **(CH₃)₂-CH-O**), 0.89 (3H, t, $J = 7.4$ Hz, **Me**); ¹³C NMR (100 MHz, CDCl₃) δ 174.0, 130.4, 130.2, 130.2, 129.4, 128.9, 128.9, 128.8, 128.8, 128.8, 128.7, 128.5, 128.3, 128.2, 128.1, 128.0, 127.8, 127.8, 127.7, 127.7, 127.6, 127.5, 125.5, 76.7, 76.4, 76.2, 69.7, 69.7, 69.6, 69.6, 69.4, 51.4, 51.4, 34.7, 34.7, 34.6, 33.5, 33.4, 32.7, 32.7, 32.6, 32.1, 31.6, 31.5, 31.5, 29.4, 29.3, 29.3, 27.4, 27.2, 27.2, 26.6, 26.6, 26.5, 25.8, 25.8, 25.7, 25.6, 25.6, 25.5, 25.2, 24.8, 24.7, 23.4, 23.4, 23.3, 23.2, 23.1, 23.1, 23.0, 22.9, 22.9, 22.7, 22.6, 22.6, 22.5, 14.1, 14.0; HRESIMS observed m/z 401.3049 [M + Na]⁺ (calculated m/z for C₂₄H₄₂NaO₃⁺, 401.3032); HPLC-MS observed multiple peaks of m/z 379 [M + H]⁺ (C₂₄H₄₃O₃⁺), t_R 61.3 - 65.4 min

n-Propoxyeicosatrienoic methyl esters (**4**, regioisomer mixture). Yield 2% (10 mg); Colorless oil; ¹H NMR (400 MHz, CDCl₃) δ 5.46-5.36 (6H, m, **vinyllic**), 3.69 (3H, s, **CO₂Me**), 3.52-3.22 (3H, m, **H₂C-O-CH**), 2.85-2.78 (3H, m), 2.35-2.22 (3H, m), 2.18-2.01 (4H, m), 1.76-1.69 (2H, m), 1.62-1.48 (4H, m), 1.39-1.27 (8H, m), 0.97-0.86 (6H, m, **Me**); ¹³C NMR (100 MHz, CDCl₃) δ 174.1, 131.8, 130.4, 130.3, 130.3, 130.2, 129.9, 129.2, 129.1, 128.9, 128.8, 128.7, 128.6, 128.4, 128.2, 128.0, 127.9, 127.8, 127.5, 126.3, 125.7, 125.3, 78.9, 78.8, 78.7, 78.6, 70.9, 70.8, 70.6, 51.4, 34.2, 34.1, 34.0, 34.0, 34.0, 33.9, 33.5, 33.5, 33.4, 32.0, 31.9, 31.8, 31.7, 31.7, 31.7, 31.6,

31.5, 29.7, 29.5, 29.4, 29.3, 29.3, 27.4, 27.3, 27.2, 26.8, 26.6, 26.5, 25.8, 25.8, 25.6, 25.5, 25.1, 24.8, 24.7, 23.5, 23.4, 23.3, 23.3, 23.2, 23.2, 22.7, 22.6, 22.5, 14.1, 14.0, 10.8, 10.7; HRESIMS observed m/z 401.3026 $[M + Na]^+$ (calculated m/z for $C_{24}H_{42}NaO_3^+$, 401.3032); HPLC-MS observed multiple peaks of m/z 379 $[M + H]^+$ ($C_{24}H_{43}O_3^+$), t_R 68.3 - 71.7 min

Synthesis of mono-epoxides (5**, regioisomeric mixture) of arachidonic acid methyl ester.**

Arachidonic acid methyl ester (1.10 g, 3.45 mmol, 1.0 equiv.) was dissolved in dichloromethane (DCM, 2 mL) and quickly added to a vigorously stirring solution of 70% *meta*-chloroperoxybenzoic acid (171 mg, 0.69 mmol, 0.20 equiv.) in DCM (30 mL). The reaction was stirred for 90 min at room temperature and quenched with saturated aq. Na_2CO_3 . The mixture was extracted with diethyl ether (4 x 10 mL), dried ($MgSO_4$), and concentrated in vacuo. The crude mixture was reconstituted in hexanes and, by monitoring fractions with TLC, purified using flash chromatography (ethyl acetate-hexanes 5:95 \rightarrow 10:90) to yield the mono-epoxides of arachidonic acid methyl ester.

Epoxyeicosatrienoic methyl esters (**5**, regioisomer mixture). Yield 88% (204 mg); Colorless oil; 1H NMR (400 MHz, $CDCl_3$) δ 5.55-5.38 (6H, m, **vinyllic**), 3.70 (3H, s, **CO₂Me**), 2.99-2.95 (2H, m), 2.87-2.82 (3H, m), 2.46-2.22 (5H, m), 2.16-2.05 (3H, m), 1.78-1.69 (3H, m), 1.38-1.28 (6H, m), 0.91 (3H, t, $J = 7.0$ Hz, **Me**); ^{13}C NMR (100 MHz, $CDCl_3$) δ 174.1, 132.9, 131.4, 131.0, 130.6, 130.4, 129.2, 129.0, 128.8, 128.5, 127.8, 125.0, 124.6, 124.4, 124.0, 123.6, 57.2, 56.4, 51.5, 33.4, 31.7, 31.5, 29.2, 27.8, 27.4, 27.2, 26.8, 26.6, 26.3, 26.2, 25.8, 25.6, 24.8, 22.6, 22.5, 14.1, 14.0; HRESIMS observed m/z 357.2429 $[M + Na]^+$ (calculated m/z for $C_{21}H_{34}NaO_3^+$, 357.2406); HPLC-MS observed multiple peaks of m/z 335 $[M + H]^+$ ($C_{21}H_{35}O_3^+$), t_R 22.0 - 24.4 min. Individual yields of 14,15-, 11,12-, 8,9-, and 5,6-EET methyl ester were 68 mg, 54 mg, 48

mg, and 34 mg, respectively, as per the corresponding regioisomeric ratio of 2.0:1.6:1.4:1.0 in the mixture.

The methyl esters of the ARA alkyl-ethers and epoxide were employed as the prodrug for therapeutic applications in cells, due to their chemical and pharmacological advantages over the carboxylic acid form.²² Stock solutions were prepared in ethanol, flushed with nitrogen or argon, and stored at -80 °C for long term use.

Soluble Epoxide Hydrolase Inhibition Assay. Purified, recombinant human sEH (hsEH) was obtained utilizing a baculovirus expression system and affinity chromatography,²³ and the inhibition assay was performed as previously described.²⁴ Briefly, a fluorometric assay that measures hydrolysis of the nonfluorescent sEH substrate CMNPC (5 μ M) to the fluorescent 6-methoxynaphthaldehyde, in the presence of different concentrations of compounds **1-5**, was employed. Fluorescence was measured at $\lambda_{\text{Ex}}/\lambda_{\text{Em}} = 330 \text{ nm}/465 \text{ nm}$ using a Molecular Devices M2 microplate reader, and the respective IC₅₀ values (μ M) against the hsEH were derived.

Cell Cultures. Porcine kidney proximal tubular epithelial cells (LLC-PK1) and human liver hepatocellular carcinoma (HepG2) cells were purchased from American Type Culture Collection (Manassas, VA, USA). LLC-PK1 cells were cultured in M199 medium, supplemented with 10% fetal bovine serum (FBS) and 1% penicillin-streptomycin (PS). HepG2 cells were cultured in Dulbecco's Modified Eagle Medium, supplemented with 10% FBS and 1% PS. Cultures were maintained in a humidified incubator at 37 °C, under an atmosphere of 5% CO₂/95% air.

MTT Cell Viability Assay. LLC-PK1 or HepG2 cells were seeded in sterile, transparent 96-well microplates at a density of 1×10^4 cells/well and incubated overnight. In general, cells were pre-treated for 1 h, in the presence or absence of 14,15-EE-5(Z)-E (3 μ M), with the vehicle

(EtOH), ARA methyl ester (0.1-10 μM), alkoxy-ARA methyl ester (0.1-10 μM , regioisomeric mixture) with or without EM (20 μM), or EET methyl ester (0.1-10 μM , regioisomeric mixture) with or without *t*-AUCB (10 μM). This was followed by exposure to cisplatin (5-20 μM) or culture media for 24-120 h. Following treatment regimens, the cell media was replaced with 100 μL /well of fresh media containing the MTT reagent (0.5 mg/mL) and incubated for 4 h in the cell culture incubator. The MTT solution was aspirated, 150 μL /well of 4 mM HCl in isopropanol was added, and plates were shaken for 15 min to dissolve the formazan crystals. Finally, absorbance was read at $\lambda_{\text{Abs}} = 570$ nm using a Molecular Devices M2 microplate reader.

CCK-8 Cell Proliferation Assay. LLC-PK1 or HepG2 cells were seeded in sterile, transparent 96-well microplates at a density of 1×10^4 cells/well and incubated overnight. Cells were then pre-treated for 1 h with the vehicle (EtOH), alkoxy-ARA methyl ester (1 μM , regioisomeric mixture), or EET methyl ester (1 μM , regioisomeric mixture), followed by exposure to cisplatin (20 μM) for 24 h. The CCK-8 assay was then conducted as per the manufacturer's instructions. Briefly, 10 μL of the CCK-8 working solution was added to the 100 μL /well cultures, plates were gently shaken for 1 min, and incubated for 2 h in the cell culture incubator. After 1 min of gentle shaking, absorbance was read at $\lambda_{\text{Abs}} = 450$ nm using a Molecular Devices M2 microplate reader.

JC-10 Mitochondrial Transmembrane Potential Assay. LLC-PK1 cells were seeded in sterile, clear-bottom black 96-well microplates at a density of 1×10^4 cells/well and incubated overnight. Cells were pre-treated for 1 h with the vehicle (EtOH), alkoxy-ARA methyl ester (1 μM , regioisomeric mixture), or EET methyl ester (1 μM , regioisomeric mixture), followed by exposure to cisplatin (20 μM) or culture media for 6, 24, or 48 h. Cells were then washed once with the wash solution (Hanks' Balanced Salt Solution with Ca^{2+} , Mg^{2+} , 0.1% Pluronic F-68). 10

μM JC-10 dye (in wash solution) was added (under dark) and cells were incubated for 1 h in the cell culture incubator. After cells were washed twice, 100 μL /well of wash solution was added and fluorescence was immediately read at $\lambda_{1\text{Ex}}/\lambda_{1\text{Em}} = 492 \text{ nm}/575 \text{ nm}$ (red aggregates) and $\lambda_{2\text{Ex}}/\lambda_{2\text{Em}} = 492 \text{ nm}/525 \text{ nm}$ (green monomers) using a Tecan Infinite Pro microplate reader. The ratio of red to green fluorescence was used as a measure of the mitochondrial transmembrane potential. FCCP (10 μM), a potent uncoupler of oxidative phosphorylation, was utilized as a positive control for the loss of mitochondrial membrane potential.

CM-H₂DCFDA General Reactive Oxygen Species Quantitation Assay. LLC-PK1 cells were seeded in sterile, clear-bottom black 96-well microplates at a density of 1×10^4 cells/well and incubated overnight. Cells were pre-conditioned with 5 μM CM-H₂DCFDA for 30 min in the cell culture incubator and washed thrice with phosphate buffered saline (PBS). Cells were then pre-treated for 1 h with the vehicle (EtOH), alkoxy-ARA methyl ester (1 μM , regioisomeric mixture), or EET methyl ester (1 μM , regioisomeric mixture), followed by exposure to cisplatin (20 μM) for 24 h. After cells were washed twice with PBS, 100 μL /well of PBS was added and fluorescence was immediately measured at $\lambda_{\text{Ex}}/\lambda_{\text{Em}} = 485 \text{ nm}/535 \text{ nm}$ using a Tecan Infinite Pro microplate reader.

MitoSOX Red Mitochondrial Superoxide Detection Assay. LLC-PK1 cells were seeded in sterile, clear-bottom black 96-well microplates at a density of 1×10^4 cells/well and incubated overnight. Cells were pre-conditioned with 2.5 μM MitoSOX Red for 10 min in the cell culture incubator and washed thrice with PBS. Cells were then pre-treated for 1 h with the vehicle (EtOH), alkoxy-ARA methyl ester (1 μM , regioisomeric mixture), or EET methyl ester (1 μM , regioisomeric mixture), followed by exposure to cisplatin (20 μM) for 24 h. After cells were

washed twice with PBS, 100 μ L/well of PBS was added and fluorescence was immediately measured at $\lambda_{Ex}/\lambda_{Em} = 510 \text{ nm}/580 \text{ nm}$ using a Tecan Infinite Pro microplate reader.

Western Blotting for Mitogen-Activated Protein Kinases. LLC-PK1 cells were seeded in sterile 6-well plates at a density of 3×10^5 cells/well and incubated overnight. Cells were pre-treated for 1 h with the vehicle (EtOH), alkoxy-ARA methyl ester (1 μ M, regioisomeric mixture), or EET methyl ester (1 μ M, regioisomeric mixture), followed by exposure to cisplatin (20 μ M) for 6 or 24 h. Cells were rinsed thrice with ice-cold PBS and harvested with ice-cold radioimmunoprecipitation assay (RIPA) lysis buffer (containing a freshly added protease/phosphatase inhibitor cocktail, 1:100). Following sonication on ice for 30 min and centrifugation at 13000 rpm and 4 $^{\circ}$ C for 25 min, the supernatants were collected and protein concentrations in lysates were normalized using a Bicinchoninic Acid (BCA) assay and a bovine serum albumin (BSA) standard. After lysate aliquots were denatured and reduced in loading buffer, 15 μ g of protein was separated by sodium dodecyl sulfate-polyacrylamide gel electrophoresis and transferred to nitrocellulose membranes. Membranes were blocked for 1 h with 5% non-fat milk or BSA in tris buffered saline-0.1% tween 20 (TBS-t) at room temperature and incubated overnight with the primary antibodies (1:1000 in TBS-t containing 2% non-fat milk or BSA) at 4 $^{\circ}$ C. Following quadruplicate washes with TBS-t, blots were incubated with the horseradish peroxidase-linked secondary antibody (1:10000 in TBS-t containing 2% non-fat milk or BSA) for 1 h at room temperature. After another set of quadruplicate washes, membranes were exposed to an enhanced chemiluminescence substrate (under dark) for 2 min and bands were visualized with a charged-coupled device imager.

Caspase -3 and -9 Activity Assays. LLC-PK1 cells were seeded in sterile 12-well plates at a density of 1×10^5 cells/well and incubated overnight. Cells were pre-treated for 1 h with the

vehicle (EtOH), alkoxy-ARA methyl ester (1 μ M, regioisomeric mixture), or EET methyl ester (1 μ M, regioisomeric mixture), followed by exposure to cisplatin (20 μ M) for 24 h. Cells were rinsed twice with ice-cold PBS and harvested with ice-cold RIPA buffer (without protease inhibitors). Following cold centrifugation, the supernatants were collected and kept on ice. 30 μ L of supernatants were incubated with 30 μ L of caspase activity buffer (50 mM HEPES, pH 7.4, 100 mM NaCl, 0.1% CHAPS, 10% glycerol, 1 mM EDTA, 10 mM DTT) containing Ac-DEVD-AMC (20 μ M, fluorogenic caspase-3 substrate) or Ac-LEHD-pNa (100 μ M, chromogenic caspase-9 substrate) for 90 min at 37 °C. Caspase activity was estimated by reading fluorescence at $\lambda_{\text{Ex}}/\lambda_{\text{Em}} = 345 \text{ nm}/445 \text{ nm}$ (Ac-DEVD-AMC) or absorbance at $\lambda_{\text{Abs}} = 400 \text{ nm}$ (Ac-LEHD-pNa) using a Tecan Infinite Pro microplate reader. The activities of caspases were normalized relative to total protein present in lysates (quantified by a BCA assay).

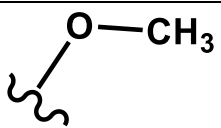
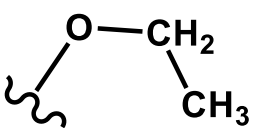
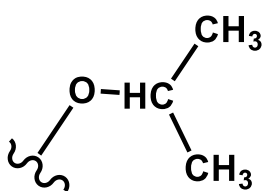
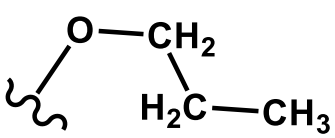
Statistics. The results are reported as the means \pm SEM. Significant differences between groups were determined by One-way analysis of variance, followed by Holm-Sidak multiple comparison testing. A p -value < 0.05 (i.e., significance level α) was considered statistically significant.

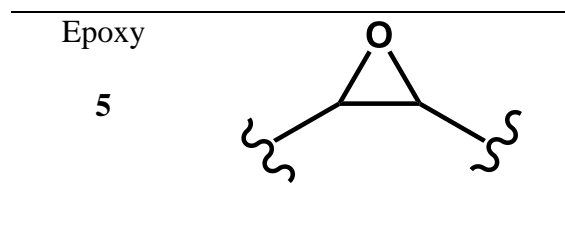
RESULTS AND DISCUSSION

Design of Arachidonic acid Alkyl-Ethers. Four different alkoxy groups (**Table 1**) were explored as potential bioisosteres for the epoxide within EETs. Due to the presence of olefins in the ARA backbone, an oxymercuration-demercuration synthetic method was employed to transform the alkenes to alkyl-ethers (**Scheme 1**). Subsequently, the mono-ethers of ARA (regioisomeric mixtures) were isolated to obtain alkoxy-containing mimics of the mono-epoxy

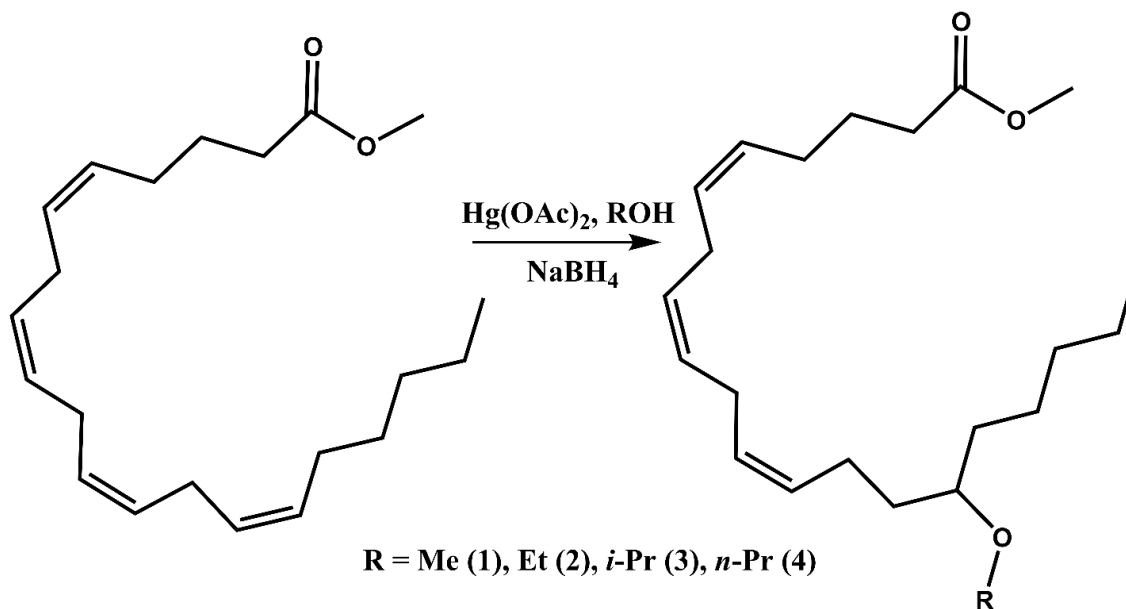
EETs. Different alkoxy groups were introduced by varying the alcohol solvent (**Scheme 1**), which served as the nucleophile reacting with the mercurinium ion to form the corresponding ether. More specifically, methanol, ethanol, isopropanol, and *n*-propanol were employed to synthesize the methoxy- (**1**), ethoxy- (**2**), *i*-propoxy- (**3**), and *n*-propoxy- (**4**) analogues, respectively.

Table 1. Structures of Four Alkoxy Bioisosteres of the Epoxide

Bioisostere	Structure of Functional Group
Methoxy 1	
Ethoxy 2	
<i>i</i> -Propoxy 3	
<i>n</i> -Propoxy 4	
Comparison Group	Structure of Functional Group



Scheme 1. General synthetic route for generation of mono-alkyl-ethers of arachidonic acid methyl ester (**1-4**, regioisomeric mixtures^a). ^aDepicted by the representative terminal regioisomer.



Initially, a concentration-response of cisplatin toxicity in LLC-PK1 cells was run (Figure S6, Supporting Information) to assess the optimal screening concentrations of cisplatin. These were determined to be 5, 10, and 20 μM for a low, moderate, and high concentration, respectively.

Ether Bioisostere Screening. Cell protective activity of the four alkoxy- EET analogues was tested against acute exposure (24 h) to a high concentration (20 μM) of cisplatin and compared to that of an EET control group (**5**, regioisomeric mixture) to gauge bioisostere functionality

relative to the epoxide. Firstly, a concentration-response of therapeutic effect against cisplatin toxicity was conducted (**Figure 1**). Compound **1** did not show significant protective activity at any of the concentrations tested (Fig. 1A). It was suspected that the generally faster rate of CYP-mediated *O*-dealkylation for methyl substituted ethers, relative to longer chain alkyl counterparts,²⁵ might be one factor that limits its action. This hypothesis was tested by co-pre-treating **1** with EM, a CYP inhibitor, to restrict potential metabolic inactivation. However, **1** was unable to significantly maintain cell viability even when incubated with the CYP inhibitor (Figure S7, Supporting Information), suggesting the lack of effect might be due to low intrinsic efficacy of the methoxy- group rather than its metabolically labile nature. On the other hand, 1 μ M of **2** and **3** significantly shielded cells from cisplatin-induced toxicity (Fig. 1B, 1C, 1F), with an efficacy comparable to that of 1 μ M **5** (Fig. 1E, 1F). 1 μ M of **4** also displayed good bioactivity (Fig. 1D), but its magnitude of effect was smaller than that of **2**, **3**, and **5** (Fig. 1F). Since all the analogues, as well as **5**, displayed maximal activity at 1 μ M, a concentration of 1 μ M was considered optimal and utilized for further experiments. To confirm that the observed effects were independent of the assay employed (i.e., MTT), a supporting viability assay (CCK-8) was also conducted (Figure S8, Supporting Information). The magnitude and trends of therapeutic action remained consistent across the two assays, reaffirming inherent compound activity.

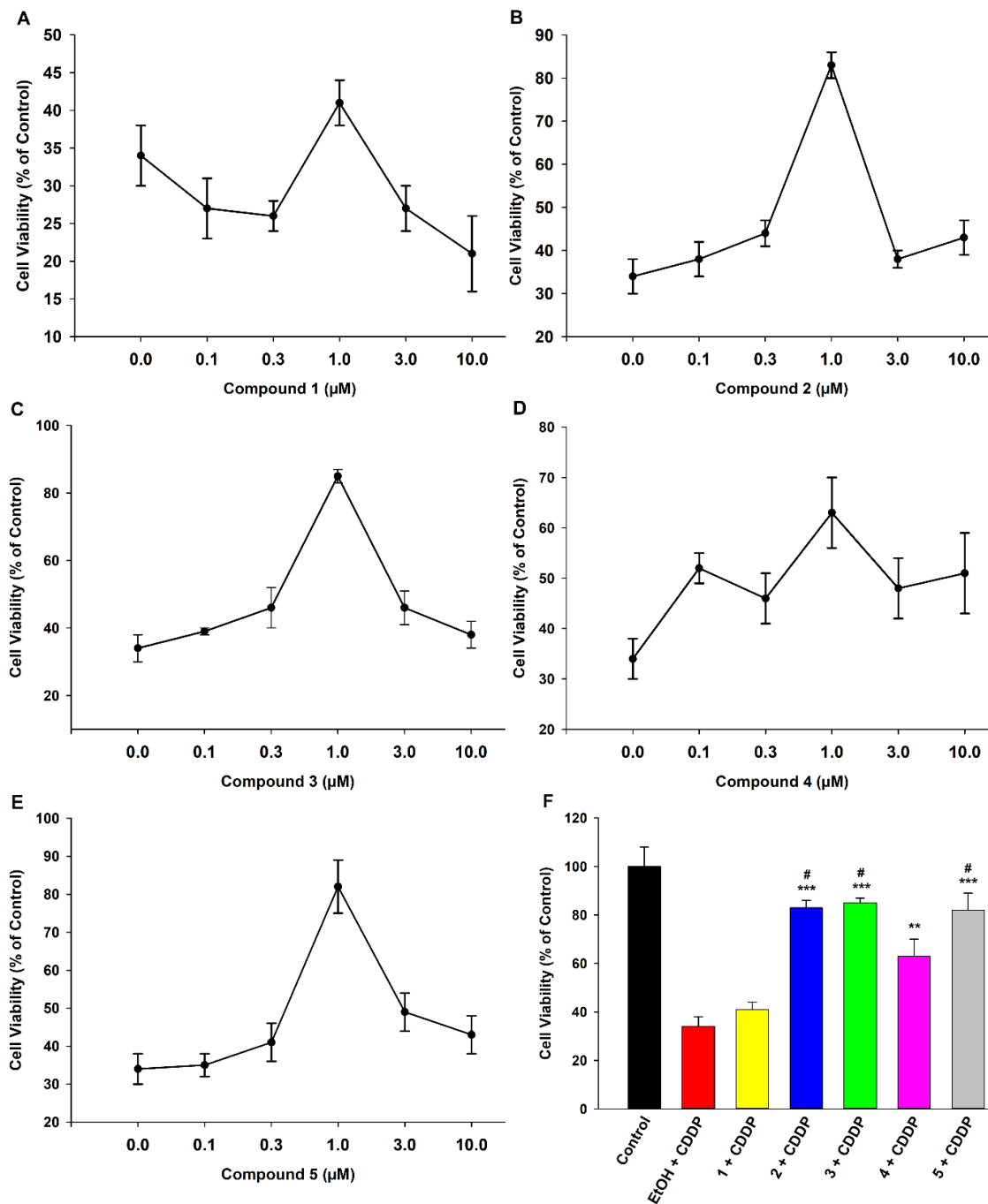


Figure 1. EET analogues **2-4** exhibit cytoprotective activity against acute cisplatin (CDDP) toxicity in LLC-PK1 proximal tubular cells in a concentration-dependent manner. Cells were pre-treated with the vehicle (EtOH), analogues **1-4** (0.1-10 μM), or compound **5** (0.1-10 μM) for 1 h, followed by exposure to CDDP (20 μM) for 24 h. (A) Compound **1** did not demonstrate

protective effects at any concentration while **(B)** compound **2**, **(C)** compound **3**, **(D)** compound **4**, and **(E)** compound **5** all displayed maximal protective activity at a concentration of 1 μ M. **(F)** 1 μ M of **2**, **3**, **4**, and **5** significantly shielded LLC-PK1 cells from CDDP toxicity (One way analysis of variance, Holm-Sidak method, *** $p < 0.001$; ** $p < 0.01$ vs. EtOH + CDDP group), and the magnitudes of action of **2**, **3**, and **5** were greater than that of **4** (One way analysis of variance, Holm-Sidak method, # $p < 0.05$ vs. **4** + CDDP group, $\alpha = 0.05$).

14,15-EE-5(Z)-E, or 14,15-EEZE, is a selective antagonist of the putative EET receptor²⁶ and was employed to study whether antagonism of EET action could pare activity of analogues **1-4**. Compounds **2-5** successfully preserved cell viability against cisplatin in the absence of 14,15-EEZE (**Figure 2**). Presence of 14,15-EEZE significantly curtailed the magnitude of therapeutic action for **2** and **3**, while completely abolishing activity of **5** (**Figure 2**). Hence, generally, alkyl ethers of ARA appear to act at least partially through agonism of the presumed EET receptor, further validating alkoxy- groups as suitable bioisosteric substitutes for the epoxide of EETs.

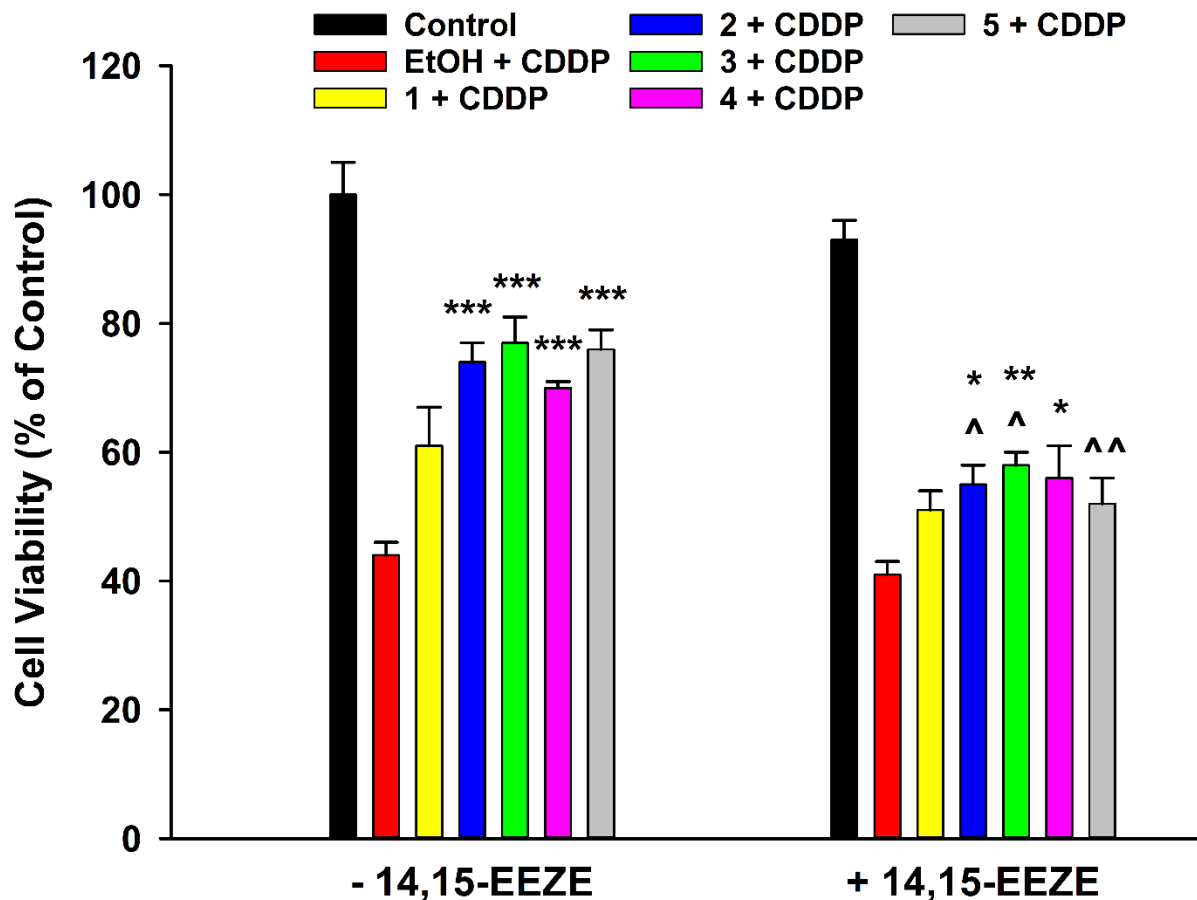


Figure 2. EET receptor antagonist 14,15-Epoxyeicosa-5(Z)-enoic Acid (14,15-EEZE) attenuates protective effects of EET analogues **2** and **3** against cisplatin (CDDP) toxicity in LLC-PK1 proximal tubular cells. Cells were pre-treated with vehicle (EtOH), analogues **1-4** (1 μ M), or compound **5** (1 μ M), in the absence or presence of 14,15-EEZE (3 μ M), for 1 h, followed by exposure to CDDP (20 μ M) for 24 h. Compounds **2-5** significantly shielded LLC-PK1 cells from CDDP toxicity in the absence of 14,15-EEZE (One way analysis of variance, Holm-Sidak method, $***p < 0.001$ vs. EtOH + CDDP - 14,15-EEZE group, $\alpha = 0.05$). Only compounds **2-4** significantly shielded LLC-PK1 cells from CDDP toxicity in the presence of 14,15-EEZE (One way analysis of variance, Holm-Sidak method, $*p < 0.05$; $**p < 0.01$ vs. EtOH + CDDP + 14,15-EEZE group, $\alpha = 0.05$). Co-pre-treatment with 14,15-EEZE reduced efficacy of **2** and **3**

and eliminated activity of **5** (One way analysis of variance, Holm-Sidak method, $^{\wedge}p < 0.05$; $^{\wedge\wedge}p < 0.01$ vs. corresponding - 14,15-EEZE group, $\alpha = 0.05$).

Additionally, a concentration-response of effect was obtained for the parent molecule ARA (Figure S9, Supporting Information), which did not sustain cell viability against cisplatin toxicity at any tested concentration. Furthermore, compounds **1-5** (and parent ARA) were tested in the absence of cisplatin to account for potential isolated effects on cells. None of the compounds stimulated cell growth, nor were they cytotoxic (Figure S10, Supporting Information). Finally, inhibitory activity of analogues **1-4** towards the human sEH was tested (Table S3, Supporting Information). The weak inhibitory potency ($IC_{50} = 6.7-32.1 \mu M$) verified their poor sEH inhibition, even relative to **5** ($IC_{50} = 3.1 \mu M$), suggesting sEH-independent action.

Time-Dependent Therapeutic Action. Activity of analogues **1-4**, relative to **5**, against prolonged exposure (48-120 h) to low or moderate concentrations (5 or 10 μM) of cisplatin was also assessed (**Figure 3**). Interestingly, **1** displayed previously unseen therapeutic activity at 72 h exposure with 5 μM cisplatin (Fig. 3C). This suggests that a degree of bioisosteric activity is associated with the methoxy- group, particularly under conditions of low acute stress. However, unlike other analogues, its activity was not sustainable against 10 μM cisplatin (Fig. 3A, 3B), or for longer durations (96 h) against 5 μM cisplatin (Fig. 3D). Analogues **2** and **3** continued to demonstrate protective effects comparable to that of **5** for earlier time points, namely 48 h and 72 h exposures to 10 μM and 5 μM cisplatin, respectively (Fig. 3A, 3C). Notably, at later durations (72 and 96 h exposures to 10 μM and 5 μM cisplatin, respectively), their activity in fact surpassed that of EETs as the extent of effects exerted by the latter subsided entirely (Fig. 3B) or partially (Fig. 3D). Co-pre-treating **5** with *t*-AUCB, an sEHI, abolished this drop-off in bioactivity (Fig. 3B, 3D), suggesting sEH-mediated degradation of EETs impedes their function

under chronic toxicity conditions. Accordingly, the necessity for dual **5**/sEHI treatment to match the activity of **2** and **3** at later toxicity time points lends confidence to the notion that the ethoxy- and *i*-propoxy- compounds would possess greater bioavailability than their epoxide equivalents and hence perhaps be more suitable for extended medicinal applications. Analogue **4** also demonstrated therapeutic effects against 5 μ M cisplatin (Fig. 3C, 3D), but the magnitude of its activity lagged slightly, relative to that of **2** and **3**, at the later (96 h) time point (Fig. 3D). However, it was still significantly more active than **5** (without sEHI) at the latter time-concentration combination, suggesting a biochemical stability advantage over EETs akin to **2** and **3**. However, **4** did not display significant activity against 10 μ M cisplatin at either the 48 or 72 h time points (Fig. 3A, 3B). None of the compounds were able to maintain cell viability after 96 h and 120 h exposures to 10 μ M and 5 μ M cisplatin, respectively (Figure S11, Supporting Information).

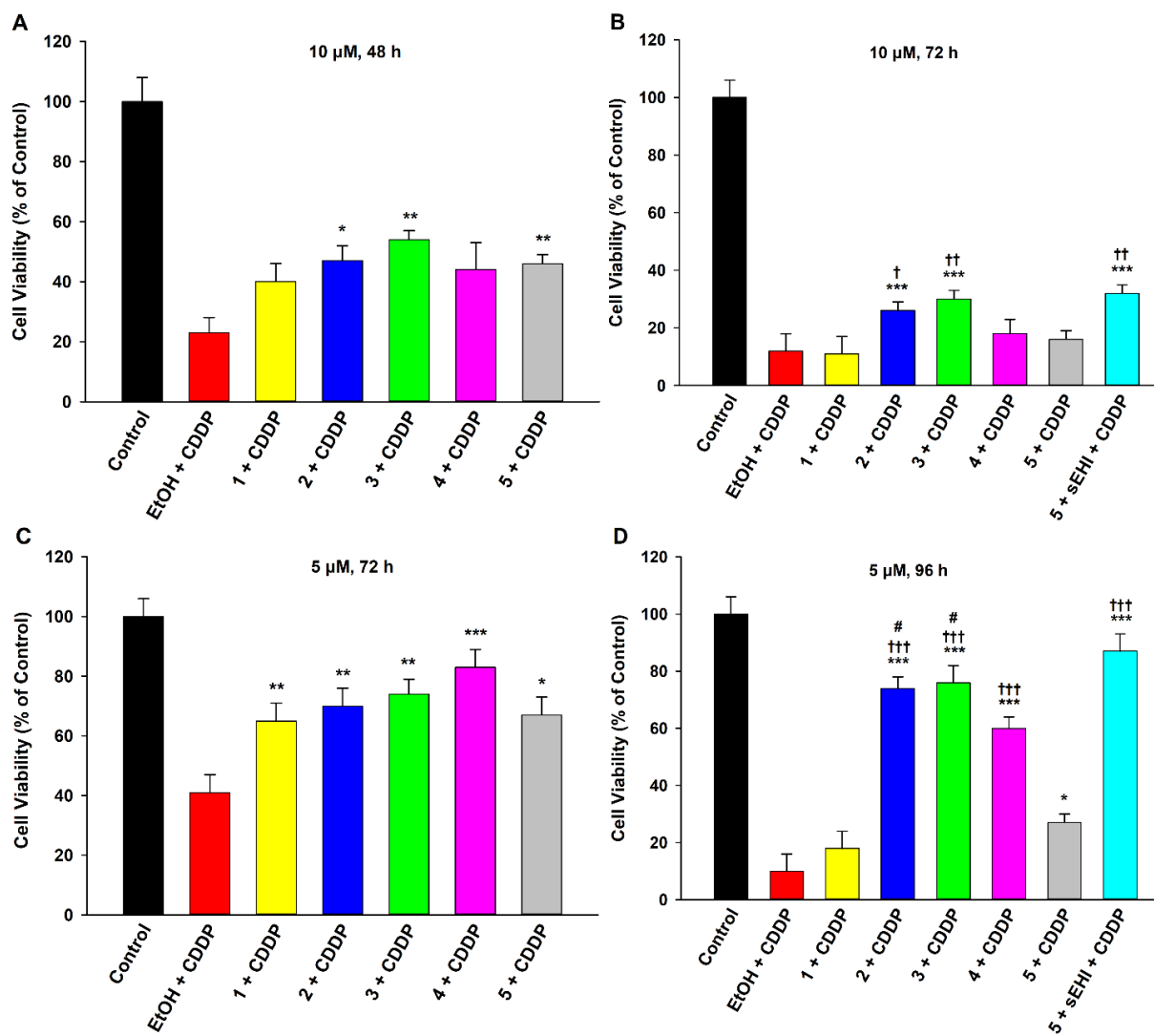


Figure 3. EET analogues 1-4 attenuate chronic cisplatin (CDDP) toxicity in LLC-PK1 proximal tubular cells in a time-dependent manner. Cells were pre-treated with vehicle (EtOH), analogues 1-4 (1 μ M), or compound 5 (1 μ M) for 1 h, followed by exposure to low (5 μ M) or moderate (10 μ M) concentrations of CDDP for 48, 72, or 96 h. (A) Compounds 2, 3, and 5 significantly maintained viability of LLC-PK1 cells exposed to 10 μ M CDDP for 48 h (One way analysis of variance, Holm-Sidak method, * p < 0.05; ** p < 0.01 vs. EtOH + CDDP group, α = 0.05). (B) Only analogues 2 and 3 significantly maintained viability of LLC-PK1 cells exposed to 10 μ M CDDP for 72 h (One way analysis of variance, Holm-Sidak method, *** p < 0.001 vs. EtOH +

CDDP group, $\alpha = 0.05$). Their activity surpassed that of **5** (One way analysis of variance, Holm-Sidak method, $^{\dagger}p < 0.05$; $^{\dagger\dagger}p < 0.01$ vs. **5** + CDDP group, $\alpha = 0.05$), as the latter failed to display protective effects. Co-pre-treating **5** with an sEHI (*t*-AUCB) maintained activity of **5** (One way analysis of variance, Holm-Sidak method, $^{\dagger\dagger}p < 0.01$ vs. **5** + CDDP group, $\alpha = 0.05$) and significantly shielded cells (One way analysis of variance, Holm-Sidak method, $^{***}p < 0.001$ vs. EtOH + CDDP group, $\alpha = 0.05$) (C) All four EET analogues **1-4**, along with **5**, significantly maintained viability of LLC-PK1 cells exposed to 5 μ M CDDP for 72 h (One way analysis of variance, Holm-Sidak method, $^{*}p < 0.05$; $^{**}p < 0.01$; $^{***}p < 0.001$ vs. EtOH + CDDP group, $\alpha = 0.05$). (D) Compounds **2**, **3**, **4**, and **5** significantly maintained viability of LLC-PK1 cells exposed to 5 μ M CDDP for 96 h (One way analysis of variance, Holm-Sidak method, $^{*}p < 0.05$; $^{***}p < 0.001$ vs. EtOH + CDDP group, $\alpha = 0.05$). Moreover, the activity of **2-4** was significantly greater than that of **5** (One way analysis of variance, Holm-Sidak method, $^{\dagger\dagger\dagger}p < 0.001$ vs. **5** + CDDP group, $\alpha = 0.05$). Co-pre-treating **5** with the sEHI bridged the gap in activity (One way analysis of variance, Holm-Sidak method, $^{\dagger\dagger\dagger}p < 0.001$ vs. **5** + CDDP group, $\alpha = 0.05$) and significantly shielded cells (One way analysis of variance, Holm-Sidak method, $^{***}p < 0.001$ vs. EtOH + CDDP group, $\alpha = 0.05$). Finally, the cell protective effects of **2** and **3** were greater than that of **4** (One way analysis of variance, Holm-Sidak method, $^{\#}p < 0.05$ vs. **4** + CDDP group, $\alpha = 0.05$).

Taken together with their effects against the acute toxicity of CDDP, all four alkoxy- EET analogues exhibited bioactivity against cisplatin toxicity in LLC-PK1 cells, ranging from excellent for **2** and **3** to good for **4** to minimal for **1**. Consequently, the two most promising analogues (i.e., **2** and **3**) were selected for further biological mechanism of action studies.

Prevention of Mitochondrial Transmembrane Potential Collapse. Cisplatin preferentially accumulates in the mitochondria, enhancing susceptibility of cells with higher mitochondrial densities (e.g., PTECs) to its noxious effects.^{3,27,28} It proceeds to trigger mitochondrial dysfunction by interfering with the electron transport chain, and perturbations typically occur in a time-dependent manner (**Figure 4**). For instance, a short exposure (6 h) to a high concentration of cisplatin did not significantly impact the mitochondrial transmembrane potential ($\Delta\Psi_m$) of LLC-PK1 cells (Fig. 4A). However, a longer exposure (24 h) resulted in substantial loss of the $\Delta\Psi_m$ (Fig. 4B). Pre-treatment with **2** or **3** (or **5**) significantly inhibited decline of the electrochemical gradient, returning it closer to basal levels (Fig. 4B), signifying that the alkoxy-based analogues of EETs exert mitochondrial protective effects. Previously, EETs were shown to reduce loss of $\Delta\Psi_m$ and thus mitigate stressor-induced mitochondrial damage in cardiac cells²⁹ and hippocampal astrocytes,³⁰ further underlining the involvement of mitochondrion-mediated action for this class of molecules. Moreover, the cell viability assays employed in this study are contingent on activity of mitochondrial reductases and hence the parallel cell-protective effects of these compounds (Fig. 1F) provide yet more evidence of a mitochondria-dependent pathway. An excessively long (48 h) exposure resulted in a nearly complete gradient collapse and pre-treatment with **2** or **3** (or **5**) was unable to preserve the $\Delta\Psi_m$ (Fig. 4C). This finding aligns closely with the observation that exposure to a high level of cisplatin for 48 h was entirely lethal to LLC-PK1 cells and pre-treatment with the compounds could not sustain viability (Figure S12, Supporting Information). Finally, none of the compounds affected the $\Delta\Psi_m$ of cells in the absence of cisplatin (Figure S13, Supporting Information).

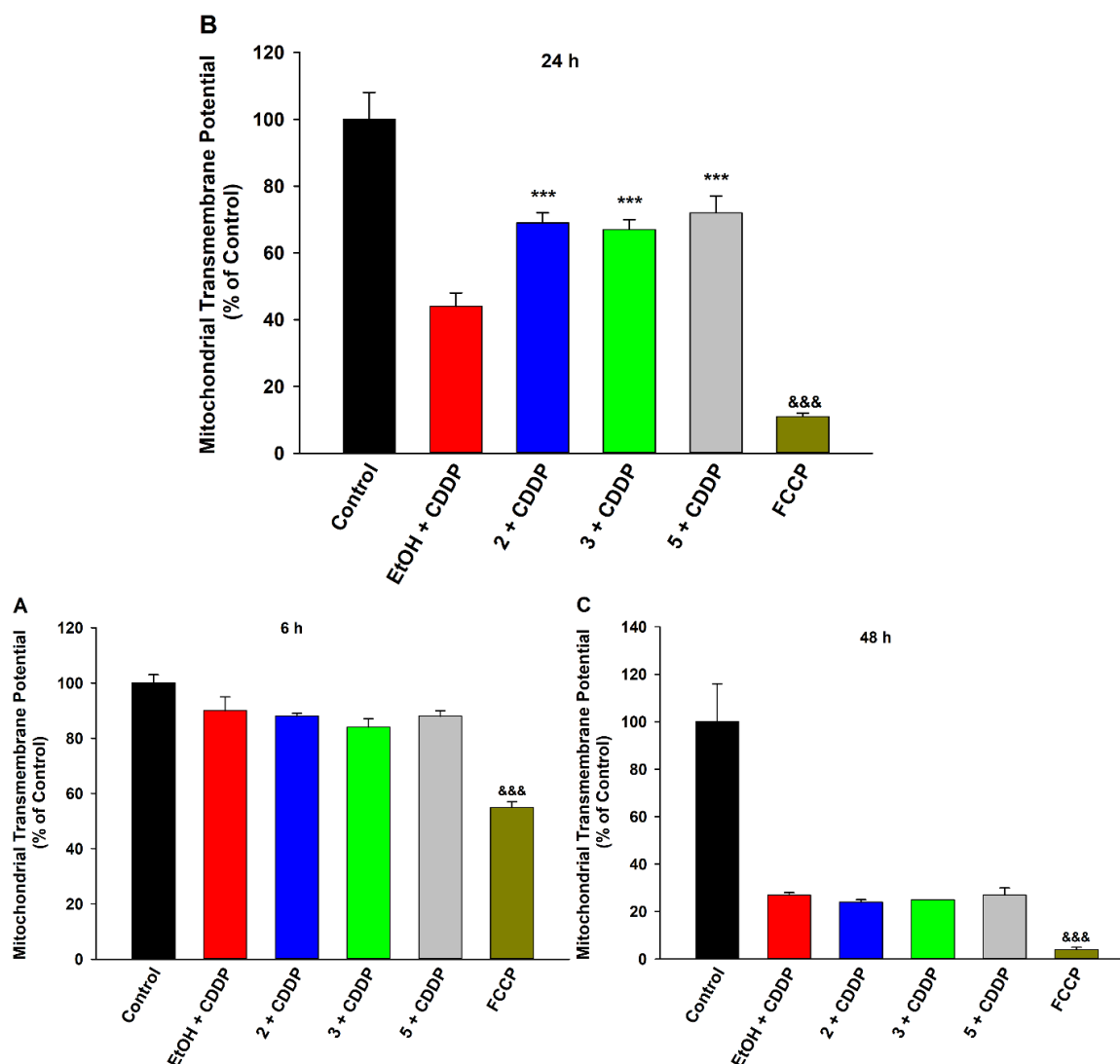


Figure 4. EET analogues **2** and **3** protect against cisplatin (CDDP)-induced mitochondrial transmembrane potential ($\Delta\Psi_m$) decline in LLC-PK1 proximal tubular cells. (A) The $\Delta\Psi_m$ was not significantly affected in cells exposed to CDDP (20 μ M) for 6 h (B) Pre-treatment with compound **2** (1 μ M), **3** (1 μ M), or **5** (1 μ M) preserved mitochondrial health by significantly mitigating loss of the mitochondrial electrochemical gradient in cells exposed to CDDP (20 μ M) for 24 h, relative to vehicle control (One way analysis of variance, Holm-Sidak method, *** $p < 0.001$ vs. EtOH + CDDP group, $\alpha = 0.05$) (C) Pre-treatment with **2** (1 μ M), **3** (1 μ M), or **5** (1 μ M) failed to mitigate the collapse of the $\Delta\Psi_m$ in cells exposed to CDDP (20 μ M) for 48 h. A

depolarized $\Delta\Psi_m$ was validated by FCCP (10 μ M), a positive control (One way analysis of variance, Holm-Sidak method, $p < 0.001$ vs. Control group, $\alpha = 0.05$).

Reduction of General and Mitochondrial Reactive Oxygen Species Generation. Cisplatin is known to induce oxidative stress,^{4,31} stimulating the generation of reactive oxygen species (ROS), particularly superoxide anion ($O_2^{\bullet-}$), H_2O_2 , and hydroxyl radical ($\bullet OH$), through both mitochondrial and non-mitochondrial pathways. Disruptions to the mitochondrial respiratory complexes are a major source of ROS. Non-mitochondrial sources include depletion of glutathione and activation of NADPH and xanthine-xanthine oxidases, which in turn can further exacerbate the mitochondrial dysfunction. Thus, effects of the EET analogues were assessed against both total cellular ROS and mitochondria-specific ROS, expressly $O_2^{\bullet-}$ (**Figure 5**). Predictably, cisplatin increased the general ROS in LLC-PK1 cells (Fig. 5A), as well as the $O_2^{\bullet-}$ generated in mitochondria (Fig. 5B). Compound **2** and **3** (as well as **5**) lessened both surges, implying oxidative stress-alleviating activity that could be both mitochondria-targeted and whole cell divergent.

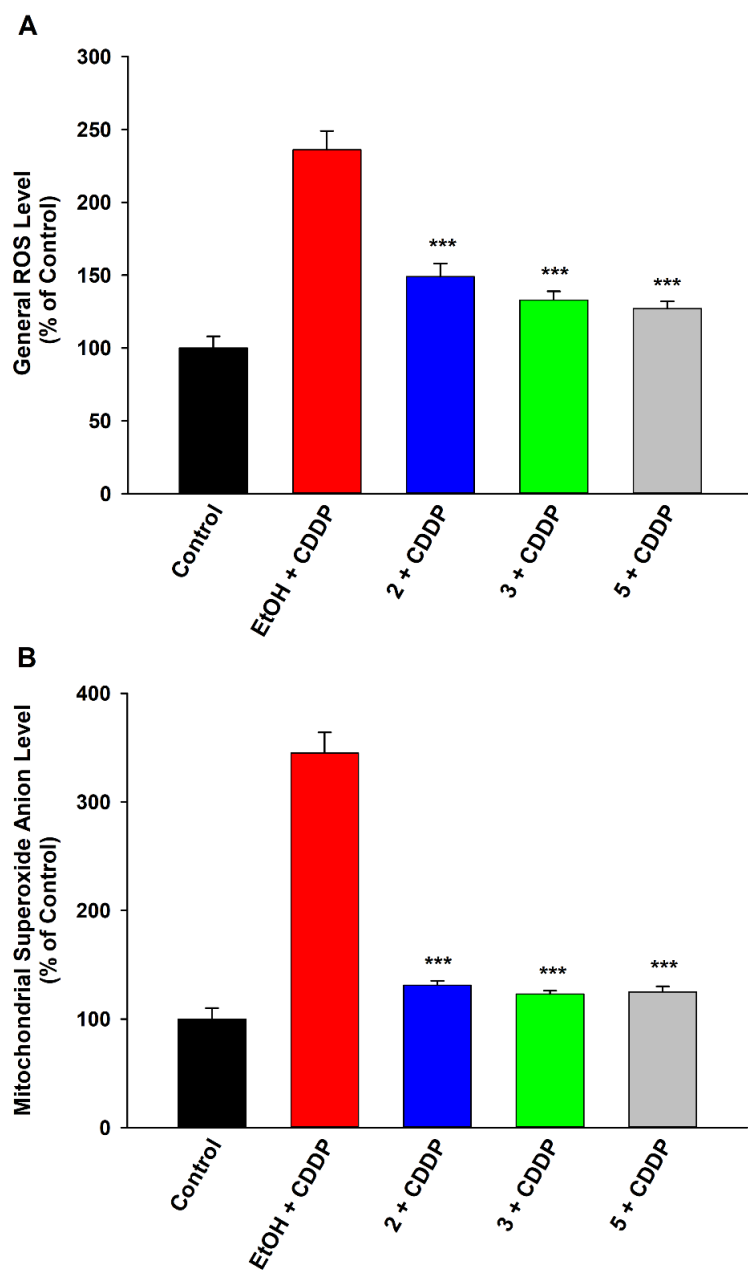


Figure 5. EET analogues **2** and **3** attenuate cisplatin (CDDP)-induced generation of reactive oxygen species (ROS) in LLC-PK1 proximal tubular cells. Pre-treatment with compound **2** (1 μ M), **3** (1 μ M), or **5** (1 μ M) significantly decreased the augmented levels of (A) general cellular ROS and (B) mitochondria-specific superoxide anion in LLC-PK1 cells exposed to CDDP (20 μ M) for 24 h, relative to vehicle control (One way analysis of variance, Holm-Sidak method, *** $p < 0.001$ vs. EtOH + CDDP group, $\alpha = 0.05$).

Decreased Ratio of Phosphorylated to Total p38 and JNK. Involvement of MAPKs, namely p38 and Jun N-terminal kinase/stress-activated protein kinase (JNK/SAPK), has been closely linked to the nephrotoxic effects of cisplatin.^{5,6} MAPKs are key regulators of the mitochondria-mediated intrinsic cellular death pathway.³² They act through recruitment of pro-apoptotic regulators and suppression of anti-apoptotic function, sensitizing the mitochondria towards cell death and activating the downstream caspase-9 pathway. Phosphorylation of MAPKs triggers their activity and cisplatin-generated ROS (in particular $\cdot\text{OH}$) are the primary cellular stressors considered to initiate this MAPK signaling. Accordingly, little to no levels of the phosphorylated MAPK variant were detectable in LLC-PK1 cells after only a brief period (6 h) of cisplatin exposure (Figure S14, Supporting Information), a time point at which mitochondrial integrity was intact (Fig. 4A). However, following an extended exposure (24 h), under conditions of verifiable cisplatin-induced mitochondrial disruption and ROS upregulation (Fig. 4B, 5), markedly augmented levels of the phosphorylated p38 and JNK/SAPK forms (relative to total variants) were observed (**Figure 6**). The ratios were significantly reduced by pre-treatments with **2**, **3**, or **5** (**Figure 6**), denoting the capacity of alkoxy- EET analogues to terminate the MAPK signaling upregulated by cisplatin.

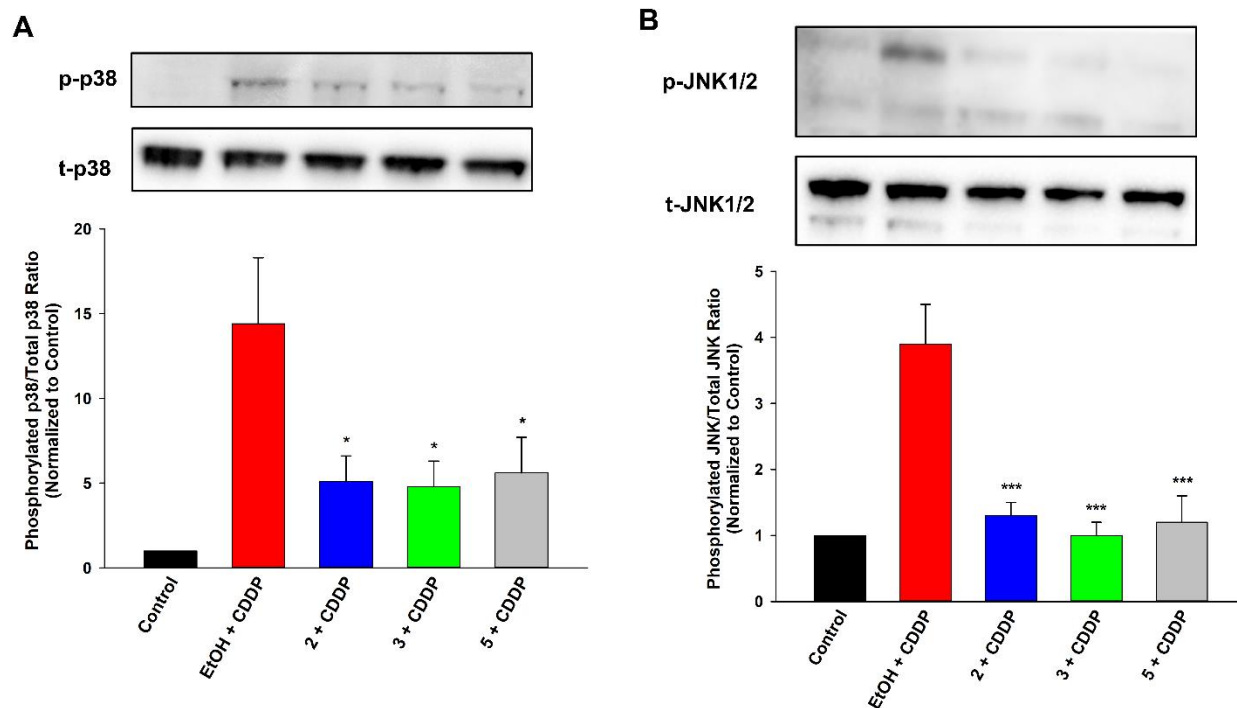


Figure 6. EET analogues **2** and **3** diminish cisplatin (CDDP)-induced MAPK signaling in LLC-PK1 proximal tubular cells. Pre-treatment with compound **2** (1 μ M), **3** (1 μ M), or **5** (1 μ M) significantly reduced the higher ratio of phosphorylated variant to total variant for MAPKs (**A**) p38 and (**B**) JNK/SAPK in LLC-PK1 cells exposed to CDDP (20 μ M) for 24 h, relative to vehicle control. Results are representative of three independent experiments (One way analysis of variance, Holm-Sidak method, * $p < 0.05$; *** $p < 0.001$ vs. EtOH + CDDP group, $\alpha = 0.05$).

Inhibition of Caspase-9 and -3 Activation. Initiation of caspase-9 and ensuing recruitment of caspase-3 is a primary mode of cisplatin-induced cell death.⁷ Disruptions to mitochondrial health, through direct agitations, oxidative damage, and MAPK-mediated pro-apoptotic signaling, trigger the caspase-9 pathway, leading to activation of the executioner caspase-3. Hence, as expected, activity of both caspase-9 and caspase-3 was greatly elevated with exposure to cisplatin (**Figure 7**). This activity was ablated by **2** and **3** (as well as **5**), suggesting the ability

of these compounds to mitigate cisplatin-induced cell death by obstructing the downstream caspase stimulation.

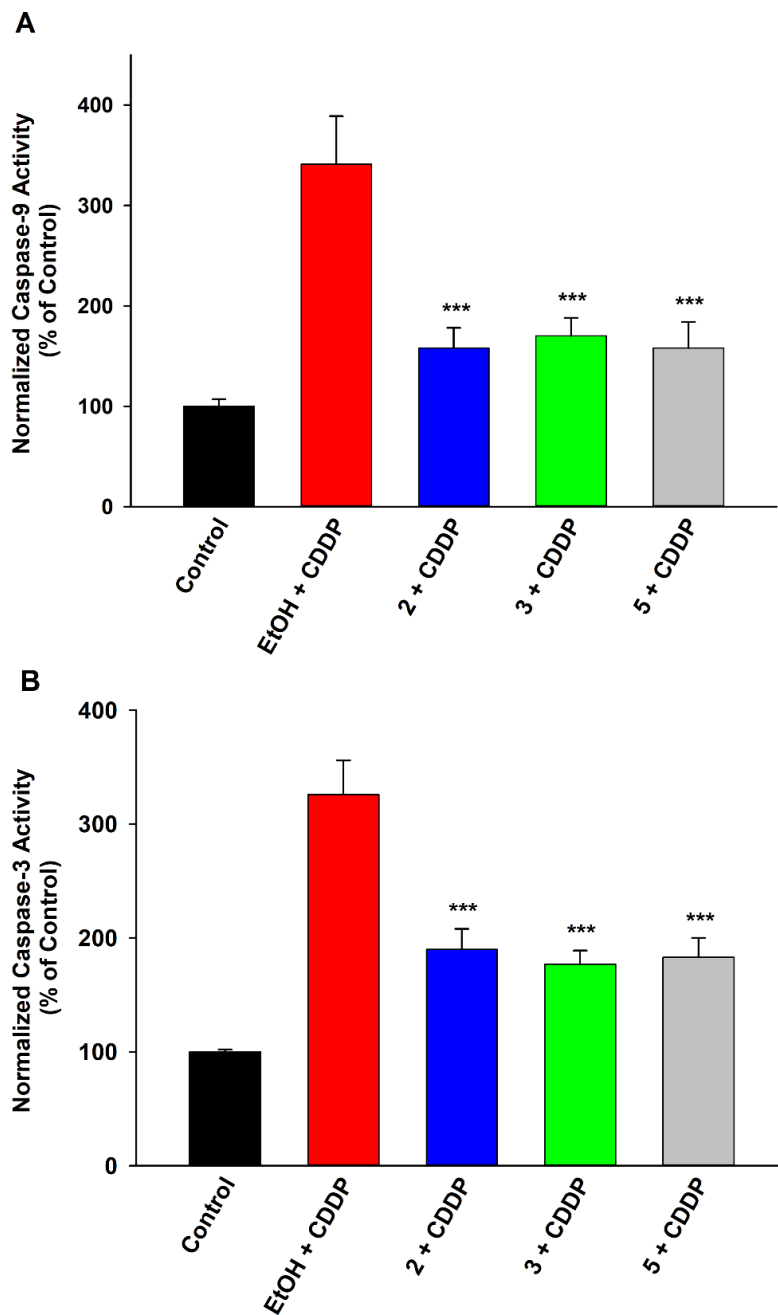


Figure 7. EET analogues **2** and **3** curb cisplatin (CDDP)-induced caspase activity in LLC-PK1 proximal tubular cells. Pre-treatment with compound **2** (1 μ M), **3** (1 μ M), or **5** (1 μ M) significantly reduced the elevated normalized activity of (A) caspase-9 and (B) caspase-3 in

LLC-PK1 cells exposed to CDDP (20 μ M) for 24 h, relative to vehicle control (One way analysis of variance, Holm-Sidak method, *** $p < 0.001$ vs. EtOH + CDDP group, $\alpha = 0.05$).

Preservation of Cytotoxicity Against Cancer Cells. While attenuating the off-target renal toxicity of cisplatin is vitally important, ensuring that the pharmacological intervention does not dilute the desired chemotherapeutic action is a key consideration. Hence, the effects of compounds **1-5** on human liver hepatocellular carcinoma cells (HepG2) were assessed (**Figure 8**). Compounds **1-5** did not shield liver cancer cells from the toxic effects of cisplatin (Fig. 8A), nor did they stimulate cancer cell growth in the absence of cisplatin (Fig. 8B). The findings were reinforced with a secondary assay (CCK-8) to ensure the lack of hindrance was assay-independent (Figure S8, Supporting Information). This implies these compounds do not interfere with the cancer cell-targeted toxicity of cisplatin, potentially expanding its therapeutic index and capacity for use.

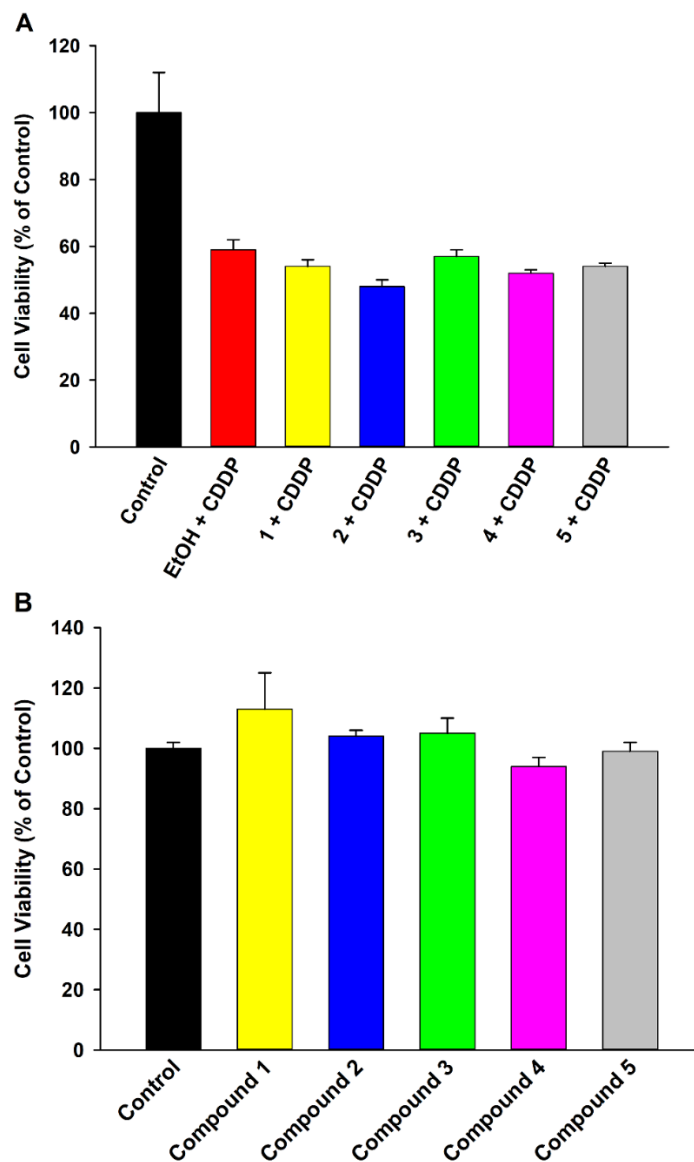


Figure 8. EET analogues **1-4** do not affect the cytotoxicity of cisplatin (CDDP) towards HepG2 liver cancer cells. **(A)** Pre-treatment with analogues **1-4** (1 μ M) or compound **5** (1 μ M) did not exert protective effects in HepG2 cells exposed to CDDP (20 μ M) for 24 h. **(B)** Compounds **1-5** (1 μ M) had no significant influence on viability of HepG2 cells.

CONCLUSIONS

Here we report new EET mimics developed as potential lead therapeutics against the off-target nephrotoxicity of the common cancer drug cisplatin. They employ alkoxy- substituents as replacement groups for the chemically stable but enzymatically labile epoxide. Since alkoxy groups are so chemically similar to the epoxide, alkyl-ethers of ARA potentially orient at the putative receptor in a manner akin to EETs. This study emphasized assessing the bioisosteric activity of common alkoxy groups in pig derived PTECs, as opposed to investigating pure regioisomers. Thus, regioisomeric mixtures of four alkoxy-ARA analogues of EETs were screened against cisplatin renal toxicity in vitro, relative to an EET regioisomer mixture. All bioisosteres exhibited activity, to varying degrees. The ethoxy- and *i*-propoxy- compounds were the most efficacious in this model and, importantly, proved more effectual than EETs at mitigating effects of prolonged cisplatin exposures. They protected PTECs from cisplatin toxicity through the same molecular modes as EETs, specifically by blocking mitochondrial dysfunction and oxidative stress and curbing subsequent MAPK signaling and caspase activation, while not influencing cytotoxicity of cisplatin against the target cancer cells. Application of an EET receptor antagonist diminished their efficacy, further authenticating mimetic functionality.

In earlier studies on alkoxy- mimics of insect JHs, large differences in biological potency were observed for the ether groups across different target species. For instance, the methoxy- was highly potent on dipterous insects (flies), relative to the weakly active ethoxy-, *i*-propoxy-, and *n*-propoxy-. In contrast, high activity of ethoxy- and *n*-propoxy- was seen in coleopterous insects (beetles), compared to low potency for methoxy and *i*-propoxy. Interestingly, the *i*-propoxy analogue of EETs was of high activity in this study but the homologous mimic of JH was over

100-fold less active than the *n*-propoxy in beetles. Hence, uniform recognition across systems cannot be assumed, and species differences and the specific bioassay of interest should be taken into account when evaluating bioisosteric potential.

More recently, there is growing interest in ω -3 EpFAs, namely eicosapentaenoic acid (EPA, 20:5)-derived epoxyeicosatetraenoic acids (EEQs) and docosahexaenoic acid (DHA, 22:6)-derived epoxydocosapentaenoic acids (EDPs), and their synthetic analogues.³³⁻³⁵ Thus, as a next step, the alkoxy- analogues of these EpFAs could also be examined, especially since EEQs and EDPs are more potent than EETs in certain disease models.^{36,37} Moreover, activity of individual regioisomers within the most promising series should eventually be explored.

Finally, while sEH-mediated hydrolysis is the primary mode of EpFA degradation, EpFAs are also metabolized by a variety of pathways including β -oxidation, chain elongation, ω/ω -1 hydroxylation, and secondary metabolism.³⁸ EpFA analogue design generally attempts to block these routes as well since they become major contributors to degradative metabolism once the hydrolytic role of sEH is blocked. Hence, the alkoxy- bioisostere approach might facilitate employment of ideal scaffolds that lead to further improved EpFA analogues. Thus, overall, future work will highlight the importance of identifying the appropriate regio- and, possibly, stereoisomer for medicinal optimization and targeted biology.

ASSOCIATED CONTENT

Supporting Information. HPLC traces and product ion spectra for compounds **1-5**, HPLC gradient, Q-TRAP MS source parameters, optimization of cisplatin screening concentrations, influence of CYP inhibitor on activity of compound **1**, CCK-8 assay-facilitated supporting

viability assessments, concentration-response of activity for parent ARA, isolated effects on PTEC viability, IC₅₀ values against human sEH, endpoints of therapeutic action against low-moderate, chronic and high, acute cisplatin exposures, isolated effects on PTEC mitochondrial health, immunoblots for MAPKs at an early exposure time point

AUTHOR INFORMATION

Corresponding Author

*Tel: 530-752-7519. Fax: 530-752-1537. Email: bdhammock@ucdavis.edu

ACKNOWLEDGMENTS

This work was partially supported by National Institutes of Health grants, National Institute of Environmental Health Sciences (NIEHS) RIVER Award R35 ES030443-01, NIEHS Superfund Award P42 ES004699, and S10 OD025271-01A1. N.S. thanks the NIEHS/UC Davis Superfund Research Program for financial support in the form of a GSR fellowship.

REFERENCES

- (1) Manohar, S., and Leung, N. (2018) Cisplatin nephrotoxicity: a review of the literature. *J. Nephrol.* 31, 15-25.
- (2) Yao, X., Panichpisal, K., Kurtzman, N., and Nugent, K. (2007) Cisplatin nephrotoxicity: a review. *Am. J. Med. Sci.* 334, 115-124.

- (3) Kruidering, M., Van de Water, B., de Heer, E., Mulder, G. J., and Nagelkerke, J. F. (1997) Cisplatin-induced nephrotoxicity in porcine proximal tubular cells: mitochondrial dysfunction by inhibition of complexes I to IV of the respiratory chain. *J. Pharmacol. Exp. Ther.* 280, 638-649.
- (4) Chirino, Y. I., and Pedraza-Chaverri, J. (2009) Role of oxidative and nitrosative stress in cisplatin-induced nephrotoxicity. *Exp. Toxicol. Pathol.* 61, 223-242.
- (5) Ramesh, G., and Reeves, W. B. (2005) p38 MAP kinase inhibition ameliorates cisplatin nephrotoxicity in mice. *Am. J. Physiol.: Renal Physiol.* 289, F166-174.
- (6) Francescato, H. D., Costa, R. S., Júnior, F. B., and Coimbra, T. M. (2007) Effect of JNK inhibition on cisplatin-induced renal damage. *Nephrol Dial Transport.* 22, 2138-2148.
- (7) Kaushal, G. P., Kaushal, V., Hong, X., and Shah, S. V. (2001) Role and regulation of activation of caspases in cisplatin-induced injury to renal tubular epithelial cells. *Kidney Int.* 60, 1726-1736.
- (8) Elmarakby, A. A. (2012) Reno-protective mechanisms of epoxyeicosatrienoic acids in cardiovascular disease. *Am. J. Physiol.: Regul., Integr. Comp. Physiol.* 302, R321-330.
- (9) Inceoglu, B., Bettaieb, A., Haj, F. G., Gomes, A. V., and Hammock, B. D. (2017) Modulation of mitochondrial dysfunction and endoplasmic reticulum stress are key mechanisms for the wide-ranging actions of epoxy fatty acids and soluble epoxide hydrolase inhibitors. *Prostaglandins Other Lipid Mediat.* 133, 68-78.
- (10) Imig, J. D. (2018) Prospective for cytochrome P450 epoxygenase cardiovascular and renal therapeutics. *Pharmacol. Ther.* 192, 1-19.

- (11) Parrish, A. R., Chen, G., Burghardt, R. C., Watanabe, T., Morisseau, C., and Hammock, B. D. (2009) Attenuation of cisplatin nephrotoxicity by inhibition of soluble epoxide hydrolase. *Cell Biol. Toxicol.* 25, 217-225.
- (12) Liu, Y., Webb, H. K., Fukushima, H., Micheli, J., Markova, S., Olson, J. L., and Kroetz, D. L. (2012) Attenuation of Cisplatin-Induced Renal Injury by Inhibition of Soluble Epoxide Hydrolase Involves Nuclear Factor κ B Signaling. *J Pharmacol. Exp. Ther.* 341, 725-734.
- (13) Liu, Y., Lu, X., Nguyen, S., Olson, J. L., Webb, H. K., and Kroetz, D. L. (2013) Epoxyeicosatrienoic acids prevent cisplatin-induced renal apoptosis through a p38 mitogen-activated protein kinase-regulated mitochondrial pathway. *Mol. Pharmacol.* 84, 925-934.
- (14) Sudhahar, V., Shaw, S., and Imig, J. D. (2010) Epoxyeicosatrienoic acid analogs and vascular function. *Curr. Med. Chem.* 17, 1181-1190.
- (15) Campbell, W. B., Imig, J. D., Schmitz, J. M., and Falck, J. R. (2017) Orally Active Epoxyeicosatrienoic Acid Analogs. *J. Cardiovasc. Pharmacol.* 70, 211-224.
- (16) Khan, M. A. H., Liu, J., Kumar, G., Skapek, S. X., Falck, J. R., and Imig, J. D. (2013) Novel orally active epoxyeicosatrienoic acid (EET) analogs attenuate cisplatin nephrotoxicity. *FASEB J.* 27, 2946-2956.
- (17) Imig, J. D., Hye Khan, M. A., Burkhan, A., Chen, G., Adebessin, A. M., and Falck, J. R. (2021) Kidney-Targeted Epoxyeicosatrienoic Acid Analog, EET-F01, Reduces Inflammation, Oxidative Stress, and Cisplatin-Induced Nephrotoxicity. *Int. J. Mol. Sci.* 22, 2793

- (18) Olearczyk, J. J., Field, M. B., Kim, I.-H., Morisseau, C., Hammock, B. D., and Imig, J. D. (2006) Substituted Adamantyl-Urea Inhibitors of the Soluble Epoxide Hydrolase Dilate Mesenteric Resistance Vessels. *J. Pharm. Exp. Ther.* 318, 1307.
- (19) Henrick, C. A., Staal, G. B., and Siddall, J. B. (1973) Alkyl 3,7,11-trimethyl-2,4-dodecadienoates, a new class of potent insect growth regulators with juvenile hormone activity. *J. Agric. Food Chem.* 21, 354-359.
- (20) Hammock, B. D., Gill, S. S., and Casida, J. E. (1974) Synthesis and morphogenetic activity of derivatives and analogs of aryl geranyl ether juvenoids. *J. Agric. Food Chem.* 22, 379-385.
- (21) Hwang, S. H., Tsai, H.-J., Liu, J.-Y., Morisseau, C., and Hammock, B. D. (2007) Orally Bioavailable Potent Soluble Epoxide Hydrolase Inhibitors. *J. Med. Chem.* 50, 3825-3840.
- (22) Singh, N., Barnych, B., Wagner, K. M., Wan, D., Morisseau, C., and Hammock, B. D. (2021) Adrenic Acid-Derived Epoxy Fatty Acids Are Naturally Occurring Lipids and Their Methyl Ester Prodrug Reduces Endoplasmic Reticulum Stress and Inflammatory Pain. *ACS Omega* 6, 7165-7174.
- (23) Newman, J. W., Morisseau, C., Harris, T. R., and Hammock, B. D. (2003) The soluble epoxide hydrolase encoded by EPXH2 is a bifunctional enzyme with novel lipid phosphate phosphatase activity. *Proc. Natl. Acad. Sci. U.S.A.* 100, 1558-1563.
- (24) Morisseau, C., and Hammock, B. D. (2007) Measurement of soluble epoxide hydrolase (sEH) activity. *Curr. Protoc. Toxicol.* Chapter 4, Unit 4.23.
- (25) Silverman, R. B., and Holladay, M. W. (2014) Chapter 8 - Drug Metabolism, In *The Organic Chemistry of Drug Design and Drug Action (Third Edition)* (Silverman, R. B., and Holladay, M. W., Eds.) pp 357-422, Academic Press, Boston.

- (26) Batchu, S. N., Lee, S. B., Qadhi, R. S., Chaudhary, K. R., El-Sikhry, H., Kodela, R., Falck, J. R., and Seubert, J. M. (2011) Cardioprotective effect of a dual acting epoxyeicosatrienoic acid analogue towards ischaemia reperfusion injury. *Br. J. Pharmacol.* *162*, 897-907.
- (27) Cullen, K. J., Yang, Z., Schumaker, L., and Guo, Z. (2007) Mitochondria as a critical target of the chemotherapeutic agent cisplatin in head and neck cancer. *J. Bioenerg. Biomembr.* *39*, 43-50.
- (28) Qian, W., Nishikawa, M., Haque, A. M., Hirose, M., Mashimo, M., Sato, E., and Inoue, M. (2005) Mitochondrial density determines the cellular sensitivity to cisplatin-induced cell death. *Am. J. Physiol: Cell Physiol.* *289*, C1466-1475.
- (29) Katragadda, D., Batchu, S. N., Cho, W. J., Chaudhary, K. R., Falck, J. R., and Seubert, J. M. (2009) Epoxyeicosatrienoic acids limit damage to mitochondrial function following stress in cardiac cells. *J. Mol. Cell Cardiol.* *46*, 867-875.
- (30) Sarkar, P., Zaja, I., Bienengraeber, M., Rarick, K. R., Terashvili, M., Canfield, S., Falck, J. R., and Harder, D. R. (2014) Epoxyeicosatrienoic acids pretreatment improves amyloid β -induced mitochondrial dysfunction in cultured rat hippocampal astrocytes. *Am. J. Physiol.: Heart Circ. Physiol.* *306*, H475-484.
- (31) Kawai, Y., Nakao, T., Kunimura, N., Kohda, Y., and Gemba, M. (2006) Relationship of intracellular calcium and oxygen radicals to Cisplatin-related renal cell injury. *J. Pharmacol. Sci.* *100*, 65-72.
- (32) Yue, J., and López, J. M. (2020) Understanding MAPK Signaling Pathways in Apoptosis. *Int. J. Mol. Sci.* *21*, 2346.

- (33) Adebessin, A. M., Wesser, T., Vijaykumar, J., Konkel, A., Paudyal, M. P., Lossie, J., Zhu, C., Westphal, C., Puli, N., Fischer, R., Schunck, W.-H., and Falck, J. R. (2019) Development of Robust 17(R),18(S)-Epoxyeicosatetraenoic Acid (17,18-EEQ) Analogues as Potential Clinical Antiarrhythmic Agents. *J. Med. Chem.* *62*, 10124-10143.
- (34) Berlin, S., Goette, A., Summo, L., Lossie, J., Gebauer, A., Al-Saady, N., Calo, L., Naccarelli, G., Schunck, W. H., Fischer, R., Camm, A. J., and Dobrev, D. (2020) Assessment of OMT-28, a synthetic analog of omega-3 epoxyeicosanoids, in patients with persistent atrial fibrillation: Rationale and design of the PROMISE-AF phase II study. *Int. J. Cardiol. Heart Vasc.* *29*, 100573.
- (35) Darwesh, A. M., Bassiouni, W., Adebessin, A. M., Mohammad, A. S., Falck, J. R., and Seubert, J. M. (2020) A Synthetic Epoxydocosapentaenoic Acid Analogue Ameliorates Cardiac Ischemia/Reperfusion Injury: The Involvement of the Sirtuin 3-NLRP3 Pathway. *Int. J. Mol. Sci.* *21*, 5261.
- (36) Morisseau, C., Inceoglu, B., Schmelzer, K., Tsai, H. J., Jinks, S. L., Hegedus, C. M., and Hammock, B. D. (2010) Naturally occurring monoepoxides of eicosapentaenoic acid and docosahexaenoic acid are bioactive antihyperalgesic lipids. *J. Lipid Res.* *51*, 3481-3490.
- (37) Wagner, K., Vito, S., Inceoglu, B., and Hammock, B. D. (2014) The role of long chain fatty acids and their epoxide metabolites in nociceptive signaling. *Prostaglandins Other Lipid Mediat.* *113-115*, 2-12.
- (38) Falck, J. R., Kodela, R., Manne, R., Atcha, K. R., Puli, N., Dubasi, N., Manthathi, V. L., Capdevila, J. H., Yi, X. Y., Goldman, D. H., Morisseau, C., Hammock, B. D., and Campbell, W. B. (2009) 14,15-Epoxyeicosa-5,8,11-trienoic acid (14,15-EET) surrogates

containing epoxide bioisosteres: influence upon vascular relaxation and soluble epoxide hydrolase inhibition. *J. Med. Chem.* 52, 5069-5075.

Supporting Information for

Chapter 3: New Alkoxy- Analogues of Epoxyeicosatrienoic Acids Attenuate Cisplatin Nephrotoxicity in vitro via Reduction of Mitochondrial Dysfunction, Oxidative Stress, Mitogen-Activated Protein Kinase Signaling, and Caspase Activation

Nalin Singh,[†] Anders Vik,[§] Daniel B. Lybrand,[†] Christophe Morisseau,[†] and Bruce D. Hammock^{†,*}

[†]Department of Entomology and Nematology and UC Davis Comprehensive Cancer Center, University of California Davis, Davis, CA, 95616, United States

[§] Department of Pharmacy, Section for Pharmaceutical Chemistry, University of Oslo, PO Box 1068 Blindern, N-0316 Oslo, Norway

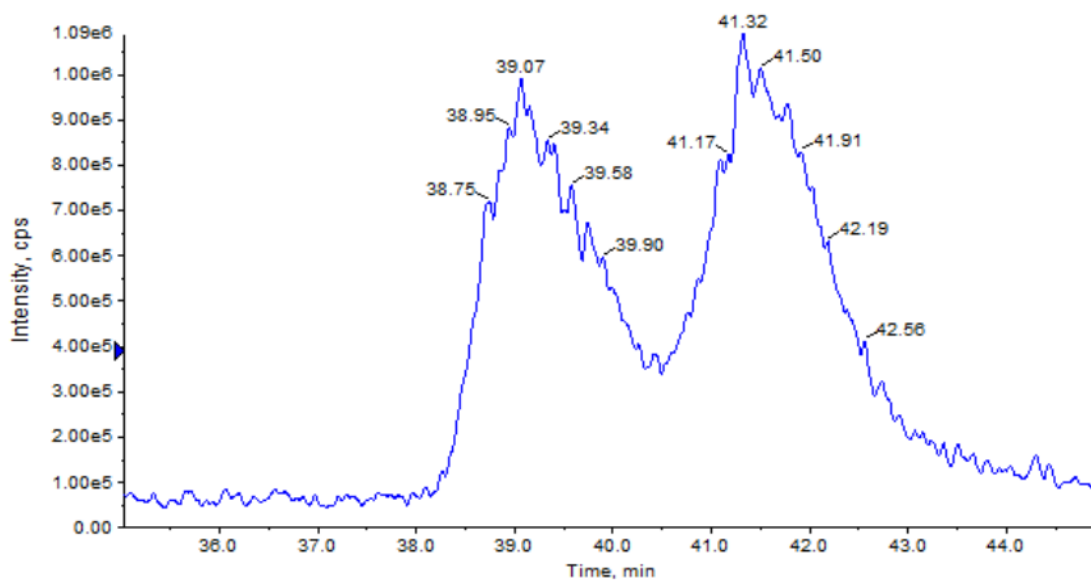
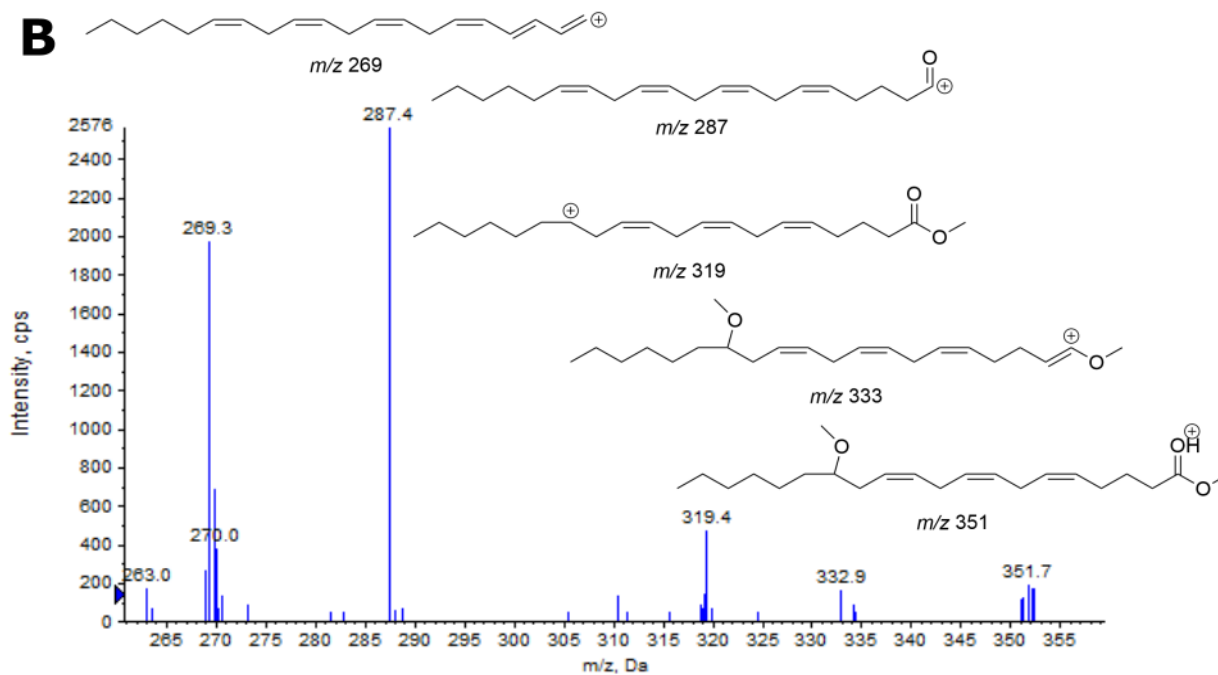
A**B**

Figure S1. HPLC-MS analysis of compound **1** (A) HPLC trace of m/z 351 with multiple regioisomer peaks (B) Product ion spectrum of m/z 351 $[M + H]^+$ precursor; putative structures for precursor and product ions of m/z 333, 319, 287, and 269 are shown.

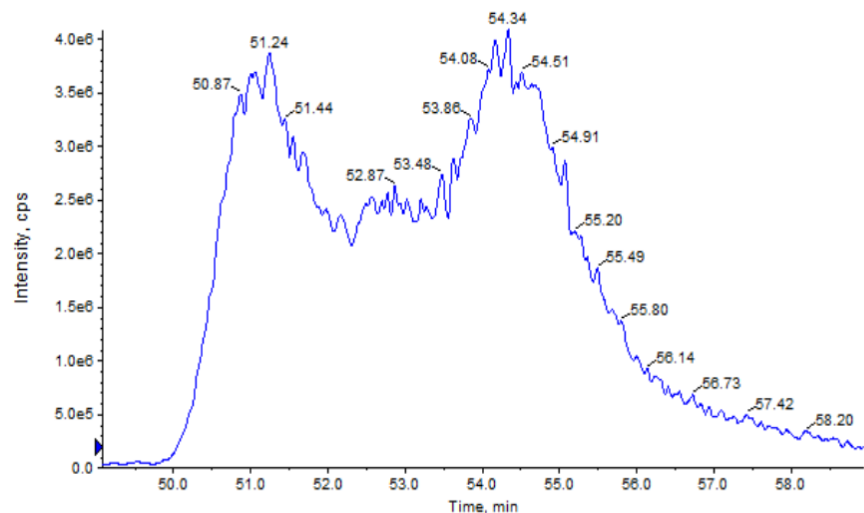
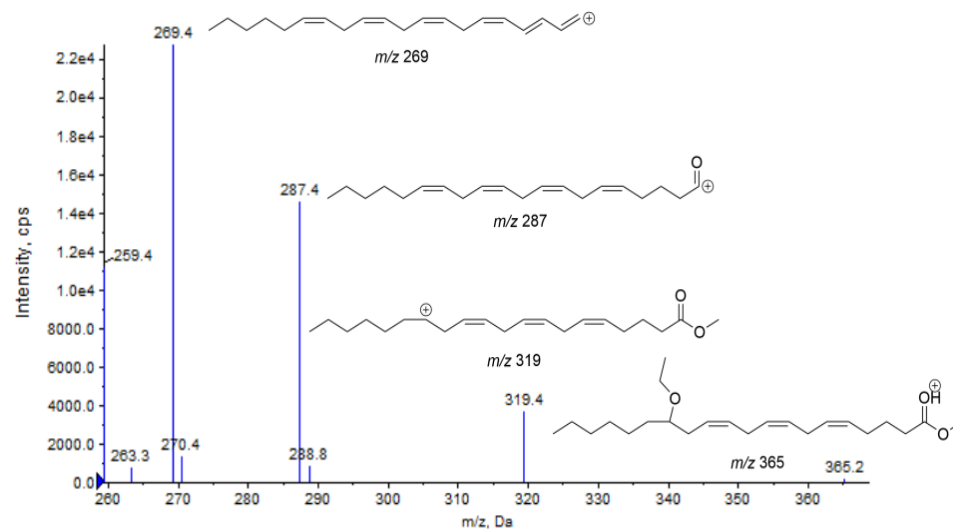
A**B**

Figure S2. HPLC-MS analysis of compound **2** (A) HPLC trace of m/z 365 with multiple regioisomer peaks (B) Product ion spectrum of m/z 365 $[M + H]^+$ precursor; putative structures for precursor and product ions of m/z 319, 287, and 269 are shown.

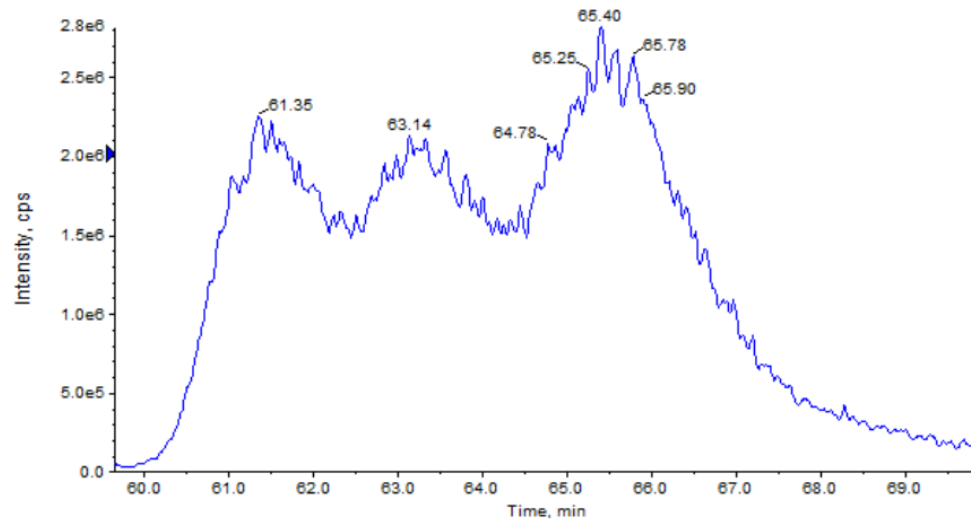
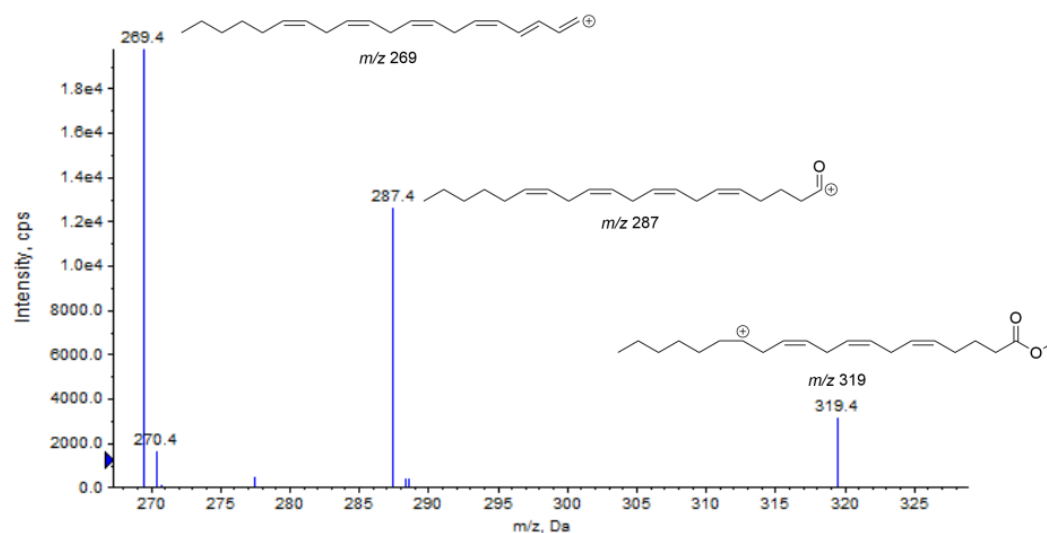
A**B**

Figure S3. HPLC-MS analysis of compound **3** (A) HPLC trace of m/z 379 with multiple regioisomer peaks (B) Product ion spectrum of m/z 379 $[M + H]^+$ precursor; putative structures for product ions of m/z 319, 287, and 269 are shown.

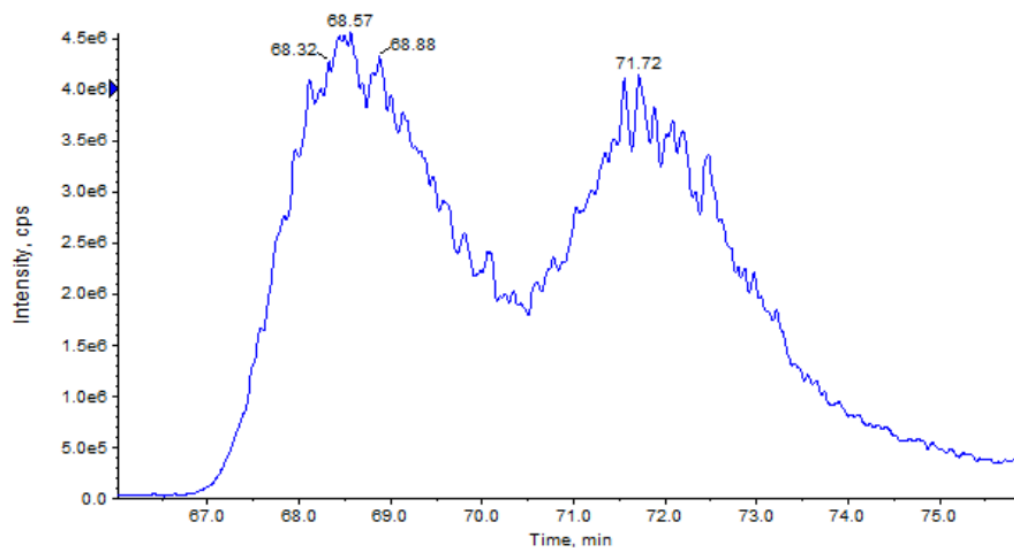
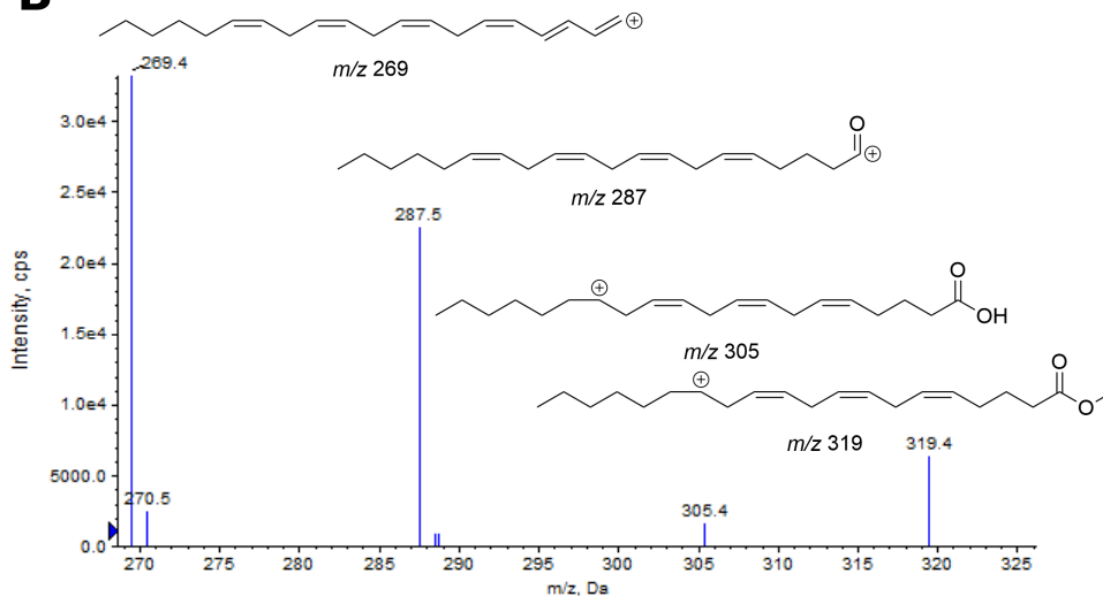
A**B**

Figure S4. HPLC-MS analysis of compound **4** (A) HPLC trace of m/z 379 with multiple regioisomer peaks (B) Product ion spectrum of m/z 379 $[M + H]^+$ precursor; putative structures for product ions of m/z 319, 305, 287, and 269 are shown.

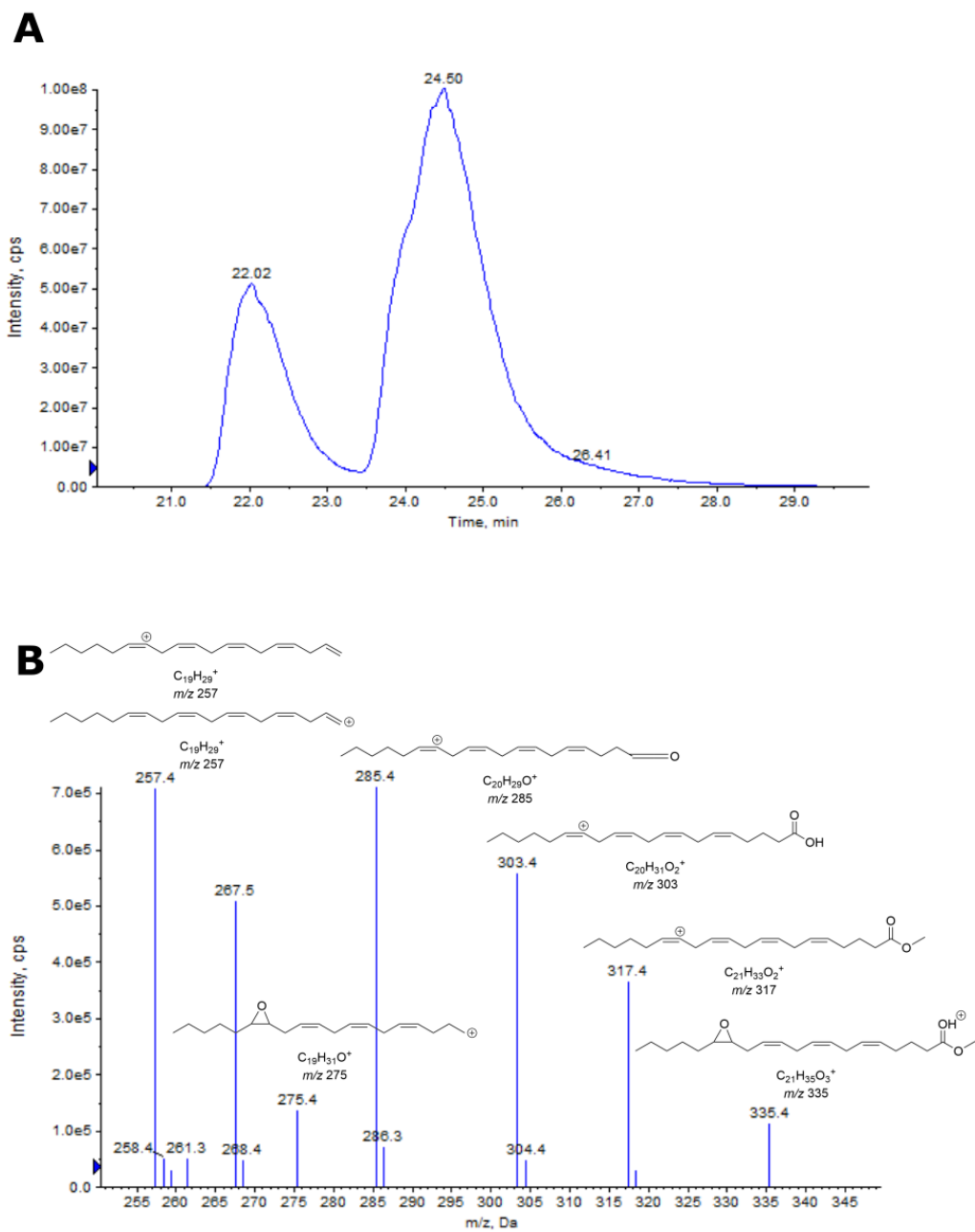


Figure S5. HPLC-MS analysis of compound **5** (**A**) HPLC trace of m/z 335 with multiple regioisomer peaks (**B**) Product ion spectrum of m/z 335 $[M + H]^+$ precursor; putative structures for precursor and product ions of m/z 335, 317, 303, 285, 275, and 257 are shown.

Table S1. HPLC Gradient employed for HPLC-MS analysis of Compounds 1-5

Time (min)	B (%)
0	25
2	25
2.01	70
82	80
82.01	100
84	100
85	25
90	25

Table S2. Q-TRAP Mass Spectrometer Conditions and Scan Range

Parameter	Q1 scan	Q3 scan
Curtain Gas (psi)	30	30
IonSpray Voltage (V)	4500	4000
Temperature (°C)	600	600
Ion Source Gas 1 (psi)	50	50
Ion Source Gas 2 (psi)	50	50
Declustering Potential (V)	60	60
Entrance Potential (V)	10	10
Collision Gas	N/A	Medium

Collision Energy (V)	N/A	30
Collision Cell Exit	N/A	10
Potential (V)		
<i>m/z</i> range (Da)	250-400	50-400

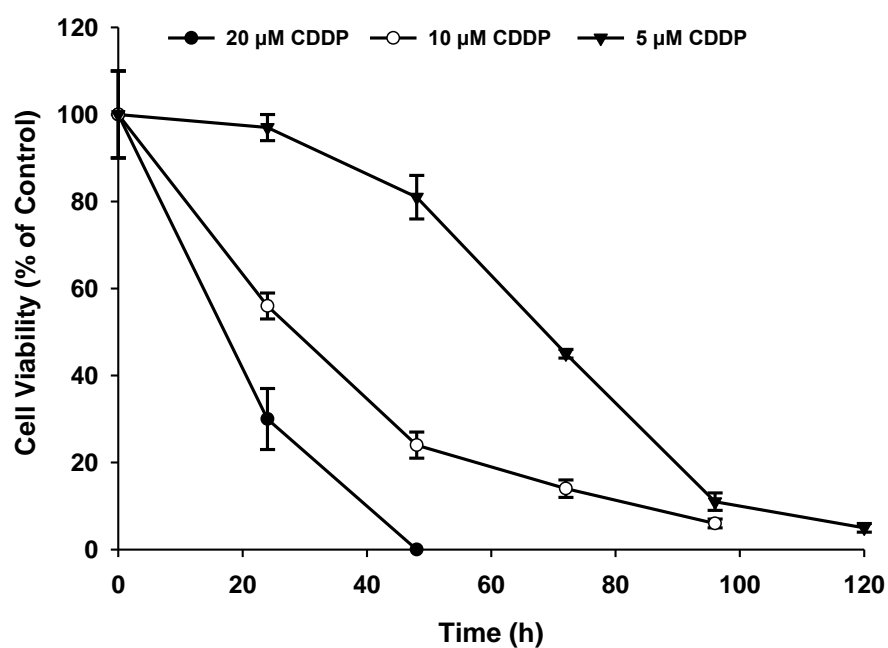


Figure S6. Concentration-response of cisplatin (CDDP) toxicity in LLC-PK1 proximal tubular cells along various exposure time points. Low, moderate, and high concentrations of CDDP were identified as 5, 10, and 20 μM , respectively.

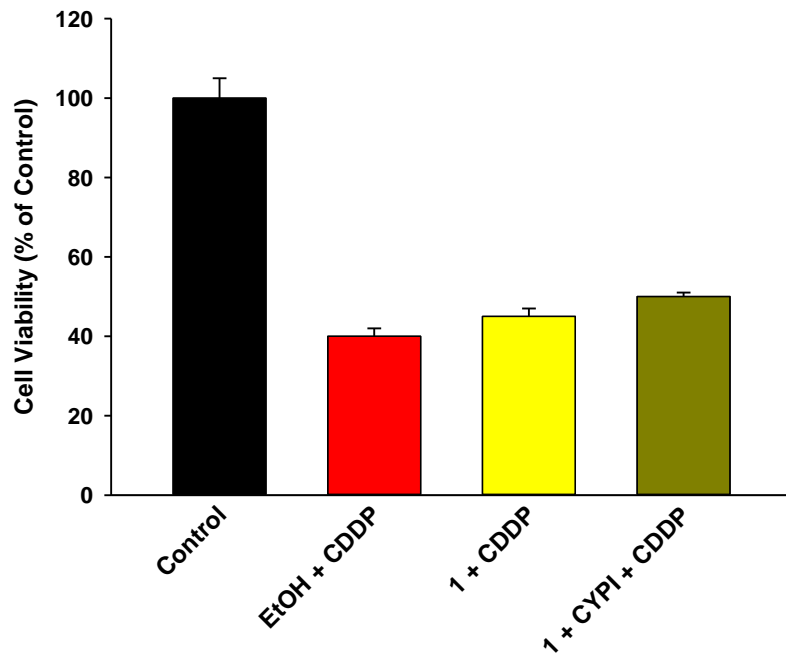
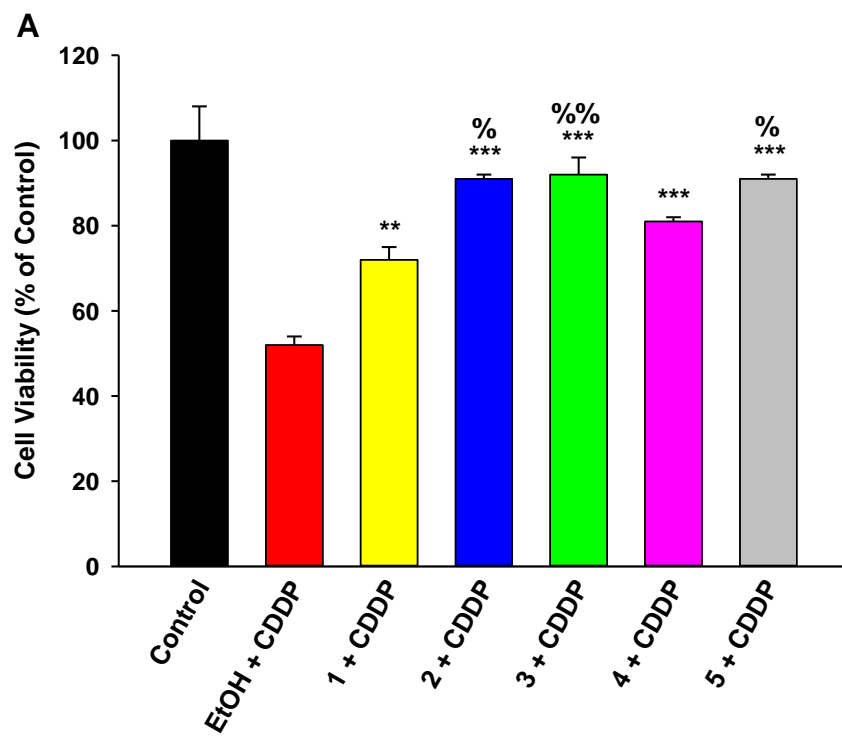


Figure S7. Co-administering EET analogue **1** with a CYP inhibitor (EM), to block potential *O*-demethylation, did not significantly improve its limited protective activity against cisplatin (CDDP) toxicity in LLC-PK1 proximal tubular cells



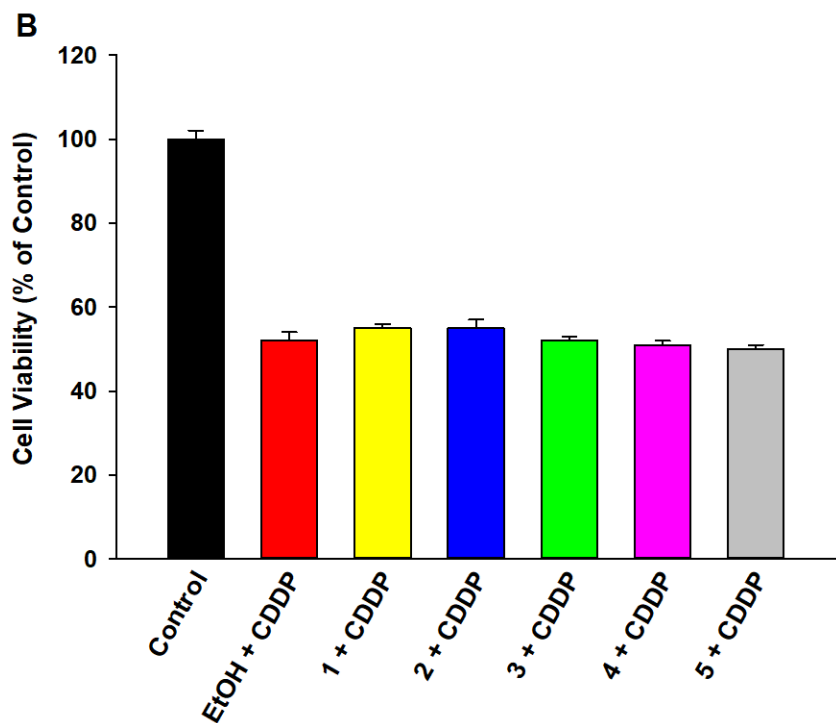


Figure S8. EET analogues **1-4** (as well as compound **5**) protect (A) LLC-PK1 proximal tubular cells but not (B) HepG2 liver cancer cells from cisplatin (CDDP) toxicity. Compounds **2**, **3**, and **5** were more active than **1**. (One way analysis of variance, Holm-Sidak method, $**p < 0.01$; $***p < 0.001$ vs. EtOH + CDDP group and ${}^{\%}p < 0.05$; ${}^{\%}{}^{\%}p < 0.01$ vs. **1** + CDDP group, $\alpha = 0.05$). Viability assessments were made with the CCK-8 in support of results from the MTT assay.

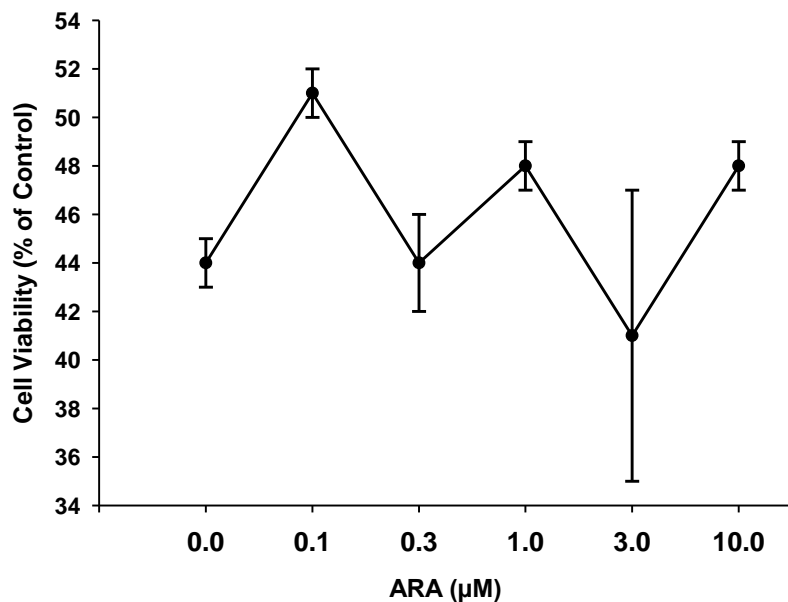


Figure S9. Concentration-response of activity of the parent ARA against cisplatin toxicity in LLC-PK1 proximal tubular cells. ARA did not protect cells at any concentration tested.

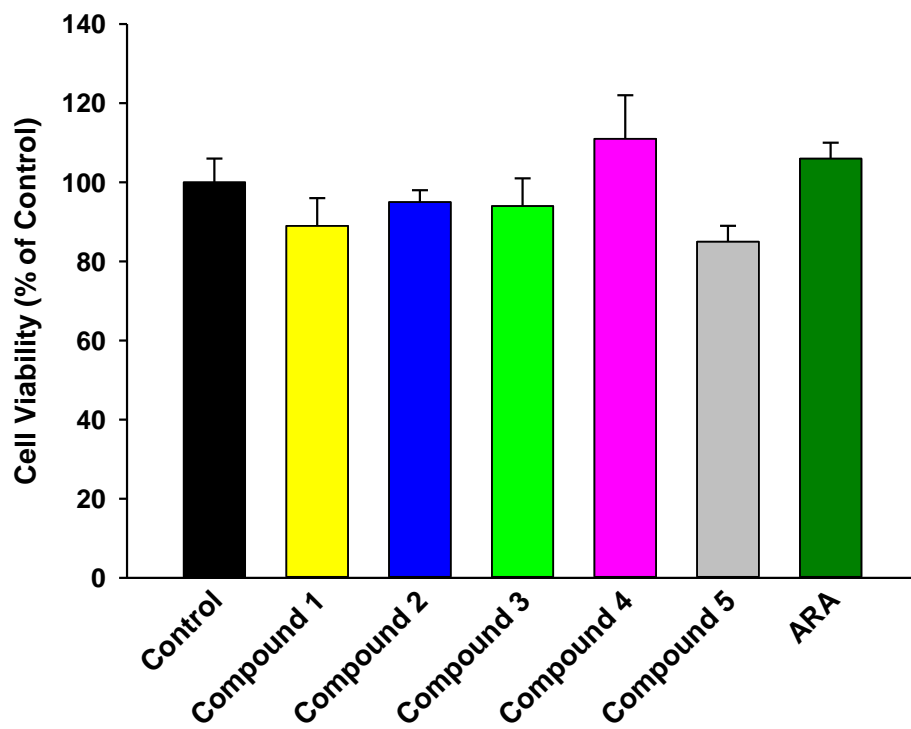


Figure S10. EET analogues **1-4**, compound **5**, and parent ARA did not influence viability of LLC-PK1 proximal tubular cells in the absence of cisplatin

Table S3. Inhibitory Potency of EET analogues **1-4** (relative to **5**) Against the Human Soluble Epoxide Hydrolase

Analogue	hsEH IC ₅₀ (μM)
1	13.6
2	15.1
3	6.7
4	32.1
Comparison Compound	hsEH IC ₅₀ (μM)
5	3.1

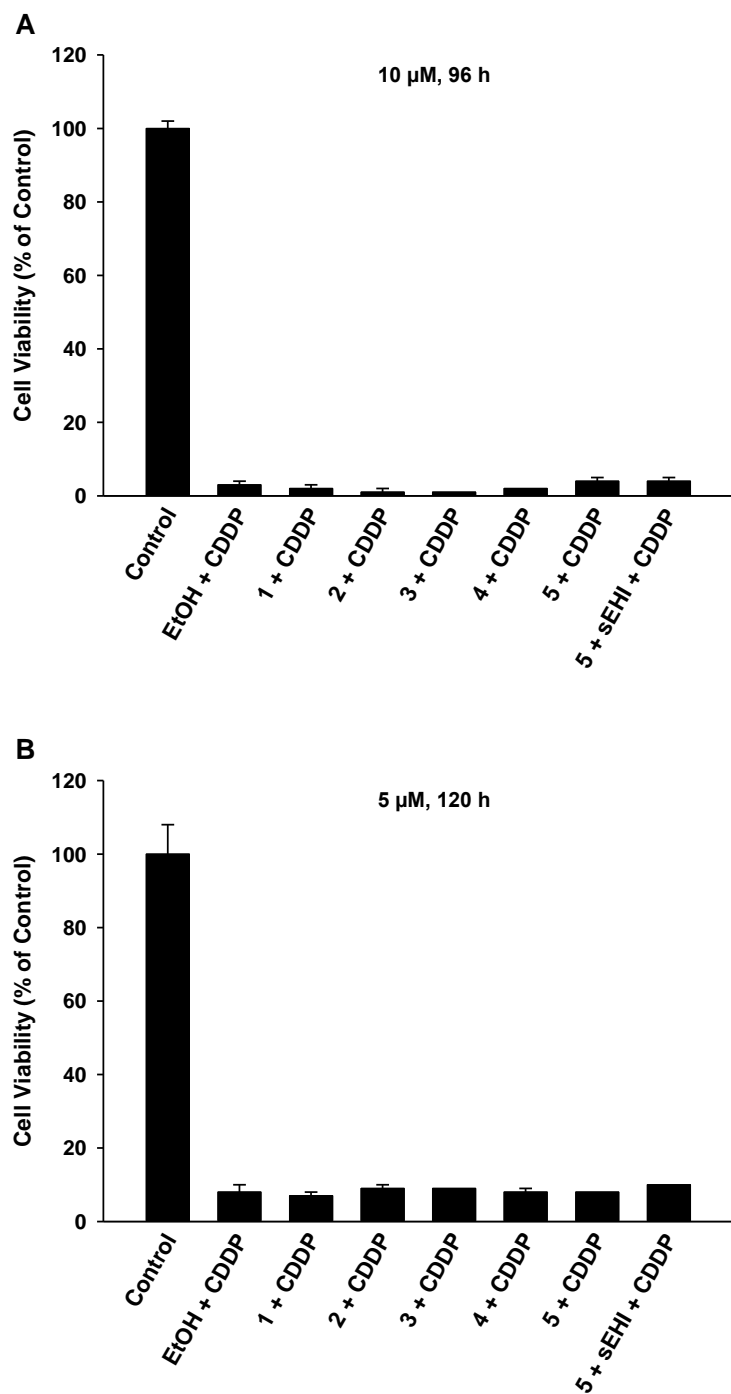


Figure S11. EET analogues 1-4, as well as compound 5 (with or without sEHI), were unable to maintain viability of LLC-PK1 proximal tubular cells exposed to (A) 10 μ M cisplatin (CDDP) for 96 h or (B) 5 μ M CDDP for 120 h

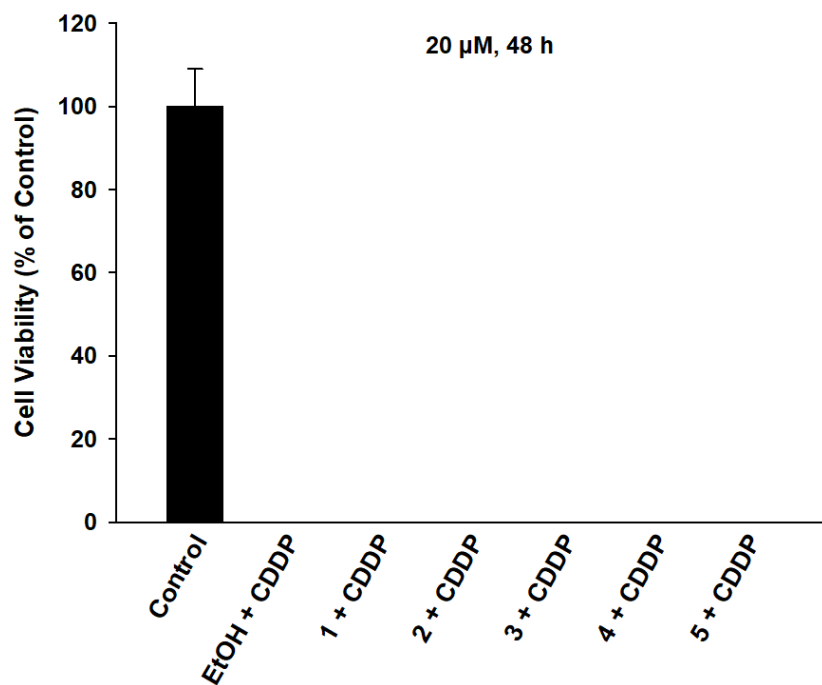


Figure S12. EET analogues 1-4 (as well as compound 5) were unable to maintain viability of LLC-PK1 proximal tubular cells exposed to 20 μ M cisplatin (CDDP) for 48 h

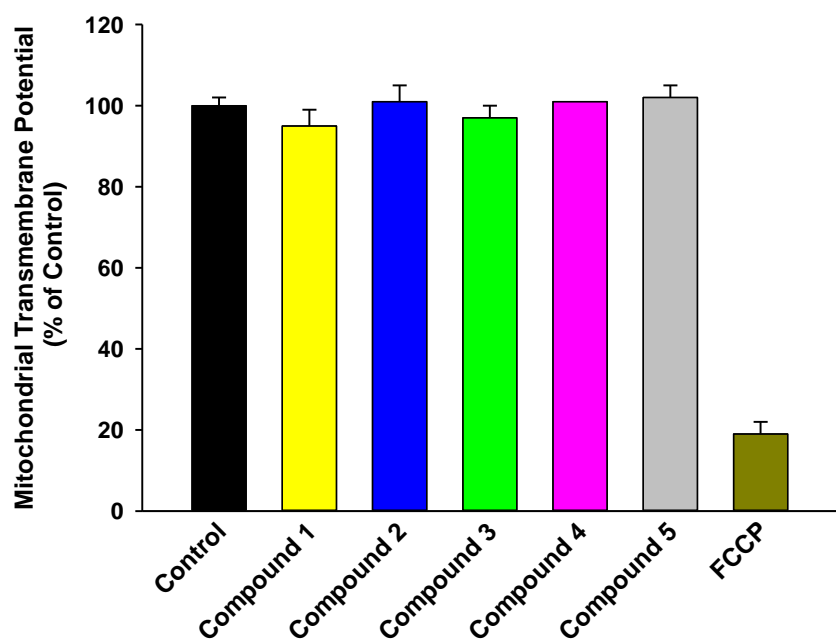


Figure S13. EET analogues **1-4** (as well as compound **5**) did not influence the mitochondrial transmembrane potential ($\Delta\Psi_m$) of LLC-PK1 proximal tubular cells in the absence of cisplatin.

FCCP is a positive control for loss of $\Delta\Psi_m$.

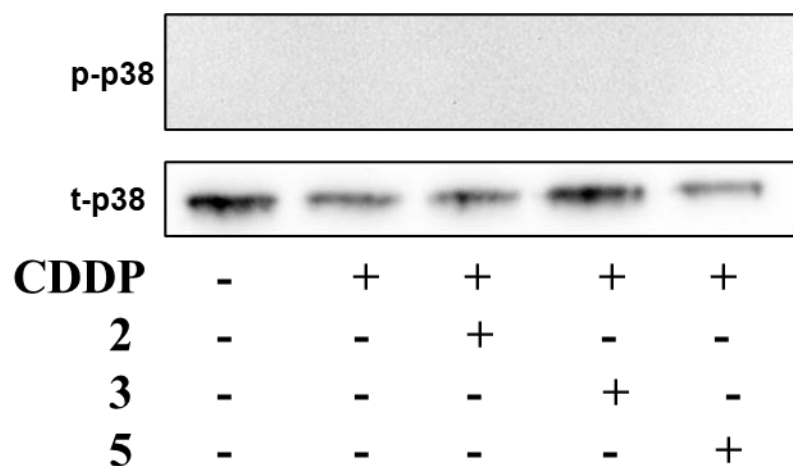


Figure S14. The phosphorylated variant of MAPK p38 was not detected in LLC-PK1 proximal tubular cells exposed to 20 μ M cisplatin (CDDP) for 6 h, in neither the presence nor absence of compounds **2**, **3**, or **5**.

Chapter 4: Improved ELISA for linoleate-derived diols in human plasma utilizing a polyHRP-based secondary tracer

Nalin Singh, Dongyang Li, Cindy B. McReynolds, Christophe Morisseau, and Bruce D.

Hammock*

Department of Entomology and Nematology and UC Davis Comprehensive Cancer Center,

University of California Davis, Davis, California, 95616, USA.

*E-mail: bdhammock@ucdavis.edu; Tel: 530-752-7519

Dihydroxyoctadecenoic acids (DiHOMEs) are cytochrome P450 pathway-derived metabolites of linoleic acid, a highly abundant dietary fatty acid. They serve thermogenic functions at low concentrations but, at high concentrations, are involved in proinflammatory and deleterious outcomes in a wide range of pathologies. Hence, the development of a reliable analytical method is critical to elucidate their potential as biomarkers of health, and enzyme-linked immunoassay (ELISA)-based approaches offer unique benefits as alternatives to traditional liquid chromatography-tandem mass spectrometry (LC-MS/MS) systems. Accordingly, an earlier ELISA for DiHOMEs was dramatically improved employing new secondary tracers and geared towards use in human plasma, a universal matrix in biomedical applications, as well as urine. Three ELISA formats, two utilizing polyHRP-based secondary labels for signal amplification, were compared. The best format involved a biotinylated detection antibody and a polyHRP-conjugated streptavidin tracer. Assay detectability was enhanced 20-fold, relative to the original immunoassay, and performance assessments validated precision, selectivity, and robustness. Fast and easy extraction-clean up steps yielded high analytical recovery and permitted the assay to operate in moderate concentrations (up to 20%) of plasma, expanding its practical relevance. Finally, the ELISA was applied towards detection of DiHOMEs in clinical samples and authenticated with complementary LC-MS/MS analysis. Hence, the method provides a valuable analytical tool to investigate the diverse and extensive roles of DiHOMEs in regulatory biology.

Introduction

Linoleic acid (LA, 18:2) is the most abundant fatty acid in western diets and, consequently, one of the most prevalent in human adipose tissue.¹ It is an essential fatty acid,² required at low levels for endogenous synthesis of ω -6 polyunsaturated fatty acids (PUFAs), particularly arachidonic acid, and plays a critical role in maintenance of skin barrier function.³ LA is a substrate of certain cytochromes P450 and is oxidized to epoxyoctadecenoic acids (EpOMEs).⁴ EpOMEs consist of two regioisomers, the 9,10-EpOME and 12,13-EpOME, otherwise known as leukotoxin (LTX) and *iso*-leukotoxin (*iso*-LTX), respectively. They are hydrolyzed downstream by the soluble epoxide hydrolase (sEH) to the dihydroxyoctadecenoic acids (DiHOMEs), 9,10-DiHOME and 12,13-DiHOME, also known as leukotoxin diol (LTXD) and *iso*-leukotoxin diol (*iso*-LTXD), respectively.⁴

EpOMEs were initially termed LTXs due to their cytotoxicity and association with poor outcomes in burn and acute respiratory distress syndrome (ARDS) patients and model species.⁵⁻⁷ However, studies utilizing EH-deficient systems and sEH inhibitors indicated hydrolytic bioactivation of LTXs is necessary for exertion of toxic effects, hence implicating the DiHOMEs (or LTXDs) as the deleterious agents.⁸⁻¹⁰ DiHOMEs cause extensive vascular permeability¹¹ and are involved in inflammatory diseases,¹²⁻¹⁵ pulmonary damage,¹⁶ sepsis,¹⁷ peroxisomal disorders,¹⁸ and burn injury,¹⁹ with high concentrations closely correlating with worsening morbidities. Recently, elevated plasma DiHOMEs were found to be excellent predictors of severe disease outcomes in patients with coronavirus disease 2019 (COVID-19).²⁰

Conversely, at low concentrations, DiHOMEs in fact act as signaling mediators in areas of metabolic dysfunction and obesity, endocrine disruption, mitogenesis, pain perception, and immune response.⁴ 12,13-DiHOME, in particular, modulates brown adipose tissue activation in

response to cold exposure and exercise, enhances glucose and fatty acid uptake, and improves cardiac mitochondrial respiration.²¹⁻²³ Accordingly, it has been classified as a thermogenic batokine and lipokine as well. DiHOMEs were also present at excessively low levels in patients with certain heart disease.²³

Hence, DiHOMEs appear to serve complex physiological roles, seemingly in a concentration-dependent manner. Thus, development of a validated analytical method with sufficient sensitivity to quantify a wide range of DiHOME concentrations is of considerable importance for their application as biomarkers of health and disease. Enzyme-linked immunosorbent assays (ELISA) are widely used for detection of a variety of analytes, including small molecules. While liquid chromatography-tandem mass spectrometry (LC-MS/MS) is the standard technique for multi-analyte analysis of oxidized lipids,^{24,25} for single analytes, ELISAs offer distinct advantages such as a lower cost, ease of operation, simplicity, speed, and high-throughput implementations. They can also be adapted to a variety of sensor platforms for multiplex application, providing greater suitability for clinical investigations.

Previously, a competitive ELISA for DiHOMEs in urine was developed by our group.²⁶ In this study, the ELISA was modified and substantially improved utilizing new secondary labels (i.e., polymeric horseradish peroxidase (HRP)-based systems) for signal amplification and enhanced detectability. Furthermore, it was applied towards use in human plasma, a ubiquitous and clinically relevant matrix, in addition to urine. Three distinct ELISA formats were compared in parallel and method validation was conducted to ensure assay reliability. For the optimal format, selectivity, robustness, analytical recovery, and matrix effects in plasma were assessed. Finally, the method was applied towards clinical samples and verified with LC-MS/MS analysis.

Materials and methods

Reagents and instrumentation

Linoleic acid (LA) methyl ester, LA, and Ricinoleic acid (OLE) were purchased from NuChek Prep Inc. (Elysian, MN, USA). EpOMEs, 9,10-dihydroxystearic acid (9,10-DiHSA), 9,10-DiHOME, 12,13-DiHOME, dihydroxyoctadecdienoic acids (DiHODEs), dihydroyeicosatrienoic acids (DiHETs), dihydroydocosatrienoic acids (DiHDTs), dihydroydocosapentaenoic acids (DiHDPs), and the tetrahydrofuran (THF)-diols of LA were prepared in-house.^{24,27} Albumin from chicken egg white (Ovalbumin) was purchased from Millipore Sigma (St. Louis, MO, USA). All reagents for synthesis are commercially available and were purchased from one of the following vendors: Millipore Sigma, Fisher Scientific Company LLC (Pittsburg, PA, USA), or VWR International (Radnor, PA, USA). Methanol, 2-propanol, glacial acetic acid, hexanes, ethyl acetate (EtOAc), and acetonitrile of HPLC grade or better were purchased from Fisher Scientific. All chemicals purchased from commercial sources were used as received without further purification. Flash chromatography was performed on silica gel (230–400 Mesh, Grade 60) from Fisher Scientific. Analytical thin layer chromatography (TLC) was performed on TLC silica gel 60 F254 plates from Merck KGaA (Darmstadt, Germany). ¹H nuclear magnetic resonance (NMR) spectra were recorded on a 400 MHz Bruker Avance III HD Nanobay NMR spectrometer. High-resolution electrospray ionization mass spectrometry (HRESIMS) data were recorded on a Thermo Q-Exactive High-field Orbitrap mass spectrometer operating in negative ion mode. MS spectra of the coating antigen were recorded on the Orbitrap operating in positive ion mode. rProteinA GraviTrap Columns were purchased from Millipore Sigma. Zeba Spin Desalting/Buffer Exchange Columns were purchased from Fisher Scientific. EZ-Link Sulfo-NHS-LC-Biotin was purchased from

Fisher Scientific. MaxiSorp clear flat-bottom immuno nonsterile 96-well plates were purchased from Fisher Scientific. Skim milk powder was purchased from Merck. HRP-conjugated Goat anti-Rabbit IgG was purchased from Jackson ImmunoResearch Laboratories Inc. (West Grove, PA, USA). Goat anti-Rabbit IgG PolyHRP40 and a Streptavidin PolyHRP40 Conjugate were purchased from Fitzgerald Industries International (Concord, MA, USA). 3,3',5,5'-tetramethylbenzidine (TMB) was purchased from Millipore Sigma. The NanoDrop™ Lite Spectrophotometer for protein quantitation was purchased from Fisher Scientific. ELISA microplates were washed automatically with a 405 TS Microplate Washer from BioTek Instruments (Winooski, VT, USA). Microplate incubations were conducted with an MTS 2/4 digital microtiter shaker from IKA (Staufen, Germany). Optical density (O.D.) was measured with a SpectraMax 190 Absorbance Microplate Reader from Molecular Devices (San Jose, CA, USA). UV-vis absorption spectra (200-800 nm) of the coating antigen were recorded with the SpectraMax Absorbance Reader. The Vortex-Genie 2 Mixer for solvent extraction/clean-up was purchased from Scientific Industries, Inc. (Bohemia, NY, USA). The accuSpin™ Micro 17R Microcentrifuge for solvent extraction/clean-up was purchased from Fisher Scientific.

Buffers and substrate

All buffers were prepared in Ultrapure water (18.1 MΩ/cm) from a MilliQ water purification system. For purification of the IgG antibody from antiserum, the binding, elution, and neutralization buffers were 20 mM sodium phosphate (pH 7.0), 0.1 M glycine-HCl (pH 3.0), and 1M Tris-HCl (pH 8.5), respectively. For the immunoassay, the coating buffer was 0.05 M sodium carbonate-bicarbonate (pH 9.6). The wash buffer was 1X phosphate-buffered saline (PBS, pH 7.4) containing 0.05% (v/v) Tween-20. The neat assay buffer was 1X PBS (pH 7.4).

The TMB substrate solution for color development was prepared from three components, the substrate buffer (pH 3.8), a 1% H₂O₂ stock, and the TMB stock, as per a previously described method.²⁸

Synthesis of DiHOME standard

The DiHOME standard (1:1 regioisomeric mixture, Fig. 1a) was synthesized as previously described.²⁴ Briefly, LA methyl ester was epoxidized with *meta*-chloroperoxybenzoic acid, followed by separation of the EpOME methyl esters by flash chromatography. The DiHOME methyl esters were obtained via perchloric acid-catalyzed hydrolysis of the epoxide. Finally, the free acid DiHOMEs were generated via base-catalyzed hydrolysis of the methyl ester and purified by flash chromatography. TLC plates (visualized with a KMNO₄ stain) revealed two conjoined spots, representing the two regioisomers ($R_f \approx 0.5$ in 60% Hexanes:40% EtOAc:0.2% glacial acetic acid developing solvent). ¹H NMR and HRESIMS data are described in the supplementary information. A stock solution of 1 mg/mL was prepared in acetonitrile, flushed with argon, and stored at -20 °C until use.

Purification of anti(α)-DiHOME antibody from rabbit antiserum

Antiserum active against DiHOMEs was from our group and was attained from an immunized rabbit as previously described.²⁶ The immunogen was a 9,10-/12,13-DiHOMEs-keyhole limpet hemocyanin (KLH) conjugate (Fig. 1b). Subsequently, the anti (α)-DiHOME IgG was purified from the antiserum via affinity chromatography with an rProteinA column, as per the manufacturer's instructions. Briefly, the column was first equilibrated with 10 mL binding buffer. 2 mL of antiserum was dissolved in 6 mL binding buffer and ran through the column (2x). After washing the column with 15 ml binding buffer, the IgG fraction was eluted with 4 ml

elution buffer into tubes containing 20% (final v/v) neutralization buffer. Quantitation by spectrophotometry revealed isolation of 9.45 mg of total IgG. Following buffer exchange to PBS, the native antibody obtained (2.7 mg/mL) was aliquoted and stored at -20 °C until use.

Biotinylation of α -DiHOME antibody

Biotinylation of the α -DiHOME antibody was conducted utilizing sulfo-NHS-biotin-mediated coupling, as per the manufacturer's instructions. Briefly, fresh sulfo-NHS-biotin (10 equiv.) was added to the native antibody (1 equiv.) in PBS and the mixture was shaken for 1 h at room temperature. The solution was desalted (2x) to eliminate excess biotin and the biotinylated antibody (0.8 mg/mL) was aliquoted and stored at -20 °C until use.

Synthesis of coating antigen

The major structurally relevant coating antigens (cAg) had previously been screened by our group.²⁶ The optimal, heterologous cAg was identified as a ricinoleic acid (OLE)-ovalbumin (OVA) conjugate (Fig. 1c) and hence utilized for the current study. Briefly, the hapten (OLE, 1.0 equiv.) was activated with 1-Ethyl-3-(3-dimethylaminopropyl)carbodiimide (2.2 equiv.) and N-hydroxysuccinimide (1.4 equiv.) in anhydrous dimethylformamide by stirring under argon for 2 h at room temperature. The solution was then added dropwise to OVA in PBS and stirred overnight at room temperature for amine coupling. Protein desalting was conducted, and the cAg was aliquoted and stored at -20 °C until use. The conjugation ratio of protein : hapten was estimated to be 1 : 3. Characterization of OLE-OVA (MS, UV-vis spectra) is shown in Fig. S1.

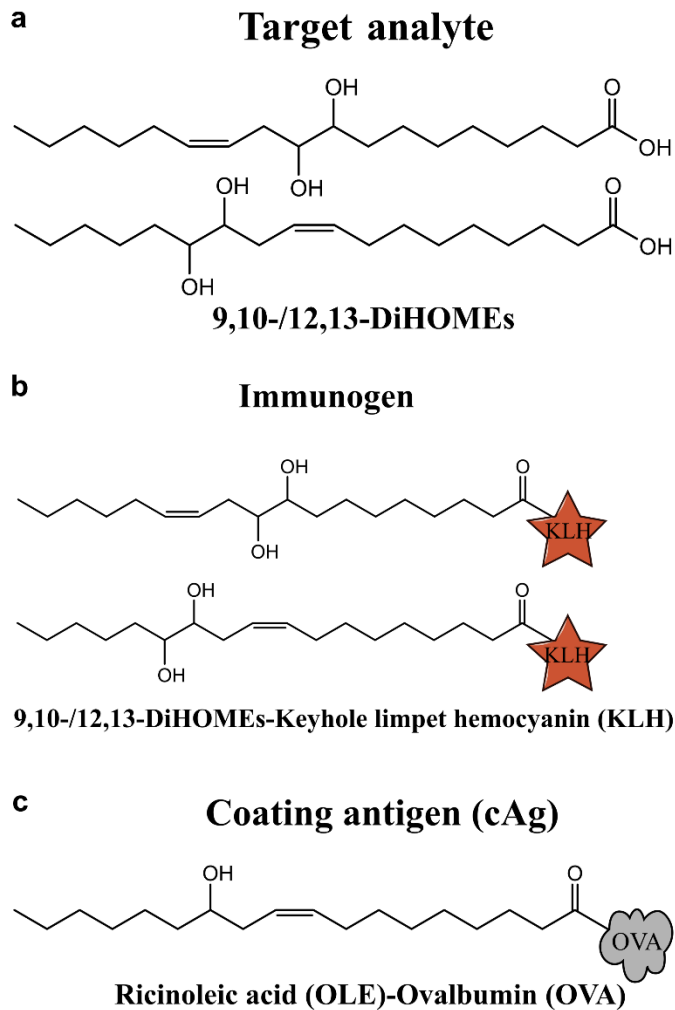


Fig. 1 Structures of the (a) target analyte standard, (b) immunogen,²⁶ and (c) coating antigen employed for development of the DiHOMEs ELISA

Competitive enzyme-linked immunoassays

ELISA microplates were first coated with OLE-OVA (0.33-0.95 $\mu\text{g}/\text{mL}$, 100 $\mu\text{L}/\text{well}$ in coating buffer) for 22 h at 4 $^{\circ}\text{C}$. After plates were washed (300 $\mu\text{L}/\text{well}$ wash buffer, 3x), wells were blocked (0.6 x g) with 3.5% (w/v) skim milk (250 $\mu\text{L}/\text{well}$ in assay buffer) for 1 h at room temperature. Plates were washed again (300 $\mu\text{L}/\text{well}$, 3x) and the analyte (100 $\mu\text{L}/\text{well}$ in assay buffer) was incubated with either the native (DetecAb) or biotinylated (BioAb) α -DiHOME

antibody (100 ng/mL, 100 μ L/well in assay buffer). The immunoreaction (0.6 x g) was allowed to proceed for 1 h at room temperature, after which plates were washed once again (300 μ L/well, 3x). DetecAb was traced (0.6 x g) with either a monomeric HRP-linked or polymeric HRP (polyHRP)-linked goat α -rabbit IgG (100 ng/mL, 100 μ L/well in assay buffer), while the BioAb was traced with the streptavidin-PolyHRP conjugate (100 ng/mL, 100 μ L/well in assay buffer) for 30 min at room temperature. After a final set of washes (300 μ L/well, 5x), the freshly prepared TMB substrate working solution (100 μ L/well) was added and permitted to react (0.6 x g) for 15 min at room temperature (protected from light). The enzymatic action was quenched with 1 M H₂SO₄ (100 μ L/well), plates were briefly shaken (10 sec), and absorbance was immediately read at $\lambda_{Abs} = 450$ nm.

Curve fitting

Calibration curves were constructed by plotting the O.D. values against the logarithm of the corresponding analyte concentration and fitted using OriginPro 8.5 software according to the 4-parameter logistic equation:

$$y = A2 + \frac{A1 - A2}{[1 + (x/x_0)^p]}$$

A1 is the maximal O.D. at zero analyte concentration, A2 is the minimal O.D. at infinite analyte concentration, p is the slope at the inflection point, and x₀ is the analyte concentration at which O.D. is 50% of the maximum (i.e., the IC₅₀). The linear working range is defined as the x values between which the O.D. is 20-80% of the maximum (i.e., the IC₂₀-IC₈₀), and was fitted according to the linear equation $y = a + kx$ where k is the slope of the linear range. The limit of detection (LOD) was defined as the x value at which $O.D. = O.D._{lowest\ standard\ point} + [3 \times (SD\ of\ O.D._{lowest\ standard\ point})]$

Method validation

Intra- and inter-assay precisions were determined by the coefficients of variation (CV, SD/mean) for sample triplicates from one plate and means of samples from three plates (run on three separate days), respectively. The % background and signal-to-noise ratio (S/N) were calculated as $(\text{observed O.D.}_{\text{min}}/\text{observed O.D.}_{\text{max}}) \times 100$ and upper asymptote (A1)/lower asymptote (A2), respectively.

Determination of cross-reactivity

Cross-reactivity (CR) was calculated as a relative IC₅₀ value for the analyte compared to the DiHOME standard, as per the equation: % CR = (IC₅₀ of DiHOME standard/IC₅₀ of test analyte) X 100

Assessment of assay robustness

Calibration curves were prepared in a) assay buffer containing varying concentrations of methanol (5-50%, v/v), b) PBS buffer (pH 7.4) containing varying concentrations of Na₂HPO₄ (5-50 mM, 0.5X-5X), and c) 1X PBS buffer of varying pH values (pH 6.4-8.4). IC₅₀ values and slopes of the linear range were compared to those of a calibration curve prepared in neat assay buffer (1X PBS, pH 7.4) to determine effects of an organic cosolvent, buffer ionic strength, and pH on ELISA performance, respectively.

Urine matrix tolerance

Calibration curves were prepared in assay buffer containing varying concentrations of spot human urine (5-50%, v/v) and compared to a calibration curve prepared in neat assay buffer to affirm serviceability of the ELISA in urine.

Extraction of DiHOMEs from plasma and extract clean-up

Human plasma (2 equiv.) was aliquoted into methanol (1 equiv.) and mixed strongly (10 sec) via a vortex mixer at maximal speed (34 x g). The solution was centrifuged at 4700 x g for 25 min. The precipitated pellet was discarded, and the collected supernatant was washed with hexanes (0.3 equiv., 3x). Briefly, the hexanes/aqueous-methanol mixture was vortexed strongly (10 sec, 34 x g) and centrifuged at 2200 x g for 5 min to partition the layers. The hexanes layer was carefully discarded, followed by addition of a fresh hexanes fraction for the next wash step. Finally, the cleaned extract was diluted in the assay buffer for the subsequent ELISA steps.

Spike recovery and matrix effects

For analytical recovery (AR) determinations, plasma samples were first pre-spiked with five concentrations of the standard (6.25, 12.5, 25, 50, and 100 ng/mL). Following MeOH extraction and clean-up, concentrations in extracts were calculated and compared to those of post-spike samples, as per the equation: $\% \text{ AR} = ([\text{DiHOME}_{\text{pre-spike}}]/[\text{DiHOME}_{\text{post-spike}}]) \times 100$. For matrix effect (ME) assessments, post-extraction diluents with varying concentrations of plasma (2.5-50%, v/v in assay buffer) were spiked with the DiHOME standard. Slopes (k) of the linear range were determined and compared to the k of a diluent prepared in neat assay buffer, as per the equation: $\% \text{ ME} = ((k_{\text{post-spike plasma}} - k_{\text{neat blank}})/k_{\text{neat blank}}) \times 100$. Negative or positive deviations were indicative of signal suppression or enhancement, respectively.

Real-sample analysis

In order to determine the ability of the assay to detect DiHOME concentrations in clinical samples, plasma obtained from healthy human volunteers who had undergone a clinical trial was analyzed using the developed ELISA. This clinical study (NCT04908995) had been conducted in

accordance with International Council for Harmonisation Good Clinical Practice guidelines and ethical principles that have their origin in the Declaration of Helsinki. Briefly, volunteers had been dosed with either a placebo or EC5026 (an sEH inhibitor), followed by *ex vivo* treatment of collected whole blood samples with lipopolysaccharides (LPS). An aliquot of the plasma fraction of whole blood isolated post-treatment was acquired and utilized for detection of DiHOMEs by the method as described above.

Confirmation by LC-MS/MS

LC-MS/MS analysis of real samples was conducted on an Agilent 1200 Series high-performance LC (HPLC) system from Agilent Technologies Inc. (Santa Clara, CA, USA), coupled to a SCIEX 4000 Q-TRAP tandem mass spectrometer from Applied Biosystems (Waltham, MA, USA), equipped with an electrospray ionization source (Turbo V), and operating in negative multiple reaction monitoring (MRM) mode. 10 μ L of samples were injected onto a reverse-phase 2.1 mm \times 100 mm, 1.7 μ m Kinetex C18 column, held at 40 °C. A gradient elution (Table S1), with a constant flow rate of 250 μ L/min, was employed for a 7 min chromatographic run (t_R of 3.08 and 3.13 min for 12,13- and 9,10-DiHOME, respectively). Mobile phase A was water with 0.1% glacial acetic acid and mobile phase B was methanol:2-propanol (1:1) with 0.1% glacial acetic acid. The distinctive MRM transitions monitored were m/z 313 (Q1) to m/z 183 (Q3_a) and m/z 201 (Q3_b) for 12,13- and 9,10-DiHOME, respectively, as previously identified.²⁹ Q-TRAP conditions and tandem MS parameters are described in Tables S2-S3.

Results and discussion

Comparison of three ELISA formats

Three competitive ELISA formats, A-C (Fig. 2), each utilizing a unique secondary label and performed in parallel with equivalent reagent concentrations, were investigated. Ideal concentrations of coating antigen and primary antibody were identified by a checkerboard titration (Fig. S2) and were determined to be 0.95 $\mu\text{g/mL}$ (ppm) and 0.1 $\mu\text{g/mL}$, respectively. Moreover, the optimal concentration of secondary tracers was 0.1 $\mu\text{g/mL}$. In formats A and B, the native α -DiHOME antibody (DetecAb) was used to bind the antigen. Taking advantage of the minimal influence of biotinylation on antibody function,³⁰ a biotinylated variant (BioAb) was utilized in format C. The DetecAb in format A was traced with a monomeric HRP-linked α -rabbit IgG. In contrast, formats B and C employed polyHRP-coupled secondary tracers for desired signal amplification, which would be expected due to the augmented specific activity of enzyme conjugates that results from the higher number of enzyme molecules present.^{30,31} A polyHRP-linked α -rabbit IgG was used in format B, while a streptavidin (SA)-polyHRP complex was utilized in format C, capitalizing on the exceptionally strong biochemical affinity between SA and biotin.^{30,31}

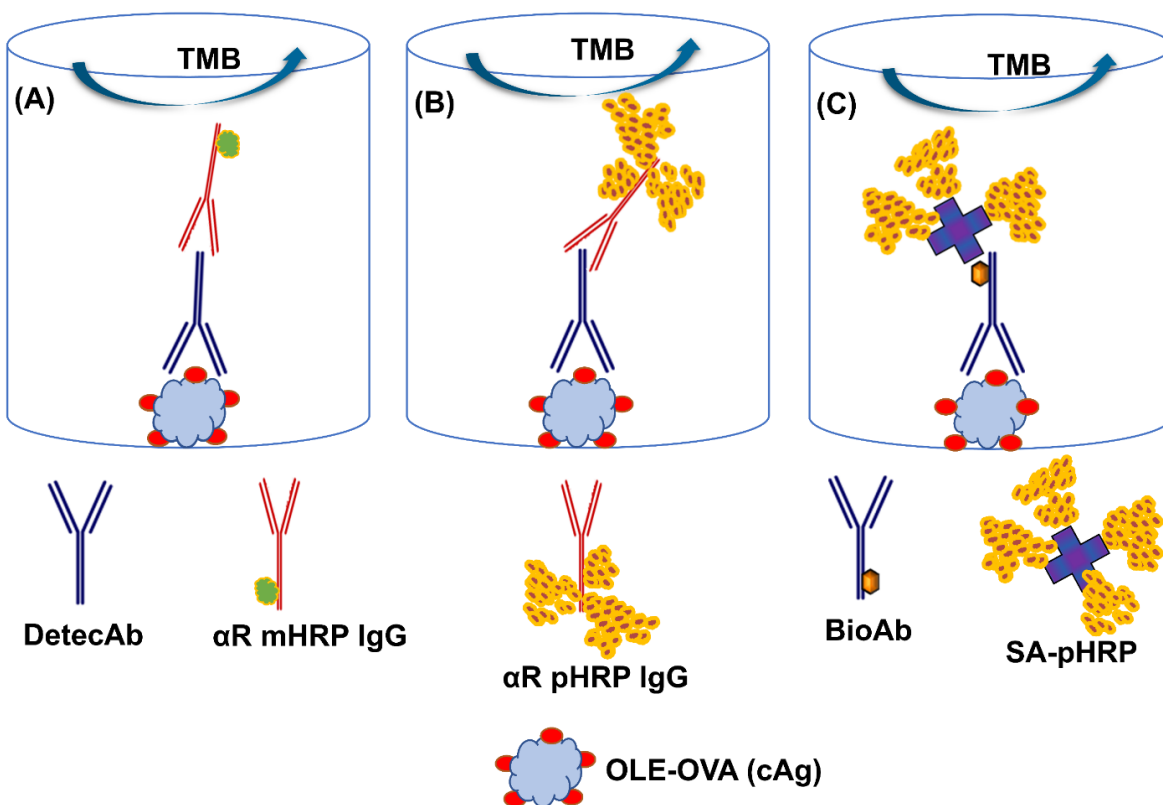


Fig. 2 Schematic of three competitive ELISA formats for DiHOMEs. **(A)** The native anti(α)-DiHOME antibody (DetecAb) was traced with a monomeric HRP-linked α -rabbit IgG (α R mHRP IgG). **(B)** The DetecAb was traced with a polymeric HRP-linked α -rabbit IgG (α R pHRP IgG). **(C)** The biotinylated α -DiHOME antibody (BioAb) was traced with a streptavidin-polyHRP complex (SA-pHRP). Illustrations are representative of the substrate-mediated color development step (post-washes).

The acquired IC_{50} values for all three formats were in the range of 0.57-0.77 ng/mL (Fig. 3), compared to the IC_{50} of 8 ng/mL for the original DiHOME ELISA.²⁶ This signifies a 10-15-fold increase in assay detectability, driven largely by application of new and enhanced secondary tracers. Importantly, for the polyHRP-based layouts B and C, the sizable improvement in detectability was attained without sacrificing signal magnitude (Fig. 3) as the maximum O.D. values observed (0.84-1.50) were comparable to that of the initial assay (0.86).²⁶

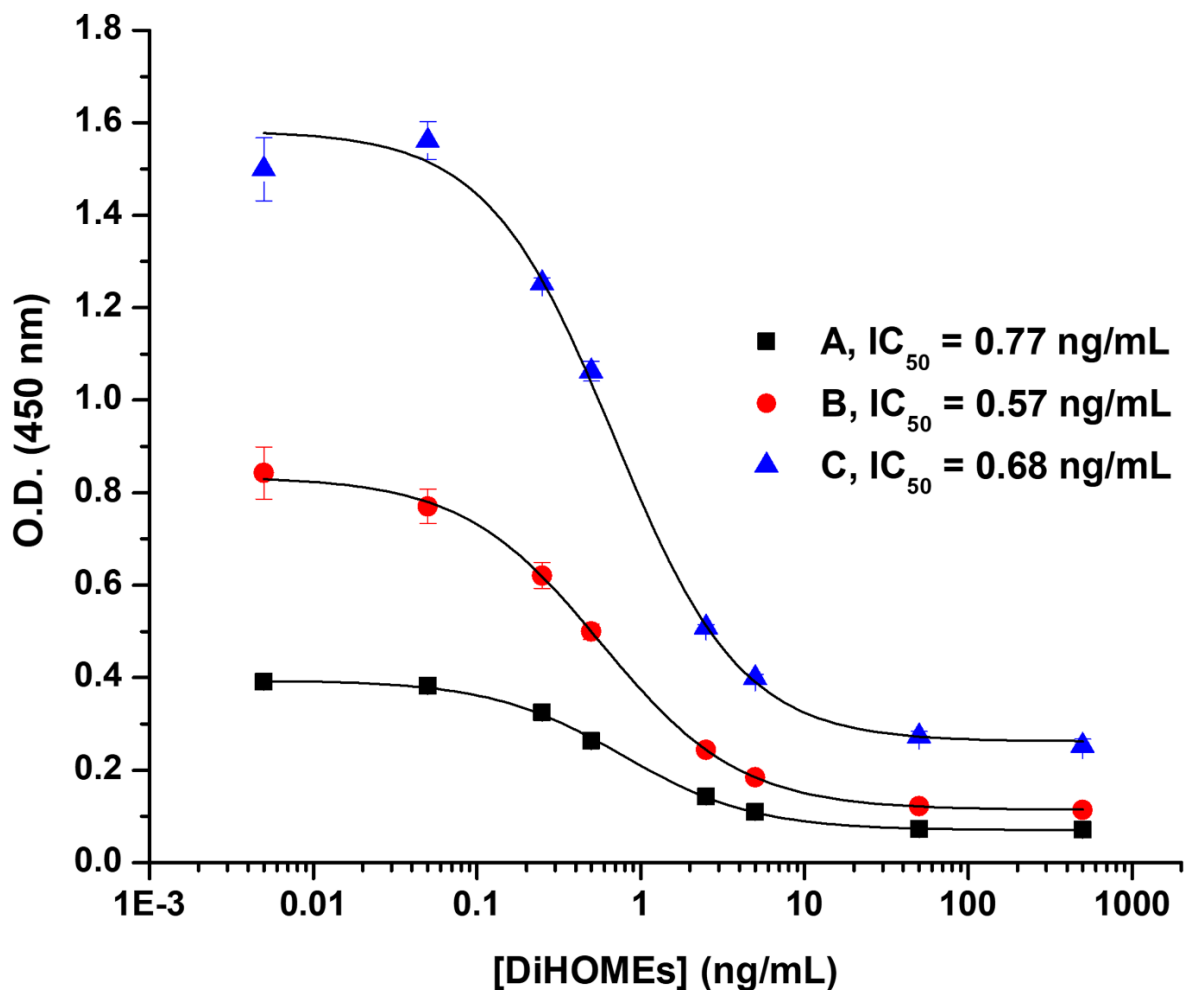


Fig. 3 Calibration curves (and IC₅₀ values) of the three ELISA formats A-C in neat assay buffer.

At equal reagent concentrations, there were few differences in the LOD, IC₅₀, and scope of the linear ranges (IC₂₀-IC₈₀) between format A and formats B and C (Table 1). Nevertheless, as noted, the signal response was considerably larger for the latter two formats (maximum O.D. of 0.84-1.50 vs. 0.39 for format A), a result of stronger polyHRP-mediated signal generation. Most prominently, the slopes of the linear range (k) for formats B and C were 2-fold and 4.5-fold greater than the k of format A, respectively (Table 1). Since k is defined as $dO.D./d[Analyte]$ and is hence a measure of assay sensitivity,³⁰ the steeper slopes indicate substantially greater discriminating power for the polyHRP systems, especially format C. In contrast, parameters such

as background and S/N were only marginally better for the polyHRP setups (Table 2). All three layouts possessed high intra- and inter-assay precision, validating their reliability, with the lowest CV seen for format C (Table 2). Altogether, primarily based on its highest amplification factor (i.e., ratio of k) and thus relative sensitivity,³⁰ the BioAb-SA-polyHRP configuration (i.e., format C) was considered optimal and adopted for further experiments.

Table 1 Parameters of logistic and linear fitting of calibration curves for ELISA formats A-C

ELISA Format	Logistic fitting				Linear fitting	
	R ²	LOD (ng/mL)	IC ₅₀ (ng/mL)	Linear range (IC ₂₀ – IC ₈₀ , ng/mL)	Slope (k)	r
A	0.9993	0.11	0.77	0.21 – 2.80	-0.071	- 0.9792
B	0.9998	0.13	0.57	0.15 – 2.20	-0.141	- 0.9889
C	0.9983	0.11	0.68	0.20 – 2.57	-0.321	- 0.9973
B/A	N/A	1.20	0.74	N/A	1.99	N/A
C/A	N/A	1.00	0.88	N/A	4.52	N/A

Table 2 Intra- and inter-assay precision, background, and S/N of ELISA formats A-C

	Precision (CV, %)	Background (%)	S/N

ELISA Format	Intra-assay ($n = 3$)	Inter-assay ($n = 3$)	O.D. _{min} /O.D. _{max}	A1/A2
A	3.40 – 10.9	7.50 – 21.6	18.0	5.62
B	2.71 – 8.44	9.57 – 22.2	13.5	7.32
C	1.44 – 5.02	2.71 – 13.6	16.2	6.05
B/A	N/A	N/A	0.75	1.30
C/A	N/A	N/A	0.9	1.08

Optimization of detectability

Because of the signal magnification afforded by the polyHRP label in ELISA format C, coating antigen (cAg) concentrations were lowered to further enhance assay detectability. Lessening the cAg typically decreases the IC₅₀ of competitive immunoassays,³² due to the increase in specificity of antibody binding. Fittingly, decreasing [cAg] by 30-50% drove down IC₅₀ values sizably (0.47-0.39 ng/mL vs. 0.70 ng/mL, Fig. 4), while retaining suitable signal strength (O.D._{max} = 1.23-0.94). However, an excessive reduction (70%) in [cAg] resulted in undesirable loss of signal (O.D._{max} = 0.69) without any appreciable improvement in IC₅₀ (0.37 ng/mL). Hence, relatively moderate concentrations of cAg were considered optimal and yielded an ELISA with a 20-fold greater detectability than the original method.²⁶

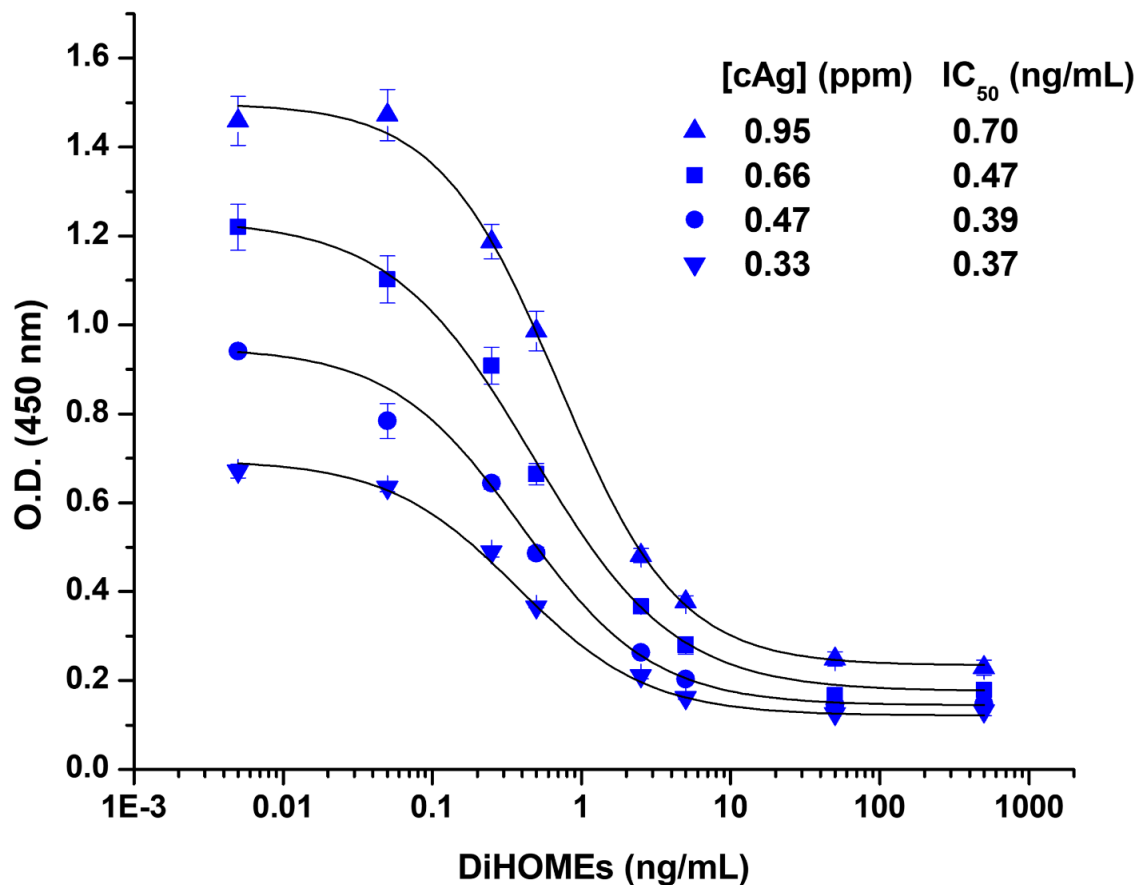


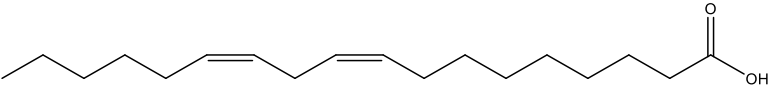
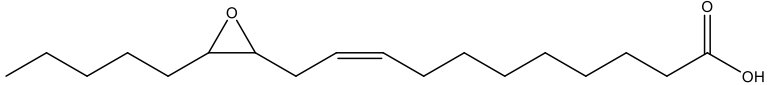
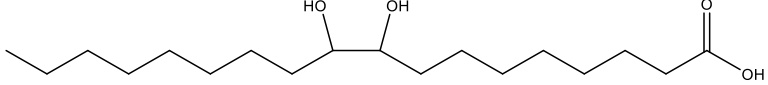
Fig. 4 Calibration curves (and IC₅₀ values) for ELISA format C at varying concentrations of coating antigen (cAg) in neat assay buffer.

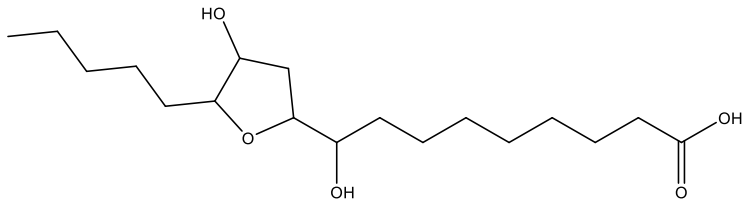
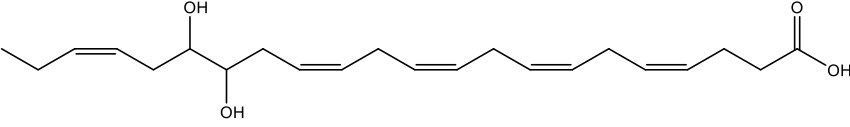
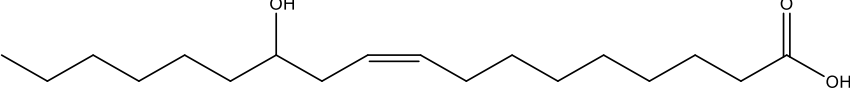
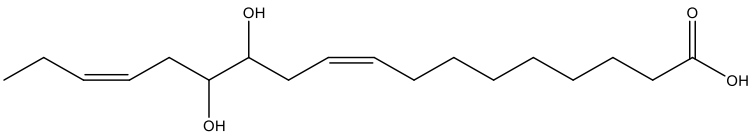
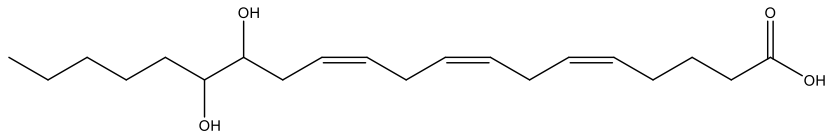
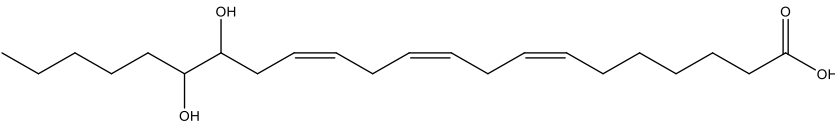
Selectivity

A cross-reactivity assessment with structurally related and biologically relevant fatty acids was conducted to ensure selectivity of the ELISA towards the target DiHOMEs (Table 3). Most critically, the ELISA did not cross-react with either linoleic acid (LA) or EpOMES (< 0.1%), indicating that the upstream precursors of DiHOMEs would not impede their detection. There was also insignificant cross-reactivity towards the THF-diols of LA (1.19%), alternative oxidized metabolites of EpOMEs.^{27,33} Expectedly, the assay exhibited a degree of cross-reactivity for OLE, a component of the coating antigen (Fig. 1c), though it was small (11.9%). Cross-reaction

with other dihydroxy fatty acids (DiHFAs) from common fatty acids was also assessed. It was negligible towards 9,10-DiHSA (0.54%), the diol derived from the abundant monounsaturated fatty acid, oleic acid (18:1). Cross-reactivity was low for ω -3-based DiHFAs, namely Docosahexaenoic acid (22:6)-derived DiHDPs (6.10%) and ω -3 alpha-linolenic acid (18:3)-derived DiHODEs (14.3%), although the relatively higher recognition for the latter is potentially due to greater structural homology. Highest cross-reactivity was seen towards ω -6 arachidonic acid (20:4)-derived DiHETs (30.0%) and their dihomo- analogues, adrenic acid (22:4)-derived DiHDTs (38.7%). This is perhaps because of the intersecting ω -6 nature of these diols, recalling that LA is the precursor for synthesis of the parent fatty acids. Still, since endogenous concentrations of linoleate metabolites far exceed those of corresponding metabolites derived from arachidonate,³⁴ the impact of this moderate non-selectivity would be trivial in real sample analyses.

Table 3 Cross-Reactivity with parent metabolites and mono- and dihydroxy fatty acids

Analyte	Representative structure	Cross-reactivity (%)
LA		< 0.01
EpOMEs ^a		< 0.1
9,10-DiHSA		0.54

THF-diols of LA ^a		1.19
DiHDPs ^a		6.10
OLE		11.9
DiHODEs ^a		14.3
DiHETs ^a		30.0
DiHDTs ^a		38.7

^aRegioisomeric mixtures

Organic cosolvent, ionic strength, and pH tolerance

Since methanol (MeOH) was employed as the organic cosolvent for extraction of DiHOMEs from plasma (as discussed in a later session), its impact on ELISA performance was evaluated. Low-moderate concentrations of MeOH (5-20%) had a limited effect on calibration curves and k values (Fig. 5a), relative to the neat assay buffer, though IC_{50} values did increase slightly at moderate MeOH concentrations (10-20%). A high concentration (50%), however, distorted the calibration curve (10-fold jump in IC_{50}) and flattened out the k , implying major interference.

Hence, ELISA performance was retained and considered functional in assay buffer containing a concentration of up to 20% MeOH. Another consideration is the ionic strength of the PBS buffer. Relative to the standard concentration of phosphate buffer (10 mM Na₂HPO₄, 1X), lower (5 mM, 0.5X) or moderately higher (20 mM, 2X) concentrations did not significantly hamper the ELISA (Fig. 5b), though k and $O.D._{max}$ did begin to drop at the latter concentration. A considerably more concentrated buffer (50 mM, 5X) adversely impacted the ELISA with a 2-fold reduction in k and diminished signal magnitude, suggesting that assay performance declines with increasing buffer ionic strength. Effects of pH fluctuations, ranging from slight acidity (pH 6.4) to slight basicity (pH 8.4), were also examined. The ELISA tolerated pH shifts in both directions quite well with minimal alterations to k and IC_{50} values (Fig. 5c), relative to neutral conditions (pH 7.4), suggesting resiliency against mildly acidic and alkaline conditions.

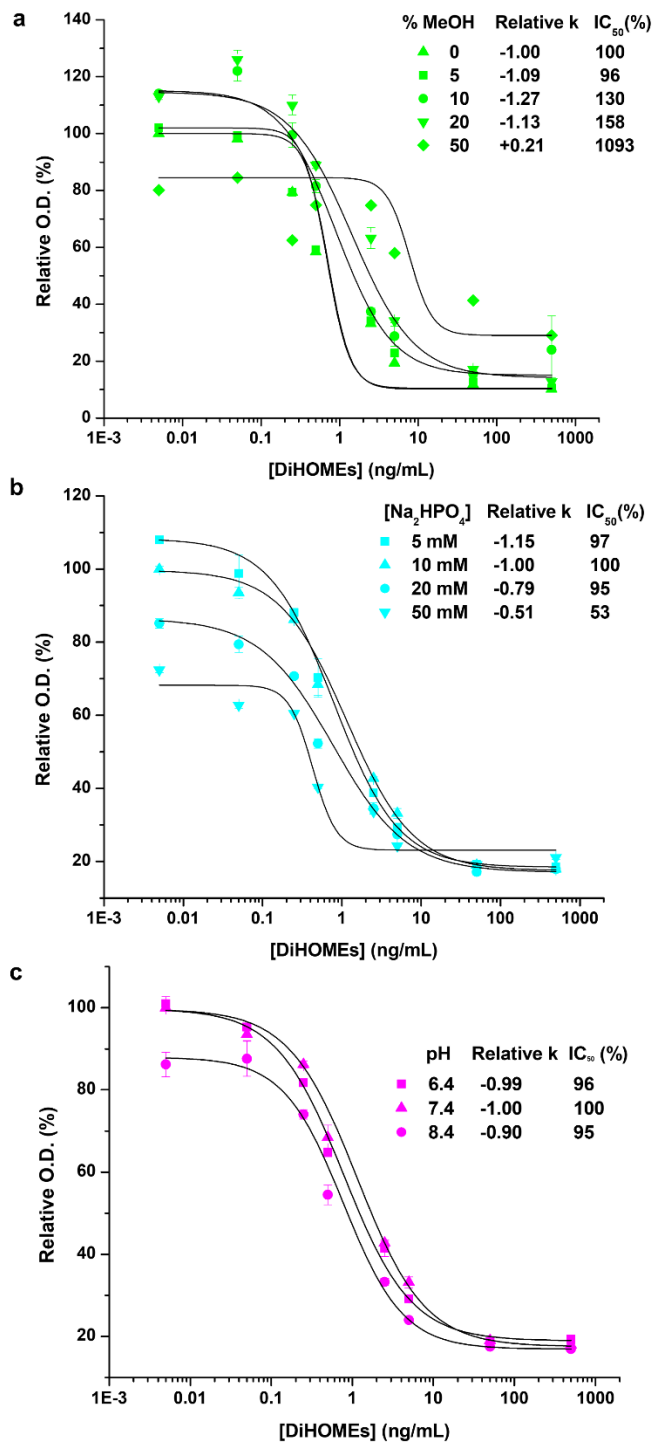


Fig. 5 Effects of (a) methanol (MeOH), (b) buffer ionic strength, and (c) pH on ELISA performance.

Solvent extraction, analytical recovery, and plasma tolerance

The original DiHOMEs ELISA was developed for application in urine samples since DiHOMEs can be metabolized and excreted as glucuronides and other conjugates.²⁶ Accordingly, functionality of the current assay was verified in human urine (useable in up to concentrations of 10%) and matching augmentations in detectability (i.e., greater than one order of magnitude reductions in the IC_{50}) were achieved (Fig. S3), indicating that the improved ELISA is also suitable for analysis of DiHOMEs in this pertinent matrix.

Nevertheless, the emphasis of the present method was on human plasma as the matrix since it is of greatest clinical relevance. Assessment and mitigation of matrix effects are key considerations to verify relevance of an assay towards real sample analysis. Typically, dilution into the assay buffer is the primary and simplest mode to reduce matrix influences. However, plasma is a complex medium with multiple polar and nonpolar elements that can adversely impact assay functionality. Hence, a quick and straightforward two-step extraction-clean-up process was employed first, to enhance sample quality and decrease the degree of dilution required for reliable method performance. In the extraction step, plasma was aliquoted into methanol, a water-miscible organic solvent commonly used as a cosolvent in ELISAs due to its relatively low influence on antigen-antibody interactions.³⁵ This extraction minimizes interference from salts and proteins (by precipitating them out) and apportions the DiHOMEs into the supernatant fraction. In the clean-up step, the methanol-aqueous extract was washed with hexanes, an immiscible nonpolar solvent. This was conducted to remove the potentially intrusive lipophilic components of plasma, while permitting retention of DiHOMEs in the polar layer, in accordance with the preferential partitioning of DiHFAs.³⁶

An analytical recovery of around 100% at five concentration levels of DiHOMEs validated this approach (Table 4), indicating efficient extraction and reliable retrieval of DiHOMEs from

human plasma. Furthermore, investigations of matrix effects revealed that low-moderate plasma concentrations (2.5-20%) did not significantly impact assay performance (Table 5). This is of particular significance since it suggests that the ELISA is operational in plasma samples after only a 5-fold-dilution, increasing potential for analysis of biological systems where DiHOMEs are present at lower concentrations. This contrasts with assays which possess high detectability in assay buffer but require 20-100-fold dilutions to be functional in real samples, a factor that restricts their tangible detection limits. However, a high plasma concentration (50%) did still result in substantial signal suppression ($\approx 60\%$) for the method (Table 5).

Table 4 Analytical recovery of DiHOMEs spiked at five concentrations into human plasma

[DiHOMEs] _{spiked} (ng/mL)	[DiHOMEs] _{measured} (ng/mL)	Recovery rate (%)
6.25	6.44	103
12.5	13.5	108
25.0	24.3	97
50.0	55.3	111
100	97.7	98

Table 5 ELISA tolerance to varying concentrations of human plasma

Plasma (%)	0	2.5	5	10	20	25	50
Relative k	-1.00	-1.15	-0.88	-1.13	-0.93	-0.74	-0.42
Matrix Effect	0	+15	-12	+13	-7	-26	-58

(%)^b

^b + = signal enhancement; - = signal suppression

Detection of DiHOMEs in real samples and correlation with LC-MS/MS analysis

Lastly, DiHOMEs were detected in plasma obtained from participants of a clinical trial for an sEH inhibitor (i.e., EC5026), to verify applicability of the developed ELISA towards clinical samples. DiHOMEs were successfully quantified in four different treatment groups (Fig. 6a), verifying pertinence of the ELISA towards real-sample analyses. Samples were also analyzed by LC-MS/MS to independently verify the detection of DiHOMEs with the previously validated analytical technique. Findings demonstrated a strong correlation (Pearson's coefficient of correlation, $r = 0.961$, Fig. 6b) between concentrations across the two methods, further bolstering reliability of the ELISA method.

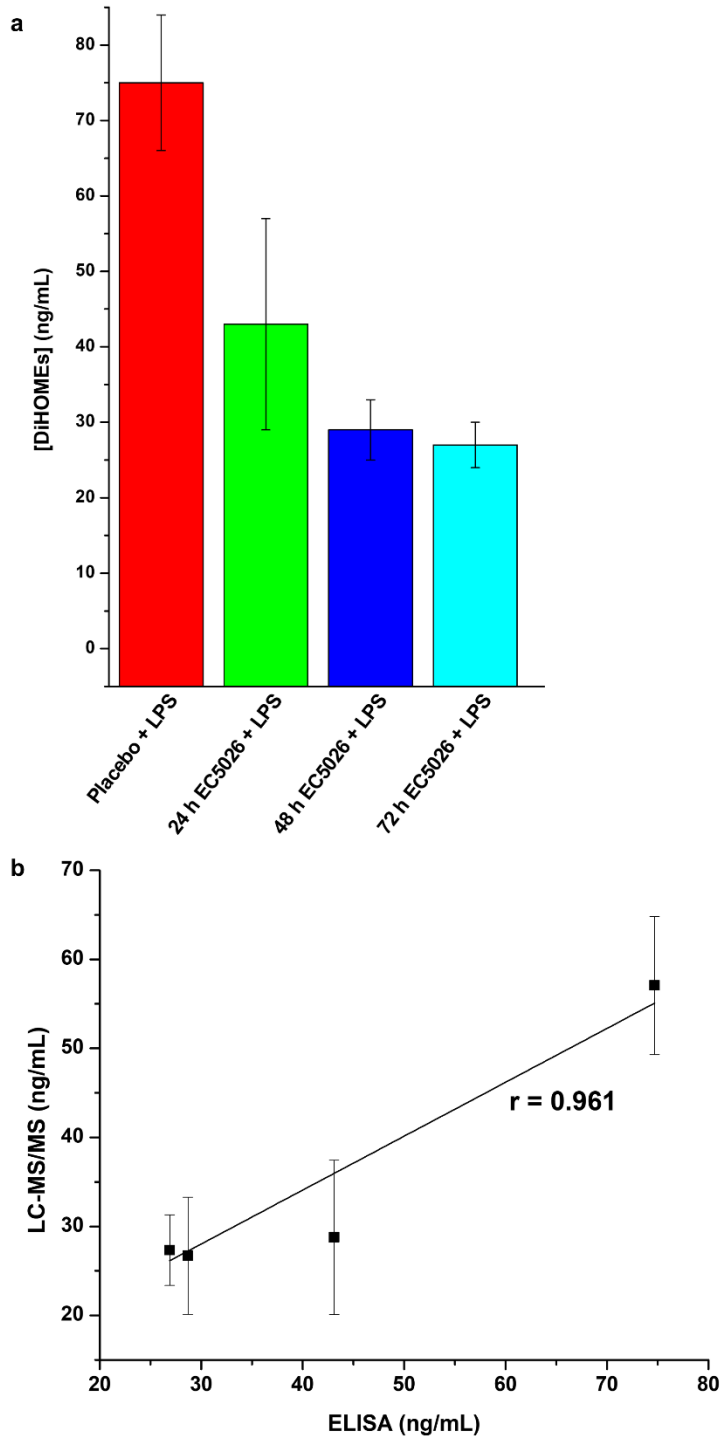


Fig. 6 Detection of DiHOMEs in clinical samples by the developed ELISA method. (a) DiHOME concentrations (\pm SD), determined by ELISA, in plasma obtained from four treatment

groups ($n = 8-16$ per group) of a clinical study. (b) Correlation between DiHOME concentrations (\pm SD) detected by LC-MS/MS and ELISA.

Conclusions

Herein, an enhanced competitive ELISA for detection of linoleic acid-derived diols was developed. Employment of a new secondary tracer improved detectability by more than one order of magnitude and various performance evaluations verified assay reliability. Tolerance to moderate concentrations of the plasma matrix and good correlation with LC-MS/MS with respect to analysis of clinical samples verified translatability for practical applications.

Differentiating the detectability between DiHOME regioisomers revealed that, intriguingly, the assay displays far greater selectivity for 12,13-DiHOME (≈ 23 -fold, Fig. 7), even though the original immunizing agent was a 9,10-/12,13-DiHOME (1:1)-KLH conjugate (Fig. 1b), suggesting strong regioisomeric-preference. This observation is likely due in part to the coating antigen used (Fig. 1c). Reactivity towards 9,10-DiHOME is sufficient enough for it to be detectable in samples with high levels of DiHOMEs but recognition would fall below the detection limit in samples with low to moderate concentrations. On the contrary, as illustrated, the ELISA exhibits excellent sensitivity towards 12,13-DiHOME, which tends to be the endogenously predominant regioisomer³⁴ and has been associated with a broader range of biologies.^{14,15,19,21-23} Incidentally, there is a commercially available competitive ELISA kit for 12,13-DiHOME (Cayman Chemical #501720). Nonetheless, the current assay possesses considerably greater detectability (≈ 7 -fold higher than reported value) towards 12,13-DiHOME and is significantly more economical.

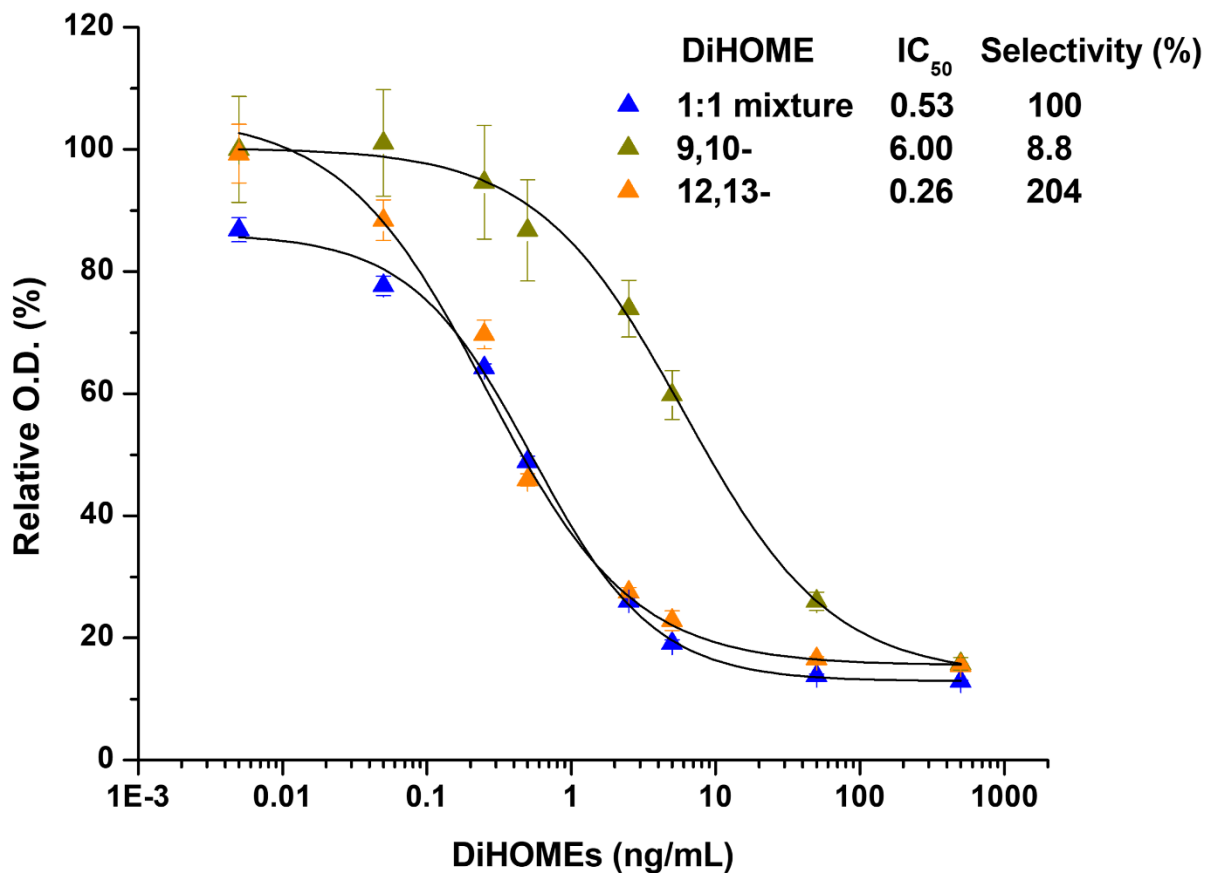


Fig. 7 Calibration curves for 9,10-DiHOME and 12,13-DiHOME, relative to the DiHOME standard (1:1 regioisomeric mixture), in neat assay buffer.

Therefore, as a next step, development of a 9,10-DiHOME-specific assay, potentially utilizing a different immunogen and/or coating antigen, could be explored for separate detection of this regioisomer since it might have some distinct biological activities. Moreover, there is growing interest in monoclonal single chain antibodies (or nanobodies) for detection of small molecules by immunoassay due to their higher specificity, relative to conventional IgG antibodies.^{31,37} Hence, nanobody-based ELISAs could be considered for regioisomer differentiation and comparable (or even enhanced) assay detectability.

While the method established in this study is far superior to older and commercially available immunoassays for DiHOMEs, its analytical performance would be unable to match that of traditionally used LC-MS/MS instruments. The LC-MS/MS methods previously reported boast an even greater sensitivity³⁸ (LOD of 0.0004-0.002 ng/mL vs. 0.05 ng/mL for ELISA) and a much larger linear working range³⁹ (four orders-of-magnitude difference between upper and lower limits vs. one order for ELISA), as well as permit synchronous differentiation of both regioisomers²⁹ (based on different fragmentation patterns, retention times). Thus, LC-MS/MS technology remains the gold standard for bioanalysis of DiHOMEs (and other oxidized lipids). However, its expensive and cumbersome nature can limit its applicability and hence the developed ELISA offers a fast and cheap alternative for high-throughput analyses, making it particularly suited for a clinical setting. Finally, the ELISA could be incorporated into multiplex platforms for simultaneous detection with other biomarkers of health and disease for a holistic evaluation of biological mechanisms and phenotypic outcomes.

Ethics statement

All procedures for acquisition of plasma from human volunteers were in accordance with International Council for Harmonisation Good Clinical Practice guidelines and ethical principles that have their origin in the Declaration of Helsinki.

Author contributions

Nalin Singh: conceptualization, methodology, validation, investigation, writing – original draft, writing – review & editing, visualization, funding acquisition. Dongyang Li: conceptualization,

methodology, resources, supervision. Cindy B. McReynolds: resources, writing – review & editing, funding acquisition. Christophe Morisseau: methodology, resources, supervision. Bruce D. Hammock: conceptualization, resources, supervision, funding acquisition.

Conflicts of interest

B.D.H. and C.B.M. are employees of EicOsis LLC, a company that focuses on bringing soluble epoxide hydrolase inhibitors (such as EC5026) to the clinic for use as analgesics

Acknowledgments

This work was partially supported by National Institutes of Health grants, National Institute of Environmental Health Sciences (NIEHS) RIVER Award R35 ES030443-01 (to B.D.H.), NIEHS Superfund Award P42 ES004699 (to B.D.H.), National Institute of General Medical Sciences (NIGMS) T32GM113770 (to C.B.M.), and National Heart, Lung, and Blood Institute (NHLBI) T32HL086350 (to N.S.).

References

1. S. J. Guyenet and S. E. Carlson, *Adv Nutr*, 2015, **6**, 660-664.
2. B. Lands, *Prog. Lipid Res.*, 2022, **85**, 101142.
3. T. Chiba, C. P. Thomas, M. W. Calcutt, W. E. Boeglin, V. B. O'Donnell and A. R. Brash, *J. Biol. Chem.*, 2016, **291**, 14540-14554.

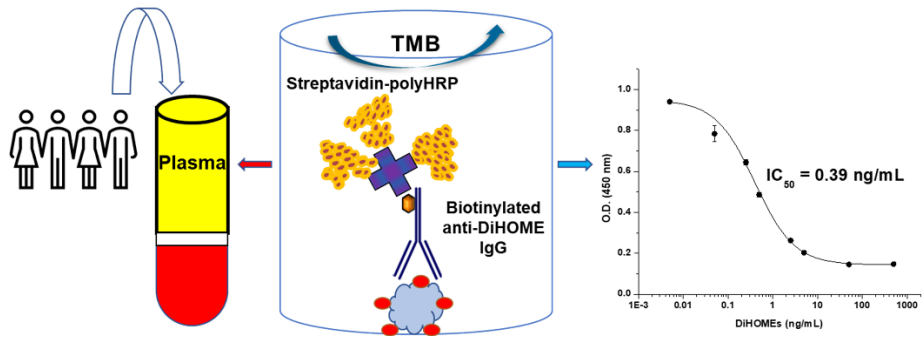
4. K. Hildreth, S. D. Kodani, B. D. Hammock and L. Zhao, *J. Nutr. Biochem.*, 2020, **86**, 108484.
5. K. Suzuki, H. Aoyama, Y. Izawa, M. Kobayashi and T. Ozawa, *Burns*, 1981, **8**, 110-117.
6. K. Kosaka, K. Suzuki, M. Hayakawa, S. Sugiyama and T. Ozawa, *Mol. Cell. Biochem.*, 1994, **139**, 141-148.
7. T. Ozawa, S. Sugiyama, M. Hayakawa, T. Satake, F. Taki, M. Iwata and K. Taki, *Am. Rev. of Respir. Dis.*, 1988, **137**, 535-540.
8. M. F. Moghaddam, D. F. Grant, J. M. Cheek, J. F. Greene, K. C. Williamson and B. D. Hammock, *Nat. Med.*, 1997, **3**, 562-566.
9. J. F. Greene, J. W. Newman, K. C. Williamson and B. D. Hammock, *Chem. Res. Toxicol.*, 2000, **13**, 217-226.
10. J. Zheng, C. G. Plopper, J. Lakritz, D. H. Storms and B. D. Hammock, *Am. J. Respir. Cell Mol.*, 2001, **25**, 434-438.
11. R. Slim, B. D. Hammock, M. Toborek, L. W. Robertson, J. W. Newman, C. H. P. Morisseau, B. A. Watkins, V. Saraswathi and B. Hennig, *Toxicol. Appl. Pharmacol.*, 2001, **171**, 184-193.
12. V. Samokhvalov, K. L. Jamieson, A. M. Darwesh, H. Keshavarz-Bahaghighat, T. Y. T. Lee, M. Edin, F. Lih, D. C. Zeldin and J. M. Seubert, *Front. Pharmacol.*, 2019, **9**, 1572.
13. K. R. Smith, K. E. Pinkerton, T. Watanabe, T. L. Pedersen, S. J. Ma and B. D. Hammock, *Proc. Natl. Acad. Sci. U.S.A.*, 2005, **102**, 2186.
14. B. Zimmer, C. Angioni, T. Osthues, A. Toewe, D. Thomas, S. C. Pierre, G. Geisslinger, K. Scholich and M. Sisignano, *Biochim. Biophys. Acta - Mol. Cell Biol. Lipids*, 2018, **1863**, 669-678.

15. S. R. Levan, K. A. Stamnes, D. L. Lin, A. R. Panzer, E. Fukui, K. McCauley, K. E. Fujimura, M. McKean, D. R. Ownby, E. M. Zoratti, H. A. Boushey, M. D. Cabana, C. C. Johnson and S. V. Lynch, *Nat. Microbiol.*, 2019, **4**, 1851-1861.
16. T. Ishizaki, T. Ozawa and N. F. Voelkel, *Pulm Pharmacol Ther*, 1999, **12**, 145-155.
17. M. Hamaguchi, H. N. Wu, M. Tanaka, N. Tsuda, O. A. G. Tantengco, T. Matsushima, T. Nakao, T. Ishibe, I. Sakata and I. Yanagihara, *Acute Medicine & Surgery*, 2019, **6**, 413-418.
18. J. M. Street, J. E. Evans and M. R. Natowicz, *J. Biol. Chem.*, 1996, **271**, 3507-3516.
19. C. B. Bergmann, C. B. McReynolds, D. Wan, N. Singh, H. Goetzman, C. C. Caldwell, D. M. Supp and B. D. Hammock, *Proc. Natl. Acad. Sci. U.S.A.*, 2022, **119**, e2120691119.
20. C. B. McReynolds, I. Cortes-Puch, R. Ravindran, I. H. Khan, B. G. Hammock, P.-a. B. Shih, B. D. Hammock and J. Yang, *Front. Physiol.*, 2021, **12**, 403.
21. M. D. Lynes, L. O. Leiria, M. Lundh, A. Bartelt, F. Shamsi, T. L. Huang, H. Takahashi, M. F. Hirshman, C. Schlein, A. Lee, L. A. Baer, F. J. May, F. Gao, N. R. Narain, E. Y. Chen, M. A. Kiebish, A. M. Cypess, M. Blüher, L. J. Goodyear, G. S. Hotamisligil, K. I. Stanford and Y.-H. Tseng, *Nat. Med.*, 2017, **23**, 1384-1384.
22. K. I. Stanford, M. D. Lynes, H. Takahashi, L. A. Baer, P. J. Arts, F. J. May, A. C. Lehnig, R. J. W. Middelbeek, J. J. Richard, K. So, E. Y. Chen, F. Gao, N. R. Narain, G. Distefano, V. K. Shettigar, M. F. Hirshman, M. T. Ziolo, M. A. Kiebish, Y.-H. Tseng, P. M. Coen and L. J. Goodyear, *Cell Metab.*, 2018, **27**, 1111-1120.e1113.
23. K. M. Pinckard, V. K. Shettigar, K. R. Wright, E. Abay, L. A. Baer, P. Vidal, R. S. Dewal, D. Das, S. Duarte-Sanmiguel, D. Hernández-Saavedra, P. J. Arts, A. C. Lehnig, V. Bussberg, N.

- R. Narain, M. A. Kiebish, F. Yi, L. M. Sparks, B. H. Goodpaster, S. R. Smith, R. E. Pratley, E. D. Lewandowski, S. V. Raman, L. E. Wold, D. Gallego-Perez, P. M. Coen, M. T. Ziolo and K. I. Stanford, *Circulation*, 2021, **143**, 145-159.
24. J. W. Newman, T. Watanabe and B. D. Hammock, *J. Lipid Res.*, 2002, **43**, 1563-1578.
25. Z.-X. Yuan, S. Majchrzak-Hong, G. S. Keyes, M. J. Iadarola, A. J. Mannes and C. E. Ramsden, *Anal. Bioanal. Chem.*, 2018, **410**, 6009-6029.
26. G. Zurek, S. J. Gee and B. D. Hammock, *Anal. Chim. Acta*, 2002, **466**, 247-256.
27. M. F. Moghaddam, K. Motoba, B. Borhan, F. Pinot and B. D. Hammock, *Biochim. Biophys. Acta – Gen. Subj.*, 1996, **1290**, 327-339.
28. D. Li, C. Morisseau, C. B. McReynolds, T. Dufлот, J. Bellien, R. M. Nagra, A. Y. Taha and B. D. Hammock, *Anal. Chem.*, 2020, **92**, 7334-7342.
29. J. Bylund, J. Ericsson and E. H. Oliw, *Anal. Biochem.*, 1998, **265**, 55-68.
30. D. Li, Y. Ying, J. Wu, R. Niessner and D. Knopp, *Microchim Acta*, 2013, **180**, 711-717.
31. D. Li, Y. Cui, C. Morisseau, S. J. Gee, C. S. Bever, X. Liu, J. Wu, B. D. Hammock and Y. Ying, *Anal. Chem.*, 2017, **89**, 6248-6256.
32. X. Wang, L. Cohen, J. Wang and D. R. Walt, *J. Am. Chem. Soc.*, 2018, **140**, 18132-18139.
33. M. Markaverich Barry, M. Alejandro, T. Thompson, S. Mani, A. Reyna, W. Portillo, J. Sharp, J. Turk and R. Crowley Jan, *Environ. Health Perspect.*, 2007, **115**, 702-708.
34. C. Schmöcker, I. W. Zhang, S. Kiesler, U. Kassner, A. I. Ostermann, E. Steinhagen-Thiessen, N. H. Schebb and K.-H. Weylandt, *Int. J. Mol. Sci.*, 2018, **19**, 180.

35. X. Cui, Q. He, D. Shen, Z. Jiang, Y. Chen, S. Zhao and B. D. Hammock, *Anal. Methods*, 2018, **10**, 2629-2635.
36. S. S. Gill, K. Ota and B. D. Hammock, *Anal. Biochem.*, 1983, **131**, 273-282.
37. Z.-F. Li, J.-X. Dong, N. Vasylieva, Y.-L. Cui, D.-B. Wan, X.-D. Hua, J.-Q. Huo, D.-C. Yang, S. J. Gee and B. D. Hammock, *Sci. Total Environ.*, 2021, **753**, 141950.
38. M. Mastrogiovanni, A. Trostchansky, H. Naya, R. Dominguez, C. Marco, M. Povedano, R. López-Vales and H. Rubbo, *Biomedicines*, 2022, **10**, 674.
39. S. Gouveia-Figueira, J. Späth, A. M. Zivkovic and M. L. Nording, *PLoS One*, 2015, **10**, e0132042-e0132042.

Table of Contents Graphic



Supplementary Information for

Chapter 4: Improved ELISA for linoleate-derived diols in human plasma utilizing a polyHRP-based secondary tracer

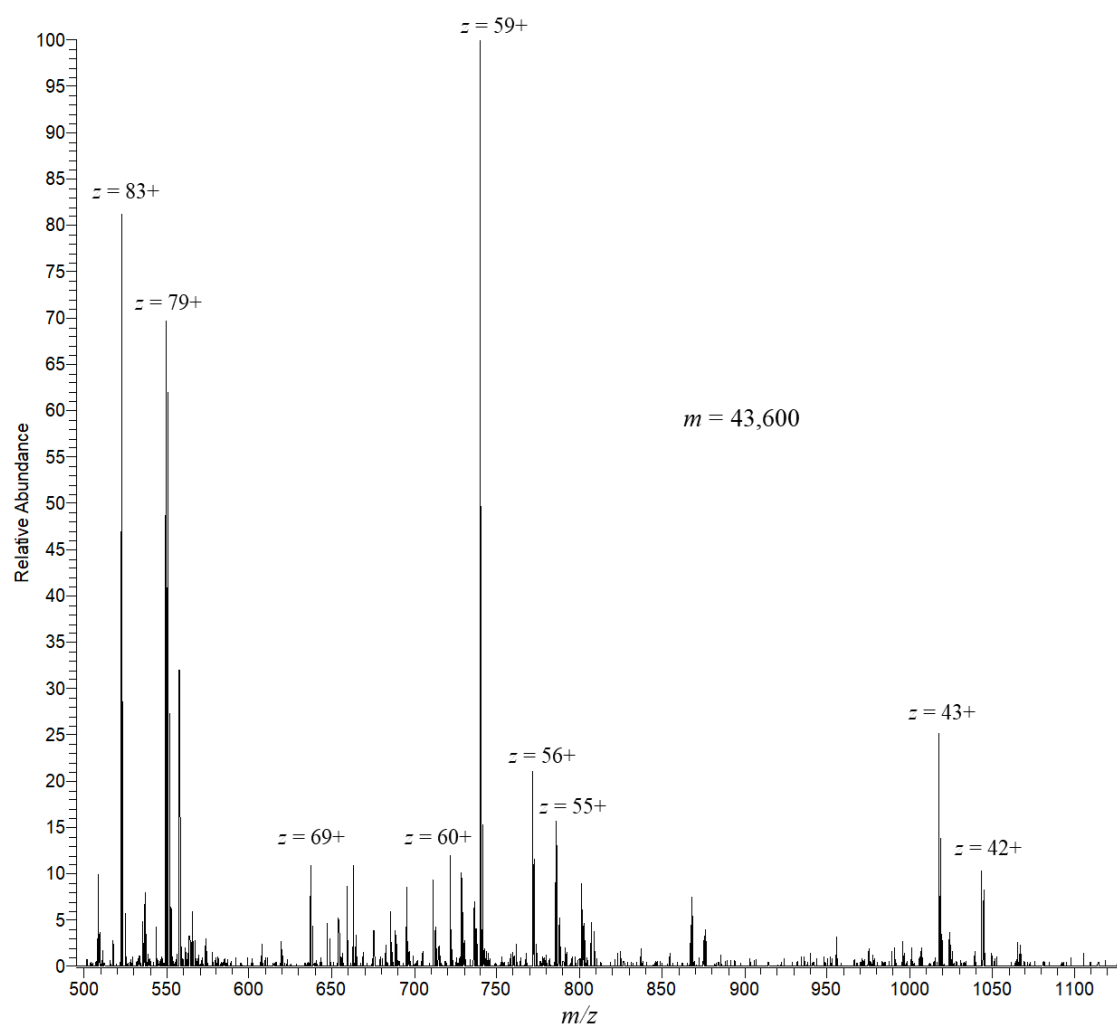
Nalin Singh, Dongyang Li, Cindy B. McReynolds, Christophe Morisseau, Bruce D. Hammock*

Department of Entomology and Nematology and UC Davis Comprehensive Cancer Center,
University of California Davis, Davis, California, 95616, USA.

*E-mail: bdhammock@ucdavis.edu

Tel: 530-752-7519

Dihydroxyoctadecenoic acids (regioisomer mixture). $^1\text{H NMR}$ (400 MHz, CDCl_3) δ 6.25-5.96 (2H, broad singlet, **OH**), 5.61-5.54 (1H, multiplet (m), **vinyllic**), 5.47-5.40 (1H, m, **vinyllic**), 3.52-3.46 (2H, m), 2.38-2.27 (3H, m), 2.11-2.02 (3H, m), 1.69-1.59 (2H, m), 1.53-1.23 (16H, m), 0.90 (3H, triplet, $J = 6.8$ Hz, **Me**); HRESIMS observed m/z 313.2388 $[\text{M} - \text{H}]^-$ (calculated m/z for $\text{C}_{18}\text{H}_{33}\text{O}_4^-$, 313.2384).



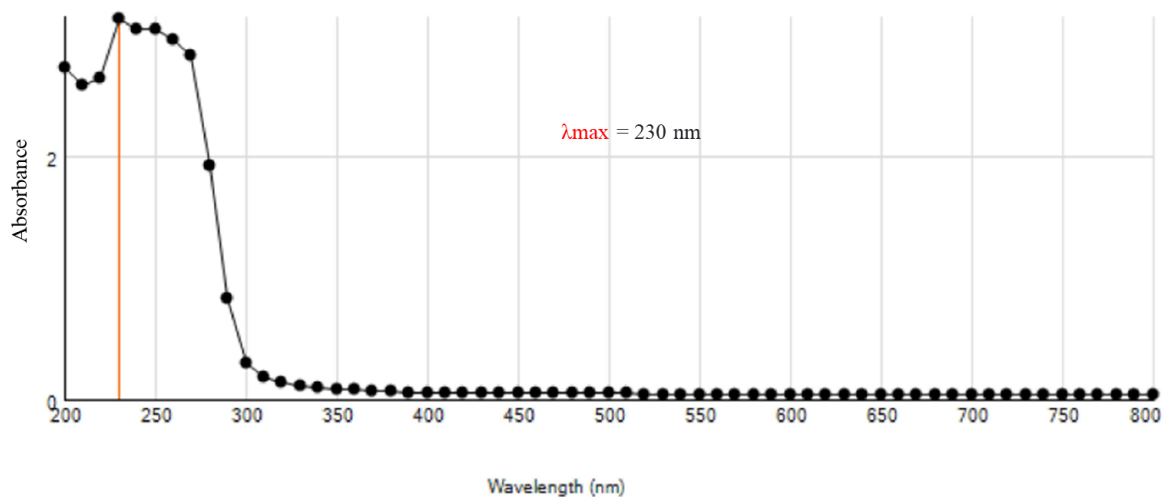


Fig. S1 MS and UV-vis characterization of OLE-OVA (coating antigen)

Table S1 HPLC gradient for elution of DiHOMEs

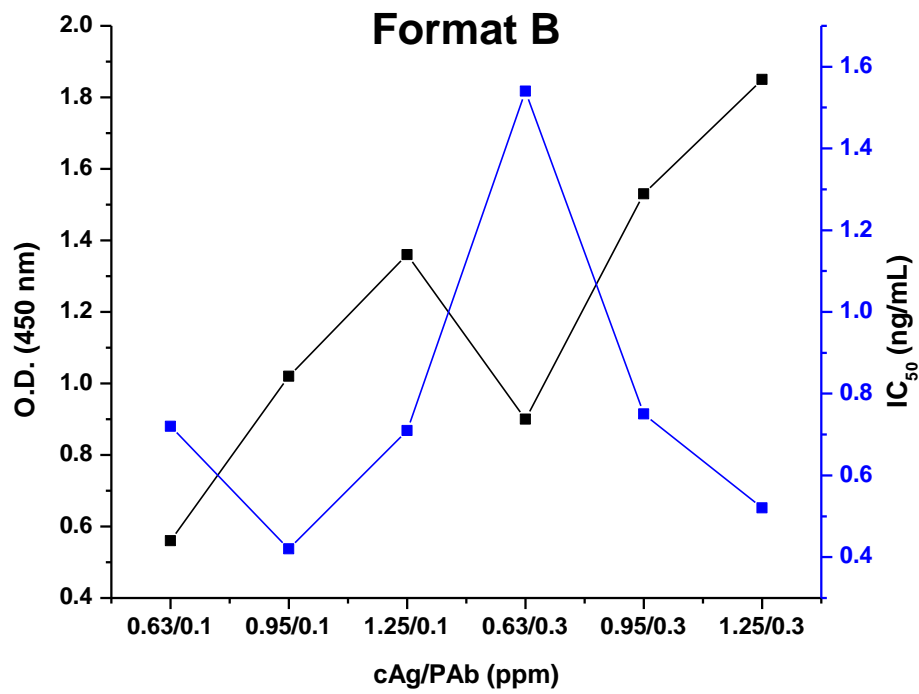
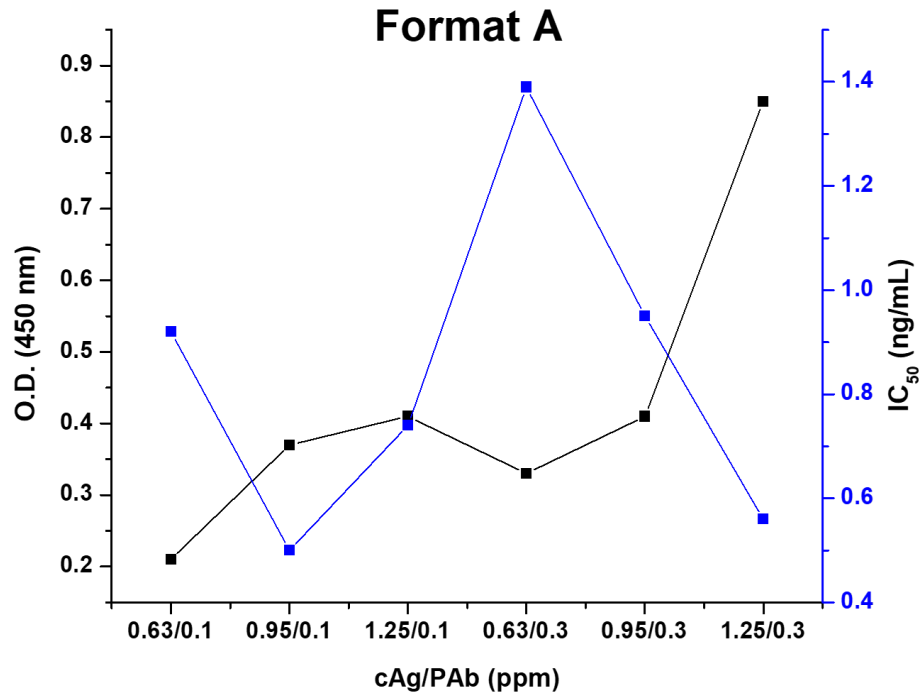
Time (min)	B (%)
0	20
1	70
5	95
6	95
7	20

Table S2 Q-TRAP mass spectrometer conditions

Parameter	Value
Curtain Gas (psi)	30
Collision Gas	Medium
IonSpray Voltage (V)	-4500
Temperature (°C)	450
Ion Source Gas 1 (psi)	50
Ion Source Gas 2 (psi)	50
Interface Heater (ihe)	ON

Table S3 Tandem MS parameters for DiHOMEs

Analyte	Declustering potential (V)	Entrance potential (V)	Collision energy (V)	Collision cell exit potential (V)
9,10- DiHOME	-50	-10	-30	-5
12,13- DiHOME	-50	-10	-30	-5



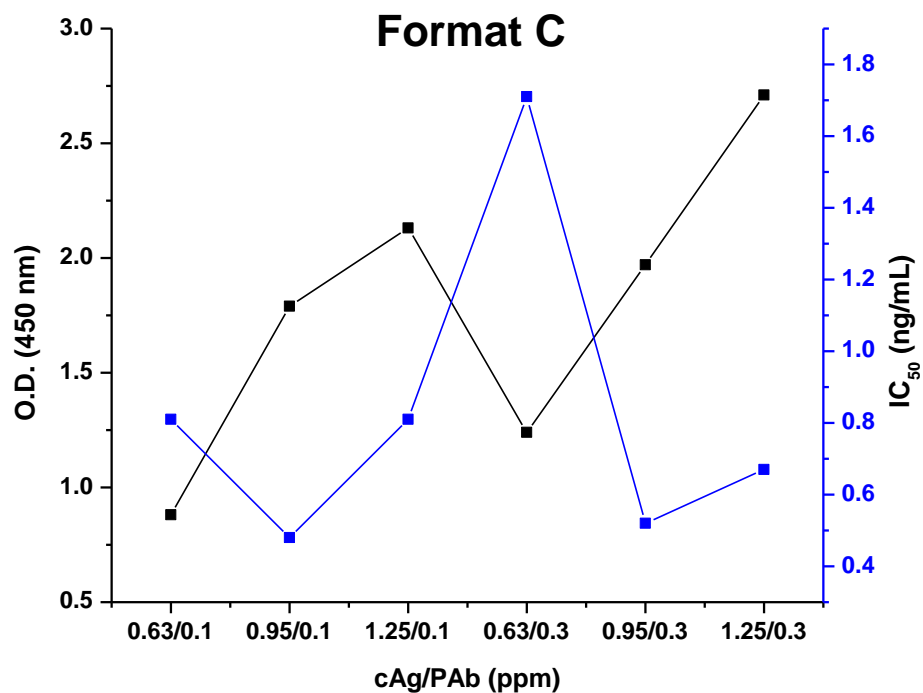


Fig. S2 Checkerboard titration-based optimization of coating antigen (cAg) and primary antibody (PAb) concentrations (ppm) for DiHOME ELISA formats A-C

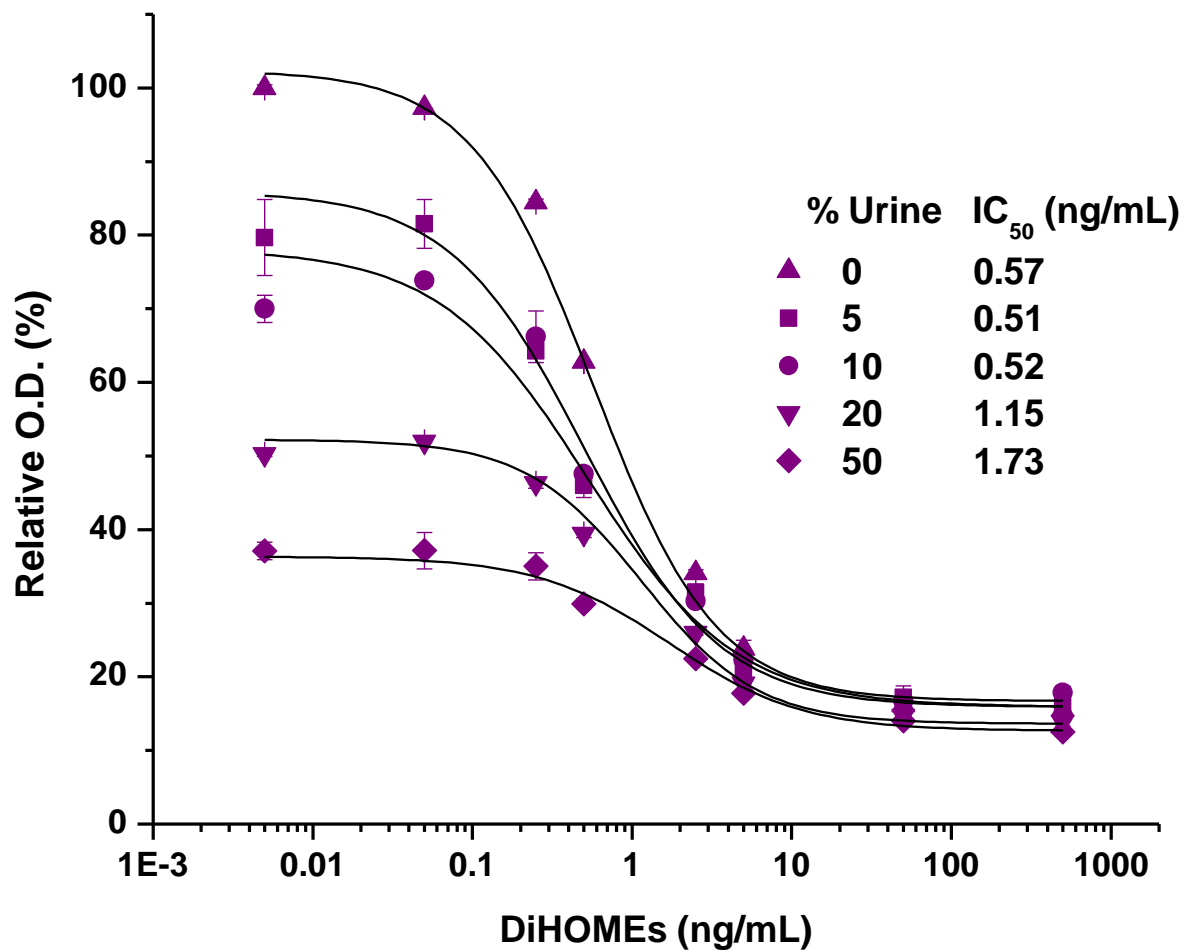


Fig. S3 Calibration curves (and IC₅₀ values) for DiHOMEs in varying concentrations (0-50% in neat assay buffer) of human urine

Conclusion

The versatility and amenability of the CYP pathway of PUFA metabolism offer multiple avenues to resolve and monitor disease outcomes and each strategy possesses its own distinct benefits and limitations.

Firstly, administration of EpFAs is the most basic and simplest means of pharmacological intervention. Typically, methyl ester forms are employed as a prodrug due to their improved cell membrane permeability. Upon entry into the cell, they are instantly cleaved to the free carboxylic acids by cellular esterases.^{1,2} Furthermore, the fact that the methyl ester penetrates membranes rapidly and the carboxylic function permeates less well works to concentrate the free acids in cells against a concentration gradient. EETs are the most widely used EpFA group and hence their 22-carbon homologues (i.e., ω -6 adrenic acid-derived EDTs) were studied and found to be another therapeutically active group of EpFAs (**Chapter 1**). Furthermore, there is growing interest in EpFAs derived from ω -3 PUFAs, namely eicosapentaenoic acid (EPA)-derived epoxyeicosatetraenoic acids (EEQs) and docosahexaenoic acid (DHA)-derived epoxydocosapentaenoic acids (EDPs), which have displayed equal or even greater potency, relative to EETs, in certain disease models.^{3,4} However, the chemically stable EpFAs have short metabolic half-lives due to rapid degradation by sEH. Past studies have required heroic efforts to obtain biological activities *in vivo* directly from EpFAs. This is probably in large part due to the high activity of epoxide hydrolase enzymes. Hence, practical application of EpFAs would likely be constrained to localized *in vivo* sites (e.g., appendage, ocular, topical, gastrointestinal). To combat this, sEH inhibitors (sEHI) can be employed to block the hydrolysis of EpFAs, facilitating systemic bioavailability and function. sEHI typically utilize urea or amide pharmacophores and act by mimicking the transition states of epoxide opening in the sEH active

site.^{5,6} Moreover, naturally derived sEHI have additional advantages since dietarily-acquired sEHI can bypass the expensive and stringent approval process required for their synthetic counterparts. Natural product sEHI have been limited pharmacologically by their poor inhibition of the sEH enzyme and/or low concentrations in plant sources.⁷ By contrast, macamides derived from maca were found to be potentially applicable naturally occurring sEHI, due to their abundance in plant root, strong inhibitory potency towards sEH, and therapeutic activity following oral administration, especially if pre- and post-harvest production can be increased (**Chapter 2**). Still, the activity of sEHI is contingent on endogenous production of EpFAs. Under certain renal or cardiovascular pathological conditions where CYP metabolism is impaired, the efficacy of sEHI could be compromised. Alternatively, synthetic analogues of EpFAs can be employed. They are designed to be more biologically stable than EpFAs and act independently of endogenous EpFA levels. Early EpFA analogues have received some criticisms for resembling and acting as traditional sEHI without accompanying verification of mimetic function. Hence, application of alkoxy- groups as epoxide bioisosteres, an approach that had previously proved successful for developing mimics of the insect juvenile hormone,^{8,9} yielded a new group of potent and stable EET analogues (**Chapter 3**). They join a new generation of EpFA analogues, which include mimics that possess non-sEH-inhibiting bioisosteres (e.g., oxamides)¹⁰ and molecules (e.g., AUDA) that exert dual mimetic/inhibitory effects.¹¹ Lastly, while sEH-produced DHFAs are of little therapeutic relevance and can in fact exert pro-inflammatory effects, these metabolites, particularly the prevalent ω -6 linoleate-derived diols (DiHOMEs), hold great potential to act as biomarkers of disease since high concentrations correlate well with poor outcomes. Accordingly, an improved¹² and validated ELISA for DiHOMEs was developed (**Chapter 4**) to obtain cheap, easy, and flexible analytical method.

Finally, assay functionality was verified by quantitation of DiHOMEs in clinical samples, accompanied by authentication with a traditional LC-MS/MS analysis.¹³

In summary, the overarching hope is that the work described in this dissertation has provided valuable therapeutic leads to alleviate the detrimental impacts of environmental exposures as well as yielded a robust analytical tool for evaluation of phenotypic outcomes.

References

1. Greene JF, Newman JW, Williamson KC, Hammock BD. Toxicity of epoxy fatty acids and related compounds to cells expressing human soluble epoxide hydrolase. *Chemical Research in Toxicology*. 2000;13(4):217-226.
2. Greene JF, Williamson KC, Newman JW, Morisseau C, Hammock BD. Metabolism of monoepoxides of methyl linoleate: bioactivation and detoxification. *Archives of Biochemistry and Biophysics*. 2000;376(2):420-432.
3. Morisseau C, Inceoglu B, Schmelzer K, Tsai HJ, Jinks SL, Hegedus CM, et al. Naturally occurring monoepoxides of eicosapentaenoic acid and docosahexaenoic acid are bioactive antihyperalgesic lipids. *Journal of Lipid Research*. 2010;51(12):3481-3490.
4. Wagner K, Vito S, Inceoglu B, Hammock BD. The role of long chain fatty acids and their epoxide metabolites in nociceptive signaling. *Prostaglandins & Other Lipid Mediators*. 2014;113-115:2-12.
5. Singh N, Hammock BD. Soluble Epoxide Hydrolase. In: Offermanns S, Rosenthal W, editors. *Encyclopedia of Molecular Pharmacology*. Cham: Springer International Publishing; 2020. p. 1-7.

6. McReynolds C, Morisseau C, Wagner K, Hammock B. Epoxy Fatty Acids Are Promising Targets for Treatment of Pain, Cardiovascular Disease and Other Indications Characterized by Mitochondrial Dysfunction, Endoplasmic Stress and Inflammation. *Advances in Experimental Medicine and Biology*. 2020;1274:71-99.
7. Sun C-P, Zhang X-Y, Morisseau C, Hwang SH, Zhang Z-J, Hammock BD, et al. Discovery of Soluble Epoxide Hydrolase Inhibitors from Chemical Synthesis and Natural Products. *Journal of Medicinal Chemistry*. 2021;64(1):184-215.
8. Henrick CA, Staal GB, Siddall JB. Alkyl 3,7,11-trimethyl-2,4-dodecadienoates, a new class of potent insect growth regulators with juvenile hormone activity. *Journal of Agricultural and Food Chemistry*. 1973;21(3):354-359.
9. Hammock BD, Gill SS, Casida JE. Synthesis and morphogenetic activity of derivatives and analogs of aryl geranyl ether juvenoids. *Journal of Agricultural and Food Chemistry*. 1974;22(3):379-385.
10. Adebisin AM, Wesser T, Vijaykumar J, Konkel A, Paudyal MP, Lossie J, et al. Development of Robust 17(R),18(S)-Epoxyeicosatetraenoic Acid (17,18-EEQ) Analogues as Potential Clinical Antiarrhythmic Agents. *Journal of Medicinal Chemistry*. 2019;62(22):10124-10143.
11. Olearczyk JJ, Field MB, Kim I-H, Morisseau C, Hammock BD, Imig JD. Substituted Adamantyl-Urea Inhibitors of the Soluble Epoxide Hydrolase Dilate Mesenteric Resistance Vessels. *Journal of Pharmacology and Experimental Therapeutics*. 2006;318(3):1307.
12. Zurek G, Gee SJ, Hammock BD. Development of an enzyme immunoassay for linoleic acid diols in urine. *Analytica Chimica Acta*. 2002;466(2):247-256.

13. Yang J, Schmelzer K, Georgi K, Hammock BD. Quantitative profiling method for oxylipin metabolome by liquid chromatography electrospray ionization tandem mass spectrometry. *Analytical Chemistry*. 2009;81(19):8085-8093.

Appendix

Chapter-publication associations

Chapter 1 is published as **Singh N, Barnych B, Wagner KM, Wan D, Morisseau C, Hammock BD. Adrenic Acid-Derived Epoxy Fatty Acids Are Naturally Occurring Lipids and Their Methyl Ester Prodrug Reduces Endoplasmic Reticulum Stress and Inflammatory Pain. ACS Omega. 2021;6(10):7165-7174.**

Chapter 2 is published as **Singh N, Barnych B, Morisseau C, Wagner KM, Wan D, Takeshita A, et al. N-Benzyl-linoleamide, a Constituent of Lepidium meyenii (Maca), Is an Orally Bioavailable Soluble Epoxide Hydrolase Inhibitor That Alleviates Inflammatory Pain. Journal of Natural Products. 2020;83(12):3689-3697.**

Chapter 3 is published as **Singh N, Vik A, Lybrand DB, Morisseau C, Hammock BD. New Alkoxy- Analogues of Epoxyeicosatrienoic Acids Attenuate Cisplatin Nephrotoxicity In Vitro via Reduction of Mitochondrial Dysfunction, Oxidative Stress, Mitogen-Activated Protein Kinase Signaling, and Caspase Activation. Chemical Research in Toxicology. 2021;34(12):2579-2591.**

Chapter 4 is published as **Singh N, Li D, McReynolds CB, Morisseau C, Hammock BD. Improved ELISA for linoleate-derived diols in human plasma utilizing a polyHRP secondary tracer. Analytical Methods. 2022; Advance Article**

List of other relevant contributions

Singh N, Hammock BD. Soluble Epoxide Hydrolase. In: Offermanns S, Rosenthal W, editors. Encyclopedia of Molecular Pharmacology. Cham: Springer International Publishing; 2020. p. 1-7

Bergmann CB, McReynolds CB, Wan D, Singh N, Goetzman H, Caldwell CC, et al. sEH-derived metabolites of linoleic acid drive pathologic inflammation while impairing key innate immune cell function in burn injury. Proceedings of the National Academy of Sciences. 2022;119(13):e2120691119.

Barnych B, Singh N, Negrel S, Zhang Y, Magis D, Roux C, et al. Development of potent inhibitors of the human microsomal epoxide hydrolase. European Journal of Medicinal Chemistry. 2020;193:112206.